University of Bath

PHD

Electrochemical and spectroscopic studies of poly-o-aminophenol

Ortega, Jose Miguel

Award date:
1996

Awarding institution:
University of Bath

Link to publication

Alternative formats
If you require this document in an alternative format, please contact:
openaccess@bath.ac.uk

Copyright of this thesis rests with the author. Access is subject to the above licence, if given. If no licence is specified above, original content in this thesis is licensed under the terms of the Creative Commons Attribution-NonCommercial 4.0 International (CC BY-NC-ND 4.0) Licence (https://creativecommons.org/licenses/by-nc-nd/4.0/). Any third-party copyright material present remains the property of its respective owner(s) and is licensed under its existing terms.

Take down policy
If you consider content within Bath's Research Portal to be in breach of UK law, please contact: openaccess@bath.ac.uk with the details. Your claim will be investigated and, where appropriate, the item will be removed from public view as soon as possible.

Download date: 05. May. 2023

Electrochemical and Spectroscopic Studies of Poly-o-Aminophenol

Submitted by José Miguel Ortega
for the degree of PhD
of the University of Bath

1996

COPYRIGHT

Attention is drawn to the fact that copyright of this thesis rests with its author. This copy of the thesis has been supplied on condition that anyone who consults it is understood to recognise that its copyright rest with its author and that no quotation from the thesis and no information derived from it may be published without the prior written consent of the author.

This thesis may be made available for consultation within the University Library and may be photocopied or lent to other libraries for the purposes of consultation.

José Miguel Ortega

UMI Number: U082957

All rights reserved

INFORMATION TO ALL USERS
The quality of this reproduction is dependent upon the quality of the copy submitted.

In the unlikely event that the author did not send a complete manuscript
and there are missing pages, these will be noted. Also, if material had to be removed,
a note will indicate the deletion.

UMI U082957
Published by ProQuest LLC 2014. Copyright in the Dissertation held by the Author.
Microform Edition © ProQuest LLC.
All rights reserved. This work is protected against
unauthorized copying under Title 17, United States Code.

ProQuest LLC
789 East Eisenhower Parkway
P.O. Box 1346
Ann Arbor, MI 48106-1346

UNIVERSITY OF EARTH
LIBRARY
21 23 AUG 1996
PHD
S105136

University of Bath

Electrochemical and Spectroscopic Studies

of

Poly-o-Aminophenol

by

José Miguel Ortega

Doctor of Philosophy

School of Chemistry

March 1996

A la memoria de aquellos
quienes me despidieron con
la esperanza de verme regresar

University of Bath

Abstract

School of Chemistry

Doctor of Philosophy

Electrochemical and Spectroscopic Studies of Poly-o-Aminophenol

by

José Miguel Ortega

Conducting poly-o-aminophenol films deposited on Pt electrodes were studied by electrochemical and spectroscopic techniques. The results suggest that the polymer is a composite of two structural forms, one corresponding to a ladder structure of alternated benzenic and phenoxazine rings and the other an opened structure similar to indophenol. Compact and uniform films were observed by SEM and their morphology and growth patterns do not depend significantly on the supporting electrolyte utilised.

The polymer exhibits conducting properties at potentials more negative that the formal potential (defined as $[E_pc + E_pa]/ 2$) of the film. This conclusion is supported by the limiting voltammetric behaviour observed during growth of the polymer and by the results of experiments with redox couples. The measured conductivity was found to depend on the pH of the solution: the lower the pH is, the higher the conductivity. The conductivity of the film at pH 0.9 was low (9.3×10^{-8} S cm^{-1})

ESR experiments indicated that formation of polarons is maximum in the region of potential where the polymer is conducting. The polaron concentration decays at positive potentials, possibly due to formation of bipolarons. However, the latter appear not to contribute to the conductivity of the film because they are trapped between non-conducting regions of the polymer.

Uv-visible spectroscopy was used to follow the changes in the oxidation state of the polymer with potential. The results revealed peaks at 414, 690 and 492 nm which were assigned to formation of polarons, bipolarons and an oxidised form of the

polymer, respectively. The absence of isobestic points and the deconvolution of the peaks indicate that a mixture of structures is formed as the oxidation occurs.

The number of molecules of water per poly-o-aminophenol equivalent in its oxidised form was determined to be approximately seven. As the reduction proceeds, swelling of the film takes place but it still exhibits rigid features. Mass changes during the oxidation-reduction of the polymer arise from a summation of various processes occurring at different timescales.

Copper deposition onto poly-o-aminophenol was carried out at potentials where the film is conducting. Electrodeposition follows an instantaneous 3D nucleation process with diffusion controlled growth at low overpotentials. At higher overpotentials, clusters are formed around a central site. A model of polymer conducting strands in a poor conducting matrix is proposed to explain these results.

Acknowledgements

I would like to express my gratitude to Prof. L. M. Peter for his guidance and advice throughout the course of this work.

Thanks are due to Dr J. Maher for letting me use his ESR spectrophotometer and to Professor R. Hillman for permitting to utilise his QCMB and the Crystal Impedance set-up and specially for the hospitality of the members of his group.

The glass work carried out by Mr. M Lock and the collaboration of Mr A. Prowse are gratefully appreciated

My acknowledgements are also to my laboratory colleagues, who shared bad and good moments with me over the years. Special mention to Dr. L. Saraby for her kindness and Dr. M. Skompska for her friendship.

Many thanks to my wife, Vilma for her understanding and support during this work. I also wish to thank Sabino and David who, during the course of this work, contributed by encouraging me. I am very grateful.

Finally, I would like to thank the Universidad De Los Andes for giving me the opportunity to further my studies. I am also indebted to the Consejo Nacional de Investigaciones Científicas y Tecnológicas (CONICIT) and the Centro de Adiestramiento de Petróleos de Venezuela (CEPET) for their financial support.

Table of Contents

CHAPTER 4: Electrochemical and Spectroscopic Studies of Pdy-o-Aminophenol.

CHAPTER 5: Electrodeposition of copper on POAP

Chapter 1

Introduction

CHAPTER 1

INTRODUCTION

1.1. Introduction

The application of the electrochemistry to transform organic compounds into dimers, oligomers and also polymers appears to be an excellent synthetic tool. Some polymers synthesised in this way have an unique electroactive behaviour due to the fact that redox reaction is accompanied by a change in the electrical properties of the film from an insulator to an electrical conductor. Due to this feature they are called *conducting polymers* or, less frequently , *synthetic metals*.

In 1977 it was reported[1,2] that polyacetylene could be chemically *p* or *n* doped (partly oxidised or reduced) with a significant increasing of its conductivity, from a semiconducting state to a *metallic* regime[3]. The doping could be carried out electrochemically and was reversible[4]. The term *p* and *n* doping refers to the partial oxidation and reduction of the polymer respectively. For an oxidation process, for example , it is possible to write:

$$(P)_x \longrightarrow [P^{y+}]_x + (xy)e^- \qquad (1.1)$$

$$[P^{y+}]_x + (xy)A^- \longrightarrow [(P^{y+})A_y]_x \qquad (1.2)$$

where P is the repetitive unit and A^- is the requisite counter-ion to preserve electrical neutrality in the system. Analogously, the reduction process can be written as follows:

$$(P)_x + (xy)e^- \longrightarrow [P^{y-}]_x \qquad (1.3)$$

$$[P^{y-}]_x + (xy)M^+ \longrightarrow [M_y^+(P^{y-})]_x \qquad (1.4)$$

where M^+ is the counter cation which preserves electrical neutrality. The conductivity of polyacetylene can be increased by up twelve orders of magnitude by the use of different dopants. Table 1.1 shows some examples of dopants and the changes in the conductivities of the polymer.

Table 1. 1

Examples of dopants for polyacetylene[5]

Substance	Conductivity (S/cm)
cis-form	1.7×10^{-9}
trans-form	4.4×10^{-5}
Oxidation (p-doping)	
AsF_5 vapor:$[(CH^{0.1+})(AsF_6^-)_{0.1}]_x$	1.2×10^3
Electrochemically: $[(CH^{0.1+})(ClO_4^-)_{0.1}]_x$	1.0×10^3
Reduction (n-doping)	
Li naphthalide: $[Li_{0.2}^+ (CH^{0.2-})]_x$	2×10^2
Electrochemically: $[Li_{0.1}^+ (CH^{0.1-})]_x$	$10^1 - 10^2$

These findings stimulated intense work in the electrochemical field due to the potential industrial applicability of this kind of conducting organic polymer. Shortly thereafter, polypyrrole[6], polythiophene[7], poly(p-phenylene)[8] and polyaniline[9] were identified and examined as conducting materials. More recently, research in this field has generated so much interest among such a wide variety of disciplines that it is not difficult to think of them as very promising futuristic materials.

1.2. Synthesis of Conducting Polymers

1.2.1 *Chemical method.*

Conducting polymers can be formed via chemical synthetic routes or via electropolymerization. In the former case, the conducting state is made by oxidative or reductive doping with electron-accepting or electron-donating species. The chemical route has been extensively utilised in the case of polyacetylene; acceptors such as bromine, iodine, AsF_5 [1,10], ClO_4^-, BF_4^- [11] and donors such as lithium[12] and sodium[13] have been reported to give conductivities of the order of 10^2 S cm^{-1}.

In other cases, the chemical method involves the mixing of strong oxidants with the monomer; for example, different oxidising agents, such as potassium dichromate[14], hydrogen peroxide[15] and ammonium persulphate[16], have been used to produce polyaniline from aniline solution. Chemical synthesis of N-substituted polyanilyne derivatives by oxidation of tetrabutylammonium salts with $(NH_4)_2 S_2O_8$ has been also reported[17]. The chemical polymerisation of pyrrole in strong oxidising medium, e.g. $FeCl_3$ [18]; leads to parasitic side reactions, especially the nucleophilic attack of the polymer positive sites by water to form hydroxides or carbonyl groups in the ring[19,20]. Soluble precursor polymers can be converted into the desired product by heating[21] or can be used in chemical oxidative polymerisation[22].

1.2.2. *Electrochemical method.*

In the last few years, electrochemistry has been the subject of a great expansion due to the discovery of conducting polymers. Most of those materials are directly synthesised in the conductive doped form by an electrochemical method. Polymers can be obtained by anodic or cathodic reactions of their monomers at the working electrode. The fact that a vast number of conducting polymers can be produced

in this simple way has tended to focus attention on this method of synthesis, rather than on others that require chemical procedures; moreover, in the chemical synthesis, generally little control can be exercised over the morphology of the product and purity of the material obtained.

The main requirements for the anodic electropolymerisation are: first of all, the monomer has an oxidation potential which is accessible in a suitable solvent system, secondly, the monomer must produce a radical cation which reacts more quickly with other monomers to form the polymer than it would with other nucleophiles in the electrolyte solution and, finally, a polymer with a lower oxidation potential than of the monomer should be produced. All aromatic systems can, in principle, act as monomers to lead to conducting polymers. However, experimental and structural factors limit the number of electropolymerisable monomers. The formation of conducting materials on electrodes has been achieved by the use of families of monomers which contain benzene and related arenes as the fundamental unit (e.g. phenylene[23], fluorene[24]), aromatic heterocycles (e.g. pyrrole[25], thiophene[26], carbazole[27]), π-conjugated systems (e.g. azulene[28], naphthalene[29]) and for polymers from which the linkage between two π-moieties is via heterochains (e.g. aniline[30], 2-substituted thiophenes[31]).

A general scheme of anodic polymerisation is shown in the figure 1.1. The activation of monomer (**Aro**) is achieved by an electron transfer from the monomer to the electrode whose potential is enough positive to overcome energy barriers. The cation radicals formed can then couple via a carbon-carbon bond to produce the dimer by proton elimination. Subsequent radical couplings and electron transfers lead to the building up of the polymer on the electrode. To grow films of significant thickness, the polymer film must itself be electroactive and capable of electrocatalytically oxidising or reducing fresh

monomer, or the film must be rather permeable to monomer. Otherwise, electrode passivation will occur.

Since increasing of the length of polyaromatic chains leads to better electronic delocalization, the oxidation potentials should ideally be in the following order: $E^{o}_{monomer} > E^{o}_{dimer} > E^{o}_{oligomer} > E^{o}_{polymer}$. As the potential needed for monomeric oxidation is always significantly higher than that required for charging of the existing polymer, the two processes, i.e. film formation and its oxidation, occur simultaneously. Figure 1.2. illustrates the building up of a conducting polymer by cyclic voltammetry.

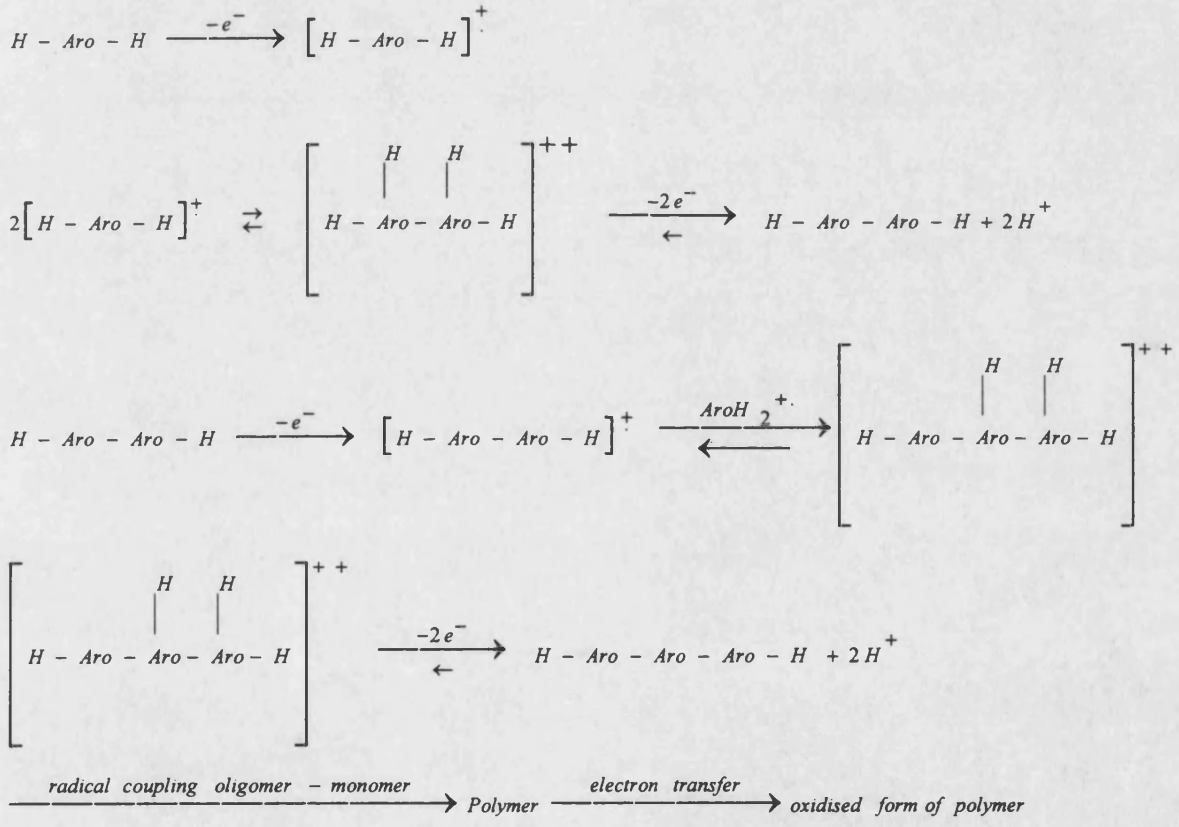

Figure 1. 1 A general scheme for the anodic electropolymerization mechanism of conducting polymers, *J. Simonet*[37].

Theoretically, the film-forming process needs 2 electrons per molecule; however, the anodic oxidation leading to conducting polymers is reported to have an electrochemical stochiometry of 2.07 to 2.6 electrons for each monomer unit[32,33]; the additional charge serves the partial oxidation-reduction of the polymer.

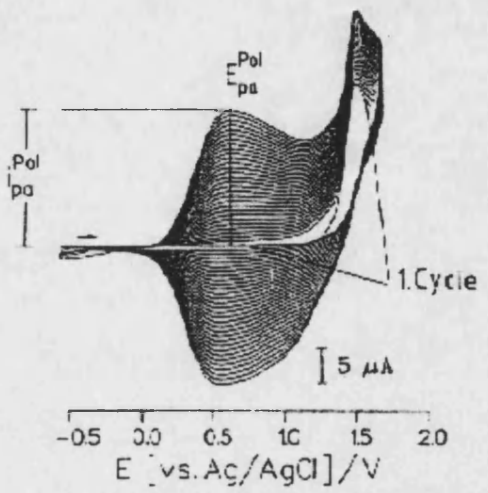

Figure 1. 2 Potentiodynamic growth of polypyrrole film in acetonitrile[34]. $\nu = 0.2\ V\ s^{-1}$

The radical coupling mechanism has been criticised[35,36] on the basis that the strong coulombic repulsion between small cation radicals renders a direct dimerization of such particles improbable. Instead, it has been postulated that a radical substrate coupling occurs. However, this suggestion is not adequate to explain the chain propagation process, since growth is observed experimentally only when the oxidation of the monomer occurs in parallel to the oxidation of the polymer[34].

The applied anodic potential during polymerisation must not be too far (± 0.1 V) from the peak corresponding to oxidation monomer[37]; too oxidising potentials could lead to material with irreversible higher oxidation state and low conductivity; on the

contrary, if the potential is too low, polymerisation will be very slow and soluble oligomers could be formed.

The n-doping corresponding to the reduction of the polymer backbone and cation insertion in order to ensure the electroneutrality is much less frequent in conducting polymers; in this case reversible oxidation results in the neutralisation of the reduced polymer which is accompanied by the cation expulsion[38]. Kinetic limitations arising probably from the slow diffusion of cations inside the polymer or the irreversible destruction of the polymeric matrix[39] have been proposed as explanations for the small number of polymers that can be electrochemically reduced .

Synthesis of conducting polymers based on the nickel catalysed reduction of dibromoaromatic substrates[40,41,42] seems to represent the cathodic alternative to produce n-type conducting polymers. However, this method is less easy to handle compare with the anodic one which is much more often used. One problem with this approach is that the polymer is obtained in its neutral (insulating) form which leads to an inhibition of the electrochemical process.

$$NiBr_2L_2 + 2e^- \longrightarrow Ni^{(0)}L_2 + 2Br^-$$

$$BrAroBr + Ni^{(0)}L_2 \longrightarrow BrAro - Ni(L_2)Br$$

$$BrAro - Ni(L_2)Br + 2e^- \longrightarrow BrAro^- + Ni^{(0)}L_2 + Br^-$$

$$BrAro^- + BrAro - Ni(L_2)Br \longrightarrow BrAro - AroBr + Br^- + Ni^{(0)}L_2$$

Figure 1.3 A general scheme for cathodic electropolymerization of conducting polymers, *Z. Xu* [43].

The cathodic synthesis of polythiophene from 2,5-dibromothiophene[43] is described by the previous scheme; the nickel (0) triphenylphosphine complex, Ni(0) $(PPh_3)_4$, was produced under galvanostatic conditions from Ni(III) $(PPh_3)Cl_2$ solution. The formation of the complex Ni $(PPh_3)_2$ (2-bromo-5-thienyl) was observed when the monomer was added; the galvanostatic reduction of this complex led, eventually, to the formation of the film. The cathodic growth yielded undoped (neutral) amorphous deposits in contrast to the organised and conductive p-doped material obtained by anodic polymerisation.

1.3 Classification of Electroactive Polymer Films

Electroactive polymers can be classified into two broad groups: electronically conducting polymers and redox polymers. Electronically conducting polymers such as polyaniline, polyacetylene, polythiophene, and polypyrrole, are π-conjugated materials which have relatively delocalized electronic states and are electronically conducting[44]. In a redox polymer, an electroactive group is covalently bonded onto a non conducting polymeric backbone[45] so that electron transport occurs only via hopping between the sites[46,47].

It has been reported that anodic polymerisation of dibenzo crown compounds[48] leads to pseudoplanar polytriphenylenes units bound together by crown ether moieties. In this kind of conducting material, electron transport occurs along triphenylene columns by a complex charge transfer mechanism[37].

Figure 1.4 Schematic representation of electronic self exchange charge mechanism for (a) ● a polymer bound redox active couple and (b) a fibrillar electronic conducting polymer. Some examples are given below pictures.

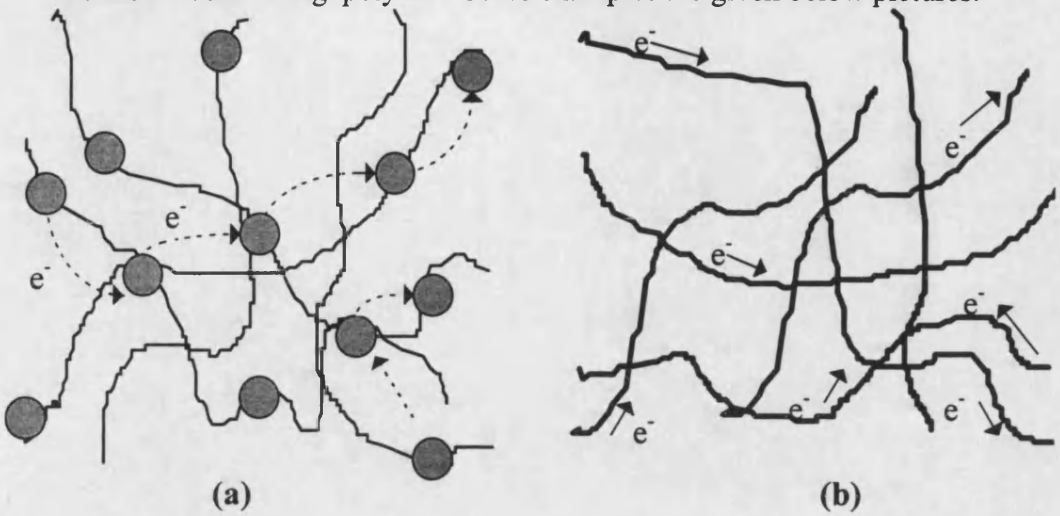

Electronically Conducting Polymer	Redox Polymer
Polyacetylene $-(CH=CH)_n-$	Poly(vinylferrocene)[50] 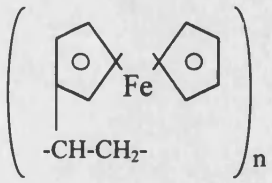
Poly(N-substituted aniline)[49] 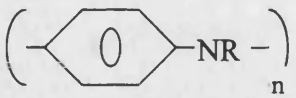	Poly(N,N'-alkylated bipyridines)[52] 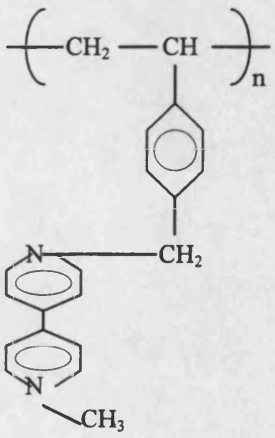
Polypyrrole 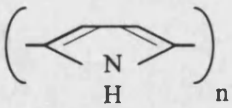	
Polyanthracene[51] 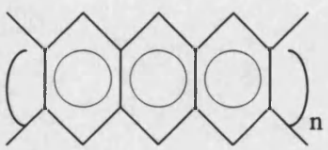	

1.4 Conduction Mechanism

In a sequence of alternating double and single bonds, π electrons are not completely localised so that a number of structures are possible for a conjugated polymer. For polyacetylene, for example, there are two possible non-degenerate *cis*-forms, the *trans-cisoid* and the *cis-transoid*; the latter is of higher energy that the former. The two *trans* forms for this polymer are essentially equivalent.

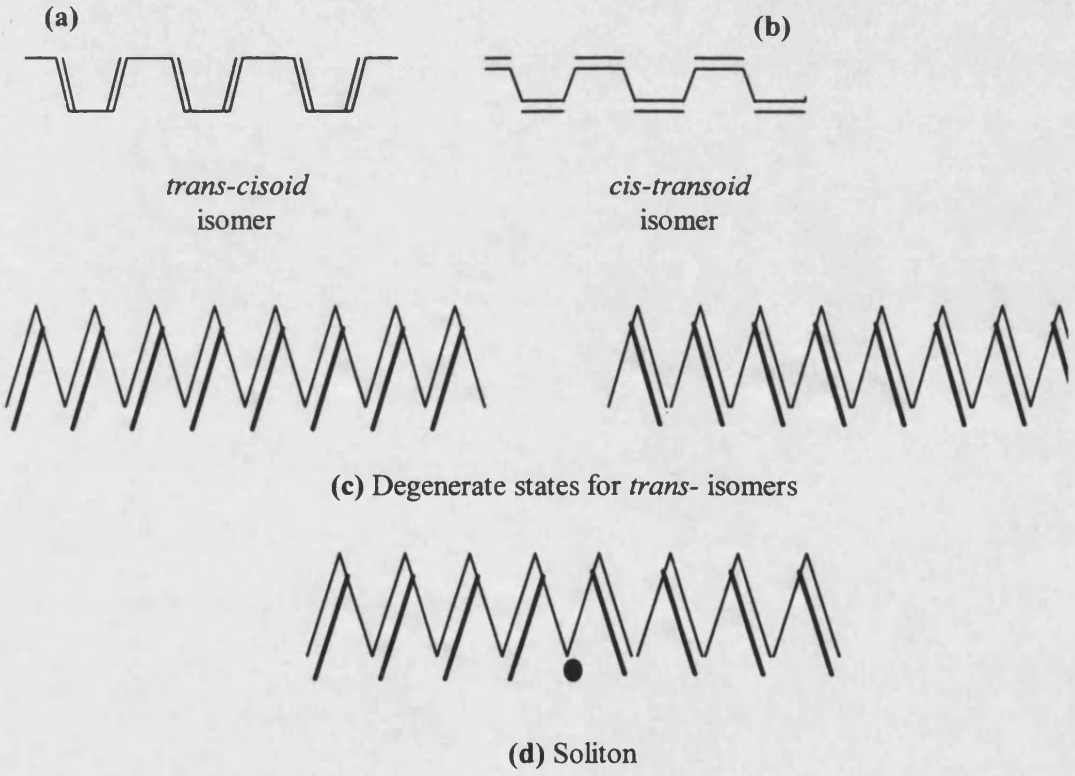

(c) Degenerate states for *trans*- isomers

(d) Soliton

Figure 1.5 Possible structures for polyacetylene chains showing the two non degenerate *cis* isomers (a), (b) and the two degenerate *trans* forms (c). A soliton defect is shown in (d) at the boundary between two degenerated *trans* domains, where the bond alternation has been reversed.

The degeneracy of the *trans* material gives rise to chains which are composed of domains[53] where the double bonds alternately belong to one type or the other. The frontier between domains exhibits a carbon atom with a nonbonding electron called a soliton[54] which it has been calculated to be delocalised over about fifteen carbon atoms[55].The space formation of charged solitons on doping gives rise to low energy configurations producing an increase in the conductivity of the film[56] .

Two neutral solitons on the same chain will tend to recombine while charged solitons will repel each other leading to two isolated charged defects. On the other hand, a neutral soliton and a charged one can achieve a minimum energy configuration by pairing

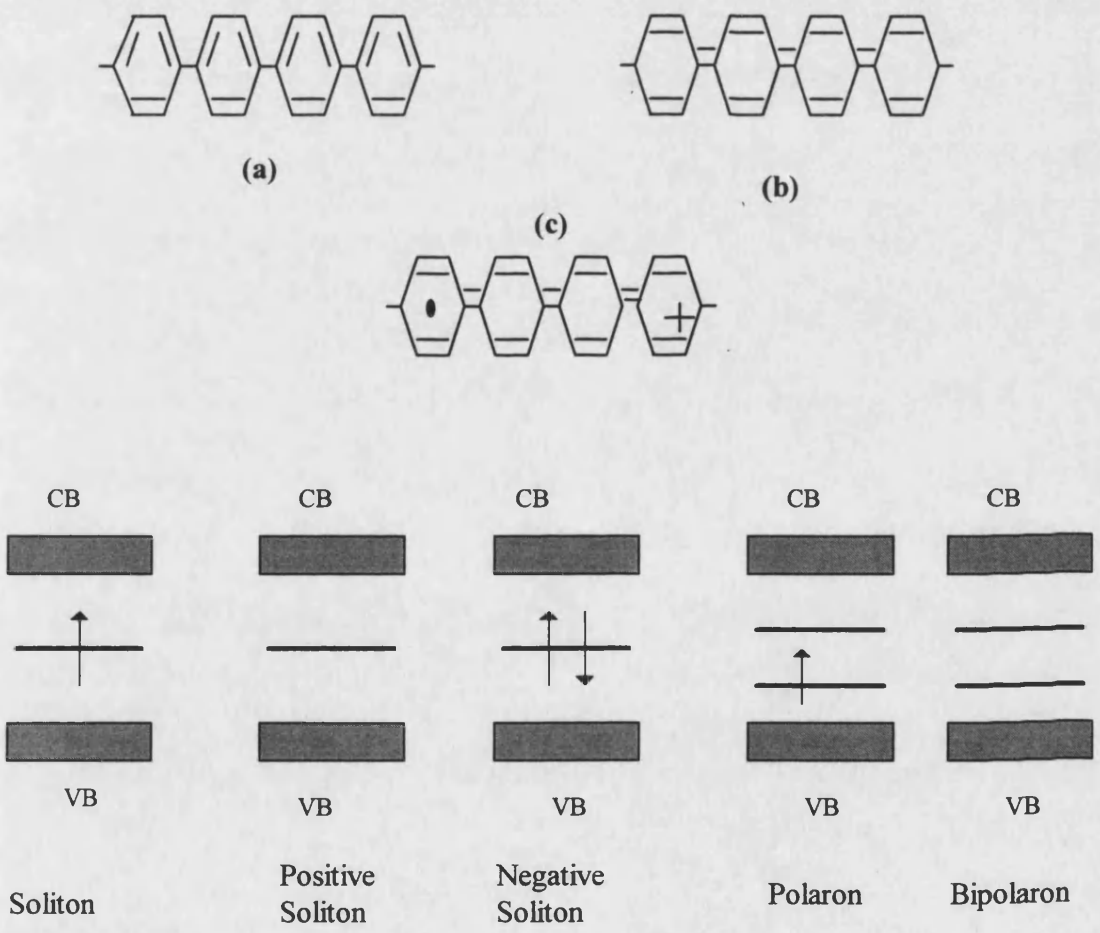

Figure 1.6 Structural diagrams for polyparaphenylene showing the non-degenerate benzenoid (a) and quinoid (b) configurations. Polaron defect (c). Below, Energy level diagrams showing electronic configurations for soliton, polaron and bipolaron defects. CB and VB are the conduction and valence bands respectively

to give rise to a polaron, which is in effect a radical cation[57] delocalised over a few polymer repeat units. Conjugated polymers, except *trans*-polyacetylene, possess non-degenerate ground states so that the formation of single solitons is energetically unfavourable and the preferred configurations involve paired defects as polarons, see figure 1.6(c) .

The pair of neutral radicals from polarons can recombine to eliminate the defect but the positively charged defects, rather than separating along the chain, are predicted to pair up to form a bipolaron, which is a dication[58] .

All these charge carriers will give rise to conductivity in materials where they occur and experimental evidence has been given by ESR[59,60] and optical measurements[61,62] to support their existence.

The mechanism of charge transport in redox polymers is assumed to occur by quantum mechanical tunnelling[63] between individual localised states. In this model it is assumed that the potential drop is concentrated at the electrode polymer interface. Thus, once potential has driven charge transfer at this interface, sequential bimolecular electron self exchange between neighbour sites will take place. Electron hopping is driven by concentration gradients of oxidised and reduced sites. It does not require the presence of an electrical potential gradient[64,65] and can be modelled in terms of a diffusional process[66,67] . Other theoretical analyses that take into account both diffusive and electric field assisted electron hopping have been reported[68] .

1.5 Redox Properties of Conducting Polymers

The interpretation of the redox behaviour is characteristic of each polymer so that a extensive variety of possible shapes of cyclic voltammograms for conducting polymer have been reported[48, 69] . However, anodic waves at the beginning of charging,

followed by a broad plat plateau as the potential increases, are frequently observed, e.g. for polypyrrole[70] and substituted polyaniline[33]. On the reverse scan a potential shifted cathodic wave appears, with a peak current that can be smaller or higher than the anodic one. This separation between peak potentials was initially interpreted as a kinetic effect associated with slow heterogeneous charge transfer. However, the hindrance of ingress and egress of counterions between the solution and the polymer in order to preserve the electroneutrality, the uncompensated charge transport resistance of the film and the polymer swelling could also all be responsible for this observation[67] . Differences between cathodic and anodic peak potentials have been related to structural changes within the solid film. During charging, benzoic based polymers stabilise through a transition from a benzoid into a quinoid-like structure and become planar[71] .

Small separation between peaks as well as symmetrical shape and proportionality of peak current to scan rate have been reported when low scan rates are applied[72,73] as is expected for a surface confined reactant[74]. Mass transport limitations have been noted at higher scan rates[75], for thick films[76],when the size of the counter ion was increased[77] or a less swelling solvent was employed[73]. The presence of electrochemically non-equivalent redox sites has been modelled[78] and it has been demonstrated that the broadening of waves can been attributed to repulsive interactions between redox centres.

The application of a potential step perturbation of short duration to a polyaniline coated ultramicroelectrode showed that the oxidative and reductive transients were very asymmetric[79]. The shape of reduction transient was found to be sensitive to IR compensation even though a microelectrode was used. By contrast, the shape of oxidation transient did not depend significantly on IR compensation and it differed from reduction

transient in that the current response was initially observed to rise, reach a maximum and then decay. This behaviour has been observed by other authors[82,83] and the normalised transients have been approximately fitted to a two dimensional instantaneous nucleation [81] or a phase propagation model[83].

1.6 Some Applications of Conducting Polymers

Electrochemical systems represent the best established family of biosensors; they can operate amperometrically, coulometrically or potentiometrically. A typical electrochemical biosensor consists of a polymeric sensing membrane containing a selective reagent, such as an enzyme, interfaced to a measurement device such as a platinum electrode. This electrode monitors the molecular or ionic species produced by the attack of the enzyme on the substrate[84]. The use of a retained electron mediator to effect electron transfer from an oxidoreductase enzyme active site to the working electrode material has been reported[85]. The two electron mediator (M) thus participates in two alternating reactions with the enzyme (E) that is first reduced by its substrate:

$$Mo + Er \longrightarrow Mr + Eo$$

$$Mr \xrightarrow[\text{electrode}]{\text{polarized}} Mo + 2H^+ + 2e^-$$

With this kind of electrode it is possible to operate at polarising voltages below those where most interferents can oxidise at the electrode. A strategy for combining the role of immobilisation and electron transfer mediation into a single material, i.e. redox polymers, has been demonstrated[86,87]. In these materials, the mediator redox couple is unable to diffuse, so that electron transport occurs by electron hopping. There are advantages in using a non-diffusing mediator: the mediator is prevented from leaching out of the sensor

membrane, thereby eliminating the need for a containment membrane while simultaneously improving the longevity of the sensor[88]. The conductivity of polymers such as polyaniline exhibits a strong dependence on the protonation state of the polymer. This property has been utilised to develop a sensor which involves immobilisation of glucose oxidase in the conducting polymer matrix. The enzyme catalysed reaction of the biomolecule results in a change in redox potential and pH of the microenvironment in the polymer matrix; this change triggers a change in the conductivity of the film which was monitored[89]. Excellent reviews about biosensors have been published [90,91,92] elsewhere.

Cables are shielded from electromagnetic interference by wrapping them in conductive tapes such as aluminium polyester laminates. Conducting polymer based tapes might be a option. However, it may be difficult to produce conducting polymer tapes in large quantities on a continuous basis. The impregnation of a microporous membrane with a conducting polymer has been achieved by sucking the monomer through a membrane on a Buchner funnel and then immersing the monomer-impregnated membrane in a solution containing a couteranion and an oxidant that polymerises the monomer. Polypyrrole[93] and polyaniline-*p*-toluenesulfonate[94] tapes obtained by this way showed conductivities in the range of 10^{-2} - 3 S cm^{-1} and high shielding efficiencies.

Electrochromic display devices make use of electroactive materials coated on an electrode (usually, indium tin oxide coated transparent glass or platinum deposited on glass producing a transparent electrode). Electrochromism is observed on changing the potential applied to an electrode coated with the polymer which can exist in at least two oxidation states with different colors. Most of the today's known conducting polymers possess electrochromic properties. However, one of the major problems that delays the commercialisation of these devices is their poor adhesion to the electrode materials and

their stabilities when polymers are switched between different oxidation states. In the case of polythiophene, more than 80% of its current activity is maintained after 1.2×10^5 switching tests whereas polyfluorene loses 5% of its activity after 10^2 cycles[37].

The problem of photodegradation of semiconductor electrodes for development of electrochemical solar cells may be overcome by coating with electrically conducting polymer. Protection of a n-GaAs photoelectrode with a polypyrrole deposit has been reported[95]. The film prevented photodegradation while permitting electron exchange with the electrolyte by acting as a barrier to ion/solvent transport. This electrode operated for a hundred hours, whereas the life time for an unprotected electrode was very short (one minute).

In a few cases, polymers have been demonstrated to be useful for microelectronic devices[96],[97]. A diode-like behaviour is achieved when two different polymers are electrochemically deposited at a platinum surface and covered with a porous thin film of gold allowing the diffusion of solvent and electrolytic salt throughout the polymer. A schematic functioning of the set up is given below.

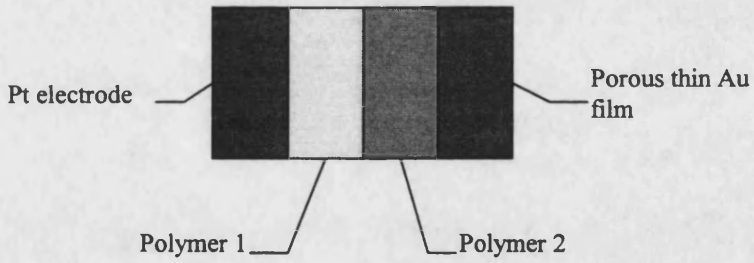

Polymer 1 is separated from the electrode by polymer 2 and $E^0_1 > E^0_2$. There will not be current toward the Au film and the solution unless that the potential applied to Pt electrode is high enough to oxidise polymer 1 and consequently the polymer 2. The redox reaction at the interface between the two polymers is dissymmetric because their very different redox potentials, resulting in a larger current in one direction than in the other.

Polymer modified electrodes exhibit sometime an electrocatalytic behaviour which is interpreted as a gain of potential[96] (reactions take place a smaller potentials than when naked electrode are used), selectivity[97] (because one well chosen polymer may lead the reaction in a desirable direction) or an increase in the current density . This catalytic effect may come from the polymeric deposit itself[98] , as a result of the creation of n-doped or p-doped states of the polymer. In other cases, the presence of reversible redox groups attached to the material[99] or the incorporation of highly dispersed metallic microparticles[100] inside the matrix contributes to the electricity transport favouring the electrocatalysis.

Others applications of conducting polymers are related to batteries[101] ,welding of thermoplastics[102] and production of conducting adhesives[92].

In this work, characteristics of conducting poly-o-aminophenol are analysed by electrochemical and spectroscopic techniques. The first part (chapter 4) involves the use of voltammetry to produce the polymer and determine its conductivity. Morphology of the films was observed by SEM. Changes of the oxidation state of the polymer with the potential of the electrode are analysed by uv- visible spectroscopy and the spectra are compared with those observed by RSE. Polymer viscoelastic effect was studied by using of quartz crystal impedance technique and changes of mass under potentiodynamic conditions are reported. The second part of this thesis (chapter 5) concerns the electrodeposition of copper on poly-o-aminophenol modified platinum electrode. Potentiostatic transients are compared with the 3D nucleation with diffusion control modelled by Scharifker[103]. SEM photographs of the nuclei formed at different overpotentials are contrasted with the behaviour predicted by the theory. Finally, a schematic model is proposed to explain the experimental results.

References

1. C.K Chiang, C.R. Fincher, Jr, Y.W. Park, A.J. Heeger, H. Shirakawa, E.J. Louis, S.C. Gau, A.G. MacDiarmid, *Phys. Rev. Lett.*, 39 (1977) 1098.
2. C.K. Chiang, Y.W. Park, A.J. Heeger, H. Shirakawa, E.J. Louis, A.G. MacDiarmid, *J. Chem. Phys.*, 69 (1978) 5098.
3. C.K. Chiang, M.A. Druy, S.C. Gau, A.J. Heeger, E.J. Louis, A.G. MacDiarmid, Y.W. Park, H. Shirakawa, *J. Amer. Chem. Soc.*, 100 (1978)1013.
4. P.J. Nigrey, A.J. MacDiarmid, A.J. Heeger, *J. Chem. Soc., Chem. Commun.*, (1979) 594.
5. R.G.Linford,*Electrochemical Science and Technology of Polymers-1*, Elsevier, London, (1987).
6. A.F. Diaz,K.K. Kanazawa, G.P Gardini, *J. Chem. Soc. Chem. Commun .*, (1979),535.
7. T.Yamamoto,K.Sanechika, A. Yamamoto, *J.Polym. Sci., Polym. Lett. Ed*, 18(1980) 9.
8. L.W Shacklette, R.R Chance, D.M. Ivory, G.G Miller, R.H. Baughman, *Synth. Metals.*, 1 (1979/80) 307.
9. A.G. MacDiarmid, J.C. Chiang, M.Halpern, W.S. Huang, S.L. Mu, N.L.D. Somassiri, W. Wu, S. Yaniger, *Mol.Cryst. Liq. Cryst.*, 21 (1985) 173.
10. C.K. Chiang, S.C. Gau, C.R. Fincher, Y.W. Park, A.G. MacDiarmid, A.J. Heeger, *App. Phys.Lett.*, 33 (1978) 18.
11. G.C. Farrington, B. Scrosati, D. Frydrych, J. DeNuzzio, *J. Electrochem. Soc.* , 131 (1984) 7.
12. A.G. Macdiarmid, R.J. Mammone, J.R. Krawczyk, S. J. Porter, *Mol.Cryst. Liq. Cryst.*, 105 (1984) 89.
13. R.B. Kaner, S.J. Porter, A.G. MacDiarmid, *J. Chem.Soc. Faraday. Trans.*, 82 (1986) 2323.
14. J.P. Travers, J. Chroboczek, F. Devreux, F. Genoud, M. Nechtschein, A.A. Syed, E.M. Genies, C. Tsintavis, *Mol. Cryst. Liq. Cryst.*, 121 (1985)195.

15. R.L. Hand, R.F. Nelson, *J. Electrochem. Soc.*, 125 (1978) 1059.
16. E.M. Genies, C. Tsintavis, *J. Electroanal. Chem.*, 195 (1985) 109.
17. C. DeArmitt, S. P. Armes, J. Winter, F.A. Uribe, S. Gottesfeld, C. Mombourquette, *Polymer.*, 34 (1993) 158.
18. R. B. Bjorklund, *J. Chem. Soc., Faraday Trans.*, 83 (1987) 1507.
19. J. C Thiéblemont, J. L. Gabelle, M. F. Planche, *Synt. Met.*, 66 (1994) 243.
20. D. S. Park, Y.B. Shim, S.M. Park, *J. Electrochem. Soc.*, 140 (1993) 609.
21. S. Antoun, D.R. Gagnon, F.E. Karasz, R.W. Lenz, *Polym. Bull.*, 15 (1986) 181.
22. Y. Wei, R. Hariharan. R Bakthavatchalam, *J. Chem. Soc., Chem. Commun.*, (1993) 1160.
23. M. Delamar, P.C. Lacaze, J.Y. Dumousseau, J.E. Dubois, *Electrochimica Acta*, 27 (1982) 61.
24. J. Rault-Berthelot, L. Angely, J. Delaunay, J. Simonet, *New J. Chem.*, 11 (1987) 487.
25. G. Ricciardi, F. Lelj, *Polyhedron*, 11 (1992) 2089.
26. G. Tourillon, F. Garnier, *J. Electroanal. Chem.*, 135 (1982) 173.
27. G. Mengoli, M.M. Musiani, B. Schreck, S. Zecchin, *J. Electroanal. Chem.*, 73 (1988) 246.
28. R. Burzynski, P. N. Prasad, S. Bruckenstein, J. W. Sharkey, *Synt. Met.*, 11 (1985) 293.
29. R. Tomat, S. Zecchin, G. Schiavon, G. Zotti, *J. Electroanal. Chem.*, 252 (1988) 215.
30. A. Kitani, J. Yano, A. Kunai, K. Sasaki, *J. Electroanal. Chem.*, 69 (1987) 221.
31. S. Naitoh, *Synt. Met.*, 18 (1987) 237.
32. R.J. Waltman, J. Bargon, A.F. Díaz, *J. Phys. Chem.*, 87 (1983) 1459.
33. E.M. Genies, C. Tsintavis, *J. Electroanal. Chem.*, 195 (1985) 109.
34. J. Heinze, *Synt. Met.*, 41-43 (1991) 2805.
35. T. Inoue, T. Yamase, *Bull. Chem. Soc. Jpn.*, 56 (1983) 985.
36. S. Asavapiriyanont, G.K. Chandler, G.A. Gunawardena, D. Pletcher, *J. Electroanal. Chem.*, 177 (1984) 229.
37. J. Simonet, J. Rault-Berthelot, *Prog. Solid St. Chem.*, 21 (1991) 1.

38. M. Aizawa, S. Watanabe, H. Shinohara, H. Shirakawa, *J. Chem. Soc., Chem. Commun.*, 5 (1985) 264.

39. G. Schivon, S. Zecchin, G. Zotti, S. Cattarin, *J. Electroanal. Chem.*,213 (1986) 53.

40. G. Schiavon, G. Zotti, G. Bontempelli, *J. Electroanal.Chem.*, 186 (1985) 191.

41. J. F. Fauvarque, M. A. Petit, F. Pfluger, A. Jutand, C. Chevrot, *Makromol. Chem. Rapid Commun.*, 4 (1983) 455.

42. S. Zecchin, G. Schiavon, R. Tomat, G. Zotti, *J. Electroanal. Chem.*, 215 (1986) 377.

43. Z. Xu, G. Horowitz, F. Garnier, *J. Electroanal. Chem.*, 246 (1988) 467.

44. J. R. Reynolds, *J. Mol. Electronics.*, 2 (1986) 1.

45. M. E. G. Lyons, H.G. Fay, J. G. Vos, A. J. Kelly, *J. Electroanal. Chem.*, 250 (1988) 207.

46. P. Audebert, G. Bidan, M. Lapkowski, *J. Electroanal. Chem.*, 219 (1987) 165.

47. A. Deronzier, D. Limosin, J. C. Moutet, *Electrochimica Acta.*, 32 (1987) 1643.

48. L. Angely, N. Simonet-Gueguen, C. Saboureau, J. Simonet, *J. Electroanal. Chem.*, 280 (1990) 195.

49. J.J. Langer, *Synt. Met.*, 35 (1990) 295.

50. G. Inzelt, L. Szabo,*Electrochimica Acta*, 31 (1986) 1381.

51. M. Satoh, F. Uesugi, M. Tabata, K. Kaneto, K. Yoshino, *J. Chem. Soc.,Chem. Commun.*, (1986) 979.

52. P. Burgmayer, R. W Murray, *J. Electroanal. Chem.*, 135 (!982) 335.

53. S. Etemad, A.J. Heeger, A.G. MacDiarmid, A.G. Ann, *Rev. Phys.Chem.*, 33 (1982) 443.

54. B.R. Weinberger, E. Ehrenfreund, A. Pron, A.J. Heeger, A.G. MacDiarmid, *J. Chem. Phys.*, 72 (1980) 4749.

55. J.L. Bredas, R.R. Chance, R. Silbey, *Phys. Rev.*, B26 (1982) 5843.

56. W. Su, J. R. Schrieffer, A.J. Heeger,*Phys. Rev.*, B22 (1980) 2099.

57. A.R. Bishop, D.K. Campbell, K. Fesser, *Mol. Cryst. Liq. Cryst.*, 77 (1980) 253.

58. J.L. Bredas, B. Themans, J. M. Andre, *Phys. Rev.*, B27 (1983) 7827.

59. F. Genoud, M. Gugliemi, M. Nechstein, E. Genies, M. Salmon, *Phys. Rev. Lett.*, 55 (1985) 118.

60. A. M. Waller, R.G. Compton, *J. Chem. Soc., Faraday Trans.*, 85 (1989) 977.

61. J. M. Ginder, A.F. Richter, A.G. MacDiarmid, A.J. Epstein, *Solid State Commum.*, 63 (1987) 97.

62. M. Vuki, Ph.D Thesis, University of Southampton, 1993.

63. N.F. Mott, *Conduction in non-crystalline materials*, Oxford University Press, Oxford, (1987).

64. P.G. Pickup, R.W. Murray, *J. Am. Chem. Soc.*, 105 (1983) 4510.

65. C.E.D. Chidsey, R.W. Murray, *J. Phys. Chem.*, 90 (1986) 1479.

66. R. J. Nowak, F. A. Schultz, M. Umaña, R. Lam, R.W. Murray, *Anal. Chem.*, 52 (1980) 315.

67. P. Daum, J. R. Lenhard, D. Rolison, R.W. Murray, *J. Am. Chem. Soc.*, 102 (1980) 4649.

68. C. J. Baldy, C. M. Elliott, S. W. Feldbergy, *J. Electroanal. Chem.*, 283 (1990) 53.

69. J. L. Bredas, *Synth. Met.*, 17 (1987) 115.

70. A.F. Diaz, J. Castillo, J. A. Logan, W. Y. Lee, *J. Electroanal. Chem.*, 129 (1986) 115.

71. K. Meerholz, J. Heinze, *Angew. Chem. Int ed. Engl.*, 29 (1990) 692.

72. R. Nowak, F.A. Schultz, M. Umaña, H. Abruña, R. W. Murray, *J. Electroanal. Chem.*, 94 (1978) 219.

73. P. Daum, R. W. Murray, *J. Electroanal. Chem.*, 103 (1979) 289.

74. Southampton Electrochemistry Group, *Instrumental Methods in Electrochemistry.*, Ellis Horwood Series in Physical Chemistry, New York, (1990).

75. X. B. Wang, J. M. Bonnet, R. Pethig, P. K. Baker, O. L. Parri, A. E. Underhill, *Journal of Molecular Electronics.*, 7 (1991) 167.

76. C. Iwakura, T. Kawai, M. Nojima, H. Yoneyama, *J. Electrochem. Soc.:Electrochemical Science and Technology.*, 134 (1987) 791.

77. M. S. Wrightin, M. C. Pallazzotto, A. B. Bocarsly, J. M. Bolts, A. B. Fischer, L. Nadjo, *J. Am. Chem. Soc.*, 100 (1978) 7264.

79 . M. S. Wrightin, M. C. Pallazzotto, A. B. Bocarsly, J. M. Bolts, A. B. Fischer, L. Nadjo, *J. Am. Chem. Soc.*, 100 (1978) 7264.

80 . P. J. Peerce, A. J. Bard, *J. Electroanal. Chem.*, 114 (1980) 89.

81 . M. Kalaji, L.M. Peter, L. M. Abrautes, J.C. Mesquita, *J. Electroanal. Chem.*, 274 (1989) 289.

82 . C. Zhong, K. Doblhofer, G. Weinberg, *Faraday Discuss. Chem. Soc.*, 88 (1989) 307.

83 . K. Akoi, Y. Tezuka, *J. Electroanal. Chem.*, 267 (1989) 55.

84 . C. Galiatsatos, Y. Ikariyama, J.E. Mark, W.R. Heineman, *Biosens. Bioelect.*, 5 (1990) 47.

85 . L. Gorton, E. Csoregi, E. Dominguez, J. Emneus, G. Jonsson-Petterson, G. Marko-Vargo, B. Persson, *Anal. Chim. Acta.*, 250 (1991) 203.

86 . B.A. Gregg, A. Heller, *Anal. Chem.*, 62 (1990) 258.

87 . P.D. Hale, T. Inagaki, H.S. Lee, H.I. Karan, Y. Okamoto, T.A. Skotheim, *Anal. Chim. Acta.*, 228 (1990) 31.

88 . M. Garguilo, N. Huynh, A. Proctor, A.C. Michael, *Anal. Chem.*, 65 (1993) 523.

89 . A.Q. Contractor, T.N. Sureshkumar, R. Narayanan, S. Sukeerthi, R. Lal, R.S. Srinivasa, *Electrochimica Acta.*, 39 (1994) 1321.

90 . M. Alvarez-Icaza , U. Bilitewski, *Anal. Chem.*, 65 (1993) 524A.

91 . M. Thompson, U. J. Krull, *Anal. Chem.*, 63 (1991) 393A.

92 . F. Scheller, P. Minh Tan, W. Moritz, *et. al*, *Analyst*, 114 (1989) 653.

93 . P. Kathirgamanathan, *Adv. Mater.*, 5 (1993) 281.

94 . P. Kathirgamanathan, *Polymer*, 34 (1993) 2907.

95 . R. Noufi, D. Tench, L. F. Warren, *J. Electrochem. Soc.*, 127 (1980) 2310.

96 . M. Aizawa, H. Shinohara, T. Yamada, K. Akagi, H. Shirakawa, *Synt. Met.*, 18 (1987) 711.

97 . G.P. Kittlesen, H.S. White, M.S. Wrighton, *J. Am. Chem. Soc.*, 107 (1985) 7373.

98 . J. Rault-Berthelot, G. Mabon, J. Simonet, *J. Electroanal. Chem.*, 240 (1988) 355.

98 . R.C. M. Jakobs, L. J. J. Janssen, E. Barendrecht, *Electrochimica Acta.*, 30 (1985) 1433.

99 . P. Moisy, F. Bedioui, J. Devynck, L. Salmon, C. Bied-Charreton, *New. J. Chem.*, 13 (1989) 511.

100 . S. Holdcroft, B.L. Funt, *J. Electroanal. Chem.*, 240 (1988) 89.

101 . T. Osaka, K. Naoi, S. Ogano, S. Nakamura, *J. Electrochem. Soc.*, 134 (1988) 2096.

102 . P. Kathirgamanathan, *Polymer.*, 34 (1993) 3105.

103 . B. Scharifker, G. Hills, *Electrochimica Acta.*, 28 (1983) 879.

Chapter 2

Techniques

CHAPTER 2

TECHNIQUES

2.1. Cyclic Voltammetry

If the potential at an electrode is varied linearly with the time a current flows as the double layer adjusts to the new voltage; then the potential reaches a value high enough to produce an electrochemical reaction and a faradaic current is eventually seen. Cyclic voltammetry is an electrochemical technique in which this kind of perturbation is applied to a working electrode up to a potential where the direction of the scan is inverted. The scan direction can be positive or negative and, in principle, the sweep rate can have any magnitude; however, high values of this parameter introduce considerable experimental difficulties due to the iR drop.

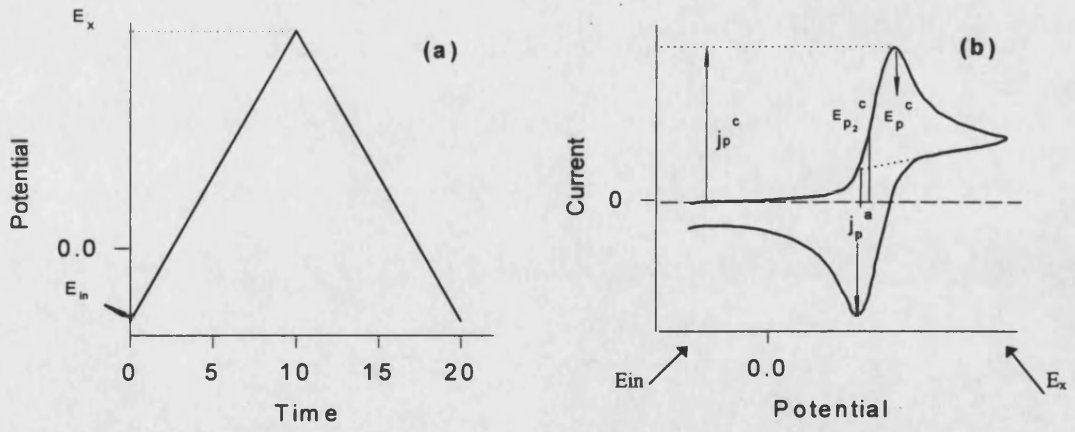

Figure 2.1 (a) Signal input to the electrochemical system, (b) typical cyclic voltammogram for a reversible system.

Figure 2.1 shows a typical voltammogram obtained for a reversible system. Some important parameters are illustrated. j_p is the current density at the maximum of the curve, E_p is the potential at which these maxima appear and $E_{p/2}$ is the potential corresponding to the half-peak current. E_{in} and E_x are the initial potential and the potential at which the direction of the scan is inverted, respectively.

2.1.1. *Reversible systems.*

The form of the current-potential plot, for a semi infinite planar electrode, is computed by solving Fick's 2nd Law for a reversible electron transfer reaction where only the reactant species (O) is present in solution initially.

$$O + ne^- \rightleftharpoons R \tag{2.1}$$

$$\frac{\partial C_O}{\partial t} = D_O \frac{\partial^2 C_O}{\partial x^2} \tag{2.2}$$

$$\frac{\partial C_R}{\partial t} = D_R \frac{\partial^2 C_R}{\partial x^2} \tag{2.3}$$

The initial and boundary conditions are

$$t = 0 \quad , \quad x = 0 \qquad C_o^{surf} = C_o^{\infty} \qquad C_R^{surf} = 0 \tag{2.4}$$

$$t > 0 \quad , \quad x \to \infty \qquad C_o \to C_o^{\infty} \qquad C_R \to 0 \tag{2.5}$$

$$t > 0 \quad , \quad x = 0 \qquad D_O\left(\frac{\partial C_O}{\partial x}\right) + D_R\left(\frac{\partial C_R}{\partial x}\right) = 0 \tag{2.6}$$

$$\left(\frac{C_O}{C_R}\right)_{x=0} = \exp\left[\frac{nF}{RT}\left(E - E_e^{\ominus}\right)\right] \tag{2.7}$$

$$-j = nFD\left(\frac{\partial C_O}{\partial x}\right)_{x=0} \qquad (2.8)$$

$$0 < t \leq \lambda \quad E = E_{in} - \nu t \qquad (2.9)$$

$$t > \lambda \qquad E = E_{in} - 2\nu\lambda + \nu t \qquad (2.10)$$

Where E_{in} is the initial potential and λ is the time at which the direction is inverted; D_o and D_R are the diffusion coefficients for the oxidised and reduced species, t is the time, C represents the bulk concentration of O or R and ν is the potential sweep rate. The subscripts *surf* and ∞ represent the boundary condition at the outer Helmholtz plane and at infinite distance from the electrode, respectively. The exponential form of the Nernst equation (2.7) defines the surface concentration ratio for all values of t and E. The first theoretical description of this system was due to Randles[1] and Sevcik[2] and its solution for a planar electrode with semi infinite dimensions at 25 °C is

$$j_p = -\left(2.69x10^5\right)n^{3/2}C_o^{\infty}D^{1/2}\nu^{1/2} \qquad (2.11)$$

j_p is the peak current density (A cm^{-2}), D is in cm^2 s^{-1}, ν is the sweep rate in V s^{-1} and C_o^{∞} is the bulk concentration of O in mol cm^{-3}.

The shape of the voltammogram for a reversible system can be explained by the creation of a concentration gradient and consumption of electroactive species O. Beyond the potential where the maximum value of current appears the current then begins to decay following a profile proportional to $t^{-1/2}$ due to depletion of O. The reaction is controlled by the diffusion of species O to the electrode surface. When the

scan is reversed there is a significant concentration of R near of electrode and it continues to be formed until the potential approaches to the equilibrium potential (E_e); R is then oxidised under similar conditions to those for the forward sweep.

2.1.2. *Irreversible systems*

Nernstian equilibrium at the electrode surface is only maintained if the electron transfer rate at all potentials is significantly higher than the rate of mass transport as is the case for a reversible system. If the electron transfer occurs at lower rate, then the equilibrium at the surface will not be maintained so that the shape of the voltammogram will change.

The theoretical description of a electrode process is given by the Butler-Volmer equation

$$j = \overrightarrow{j} + \overleftarrow{j} = j_o\left[\exp\left(\frac{(1-\alpha_c)\,nF\eta}{RT}\right) - \exp\left(-\frac{\alpha_c nF\eta}{RT}\right)\right] \quad (2.12)$$

where j_o, the exchange current density, is a scaling factor that depends on the values of the standard rate constant and of the concentrations of O and R species. The terms in brackets represent the anodic and cathodic contributions to the net current density, j, respectively ; η is defined as the deviation of the potential from equilibrium value, i.e. $\eta = E - E_e$; α is the cathodic transfer coefficient which is considered as the fraction of the change in the overpotential which leads to a change in the rate constant for electron transfer and commonly it has a value close to 0.5 for simple outer sphere redox systems. The term n represents the number of electrons involved in the electrode reaction, F is the Faraday constant, R is the gas constant in J K^{-1} mol^{-1} and T is the temperature in K.

From the figure 2.2 it can be noted that the current does not grow indefinitely as predicted by (2.12) but is limited by transport of species to the electrode at higher potentials. An increasing peak separation with increasing sweep rate is the most noticeable effect of the irreversibility; the shorter the scale of the experiment, the greater will be the peak separation. The peaks are also broader and lower with respect to reversible system waves.

To solve (2.2) and (2.3) for a irreversible system, a new boundary condition must be written for t >0, x = 0 , which becomes

$$\frac{-j}{nF} = D_o\left(\frac{\partial C_o}{\partial x}\right)_{surf} = \vec{k}(C_o)_{surf} \qquad (2.13)$$

where $\vec{k}$ is the rate constant for the cathodic process (cm s^{-1}); finally (2.13) leads to the following equation for the peak current density at 25 °C:

$$j_p = -\left(2.99x10^5\right)n(\alpha_c n_\alpha)^{1/2} C_O D_o^{1/2} v^{1/2} \qquad (2.14)$$

where n_α is the number of electrons transferred up to, and including, the rate determining step.

A more detailed explanation for the application of cyclic voltammetry to a wide variety of electrochemical systems can be found in the literature[3,4,5]; some diagnostic criteria for determining the reversibility of a system are summarised in Table 2.1.

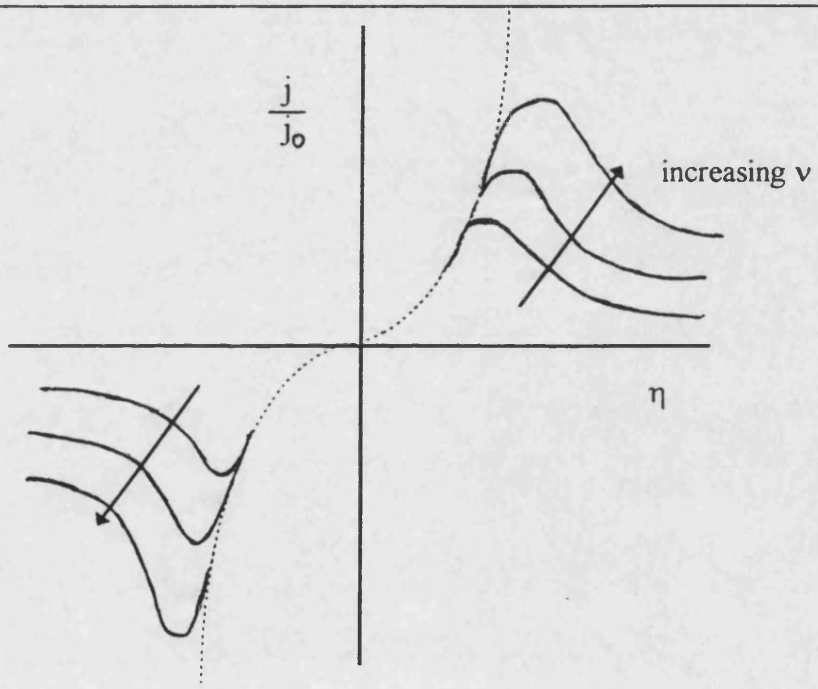

Figure 2.2 (----) Current-voltage characteristics predicted by (2.12) for $\alpha_c = 0.5$.
(——) Effect of the mass transfer on the curve.

Table 2. 1. Diagnostic test for cyclic voltammograms of reversible and irreversible systems at 25°C

Reversible case	Irreversible case
$\Delta E_p = E_p^a - E_p^c = 59/n$ mV	$E_p^a - E_p^c > 59/n$ mV
$\lvert E_p - E_{p/2} \rvert = 59/n$ mV	$\lvert E_p - E_{p/2} \rvert = 48/\alpha n_\alpha$ mV
$\lvert I_{pa} / I_{pc} \rvert = 1$	-
$I_p \propto \nu^{1/2}$	$I_p \propto \nu^{1/2}$
E_p is independent of ν	E_p^c shifts $-30/\alpha n_\alpha$ mV per decade increase in ν

2.1.3 *Electron reactions involving adsorbed species.*

Consider a surface attached redox system

$$O + ne^- \rightleftharpoons R$$

If the electron transfer is sufficiently rapid to maintain the equilibrium at all times under potentiodynamic conditions, then the system can be described by the Nernst equation, in the form

$$\frac{x_O}{1-x_O} = \exp\left\{\left(\frac{nF}{RT}\right)\left(E - E^0\right)\right\} \qquad (2.15)$$

where x_o and $1\text{-}x_o$ represent the mole fractions of O and R respectively, i.e. assuming ideal mixing over the whole composition range. If a dimensionless potential is defined as $\xi = (nF/RT)(E - E^0)$, then x_O can be written in the form

$$x_O = (\exp \xi)(1 + \exp \xi) \qquad (2.16)$$

The charge density required to oxidise the film to a particular composition x_o is given by

$$Q = nF\Gamma x_O \qquad (2.17)$$

where Γ is the total coverage with the redox species (mol cm^{-2}). The current density is defined by the relations

$$j = \frac{dQ}{dt} = \left(\frac{dQ}{dE}\right)\left(\frac{dE}{dt}\right) = nF\Gamma\left(\frac{dx_o}{dE}\right)\left(\frac{dE}{dt}\right) \tag{2. 18}$$

$$j = nF\Gamma\nu\left(\frac{dx_o}{dE}\right)$$

The derivative (dx_o / dE) is equal to (dx_o/ $d\xi$)($d\xi$/ dE). From Equation (2.16) and the expression of the dimensionless potential ξ , the current density is then given by

$$j = \left(\frac{n^2F^2\Gamma\nu}{RT}\right)\left\{\frac{(\exp\xi)}{(1+\exp\xi)^2}\right\} \tag{2. 19}$$

Equation (2.19) has a maximum when $\xi = 0$, i.e. $j(\xi) = (1/4)\ (n^2\ F^2\ \Gamma\ \nu/RT)$, see figure 2.3.

The charge associated with the voltammogram is related to the number of sites in the film where the oxidation can occur. The peaks are symmetrical with the density current raising from zero and falling again to zero beyond the peak when the polymer is fully transformed. The separation between the forward and reverse peaks is zero for rapid electron transfer in thin films because diffusion plays no role in the process. The charges associated with the anodic and cathodic processes are equal because of the fixed number of active sites in the polymer; moreover, the charges are independent of the potential scan rate.

2.2. Chronoamperometry

This technique is based on an excitation function of one or more potential steps that are applied to an electrode immersed in a nonstirred solution; currents are monitored as a function of the time following the application of the potential step.

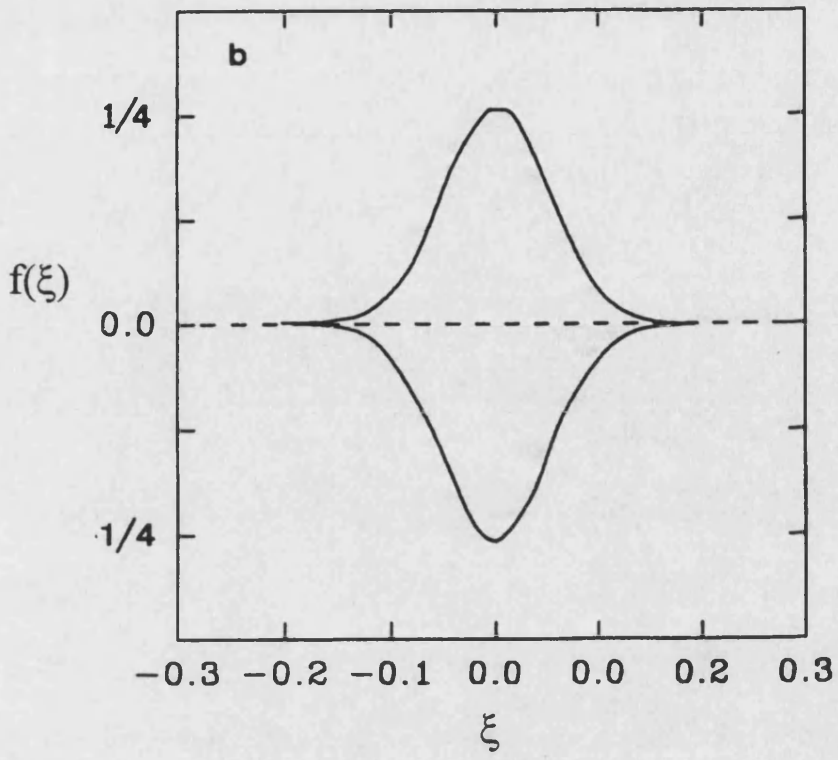

Figure 2.3 Cyclic voltammogram predicted for attached polymeric redox system

Figure 2.4. Chronoamperometry. (a) Potential excitation signal. (b) Current-time response signal (chronoamperogram).

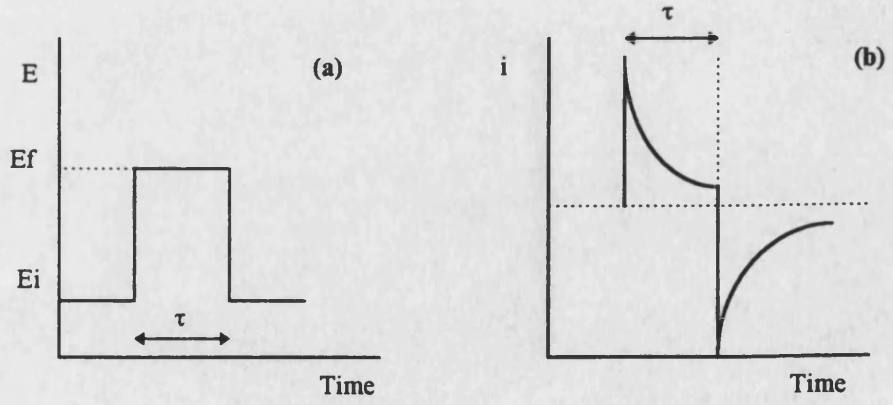

The square-wave voltage signal steps the potential of the working electrode from a value at which no faradaic current occurs, *Ei*, to a potential *Ef*, at which the surface concentration of the electroactive specie "O", for the generalised reaction (2.1), is effectively reduced to R. The potential can either be maintained or be reversed after some interval of time, τ , has passed.

The electrochemical depletion of O in the solution adjacent to the electrode generates a net diffusion from the bulk solution to the depleted region. The rate of loss of O and consequent rate of formation of R are both controlled by the rate of diffusion of O to the electrode surface under a concentration gradient effect.

The integration of curve 2.4(b), during the interval of time τ, gives the charge q passed across the interface, which it is related to the amount of material that has been converted. The current density is related to the instantaneous rate at which this conversion occurs, so it can be defined as the rate of charge flow;

$$q = nFAN \tag{2.20}$$

where N is the number of moles converted in a given time interval. The instantaneous current density at time t is

$$j_t = \left(\frac{dQ}{dt}\right)_t = nF\left(\frac{dN}{dt}\right)_t \tag{2.21}$$

where Q is the charge density in C cm^{-2} .The rate of conversion, dN/dt, is proportional to the flux of material as derived from Fick's first law

$$j_{t=nFD_o}\left(\frac{\partial C_o}{\partial x}\right)_{x=0,t} \tag{2.22}$$

$(\partial Co/\partial x)x=0$ represents the slope the concentration versus distance profile for species O at electrode surface at time *t*; these slopes decrease with the time due to the extension of the diffusion layer so that the current must decay smoothly and approaches asymptotically to zero with increasing time as described by the Cottrell equation[6] for a planar electrode

$$i_t = \frac{nFAC_o D_o^{1/2}}{\pi^{1/2} t^{1/2}} \tag{2.23}$$

It follows from this equation that the product $it^{1/2}$ should be constant. Deviations from this constancy can be produced by coupled chemical reactions, convection in the cell, etc.

For a potential step into the mixed controlled region is not possible use the Nernst equation to define the surface concentration. This leads to more complex boundary conditions. The result is given by

$$j = nF \vec{k} C_o \exp\left[\left(\vec{k} + \overleftarrow{k}\right)^2 \frac{t}{D}\right] erfc\left[\left(\vec{k} + \overleftarrow{k}\right)\frac{t^{1/2}}{D^{1/2}}\right] \tag{2.24}$$

where $\vec{k}$ and $\overleftarrow{k}$ are the rate constants for the cathodic and anodic process respectively. D_o and D_R are supposed to be identical. For negative potentials, far from equilibrium potential, the cathodic rate constant is much greater than the anodic one so the equation (2.24) can be simplified

$$j = nF \vec{k} C_o \exp \vec{k} \frac{t}{D} erfc\left(\vec{k} \frac{t^{1/2}}{D^{1/2}}\right) \tag{2.25}$$

For low values of $\vec{k}$, the current densities determined by (2.25) are independent of time and much lower that those calculated from the Cottrell equation (2.23).For

intermediate values of the rate constant, a decaying transient is observed, but j remains low compared with the diffusion limited values. At high values of the rate constant, the transients tends to that predicted by Cottrell equation. Figure 2.5 illustrates these tends.

Equation (2.24) has two limiting forms:

at short times

$$j \cong -nF \vec{k} C_o \left(1 - \frac{2\left(\vec{k} + \overleftarrow{k}\right) t^{1/2}}{\pi^{1/2} D^{1/2}} \right) \qquad (2.26)$$

at long times

$$j \cong -\frac{nF \vec{k} C_o D^{1/2}}{\pi^{1/2}\left(\vec{k} + \overleftarrow{k}\right) t^{1/2}} \qquad (2.27)$$

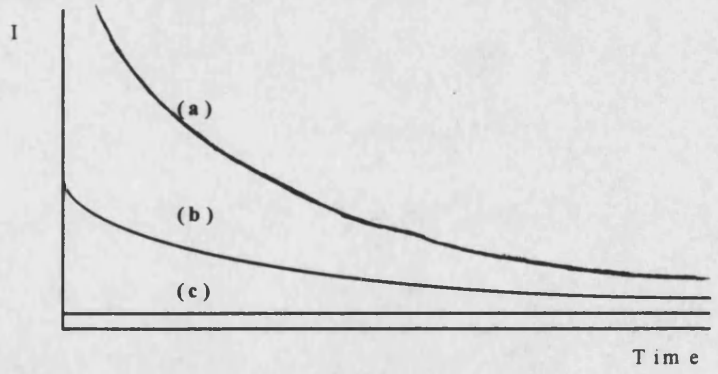

Figure 2.5 Current density versus time profiles for (a)diffusion control (b)mixed control and (c) electron transfer control in potential step experiments.

At cathodic overpotentials $\overleftarrow{k}$ is negligible and the equation (2.27) reduces to the Cottrell equation. The curves in figure 2.4 tend to superimpose one on another at long times.

Chronoamperometry has been used to determine heterogeneous rate constants[7] and to study systems where chemical reactions are coupled to the electrochemical step[8,3]. It has also been used to calculate charge transport diffusion rates in conducting polymers[9]. Further information about this technique can be found in references 3 and 7.

2.3. Ultramicroelectrodes

Miniaturisation of electrodes to dimensions of 1 - 10 μm gave rise to the term ultramicroelectrodes which are simply electrodes with at least one dimension small enough that their properties, e.g. mass transport regime, are function of size[10]. In the last decade a large number of publications related to these devices has appeared[11,12,13] and the impact of ultramicroelectrodes in several branches of the electrochemistry is still developing.

There are dramatic changes to conventional electrochemical responses when ultramicroelectrodes are utilised. First af all, mass transport rates to and from the electrode are increased; secondly, the double layer capacitance is reduced due to the decrease in surface area and finally, the ohmic loss is reduced due to hemispherical geometry. All this allows electrochemistry to be done under unusual conditions, for example, in absence of supporting electrolyte so that the oxidation wave of the supporting electrolyte will not obscure those of the sample. Under these conditions the oxidation of alkanes[14] to the highly reactive carbenium ion (R^+) and the rare gases[15] at high potentials has been reported. On the other hand, their size and the small currents make ultramicroelectrodes interesting devices for *in vivo* analysis[16].

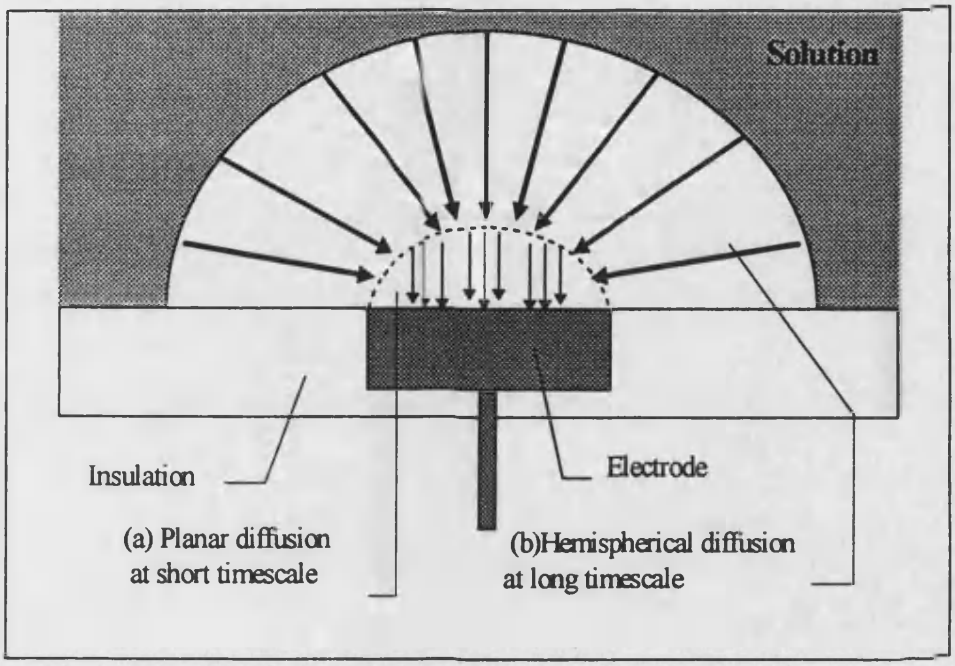

Figure 2.6 Diffusion of species at an ultramicroelectrode. (a)Profile at short times as in a rapid cyclic voltammetry (10 V s^{-1}). (b) Profile at longer times as in slower cyclic voltammetry (0.01 V s^{-1}).

2.3.1. *Mass transport at ultramicroelectrodes*

For a system like (2.1) the diffusion of electroactive species to a spherical electrode may be described by Fick's second law in spherical coordinates

$$\frac{\partial Co}{\partial t} = D_o \frac{\partial^2 C_o}{\partial r^2} + \frac{2D_o}{r}\frac{\partial C_o}{\partial r} \qquad (2.28)$$

The initial condition is

$$\text{at } t = 0 \text{ and } r \geq r_s,\ C_o = C^{\infty} \qquad (2.29)$$

and the boundary conditions for $t > 0$ are

$$\text{at } r \rightarrow \infty,\ C_o \rightarrow C^{\infty} \qquad (2.30)$$

$$\text{at } r = r_s,\ C_o = 0 \qquad (2.31)$$

where r is the distance from the centre of the sphere, r_s is the radius of the sphere; the sign ∞ represents parameters relating to distance far from the electrode surface. If the potential is stepped from a value where no electrode reaction occurs to one where the species O is reduced at a diffusion controlled rate, then the solution to the previous set of equations is found using the Laplace transform method. The equation for a microsphere can be modified to be applied to a microdisc by the substitution $r_s = \pi r_d / 4$, where r_d is radius of the disc.

The final equation is

$$j_d = \frac{4nFD_oC_o^{\infty}}{r_d \pi} + \frac{nFD_o^{1/2}C_o^{\infty}}{\pi^{1/2}t^{1/2}} \qquad (2.32)$$

The second term in (2.32) will always be dominant for conventional electrodes because r_d is big. This second term corresponds to the Cottrell equation. For ultramicroelectrodes, however, the response is determined by both terms. At short

times, equation (2.32) tends to the Cottrell equation, so that any transient will exhibit the same shape as observed with a planar electrode with linear diffusion. At long times, (2.32) will reach a steady state value given by the first term of the equation. At intermediate times both term are significant, complicating the interpretation of results.

2.3.2. *iR drop.*

During any electrochemical experiment, a current flows between the working electrode and the counterelectrode. In addition to the equilibrium potential and the overpotential at the working electrode there is a component of the potential caused by the resistance of the electrolyte between the working and reference electrode, i.e.

$$E_{iR} = iR_u \qquad (2.33)$$

where R_u is the uncompensated solution resistance , i is the cell current and E_{ir} is the so called ohmic drop. For large electrodes, the iR drop is usually minimised by the use of a three electrode system coupled to a potentiostat. However, significant iR distortion of cyclic voltammograms is commonly observed at sweep rates exceeding 100 V s^{-1} and poorly conductive media. Under such conditions, positive feedback compensation is applied until the potentiostat begins to oscillate. However, some uncompensated resistance is required for the stability of the potentiostat so that the maximum compensation is usually limited to about 90%.

Electrochemical currents at disc electrodes of 4 μm radius are four to five orders of magnitude smaller than those seen at electrodes of conventional size so that the iR term is much less important. Wightman[17] has examined the oxidation of ferrocene in acetonitrile with low concentration of supporting electrolyte (10^{-3} mol dm^{-3}); Nernstian behaviour was observed with a 6.5 μm radius ultramicroelectrode.

Under the same conditions, the voltammogram at a 0.4 mm radius electrode showed a 240 mV peak separation . This result demonstrates that electrochemistry of low conducting electrolytes is now feasible by using ultramicroelectrodes.

2.3.3. *Charging current.*

The application of a potential to the electrode causes excess of charge in the electrode surface; oppositely charged ions in solution are then attracted to the electrode. The arrangement of these ions close to the interface gives rise what is known as the *electrical double layer*. This double layer acts as a capacitor so that a charging current is detected. For a potential step, the charging current is given by

$$i_{dl} = \frac{\Delta E}{R} e^{-t/RC} \qquad (2.34)$$

where ΔE is the amplitude of the pulse, C is the double layer capacitance, t is the time measured from the application of the pulse and R is the uncompensated resistance of the electrochemical cell. For a hemispherical ultramicroelectrode, R is given by

$$R = \frac{1}{2\pi\kappa r} \qquad (2.35)$$

where κ is the specific conductivity of the electrolyte solution and r is the radius of the hemisphere. Equation (2.35) shows that $R \propto 1/r$. Since the capacitance is function of the area of electrode, i.e. $C \propto r^2$; the product RC must then be proportional to r. The smaller r is, the smaller the RC time constant will be. This reduction of the time constant is important since this parameter determines the shortest time at which meaningful measurements of faradaic current can be made.

2.4. The Electrochemical Quartz Crystal Microbalance

The application of an electric field across a piezoelectric material induces a deformation[18]. If the geometry and properties of the sample are the suitable, the frequency of the applied electric field will give rise to an oscillation in a mechanically resonant mode. In an electrochemical Quartz Crystal Microbalance, (EQCM), this resonant mode corresponds to the creation of an acoustic shear wave within a quartz crystal. The node of the produced wave is at the midpoint between the two faces of the crystal and the antinodes are at the two faces of the disc. Two vapour deposited electrodes are attached on both faces of the crystal so those mass changes that occur at the surface of them are detected by the resonator.

A view of an EQCM disc is shown in the figure 2.7. The vertical dashed line passes through the centre of the electrode pad; the sizes of the arrows represent approximate magnitudes of the shear deformation within the bulk of the crystal disc. The use of electrochemical techniques to induce redox processes at ones of the disc electrodes and the recording of the changes these processes produce in the resonant oscillation of the quartz is the physical basis of the operation of the electrochemical quartz microbalance.

Quartz crystals can be obtained from commercial sources and are generally cut into discs with the angle of the cut defining the direction of propagation of the acoustic wave[19]. Only crystals cut with the proper angles with respect to the crystalline axes exhibit shear displacements; the cut angle also determines the temperature stability of the oscillation resonant frequency[20]. AT-cut crystals are the more commonly used because of their low sensitivity to temperature variations around room temperature, see figure 2.8. These crystals consist of a thin quartz wafer

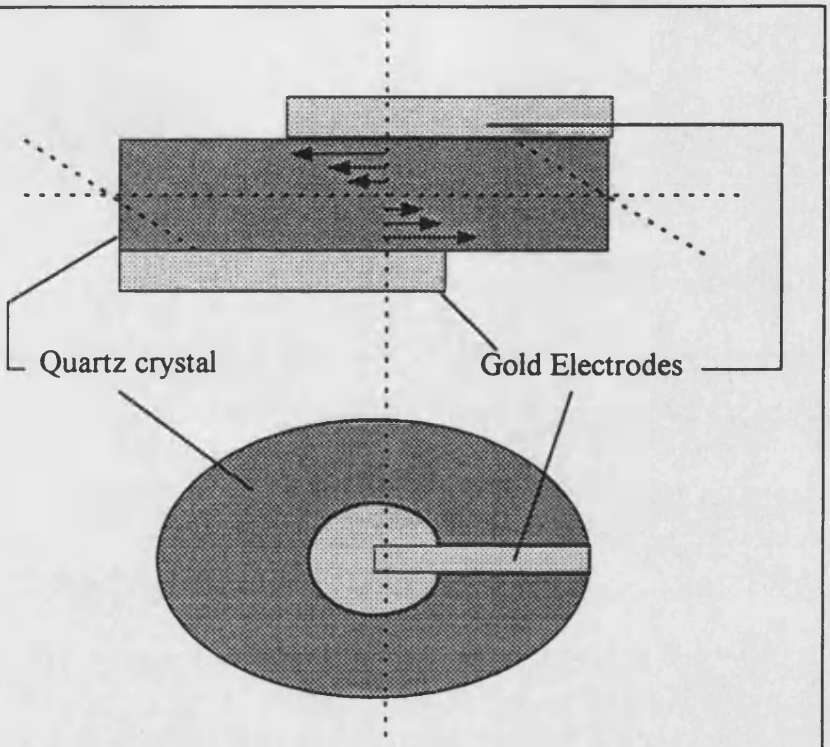

Figure 2.7 Top and edge views of a EQCM crystal with vapor deposited gold electrodes

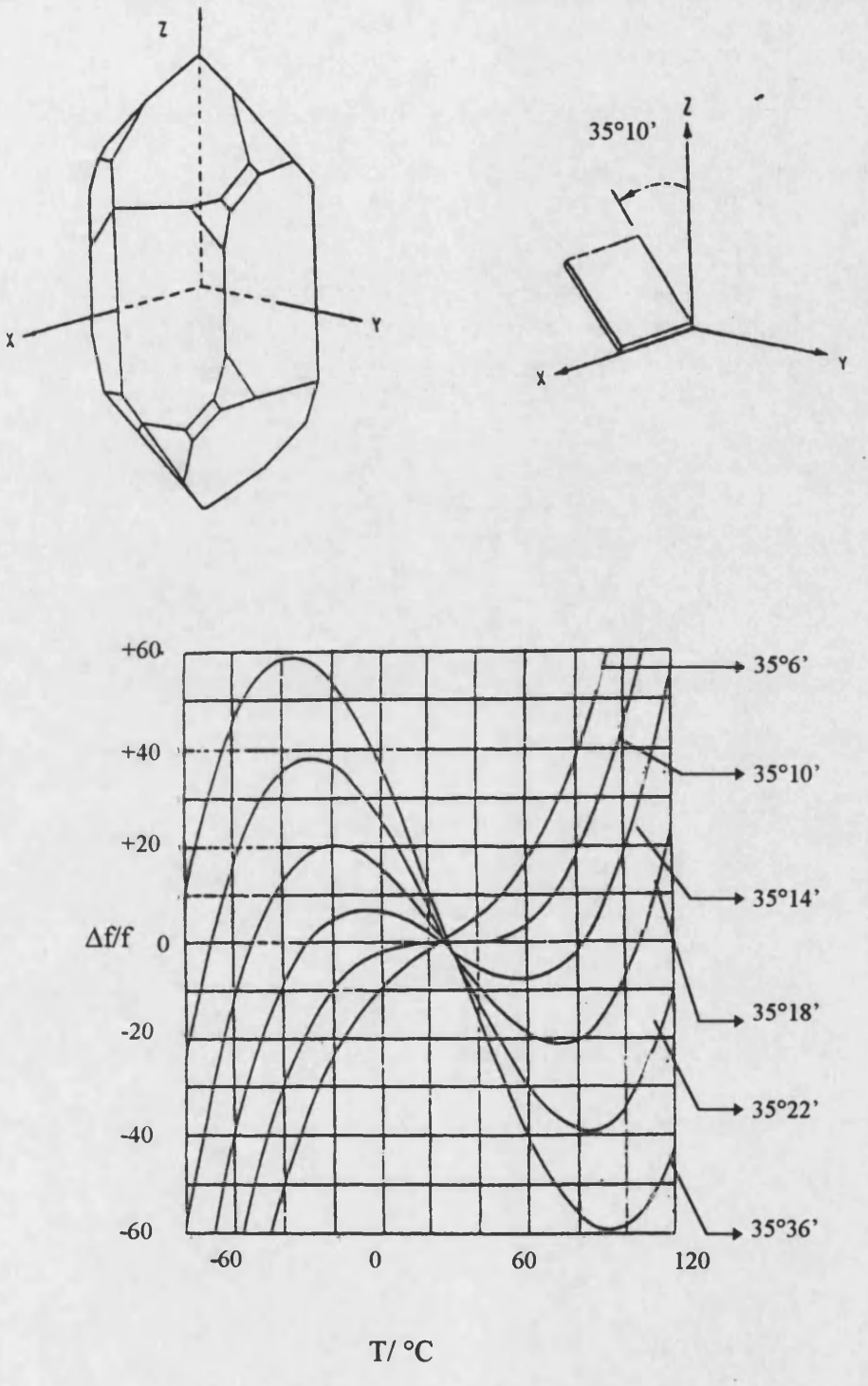

Figure 2.8 Assignment of axes to a quartz block and the angle of an AT-cut quartz crystal,above. Temperature-dependence of oscillation resonant frequency for quartz crystals of various cut angles, below.

prepared by slicing through a quartz rod at an angle of approximately 35 ° with respect to the x axis[21].

Sauerbrey[22] has related the mass changes at the electrodes to the frequency changes in the crystal

$$\Delta f = -\frac{f_o^2 m}{N\rho} = -\frac{2f_o^2 m}{n(\rho\mu)^{1/2}} \qquad (2.36)$$

where Δf is the frequency change induced by the gain or loss of mass; f_o is the resonant frequency (in Hz) prior to the addition or removal of mass; m is the mass per unit area of the deposit (g cm^{-2}); N is the frequency constant of the quartz crystal used (for example, for a AT-cut quartz with 5 MHz of resonant frequency N is 0.167 x 10^6 Hz cm); n is the harmonic number of the oscillation, ρ is the density of quartz (2.648 g cm^{-3}) and μ is the shear modulus of quartz (2.947 x 10^{11} g cm^{-1} s^{-2}). Equation (2.36) simplifies to

$$\Delta f = -C_f m \qquad (2.37)$$

in which C_f is a constant containing all the previous material properties and the resonant frequency of the resonator. The negative sign in the equation (2.36) and (2.37) indicates that addition of mass to the resonator results in a decrease in its resonant frequency. Both equations are based on the assumption that all of the mass is present at the anti node, that is where the crystal has its maximum deformation; the deposit by itself does not undergo any deformation so that this situation is referred to the thin film limit.

When the deposit is thick enough to experience shear deformation, the frequency changes are very high; 40% of the original resonant frequency is expected in contrast to less than 2% change for a rigid thin film. Under such conditions the

properties of the deposit have to be taken into account to relate the changes of the frequency to the mass involved in the process. Although an equation that relates Δf to m for this kind of deposit has been derived [23], the analysis of these systems becomes considerably more complicated because it requires knowledge of density and the shear modulus of the film as well as the speed of sound in the material.

The ability of the EQCM to monitor the mass changes that accompany the redox processes in rigid films makes it an interesting technique to study the ion and solvent transport in conducting polymers [24,25,26] and to characterise underpotential deposition of metals[27]. *In situ* mass changes of 1 ng cm^{-2} can routinely be detected[28]. In some cases, the formation of layers, dissolution or changes in the composition of the interface can be related to the presence of species in the ambient medium, providing the basis for building sensor devices[24, 29]. A disadvantage of this technique is the lack of molecular specificity since the only observable parameter is the mass change. Fortunately, there are some methods to deconvolute the contributions of several species to the net mass change, such as using a series of supporting electrolyte with different counterions but known molecular masses and using isotopically labelled solvents or ions.

2.5 Admittance Behaviour of Quartz Crystals

The properties of the quartz resonator can be described conveniently by the admittance of the resonator[30]

$$Y = G + jB$$
$$|Y| = \left(G^2 + B^2\right)^{1/2} \qquad (2.38)$$

where Y is the admittance, G and B are the conductance and susceptance of the system. |Y| represents the magnitude of the admittance and can be determined from

the resultant of the real and imaginary vectors. The frequency-dependent properties of the resonator admittance can be displayed in the complex plane. Figure 2.9 schematically illustrates an admittance locus for a series LRC network, named the motional branch of the quartz resonator[31] . The circuit shown in figure 2.9(a) includes an inertial parameter related to the displaced mass (L), a capacitor representing the energy stored during oscillation (C) and a resistance due to energy dissipation (R). As the frequency increases from f=0, the imaginary component (jB) reaches a maximum at f_1 . Upon increasing the frequency the admittance crosses the abscissa, the real component of admittance is maximum (at $f=f_r$), this occurs at the resonant frequency of the resonator. At $f=f_2$, the imaginary component of the admittance reaches a minimum.

The actual electrical circuit of the resonator includes a capacitance, C_o , in parallel with the motional branch. This component represents the static capacitance arising from the two electrodes separated by the insulating quartz[32] . The admittance locus is raised along the imaginary axis by ωC_o (see figure 2.9b).The maximum and minimum B values still occur at f_1 and f_2 , respectively, but the frequency of the maximum admittance is located at lower frequency than the maximum of real admittance, f_{Gmax}. Resonance is now satisfied at two frequencies, f_s and f_p , where the phase angle is zero. At f_s the real part of the admittance is slightly less than that the real maximum whereas at f_p the real part of admittance is slightly greater than zero. The f_s is named the series resonance frequency which is generally measured in QCM experiments. Impedance and reactance equations for the series and parallel conditions have been reported by Buttry[33] et al.

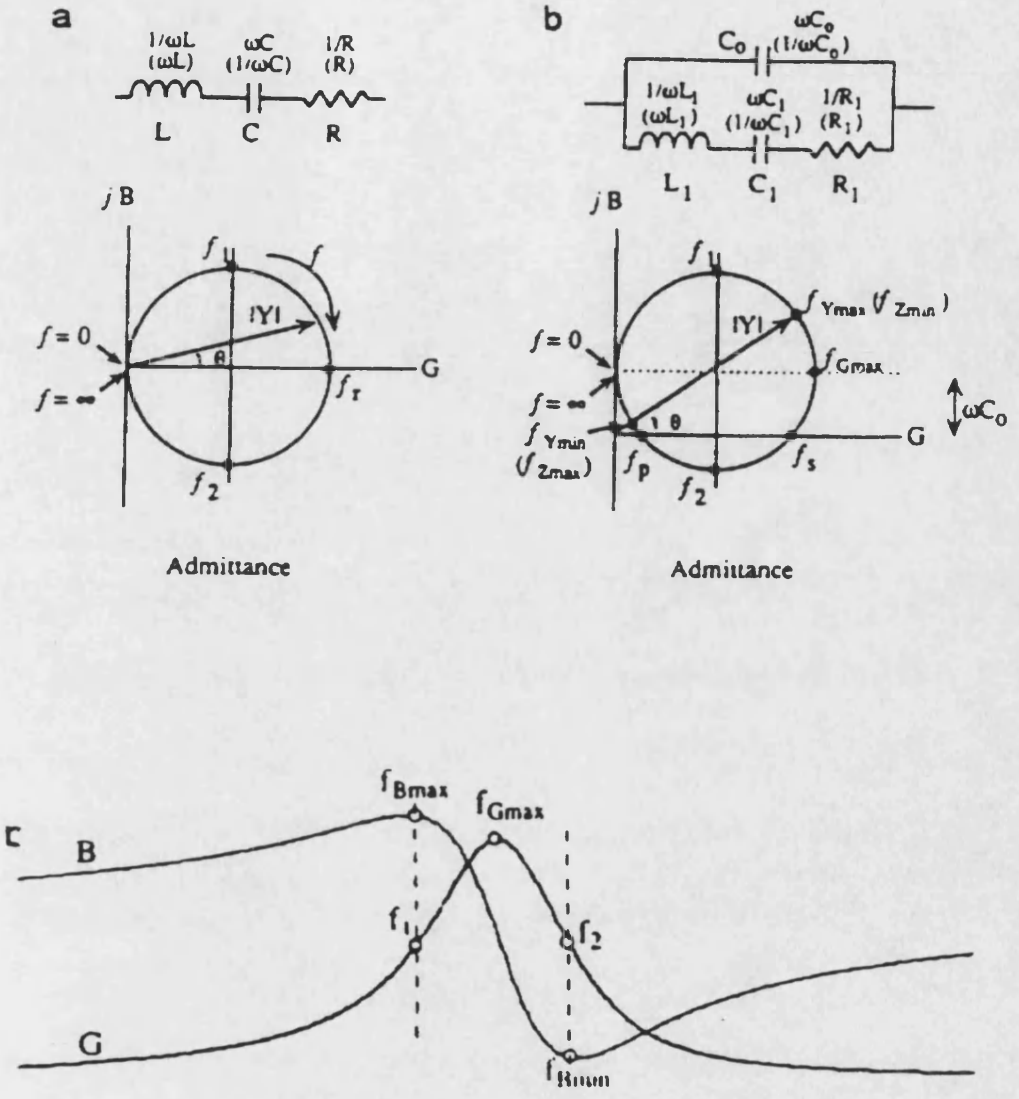

Figure 2.9 Admittance locus for (a) a series LCR circuit, (b) for the equivalent circuit of a quartz resonator. (c) Typical admittance and the imaginary part of the admittance, B, plots in the resonance region of a AT-cut quartz resonator.

Figure 2.9(c) illustrates B-G plots in the resonance region of an AT-cut quartz resonator. The G plot shows that the current flows most easily through the resonator only at frequencies in the vicinity of f_{Gmax}. New electrical components are considered when a resonator is in contact with a viscous liquid[34,35] or/and a polymer film[33]. The equivalent circuit is modified to include the mass loading density component (L_l) and viscosity (R_l) of the liquid as well as similar components for the polymer (L_f and R_f). The mass loading of the film, (L_F), and a resistive component (R_d) representing the energy dissipation of the film are added to the circuit. Finally, effects from elasticity of the film are representing by a capacitance (C_f), see figure 4.38. As any of these components increases, the diameter of the admittance loci decreases and the resonant frequency (f_s) as well. A shift in f_s indicates changes of mass at the surface of the quartz crystal, while changes in the bandwidth can be related to viscoelastic properties of the added mass[36] or/and viscosity of the liquid in contact with the crystal[32].

The contribution of viscous coupling of the crystal to the liquid can be incorporated into the Sauerbrey equation to give

$$\Delta f = -\left[2f_s^2/(\mu\rho)^{1/2}\right]\left[(\Delta m/A) + (\rho_L \eta_L/4\pi f_s)^{1/2}\right] \qquad (2.39)$$

where ρ_L and η_L are the density and viscosity of the liquid, respectively. If the product $\rho_L\eta_L$ is constant, equation (2.39) reduces to Sauerbrey equation. Polymers commonly are viscoelastic in nature and the contribution of η_F , ρ_F and μ_F to the resonant frequency of must be considered. The admittance spectrum can be used to study the viscoelastic properties of a polymer in order to know if the film is rigid enough to use the Sauerbrey[22] equation. Thin films of poly-nitrostyrene[37] were

observed to swell extensively with solvent during cycling in acetonitrile so that ingress of solvent and counterions can result in changes in the viscosity or elasticity of the film. Those changes in the viscosity or elasticity of the film give rise to large changes in the resonant frequency of the crystal which are not related to mass changes; similar results were observed for Os-poly-vinylpyridine films in p-toluenesulphonic acid[36].

References

1. J.E.B Randles, *Trans.Faraday Soc.*, 44 (1948) 327.
2. A. Sevcik, *Coll. Czech. Chem. Comm.*, 13 (1958) 349.
3. Southampton Electrochemistry Group, *Instrumental Methods in Electrochemistry.*, Ellis Horwood Series in Physical Chemistry, New York, (1990)
4. D. Pletcher, *A First Course in Electrode Processes.*, The Electrochemical Consultancy, Romsey,(1991).
5. J. Koryta, J. Dvorák and L. Kavan, *Principles of Electrochemistry,* Second Edition, Jhon Wiley & Sons, Chichester,(1993).
6. F. G. Cottrell, *Zphysik. Chem.*, 42 (1902) 385.
7. A. J Bard, L. R Faulkner, *Electrochemical Methods: Fundamentals and Applications.*, John Wiley & Sons, Chicester, (1980).
8. G. S. Alberts, I. Shain, *Anal. Chem.*, 35 (1963) 1859.
9. P. Daum, R. W. Murray, *J. Phys. Chem.*, 85 (1981) 389.
10. M. I. Montenegro, M. A. Queirós, J. L. Daschbach (Ed), *Microelectrodes: Theory and Applications.*, NATO ASI Series, Vol. 197, Kluwer Academic Publisher, Dordrecht, (1990).
11. R.M. Wightman, D.O.Wipf, *Electroanalytical Chemistry: A Series of Advances.*, A.J. Bard (Ed), Vol 15, Marcel Dekker, (1988).
12. M. Fleischmann, S. Pons, D. R. Rolison, P. P. Schmidt, *Ultramicroelectrodes.*, Datatech Systems Inc, Morganton, (1987).
13. R. M. Wightman, *Science*, 240 (1988) 415.
14. J.Cassidy , S.B. Khoo, S. Pons, M. Fleischmann, *J. Phys.Chem.*, 89 (1985) 3933.
15. T. Dibble, S. Bandyopadhyay, J. Ghoroghchian, J. J. Smith, F. Sarfarazi, M. Fleischmann, S. Pons, *J. Phys.Chem.*, 90 (1986) 5275.
16. R. T. Kennedy, J. W. Jorgenson, *Anal. Chem.* 61 (1989) 436.
17. R. M. Wightman, *Anal. Chem.*, 53 (1981) 1125A.

18. *Applications of The Piezoelectric Quartz Crystal Microbalance. Methods and Phenomena"*., C. Lu and Czanderna (Ed), Vol 7, Elsevier, New York, (1984).

19. *Electrochemical Interfaces. Modern Techniques for in situ Interface Characterization.*, H. D. Abruña (Ed), V.C.H. Publishers Inc., New York, (1991).

20. C. Lu, A. W. Czanderna (eds.),*Applications of Piezoelectric Crystal Microbalances.*, Vol.7, Elsevier, New York, (1984).

21. D. A. Buttry, Michael D. Ward, *Chem. Rev.*, 92 (1992)1355.

22. Sauerbrey G. Z., *Phys.*,155 (1959) 206.

23. Lu, C., Lewis, O., *J. Appl. Phys.*, 43 (1972) 4385.

24. A. R. Hillman, D. C. Loveday *et. al*, *Macromol. Symp.*, 80 (1994) 323.

25. M. C. Miras, C. Barbero, R. Koltz, O. Hass, *J. Electroanal. Chem.*, 369 (1994) 193.

26. Reynolds, J. R., Sundaresan, N. S., Pomerantz, M., Basak, S., Baker, C. K., *J. Electroanal. Chem.*, 250 (1988) 355.

27. Deaking, M.R., Melroy, O., *J. Electroanal.Chem.*, 239 (1988) 321.

28. A. R. Hillman, D. C. Loveday, M. J. Swann, S. Bruckenstein, P. Wilde, *ACS Symposium Series.*, Vol. 487, (1992) 150.

29. Hillman A. R., Loveday D. C., Bruckenstein S., *Langmuir*, 7 (1991) 191.

30. M. Thompson, A. L. Kipling, W. C. Duncan-Hewitt, L. V. Rajakovic, B. A. Cavic-Vlasak, *Analyst.*, 116 (1991) 881.

31. W. G. Cady, *Piezoelectricity*, Dover, New York (1964).

32. Z. A. Shana, H. Zong, F. Josse, D. C. Jeutter, *J. Electroanal. Chem.*, 379 (1994) 21.

33. D. A. Buttry, M. D Ward, *Chem. Rev.*, 92 (1992) 1355.

34 S. Bruckenstein, M. Shay, *Electrochim Acta.*, 30 (1985) 1295.

35. T. A. Zhou, L. H. Nie, S. Z. Yao, *J. Electroanal. Chem.*, 293 (1990) 1.

36. A. R. Hillman, D. C. Loveday, A. Glidle, J. G. Vos, A. P. Clarke, D. Kelly, S. Bruckenstein, *Macromol. Symp.*, 80 (1994) 323.

37. R. Borjas, D.A. Buttry, *J. Electroanal. Chem.*, 280 (1990) 73.

Chapter 3

Experimental

CHAPTER 3

EXPERIMENTAL

3.1. Reagents.

o- aminophenol (Fluka, purum 90%) was purified by recrystallizing it three times in ethyl acetate (Fisons,SLR grade). The very pale white plates were then dried in a warm water bath under vacuum to eliminate residual solvent. The monomer was stored in a desiccator under vacuum until required.

$NaClO_4$ (Aldrich, 99%), Na_2SO_4 (Fluka, 99%), NaCl (Fisons) and $NaNO_3$ (Fisons, reagent) were all used as supporting electrolytes without further purification as well as copper(II) perchlorate hexahydrate (Aldrich, 98%), $FeCl_2.4H_2O$ (BDH), europium(III) carbonate (Aldrich, 98%) and methylviologen (BDH). Sulphuric (Aldrich, 98%), nitric (Aldrich, 70%), perchloric (Fluka, 70%) and hydrochloric (BDH, 36%) acids were diluted and utilised to control the pH in solutions with the same anion. Ultrapure water (18.2 MΩ), from a MilliQ system, was used for the preparation of all aqueous solutions. Aluminium oxide (Avocado, neutral 50-160μm, 99%) was activated by drying it in an oven at 150 °C for 24 hours, under vacuum; it was added to acetronitrile (Fisons, spectrograde) in order to absorb moisture.

3.2. Glassware.

All glassware was cleaned with acetone to remove residual organics. Afterwards, it was immersed in 1:1 a mixture of sulphuric and nitric acids. Next, it was generously rinsed with ultrapure water and eventually dried in an oven at low temperature. An alternative cleaning solution, made by mixing equal proportion of H_2O_2 (Fisons, 20%) and concentrated H_2SO_4, was also utilised to remove impurities from glassware.

3.3. Electrochemical cells.

Figures 3.1, 3.2 and 3.3 show the electrochemical glass cells utilised during experiments. All of them, except that used for methylviologen and Eu(II) reduction, had one compartment . The cell incorporated an entrance and exit for nitrogen gas as well as a trap to prevent oxygen from entering cell. Electrodes were constructed to fit to that cell so that two or three electrode arrangements could be utilised. An almost identical cell design to that shown in figure 3.1 was utilised for quartz crystal experiments; in this case the bottom of the cell incorporated an opening which permitted the fitting of the quartz crystal. A flat quartz electrolytic cell (Wilmad, part number WG-810-A) was utilised for ESR experiments.

3.4. Electrodes.

Microelectrodes were constructed from platinum wire, about 10 μm diameter, supplied by Goodfellow Metals (99.9%) embedded in a soda glass tube. Disc electrodes with diameter of 0.65 and 0.05 cm were used for voltammetric and potential step experiments. A dismantleable and reusable platinum disc electrode was

designed in for the scanning electron microscope, figure 3.4. In this electrode, the head was fitted to the body by a heat-shrink plastic tube and electrical connection is achieved by a mercury drop and a nickel wire. Once the polymer had been deposited on the surface, the head was removed and attached to a metallic disc by silver conductive paint (RS).

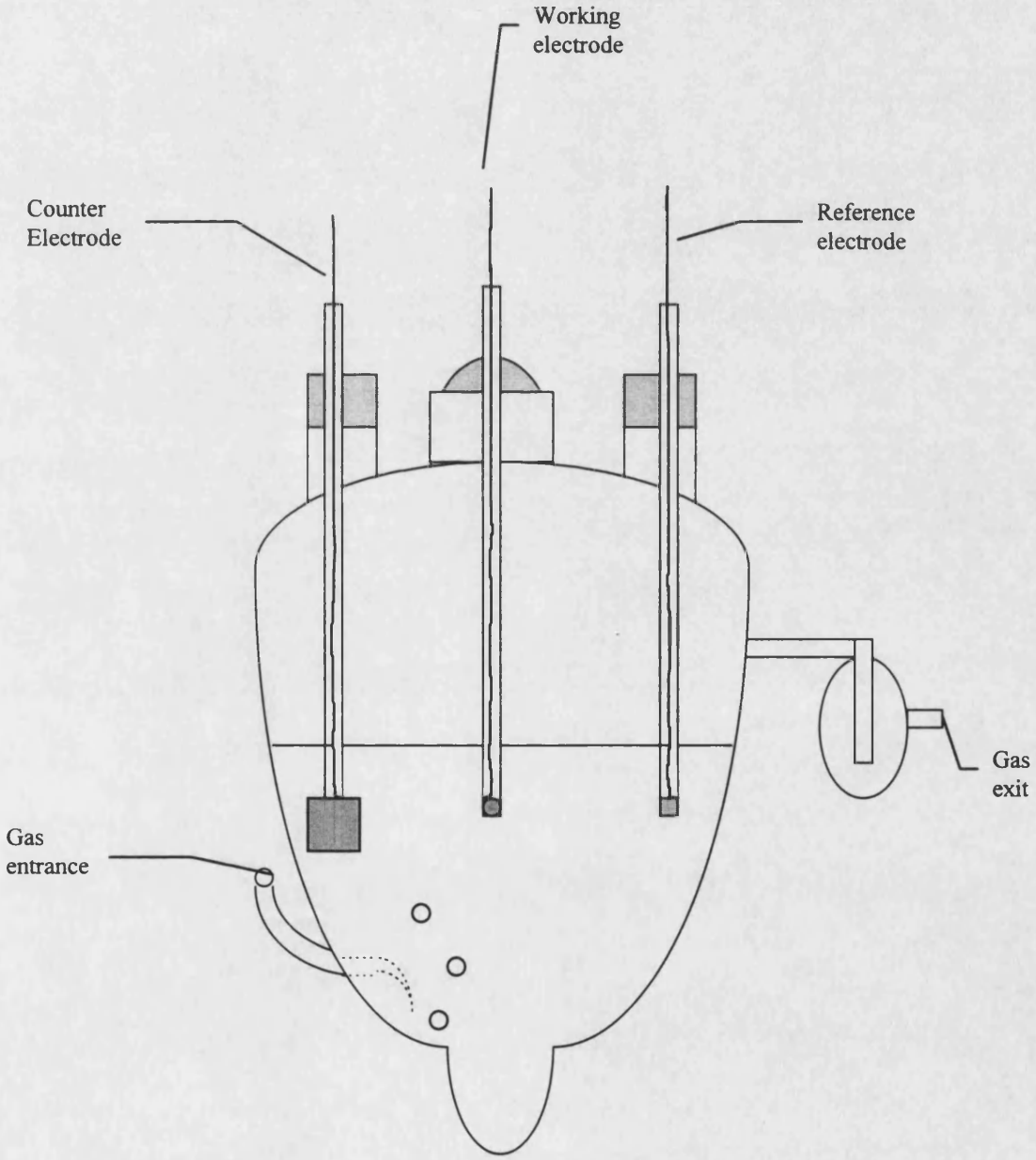

Figure 3.1 Electrochemical cell for voltammetric and chronoamperometric experiments

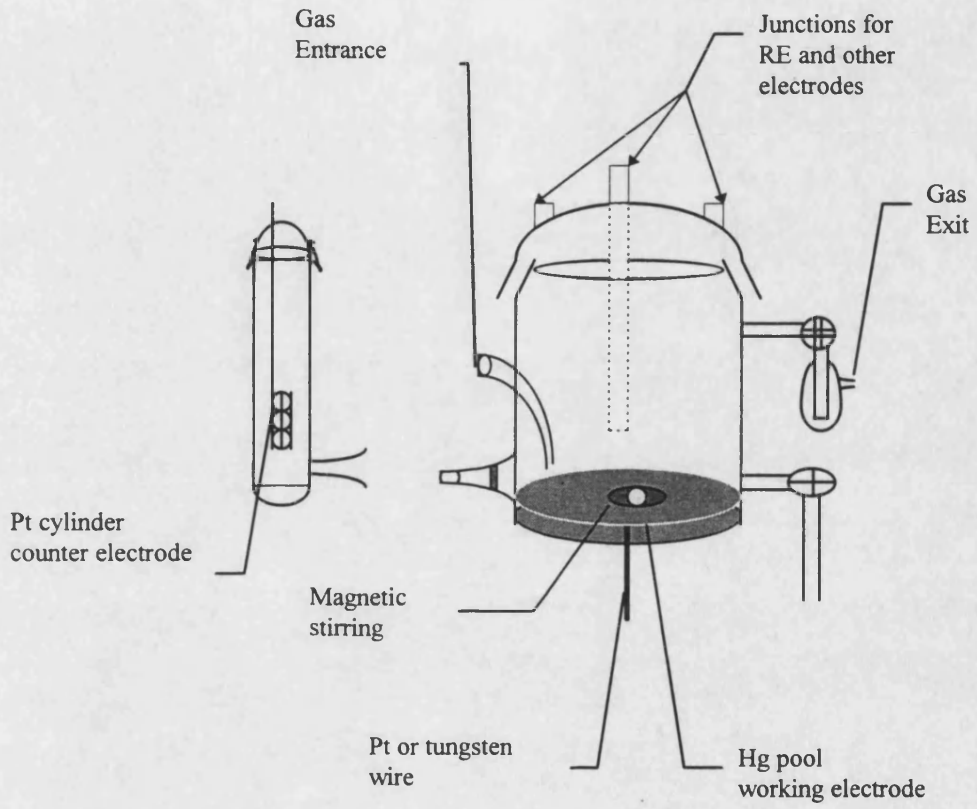

Figure 3.2 Electrochemical cell for reduction of europium(III) and methylviologen.

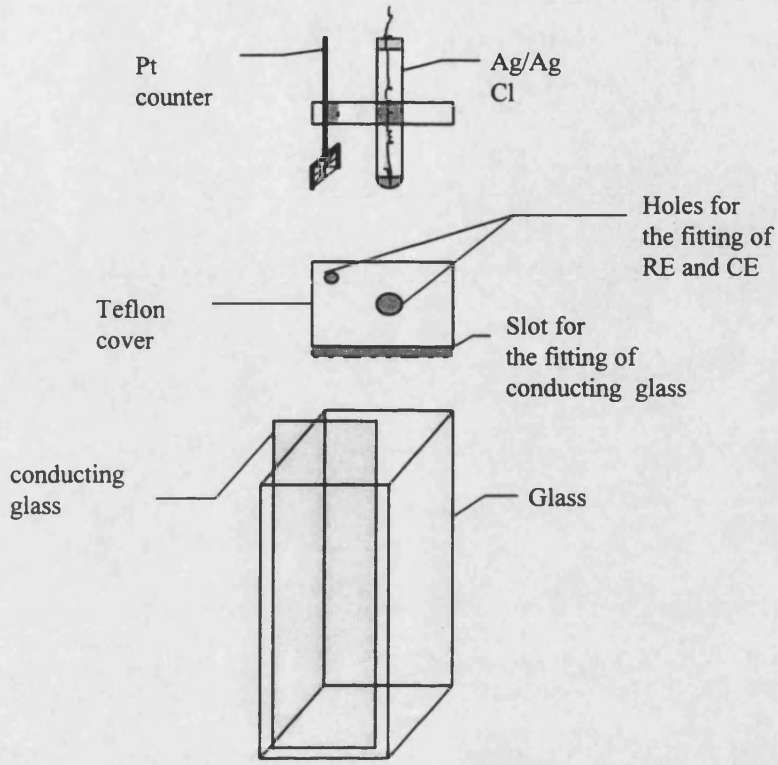

Figure 3.3 Electrochemical cell for visible spectroelectrochemical experiments.

All Pt working electrodes were polished initially on emery paper. This was followed by polishing in a series of finer grades of alumina powder (Leco) from 3 μm down to 0.05 μm. Electrodes were then thoroughly rinsed with purified water and introduced into a an ultrasonic bath after each polishing step in order to ensure that all the polishing particles are effectively removed. Further polishing was made only with the finest grade of alumina (0.3 and 0.05 μm) to remove polymer films. If any leakage or contamination were observed from cyclic voltammograms then the polishing procedure was repeated from the beginning.

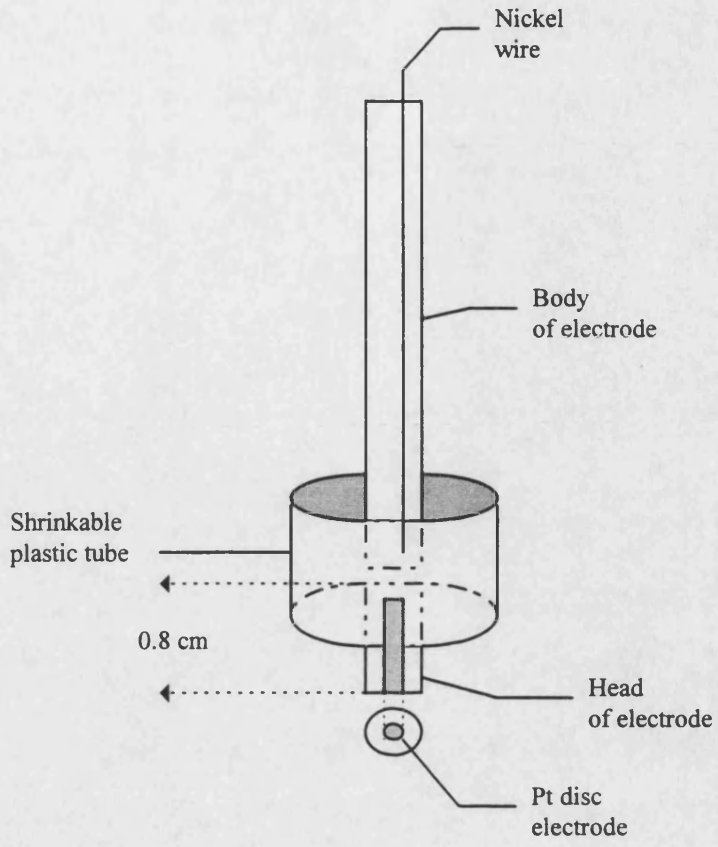

Figure 3.4 Recyclable electrode used as support for SEM of polymer modified electrode.

Tin oxide transparent electrical conducting glass (Libbey Owens Ford) was cut in 0.8 x 6.4 x 0.1 cm plates. They were then washed with soap and vigorously rinsed with ultrapure water. Next, electrodes were introduced into a thimble in a Soxhlet that contained isopropanol (Sigma) and cleaned under reflux for three hours to remove organic impurities. Finally, the electrodes were rinsed in water and stored in a container to protect them from dust.

A conventional potassium chloride saturated calomel electrode was used for experiments in aqueous solutions; a silver wire acted as a pseudo reference electrode for measurements in acetronitrile and dichloromethane. For visible spectroscopic experiments an Ag/AgCl reference electrode was prepared by introducing a silver wire in 20% H_2O_2 for five hours in order to oxidise the metal and produce a clean

surface. The wire was then rinsed and immersed in 0.2 mol dm^{-3} HCl for 48 hours to oxidise the surface to AgCl. The electrode was again rinsed place in saturated NaCl until it reached equilibrium. The potential of the built electrode was measured against a saturated calomel reference electrode (SCE) and recorded against time. Figure 3.5 shows the variation of potential versus time for this electrode. A stable potential of -49 ± 0.8 mV was reached after 20 hours. This potential was rechecked after each set of experiments in order to ensure its stability.

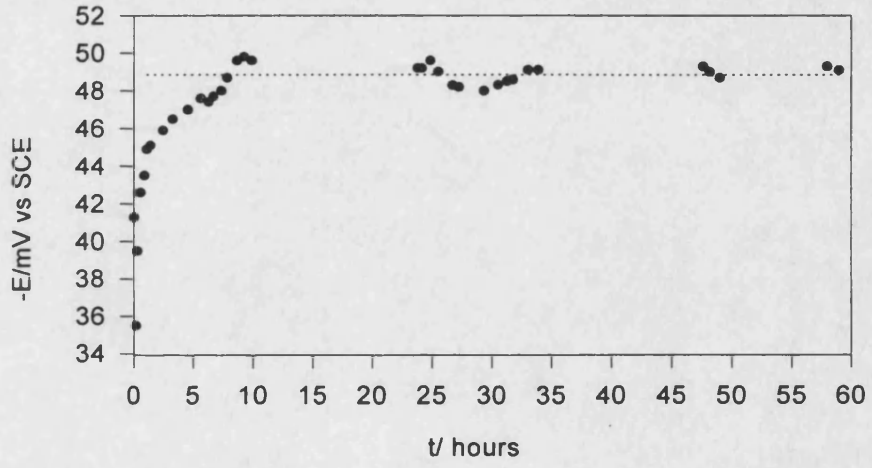

Figure 3.5 Variation of Ag/AgCl reference electrode potential as a function of time. Potential was recorded versus SCE.

Counter electrodes were made of Pt foil or gauze, with geometric areas of about 1 cm^2 for voltammetric and chronoamperometric experiments and 3 cm^2 for measurements related to the reduction of methylviologen and Europium(II). Counter electrodes were cleaned before and after each set of experiments by flaming in a bunsen burner.

3.5. Procedure for experiments.

Voltammograms of platinum in 1.0 mol dm^{-3} sulphuric acid were recorded in order to determine the effective area of the ultramicroelectrodes. Average charges corresponding to hydrogen adsorption and desorption of a monolayer were calculated by digitising the area under the voltammograms in the negative potential region. The charges are related to the total hydrogen coverage of the surface platinum assuming that one hydrogen atom is adsorbed per platinum atom. The theoretical charge associated with the formation of a monolayer of hydrogen on a polycrystalline platinum surface under the same conditions has been reported[1] to be 210 $\mu C\ cm^{-2}$. The effective area was calculated from the ratio between experimental value of charge and the theoretical charge density[1]. Correction for the double layer charging was carried out by linear extrapolation from the double layer region assuming that the capacity is constant in the potential range -0.24 to 0.4 (SCE) and that the contribution of the hydrogen adsorption-desorption process is not significant. The radius of the microdisc was evaluated by using

$$A = \pi r^2 \qquad (3.1)$$

where A is the effective area of the electrode in cm^2 and r is the radius of the microdisc.

The effective area was also determined by recording voltammograms, at low scan rates, of the oxidation of $Fe(CN)_6^{4-}$ in 1.0 mol dm^{-3} KCl as supporting electrolyte. The radius was then worked out from the value of limiting current, taking

as diffusion coefficient of $Fe(CN)_6^{4-}$, under the same experimental conditions at 25°C, 7.1 x 10^{-6} cm^2. s^{-1} [2] in the equation for steady state current at a microdisc[3]

$$i_d = 4nFDC^{\infty}r \qquad (3.2)$$

where i_d is the diffusion current, D is the diffusion coefficient of $Fe(CN)_6^{4-}$, C^{∞} its concentration in mol cm^{-3} , n= 1 is the number of electrons transferred during oxidation of this species, F is the Faraday constant and r is the radius of the microdisc.

Poly-*o*-aminophenol films were grown by cycling the potential of Pt between -0.250 and 0.750 V (-0.45 to 0.98 V for conducting glass electrodes) versus SCE in a 10^{-2} mol dm^{-3} monomer solution which contained sodium perchlorate 0.4 mol dm^{-3}, pH 0.9. The potential was scanned at 100 mV s^{-1} . After the growth, the films were transferred into a cell containing monomer free solution with the same supporting electrolyte. Voltammograms were then scanned from -0.25 V to 0.75 V at sweep rates of 100 and 20 mV s^{-1} . This procedure was followed when the polymer was grown in Na_2SO_4/ H_2SO_4 and NaCl/ HCl solutions. Changes in the solution pH were achieved by adding small volumes of a more concentrated acid solution with the same supporting electrolyte concentration; changes in the supporting electrolyte concentration were always at constant pH. Potential step measurements were carried out by stepping the potential from -0.200 to a series of potentials more positive than the anodic peak potential. A waiting time of 2-3 minutes was applied before each potential step while nitrogen gas was passed through the cell.

Nucleation of copper on polymer modified electrodes was studied in a 3.5 x 10^{-2} mol dm^{-3} $Cu(ClO_4)_2$ solution. The electrode was kept at +0.279 V (SCE)

for six or eight minutes before each cathodic pulse to ensure a total redissolution of metallic copper deposited in previous steps. Any change in thickness of the film or in its electroactivity can be detected by a change in the peak height and/or peak potential. The integrity of film was then checked by cyclic voltammetry before and after any set of experiments.

Visible spectra of poly-*o*-aminophenol were recorded at different potentials. A waiting time of ten or twelve minutes preceded each experiment in order to allow the polymer film to equilibrate. It was very difficult to fit a gas entrance and exit to the cell due to its dimensions so that the solution contained in it was renewed by a fresh and oxygen free solution every thirty minutes. The reference cell was filled with blank solution, and a strip of conducting glass was also introduced in order to compensate any absorption coming from the glass electrode.

The quartz crystals employed were 10 MHz AT-cut (International Crystal Manufacturing Company Inc.), with Au electrodes of electroactive area 0.23 cm^2. The calibrated mass sensitivity was 4.4 ng cm^{-2} Hz^{-1}. The crystals were fixed to the base of the electrochemical cell using non-corrosive silicone rubber sealant (RTV1000 Dow Corning), and allowed to cure for several hours. Calomel electrodes were used as reference in all the experiments.

The low conductivity of the film made it difficult to obtain scanning electron photographs of the polymer by electrical connection between platinum wire and the metallic disc of microscope, so that it was necessary to sputter a thin layer of gold onto the polymer modified electrodes for four minutes.

3.6. Instrumentation.

Cyclic Voltammetry and chronoamperometry were carried out using a waveform generator (Hitek Instruments), a potentiostat built in house (maximum sensitivity: 0.1 μA V^{-1}) coupled to a digital storage oscilloscope (Hitachi, model VC-6265) and a *xyt* recorder (Phillips, model PM8271). A current amplifier with a low pass filter (Kethley model 427) was also utilised to detect small currents on ultramicroelectrodes at lower scan rates. Charges obtained during transients were measured by an electronic integrator built in house (sensitivity: 10 C V^{-1}). Coaxial cables and a Faraday cage were utilised in order to minimise the noise in all the experiments.

Currents involving faradaic processes increase as the area of the disc electrode becomes bigger. For electrodes whose diameter exceeded 50 μm it was then necessary to use a potentiostat and a three electrode system to avoid the polarisation of the reference electrode, even at low potential scan rates.

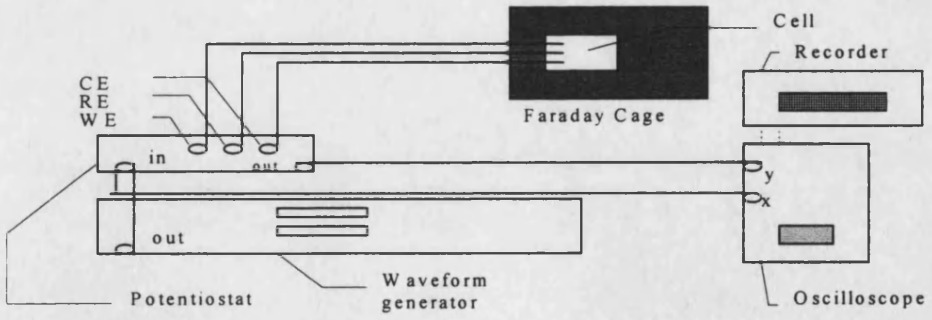

Figure 3.6 Instrumental arrangement for voltammetric experiments with conventional electrodes. The oscilloscope was used for high scan rates.

A Jeol JSM-T330 Scanning Microscospe was used to obtain the SEM images of the polymer grown under different experimental conditions. The samples were sputtered with gold in an Edwards S150B Sputter Coater.

Visible spectra of the film were recorded in a dual beam Perkin-Elmer 330 UV-Visible Spectrophotometer; identical conventional glass cells of 1 cm (Chandos Products Ltd) were introduced in the reference and sample compartment. Infrared spectra of the polymer on the electrode were obtained with a Nicolet 510P FT-IR Spectrometer with a fixed grazing angle specular reflectance unit (Spectra Tech, FT-80). The incidence angle on the polymer modified electrode was 80°. A special device was constructed to fit the electrode into the reflectance unit.

Figure 3.7 Instrumental arrangement for chronoamperometric experiments.

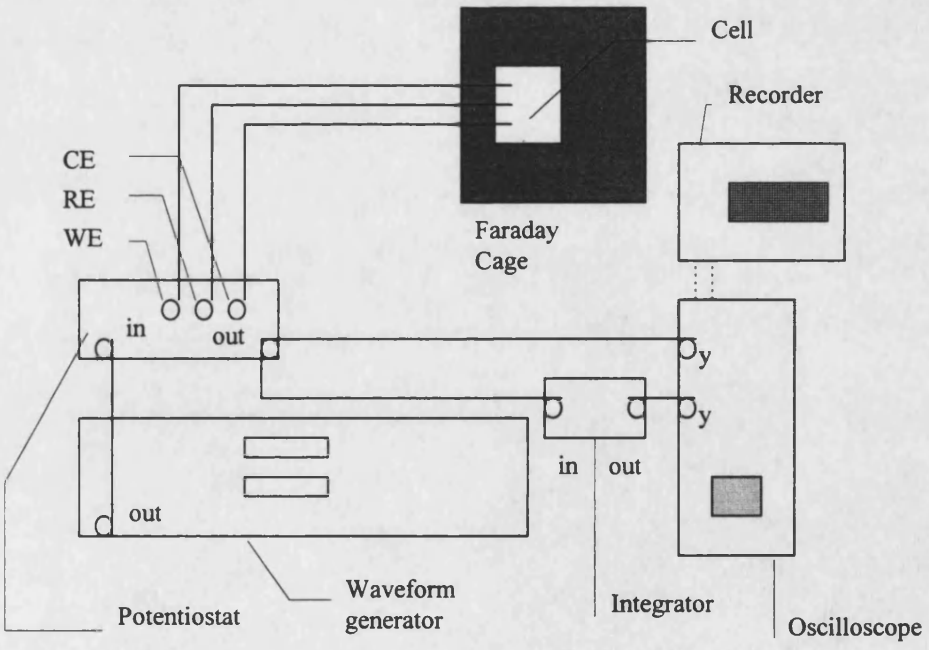

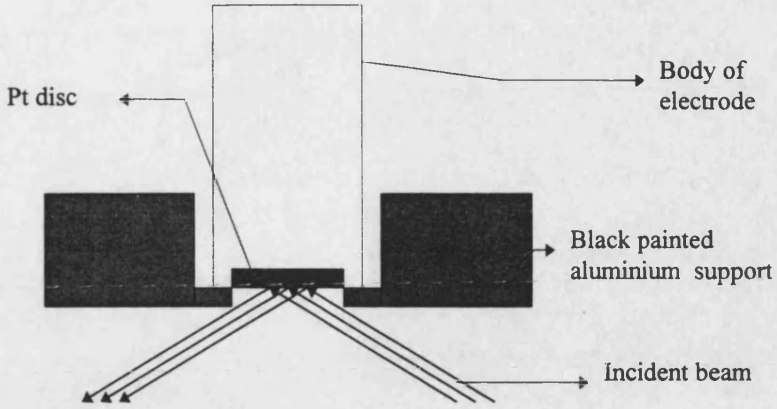

Figure 3.8. Device fixed to the spectrometer for obtaining FTIR spectra of polymer films.

The frequency response of the crystal was performed as a passive element, i.e. it was applied a sinusoidal voltage a various frequencies across the terminals of the crystal, by using a Hewlett-Packard 8751A network analyser used in reflectance mode. Scans were made over 16 kHz bandwidth centred on the peak admittance maximum. The sweep time was 15 ms and a sweep repetition rate of 1 and 10 minutes. Calibrated sensitivity was 1.1 Hz ng^{-1}. The computer acquired data were stored in a compact binary file and converted into an ASCII file suitable for importing into an any worksheet for analysis. For the mass changes associated with the redox switching of the polymer the quartz crystal was connected between the output and input of an oscillator amplifier and provides positive feedback that causes oscillation of the circuit. The resonant frequency of the crystal was measured by a electronic counter (Hewlett Packard 5334B) and stored in a interfaced ATX computer.

3.7. Determination of polymer film thicknesses.

The thickness of polymer films produced was dependent on deposition time. The thickness of the film was determined by monitoring the total charge in a half a cycle of voltammograms at low scan rates: 20 mV s^{-1} in monomer free solutions. It corresponds to a completely oxidised or reduced polymer. For films of area A and density ρ, the thickness d was calculated from the relationship 3.3 assuming that the total charge is completely associated with the redox reaction in the polymer [4,5,6]

$$d = \frac{qM_w}{FA\rho} \qquad (3.3)$$

where F and are the Faraday constant and M_w is the molecular weight of the polymer repeating unit plus anion from the supporting electrolyte. The value of ρ used for poly-*o*-aminophenol films was 0.8 g cm^{-3} due to the absence of data from the literature. Oxidation charges obtained during the cycling of poly-o-aminophenol at a scan rate of 20 mV s^{-1} were utilised for the calculation of the thicknesses.

References

1. R. Woods in "Electroanalytical Chemistry", (ed. A.J. Bard), vol.9, Interscience, New York, (1976), pp 48-57 .
2. J.E. Baur, R.M. Wightman, *J. Electroanal. Chem.*, 305 (1991) 73.
3. M. Irene Montenegro, M. Arlete Queirós, John L. Daschbach (Eds), *Microelectrodes: Theory and Applications*., NATO ASI Series, Vol. 197, Kluwer Academic Publisher, Netherlands (1990)
4. M. I. Florit, M.E. Martins, A.J. Arvia, *J. Electroanal. Chem.*, 269 (1989) 209.
5. X. B. Wang, J.M. Bonnett, R. Pethig, P. K. Baker, O. L. Parri, A. E. Underhill, *Journal of Molecular Electronics*, 7 (1991) 167.
6. B. E. Conway, H. Angerstein-Kozlowska, *Acc. Chem. Res.*, 14 (1981) 49.

Chapter 4

Electrochemical and Spectroscopic Studies of Poly-o-Aminophenol

CHAPTER 4

ELECTROCHEMICAL AND SPECTROSCOPIC STUDIES OF POLY-o-AMINOPHENOL

4.1 Introduction

A considerable effort has focused on attempts to obtain conducting polymers from phenols and anilines. The electropolymerization of substituted anilines has been studied in view of the formation of soluble polymeric films with improved processability and preservation of their electrical properties[1]. However, electropolymerization of benzyl monomers containing both $-NH_2$ and -OH groups is more recent and less explored. Orthoaminophenol(oAP), for example, gives a surface film of interesting electrochemical and electrochromic properties when it is electropolymerised in acid medium[2].

As in the case of many organic molecules[3,4], the electropolymerization reaction of oAP is initiated by oxidising the respective monomer to a radical cation. Once the oAP radical cation is formed it can dimerize by C-C, N-N or C-N coupling; see a, b and c Figure 4.1. Each dimer may then undergo two electron oxidation to the products *a'*, *b'* and *c'*. Two of these species (*a'* and *b'*) could oxidise and further coupling would lead to the formation of polymers. Coupling through para carbon to amino group (meta carbon to OH group) is also possible[5] giving rise to a cyclic dimer formed by a relatively slow cyclization reaction . This compound is known as 3-APZ (3-aminophenoxazone). SERS spectra[6,7] have showed that the major products of oAP oxidation are 3-APZ[8] and 2,2'-dihydroxyazobenzene; the relative amount of each species depends on pH. At lower pH, the cyclic dimer is favoured while in alkaline media N-N coupling results in the formation of azo species. Further oxidation of 3APZ

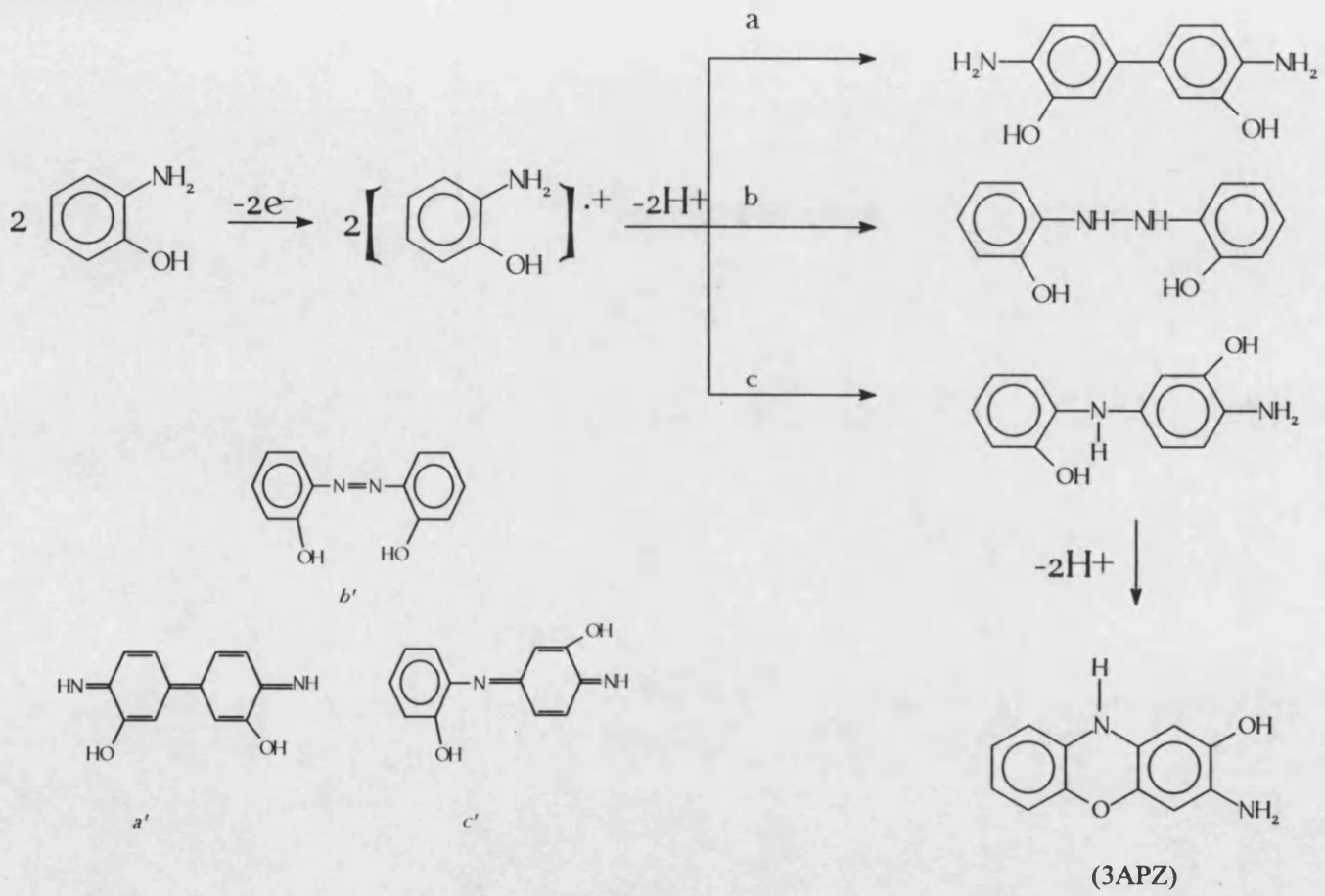

Figure 4.1 Scheme for the electrooxidation of oAP in acid medium.

gives rise to a polymer with a ladder phenoxazine-like structure which is named poly-o-aminophenol (POAP). The blocking of the *para* position in oAP leads to the inhibition of film formation as predicted by the shown mechanism[2].

Previously it has been reported[9] that the chemical polymerization of oAP achieved by using PbO_2 and potassium hexacyanoferrate (III), in several organic solvents, gives rise to the same ladder structure of the polymer as does the polycondensation of 4,6-diaminoresorcinol hydrochloride with 2,5-dihydroxy-*p*-benzoquinone[10] and 2,5-dichlorophenylenediamine with 2,5-dihydroxy-*p*-benzoquinone[11].

Other aminophenols have already been studied. It is accepted that anodic oxidation of *p*-aminophenol in aqueous solutions gives benzoquinone with the reaction occurring in homogenous medium; no electrode coating was observed [2,12]. However, a dark brown coloured conducting film was obtained on Pt when DMF and MeOH were used as solvents [13]; a destabilising effect of electron withdrawing groups on the radical cation decreases its lifetime and favours rapid reaction with solvent to form soluble products. Thin films of poly-*p*-aminophenol have also been obtained from concentrated monomer solution in hydrochloric acid; AFM showed that the surface was composed of small, elongated bundles with dimensions ranging from 50 $Å^2$ to 2000 $Å^2$ which are distinctly separated[14]. On the other hand, the anodic oxidation of *m*-aminophenol in acetonitrile[15], MeOH[16] and aqueous[2] media produces a non conductive and non permeable film attributed to extensive crosslinking. This feature could make it very attractive for use as material for protective coatings. However, studies based on X-rays and IR analyses revealed that pinholes of various sizes and shapes are present[17], which

explains the electroactivity of some species by diffusion through the polymer layer and indicates that poly-*m*-aminophenol may not be a good corrosion protector.

The first example of a ladder polymer film prepared electrochemically from its monomer was poly-*o*-phenylenediamine[18]. By analogy with phenylenediamine, oAP was thought to form a similar repeating unit and polymer structure, that is an alternated set of benzenic and phenoxazine rings. IR absorption spectra of POAP film in its oxidised form[19] showed the vibration modes of C-H, C=C of aromatic centres (3000 and 1430-1605 cm^{-1}, respectively), C-N at 1250 and 1310 cm^{-1} as well as the N-H and C=N stretching vibrations of the imino groups at 3420 cm^{-1} and 1645 cm^{-1}; C-O-C , C=O and 1,2,4,5 tetrasubstituted benzene bands were also observed. These results suggest a ladder structure similar to poly-*o*-phenylenediamine; however, partially ring opened structures are also conceivable.

The relative intensities of the Raman peaks[7] at 1235 cm^{-1}, corresponding to C-O-C stretching vibrations, are quite close for the 3APZ monomer and the POAP which indicates the presence of a considerable number of C-O-C bonds. However, the Raman spectra of the oligomers produced by 3APZ electrooxidation did not indicate bonding through C-O-C bonds but most probably through -C=N- bonds; this seems to support the idea of a mixture of opened and closed structure for the polymer .

The POAP film coated electrode displays electrochromic character when the potential is driven from -0.1 to 0.7 V vs. SCE: the oxidised form exhibits a bronzy brown colour and the reduced form is reported to be very pale green[20], yellow[21,2]. The uv/visible absorption spectra of the oxidised and reduced forms of POAP have been reported; however, there are significant differences between the reported spectra that cannot be attributed to the experimental conditions. A maximum at approximately 530 nm for the reduced form and a quite broad band in the range 420 to

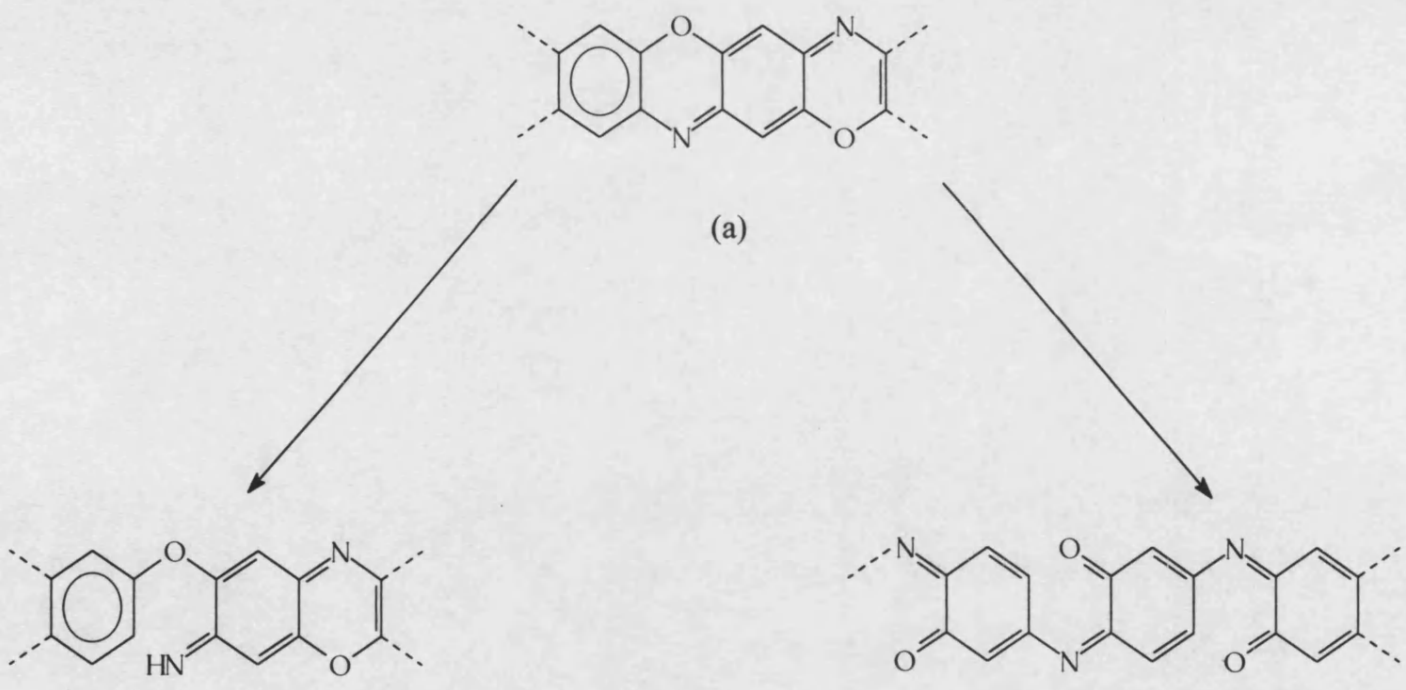

(b) (d)

Figure 4.2 Ring-closed (a) and ring-opened (b and c) possible structures for poly-o-aminophenol. *Kunimura* [19]

600 nm for the oxidised form of the polymer were observed by Barbero[22] *et al.* while well-defined peaks at 440 nm and *ca* 600 nm corresponding to oxidised and reduced forms, respectively were observed by Ohsaka[20] *et al.*; see figure 4.3. The latter author found that the brown colour of the oxidised form remained substantially unchanged even after standing in air at open circuit for six months. On the contrary, the reduced form was gradually oxidised by oxygen in air and consequently became coloured.

The cyclic voltammetric behaviour of POAP film deposited on pyrolytic graphite in 0.2 mol dm^{-3} $NaClO_4$ aqueous solution (pH 1.0) showed a reversible redox response, similar to an electrode reaction of a solution phase redox species that diffuses to the electrode surface[19,20]. The cathodic and anodic peaks currents were found to grow linearly with the square root of potential scan rate in the range from 5-200 mV s^{-1}, suggesting that the charge transport process within film is diffusion controlled[23]. The calculated apparent diffusion coefficients (D_{app}) for oxidation and reduction processes, determined by chronoamperometry, chronocoulometry and normal pulse voltammetry, were in the order of 10^{-10} cm^2 s^{-1}; D_{app} for reduction was generally *ca* 50% higher than for the oxidation of the film[19,20].

POAP is electroactive in aqueous and nonaqueous solutions containing protons. No response is observed at pH values higher than 7. Peak currents increase and peak potentials are displaced to more negative potentials as the pH increases[24]. The redox reaction is believed to involve the processes of addition/ elimination of protons coupled with reversible electron transfer[20,24,25], see figure 4.4 .

The electrical conductivities of the films in dry state are reported[19] to be very low: 4 $x10^{-7}$ S cm^{-1} ; however, the determination of conductivity in the dry state provides little information about the real conductivity in the electrochemical situation because of the absence of an electrolyte. Barbero[24], determined the conductivity of

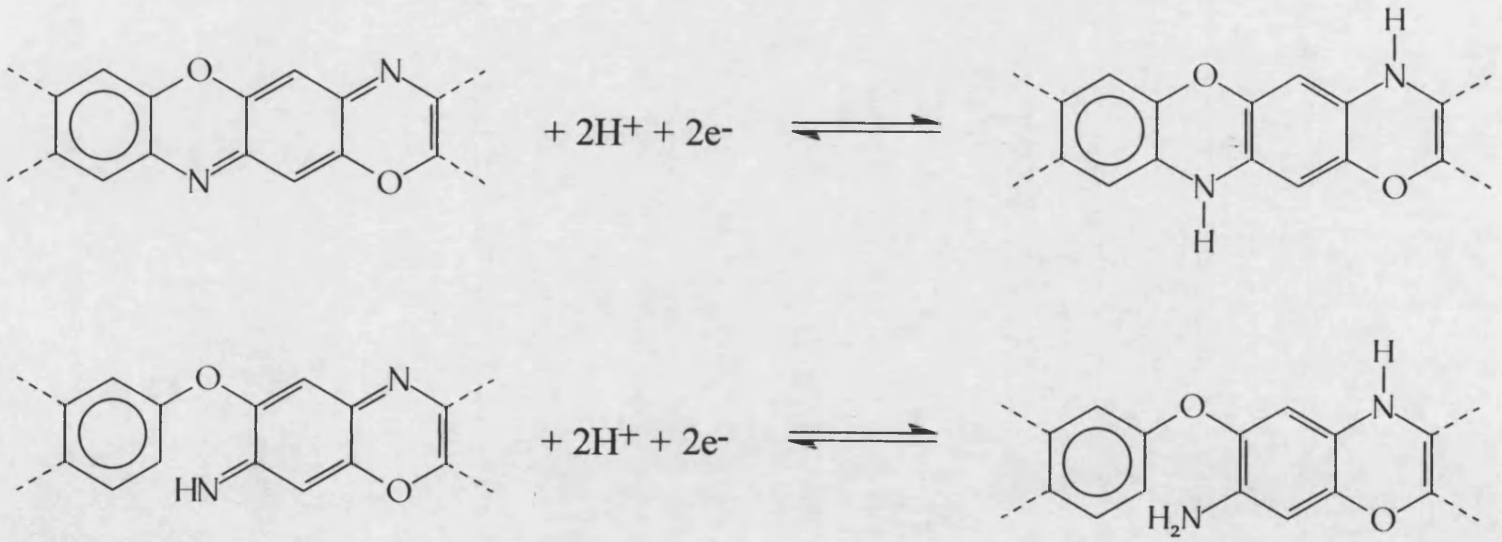

Figure 4.4 Proposed redox mechanism of POAP films.*Kunimura*[19].

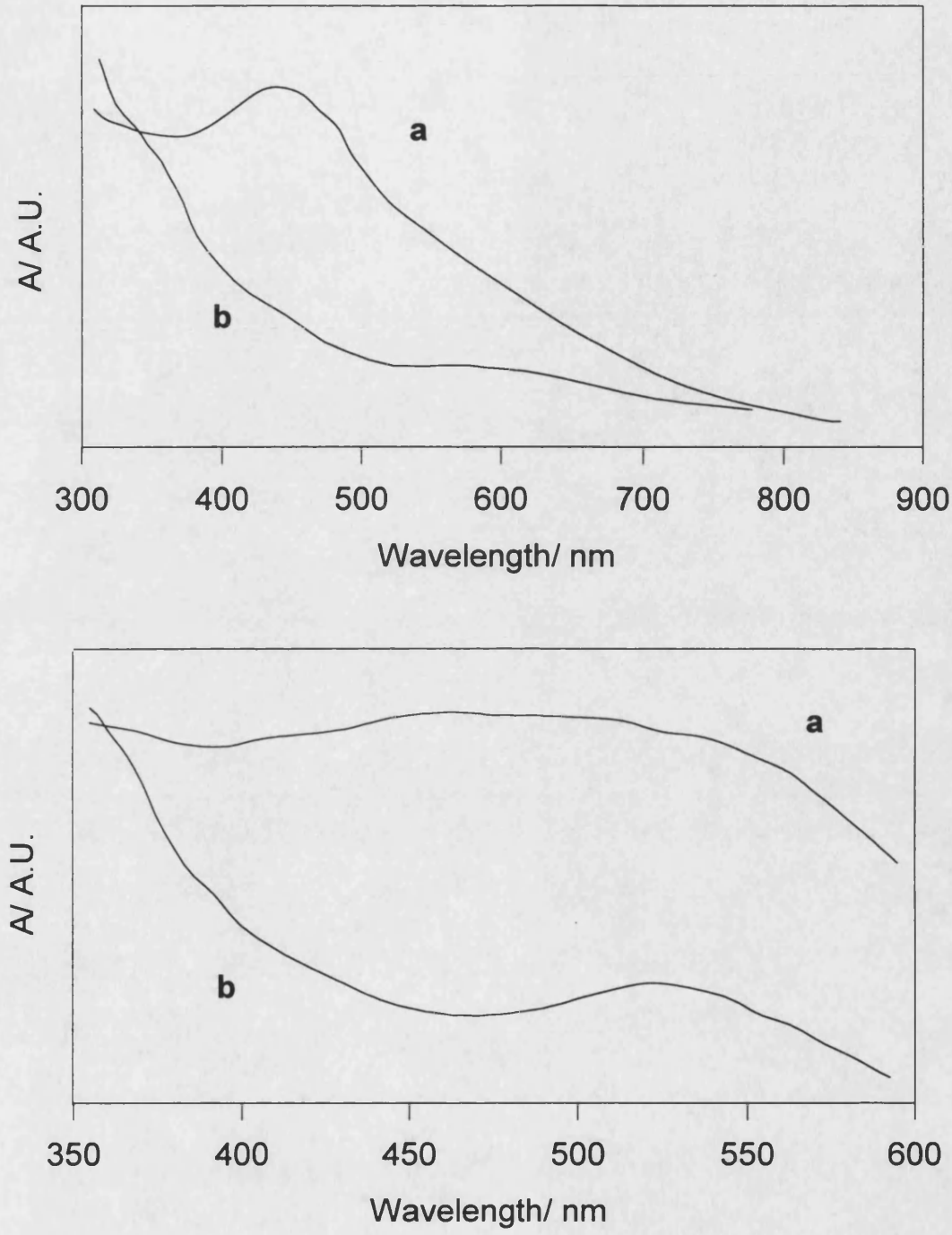

Figure 4.3 Relative absorbance as a function of wavelength for **(a)** oxidised and **(b)** reduced POAP. The upper plot was reported by Ohsaka[20] while the lower one was given by Barbero[22].

POAP films based in the quasi-reversible behaviour observed for the oxidation of $K_4Fe(CN)_6$ as the polymer thickness increases; this effect was attributed to the film resistance with the assumption of a fast charge transfer at the electrode/film and film solution interfaces. The value of conductivity determined in this way was 1.34×10^{-4} S cm^{-1}. This author found that species with reduction potentials more negative than E_{pa} of the film (Cr^{3+}, Cd^{2+} and Cu^{2+}) were not be reduced on POAP modified electrode, with the exception of the H^+. On the other hand, couples with E^0 more positive than E_{pa} of the film (ascorbic acid and hydroquinone) were oxidised. This supports the conclusion that the film is conductive in its oxidised state.

The variety of results reported in the literature show that the electrochemical response of POAP is strongly influenced by the experimental procedure followed to produce the polymer film. Some authors used oAP without further purification[5,6,21] , reporting the formation of coloured solutions. Under such circumstances, the products of the oxidation in air of oAP can react electrochemically to form composite polymers. In this chapter, the cyclic voltammetry, chronoamperometry, and spectroscopic measurements of poly-o-aminophenol are discussed. The monomer was rigorously purified before the deposition of the polymer (see *Chapter 3).*

4.2 Electropolymerization of oAP

A typical cyclic multisweep voltammogram of oAP at a Pt electrode in an aqueous solution containing 0.4 mol dm^{-3} of $NaClO_4$ and 10^{-2} mol dm^{-3} of the monomer is shown in figure 4.5. The potential of electrode was continuously swept at 100 mV s^{-1} between -0.25 and 0.750 V vs. SCE. On the first positive sweep, only one irreversible peak is defined at 650 mV (figure 4.5 **a,** visible at lower sensitivity) which can be attributed to oxidation of monomer to the monocation radical. No

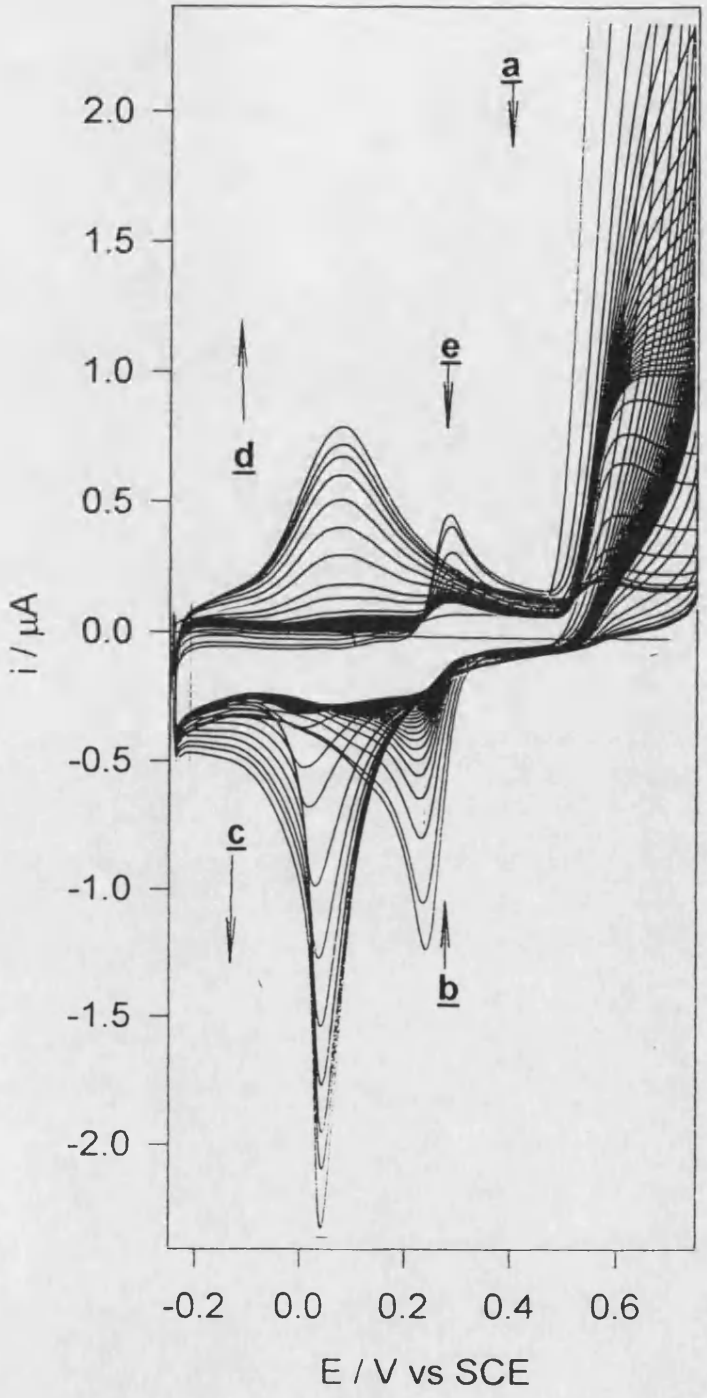

Figure 4.5 Cyclic voltammogram of o-AP at pH 0.9; ν= 100 mV s^{-1}.
Area 1.9 x 10^{-3} cm^2, [o-AP] = 10^{-2} mol dm^{-3}; solution contained 0.4 mol dm^{-3} $NaClO_4$ and 0.12 mol dm^{-3} $HClO_4$. Arrows indicate the changes in the peak height as electropolymerization is taking place.

complementary peak to **a** is observed, on the negative scan, while an large peak appears at 230 mV (figure 4.5 **b**). This peak has a complementary one (**e**) at 290 mV in the next positive scan, (ΔE= 60 mV) corresponding possibly to the redox reaction of the dimer **c**, figure 4.1. By continuous cycling it is observed that peak **a** decreases rapidly and continually up to a minimum, peaks **b** and **e** fall correspondingly. After eight or ten minutes cycling (24th to 30th cycle), the current response in the range from 0.0 to 0.2 mV begins to increase continuously with successive potentials scans, giving rise to peaks **c** and **d** which indicate the build-up of an electroactive polymeric product on the electrode surface.

Neither polymer nor couple **b** and **e** are formed if the potential scan does not reach 650 mV. On the other hand, peaks **b, e, c** and **d** do not appear when potential cycling takes place under continuous nitrogen bubbling; it seems that under stirred conditions the intermediate corresponding to **b** and **e** is moved away from electrode so that its further transformation into polymer is prevented. This conclusion is in agreement with that reached by Barbero[2] *et al.* who suggest that the polymer is produced by a comparatively slow cyclization reaction of dimer *c'* (figure 4.1) to form 3APZ and that the peaks **c** and **d** correspond to this species and its polymer.

The anodic I_p (**e**) was always smaller than the cathodic peak (**b**). This decrease could be related to the quantity of dimer which was consumed by the cyclization reaction during each voltammetric cycle. A rapid diffusion of the dimer away from electrode should not be ruled out. Voltammograms of the two first cycles of the electropolymerization process were recorded using a Pt disc electrode which was polished with a series of finer grades of alumina powder, thoroughly rinsed with purified water and cleaned in an ultrasonic bath. The electrode was then polished with

the finest alumina powder (0.05 μm) before each experiment in order to avoid greater changes in the roughness of the electrode surface. If the diffusion into the bulk solution was the dominant process, then the charges involve in peak **e** would be sensitive to the potential scan rates. The charge ratio, $q_{anodic}/q_{cathodic}$,, should increase with the potential scan rate because species will not have time enough to diffuse away from electrode. The lower the scan rate, the longer the time this species has to diffuse into bulk solution. Figure 4.6 illustrates the behaviour of charge ratio as a function of the scan rate. A progressive decrease of this parameter is observed with increasing sweep rate. This behaviour suggests that a slow chemical reaction is coupled to the peaks **b** and **e** instead of a rapid diffusion of species away from the electrode. The fraction of species **b** consumed by this path is given by the decrease of its complementary peak **e**. At higher scan rates, the concentration of formed dimer is low so that the fraction of this species which is transformed to 3APZ is relatively larger .

The chain propagation appears to proceed slowly; the last curve shown in the figure 4.5, corresponds to 180th cycle. After two or three hours cycling there is no change in the peaks corresponding to the build-up of the polymer. It is possible that oAP species have to diffuse through the film to reach the electrode and produce more monocation radical; for this reason peaks **a**, **b** and **e** decrease with the time. This supports the idea that the oxidised state of the polymer is non-conducting, which is opposite to the conclusion reached by Barbero[24]. Moreover, the fact that the growth of polymer starts after an induction time, much later than when the peaks corresponding to oAP radical cation and dimers become very small, and it stops after three hours suggests that the propagation process is further oxidation and coupling of 3APZ. However, cyclic voltammetry of 3APZ [7] appears to show that this compound oxidises

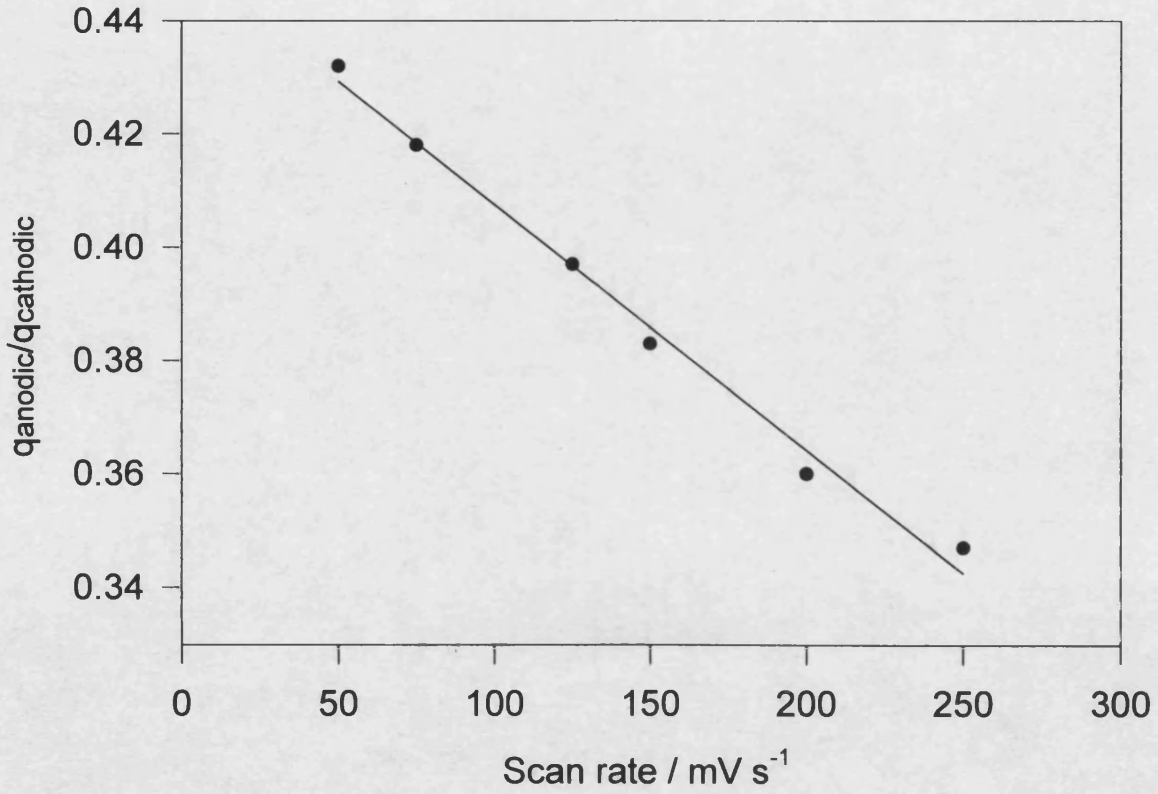

Figure 4.6 $q_{anodic}/q_{cathodic}$ as a function of the scan rate for the couple **b-e** in the cyclic voltammogram for electropolymerization of oAP. Area 1.9×10^{-3} cm^2, [oAP] = 0.01 mol dm^{-3}

and dimerises but does not polymerise, which disagrees with the coupling of 3APZ units. Unfortunately, the authors do not state how long the system was cycled, see figure 4.7. On the other hand, the voltammograms of 3APZ corresponding to the first cycles reported by Barbero[2] show the characteristic behaviour of an electroactive deposited substance with currents increasing with cycling, figure 4.8. Peak potentials for both the monomer and polymer from 3APZ were the same and they correspond exactly to the peak potentials of **c** and **d** from figure 4.5. The coupling of 3APZ units to form the polymer seems to be the process that is taking place during the propagation of the polymeric chains.

During synthesis by cyclic voltammetry, conducting polymers are partially oxidised and reduced, and ions from the electrolyte must move into or out of the polymer film and in order to preserve electroneutrality. This movement can also involve some water or salts, so that the supporting electrolyte could be a major component of the total mass of the film[26,27]. The nature of the supporting electrolyte can alter the morphology and electrical characteristics of the film[28]. POAP films were therefore grown in different media in order to see the effect on the patterns of growth. By area integration of the peaks **c** and **d**, anodic and cathodic charges were calculated from cyclic voltammograms during the growth of the polymer and plotted as a function of the time. Three different monomer concentrations were used. Figures 4.9, 4.10, 4.11 and 4.12 summarise the observed behaviour. The patterns of growth, recorded by cyclic voltammetry, were always similar; however, small differences can be seen in figures 4.9-4.12. First of all, there is an induction time which depends on monomer concentration. The higher the monomer concentration is, the shorter the induction time becomes. This effect is most clearly observed in $NaClO_4$ medium; at short times there

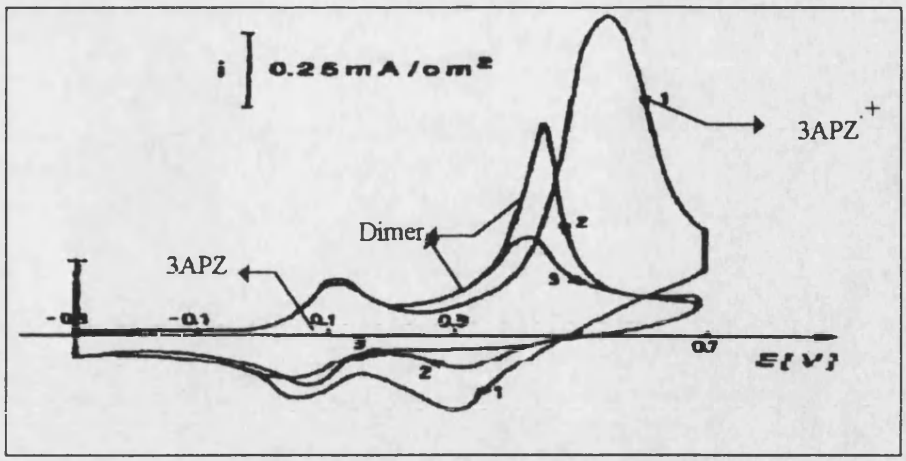

Figure 4.7 Cyclic voltammogram of 3APZ in 0.1 mol dm^{-3} $LiClO_4$ + 0.1 mol dm^{-3} $HClO_4$ on Au electrode(0.2 cm^2), ν= 40 mV s^{-1} . Numbers indicate the number of cycles, *Jackowska*[7].

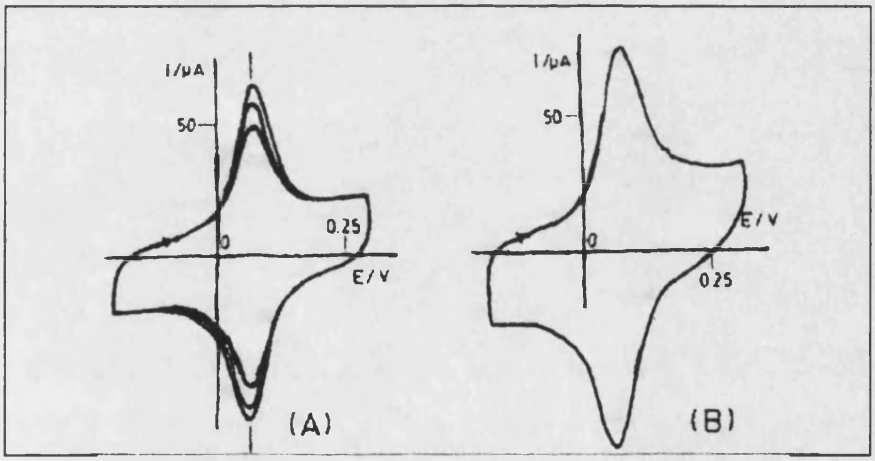

Figure 4.8 Cyclic voltammograms of (A) [3APZ]=1 x 10^{-3} mol dm^{-3} and (B) from A, after the first ten cycles, in a monomer free solution. ν= 0.1 V s^{-1}, glassy carbon electrode 0.0071 cm^2; 0.4 mol dm^{-3} $NaClO_4$ + 0.1 mol dm^{-3} $HClO_4$. *Barbero*[2].

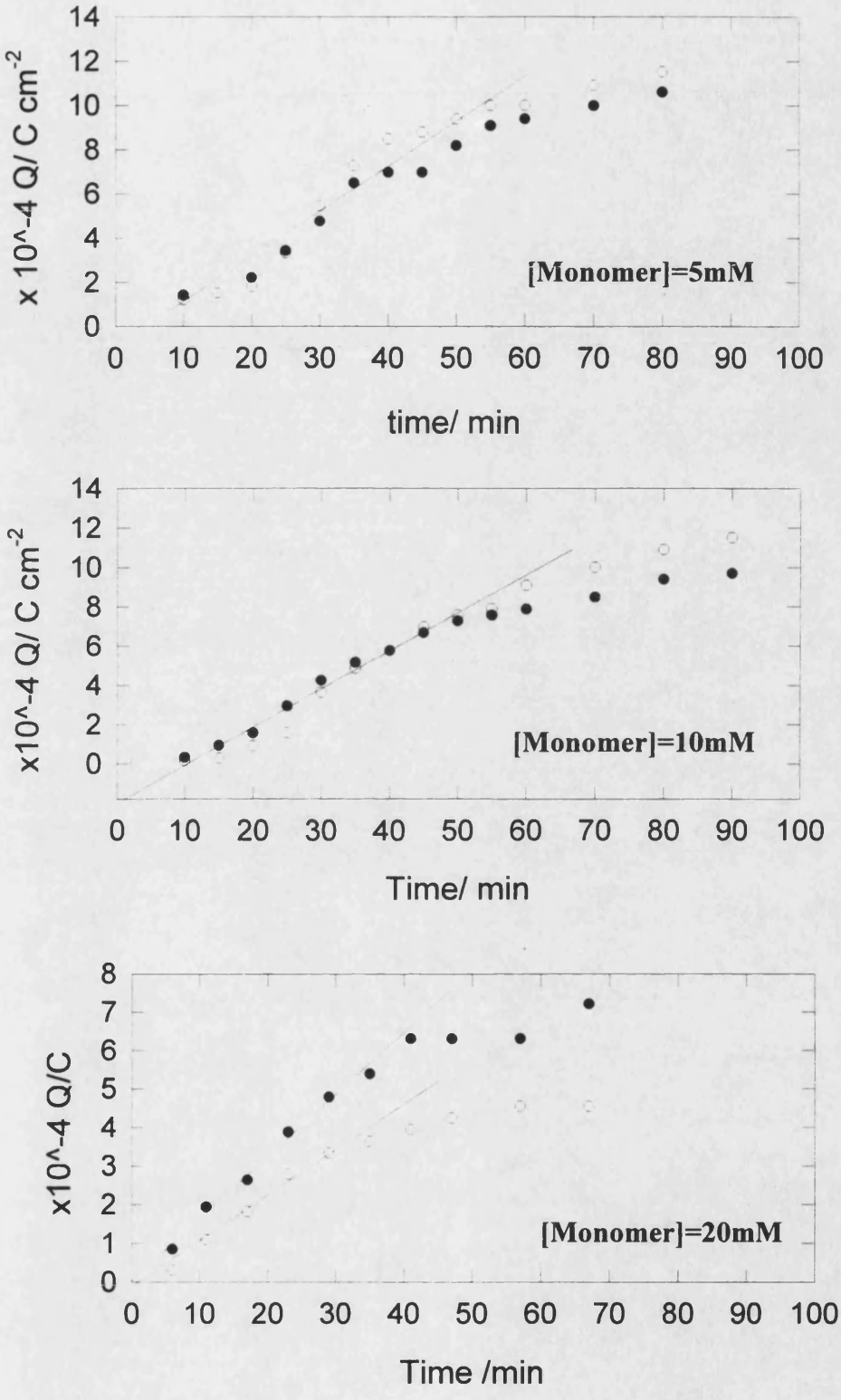

Figure 4.9 Anodic and cathodic charge for peaks c and d (figure 4.5) during the growing process as a function of time. $NaClO_4$ (0.4 mol dm^{-3}) and $HClO_4$ (pH 0.9).
○ Anodic process • Cathodic process

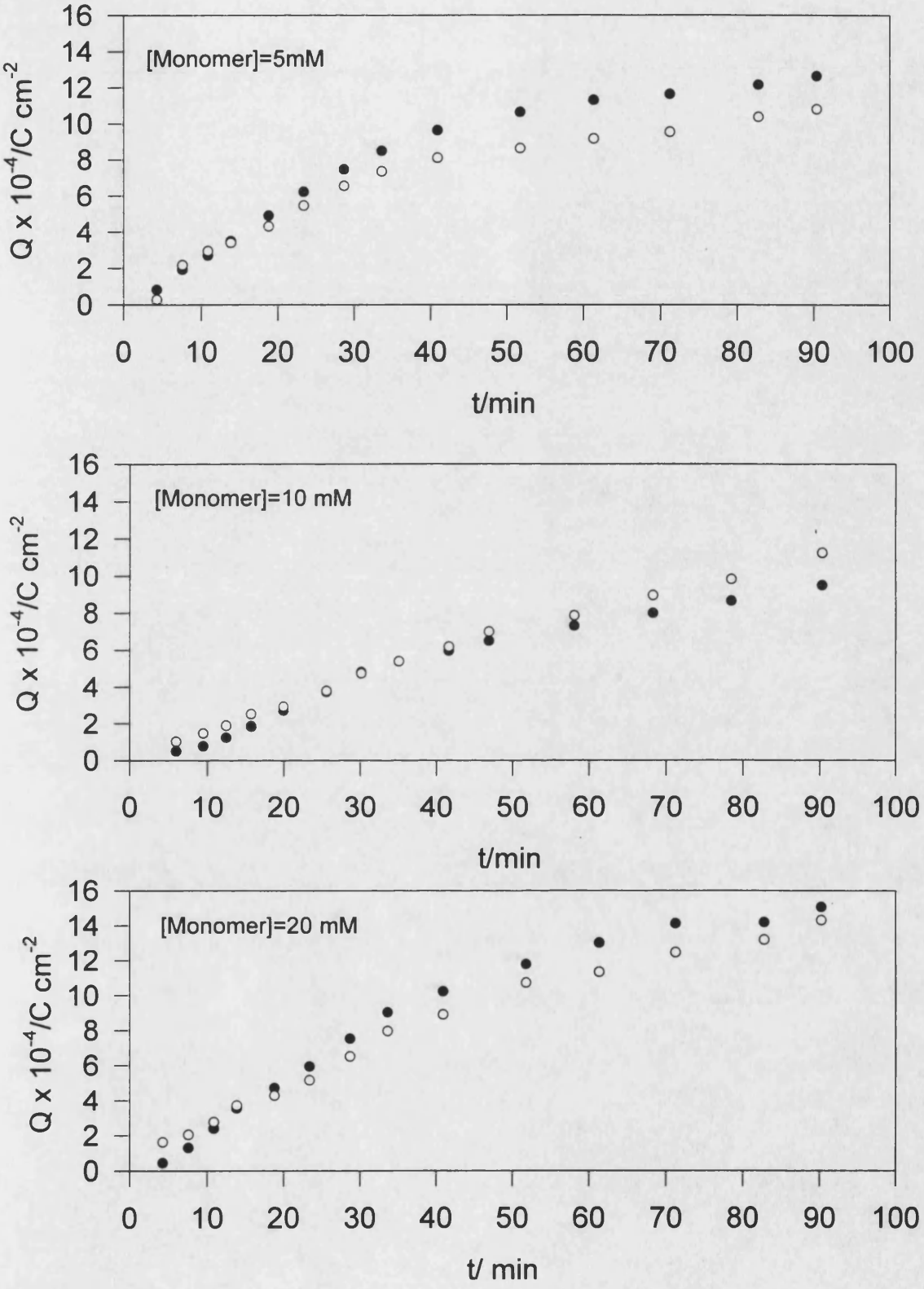

Figure 4.10 Anodic and cathodic charge for peaks c and d (figure 4.5) during the growing process as a function of time Na_2SO_4 (0.4 mol dm^{-3}) and H_2SO_4 (pH 0.9).

• Anodic process ○ Cathodic process

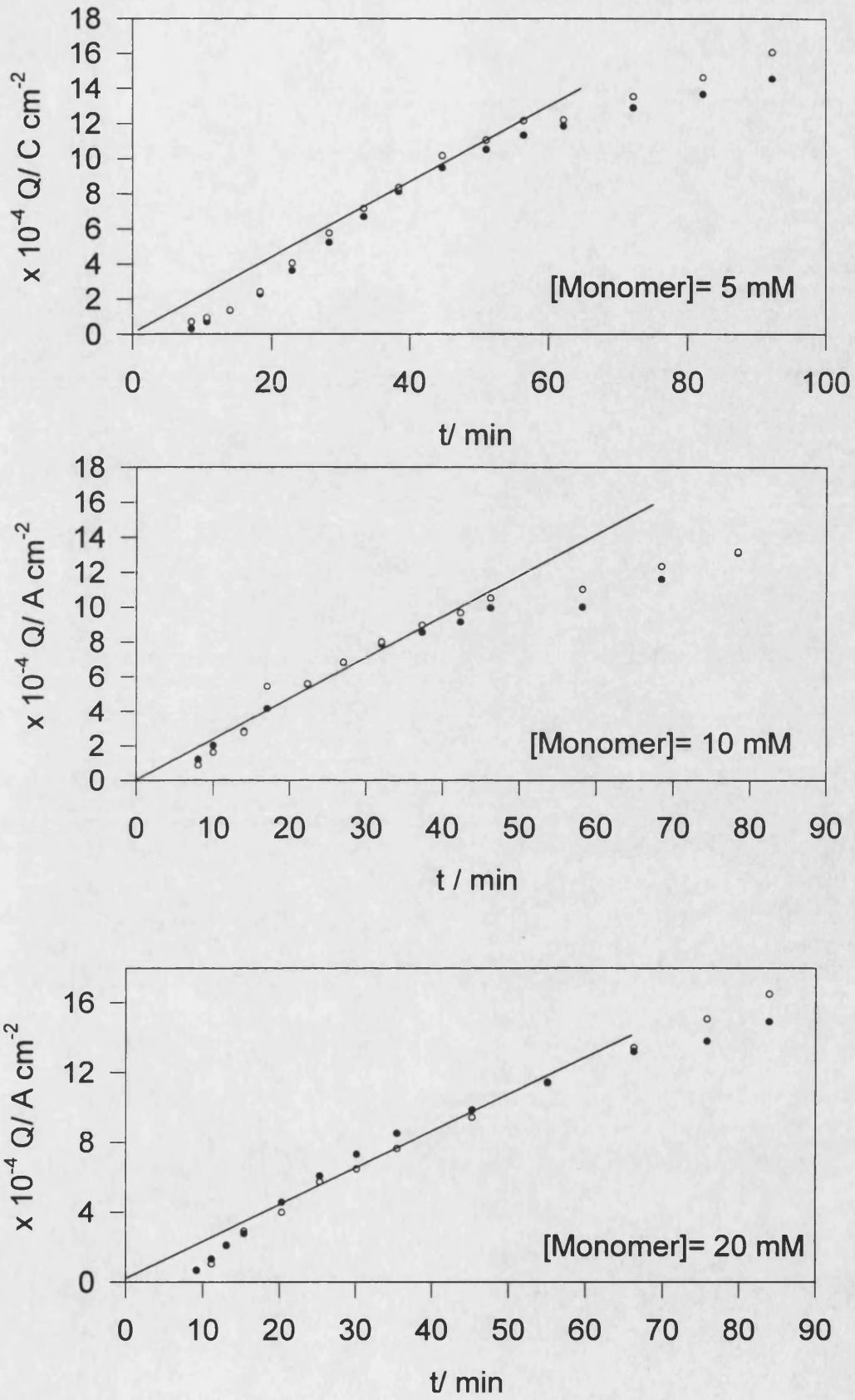

Figure 4.11 Anodic and cathodic charge for peaks c and d (figure 4.5) during the growing process as a function of time. NaCl (0.4 mol dm^{-3}) and HCl (pH 0.9).
• Anodic process ◦ Cathodic process

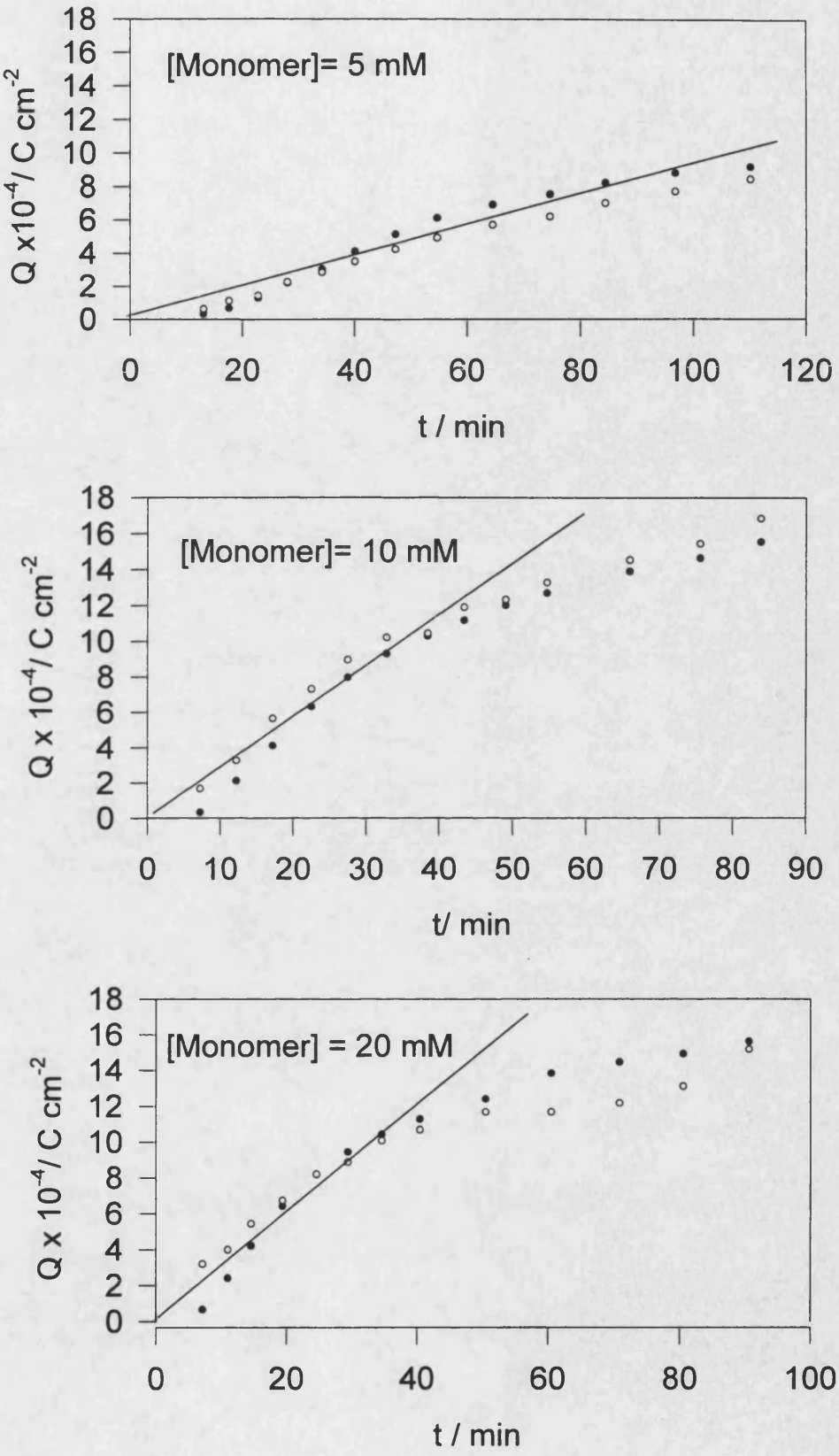

Figure 4.12 Anodic and cathodic charge for peaks c and d (figure 4.5) during the growing process as a function of time. $NaNO_3$ (0.4 mol dm^{-3}) and HNO_3 (pH 0.9).
• Oxidation ° Reduction

is a deviation from the linear behaviour due possibly to the difficulty of precipitating the cyclic dimer or its polymer at low concentration. This agrees with the decrease of the induction time when the polymer was grown in previously electrolysed solution. However, the polymer was never detected before the first five minutes cycling.

Secondly, there is a region, immediately after the induction time, where a constant polymer growth rate is observed. Figure 4.10 shows the pattern of polymer growth in sodium sulphate; the plot does not exhibit the negative deviation observed at shorter times and lower concentrations, when NaCl, $NaClO_4$ and $NaNO_3$ were used as supporting electrolytes. On the contrary, a wide linear region can be seen. It is possible that the solubility of the polymer in this medium is lower than in the others or that the higher concentration of Na^+ ions favours the precipitation of the film. For all the cases, the linear polymer growth region ceases after forty-fifty minutes cycling or when 0.8-1.0 mC cm^{-2} are consumed. This corresponds to a thickness of about 30 nm (calculated from equation 3.3, section 3.7); after that point, the polymer carries on growing but much slowly than in the early stages of the process. The fact that the nature of the supporting electrolyte and the concentration of monomer do not significantly affect on this change suggests the presence of some kind of hindrance to the propagation of the polymer chain; a larger chain could mean a greater proportion of the opened-ring structure in the film so that its conductivity would decrease with the polymer growth. However, the coupling of opened-ring structures to the growing chain is a random process that would not lead to a well defined change when the film thickness reaches at 30 nm. It seems more likely that a non-conducting oxidised form of the polymer grows continuously until the pores become small enough to hinder the movement of oAP units to the electrode surface to produce more radical cations.

Attempts were made to produce the film potentiostatically by an oxidation step from 0.0 to 0.75 V, but no film was observed by cyclic voltammetry even after three hours. However, a train of pulses from -0.25 → 0.75V (with a duration of five seconds per step, applied for two hours) gave rise to a polymer of identical electrochemical behaviour and morphology to that formed by cyclic voltammetry. Clearly the oxidation-reduction of the cyclic dimer of oAP is a necessary process which leads to the formation of the polymer.

POAP films were deposited on Pt disc ultramicroelectrodes (about 10 μm diameter) by cycling the potential between -0.25 and 0.7 V; however, the peaks corresponding to the polymer were not observed when the modified electrode was transferred to a monomer free solution. It is possible that POAP is partially soluble in the medium. The loss by solubility of the film is more important when ultramicroelectrodes are used because of the small mass deposited on the electrode surface, no saturation of the solution and the highly efficient radial diffusion[29]. Attempts were made to saturate the free monomer solution with polymer in other to avoid or minimise this loss by solubility effect. For this, a large area polymer modified electrode (1 cm^2) was introduced into the solution and left there for four hours. However, no polymer was detected on the ultramicroelectrode after this procedure.

4.3 Morphology of POAP films

Samples of POAP film were deposited on the Pt disc electrodes shown in figure 3.4. Aqueous solutions of different supporting electrolyte ($NaClO_4$, Na_2SO_4, $NaNO_3$, NaCl , 0.4 mol dm^{-3}) at pH 0.9 were used as media for the growth of the polymer. All the films were grown for about ninety minutes. Afterwards, electrodes were dismantled and allowed to dry overnight in a dessicator that contained silica gel.

Finally, the head of the electrode was fixed on a metallic disc by using electrically conductive silver paint. Direct observation of the film was not possible due to the low conductivity of the film, so that a thin layer of gold was sputtered over the electrodes. Figure 4.13 shows a view of the polymer modified electrode formed in $NaClO_4$ solution. A very compact and uniform layer of polymer was deposited all over the available electrode surface.

Because of the very smooth surface and the uniformity of the film, it was difficult to find differences between the polymer modified electrode surface and the naked platinum electrode. It was therefore necessary to scratch the surface to observe the detailed morphology of the films (figures 4.13 - 4.15). The film is seen as a compact sheet which breaks into pieces when it is scratched by a pin. This appearance is quite similar to those obtained when the other supporting electrolytes were used. This morphology differs from the granular appearance reported by Kunimura[19] for POAP film deposited on ITO glass electrode or the nanometer-scale bundles structures of polyhydroxyaniline deposited on Pt[30,31] . In the latter case, the samples were maintained under high vacuum for forty eight hours prior to STM analysis so that some loss of solvent could have taken place.

4.4 IR Spectrum of POAP

A film formed by potential cycling of a Pt electrode in 10^{-2} mol dm^{-3} orthoaminophenol solution was washed and dried overnight in dessicator containing silica gel. The polymer film is quickly oxidised when it is exposed to the air. The modified electrode was then fixed in the device showed in figure 3.8 and fitted into the FTIR spectrophotometer. Reflection spectra were averaged over one hundred scans.

Figure 4.16(a) shows IR spectra obtained from the POAP film in this work. The broad band centred at 3400 cm^{-1} may be assigned to the stretching of N-H bonds,

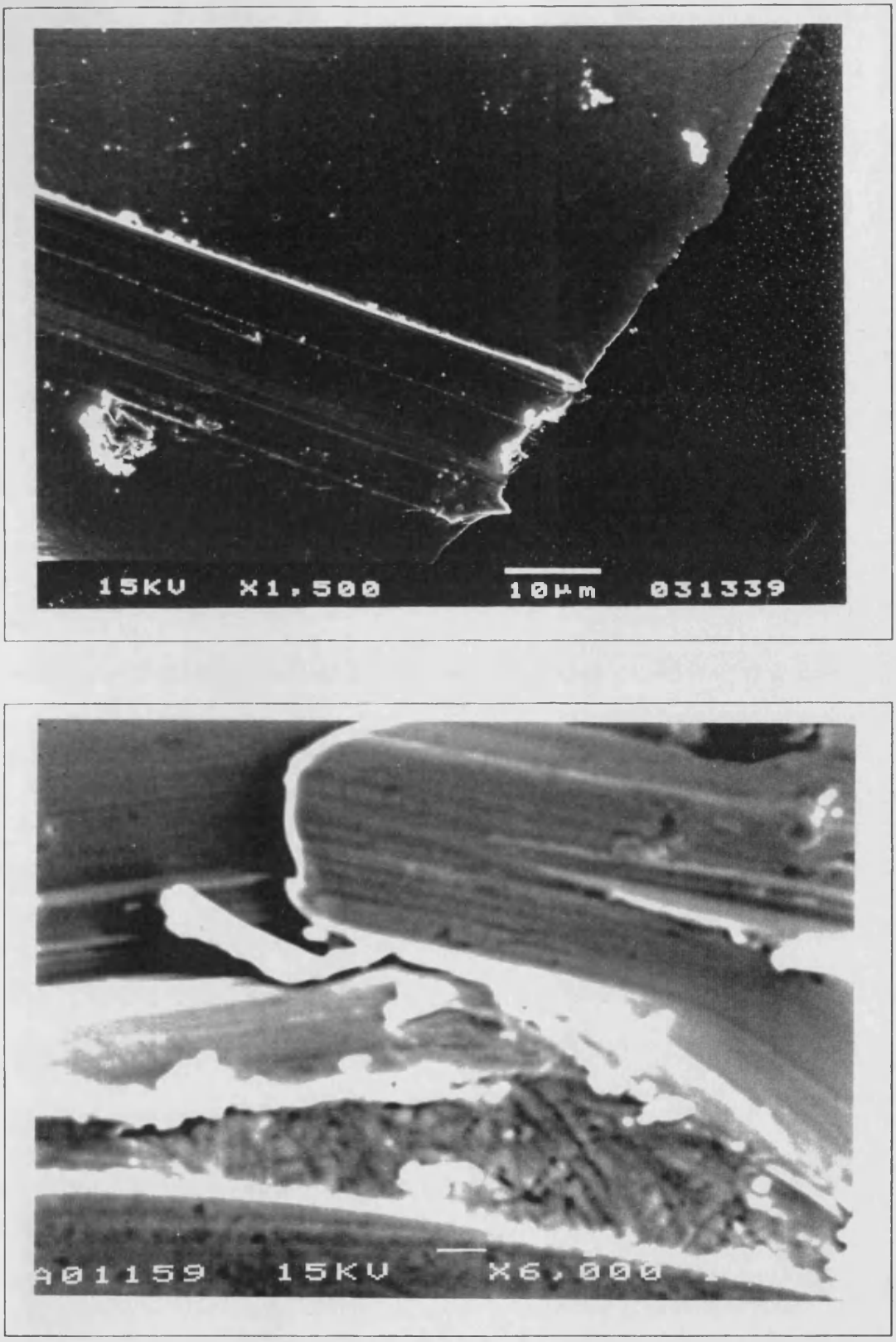

Figure 4.13 Above, view of a scratched POAP modified platinum electrode . Below, a more detailed SEM photograph of the polymer. In both cases the polymer was grown in $NaClO_4$ (0.4 mol dm^{-3}) solution at pH 0.9.

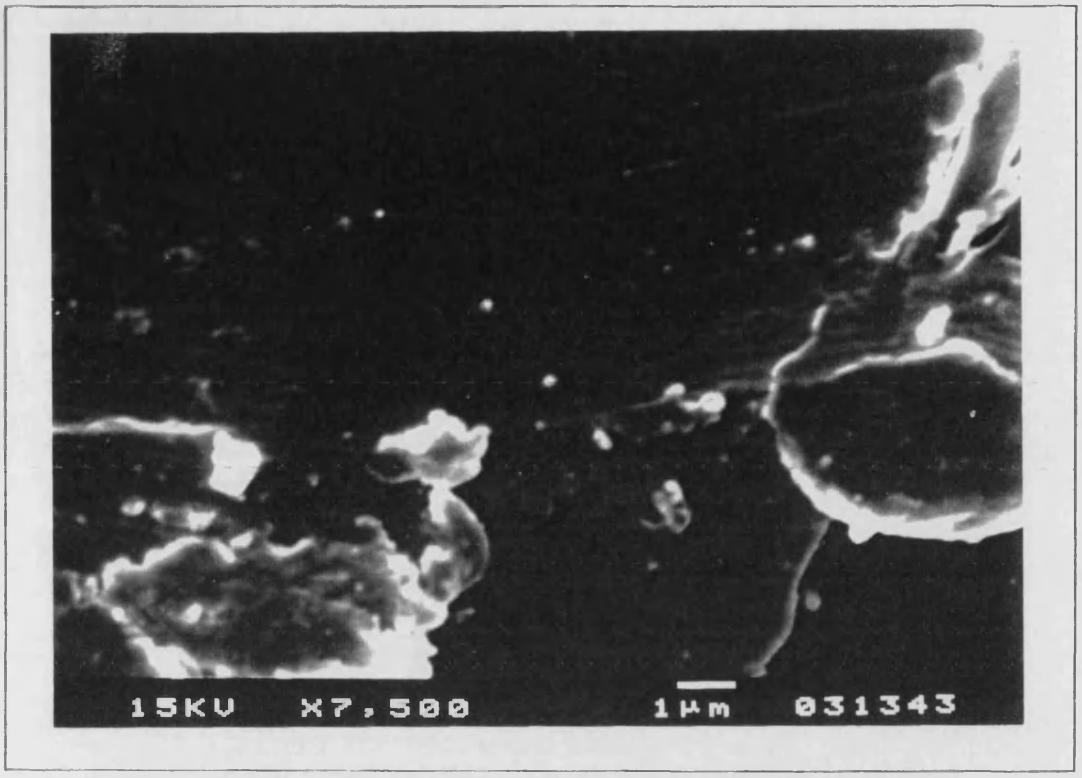

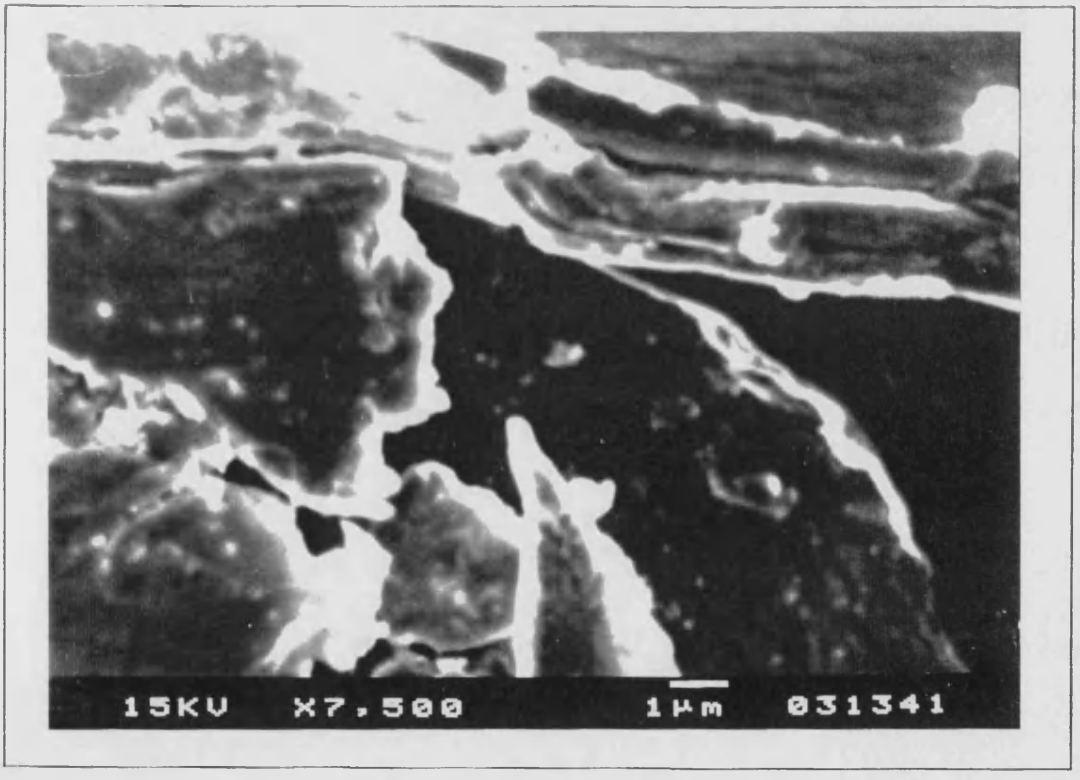

Figure 4.14 SEM photographs of POAP grown in : above, $NaNO_3$ (0.4 mol dm^{-3}) HNO_3 (pH 0.9) solution; below, Na_2SO_4 (0.4 mol dm^{-3}) and H_2SO_4 (pH 0.9)solution.

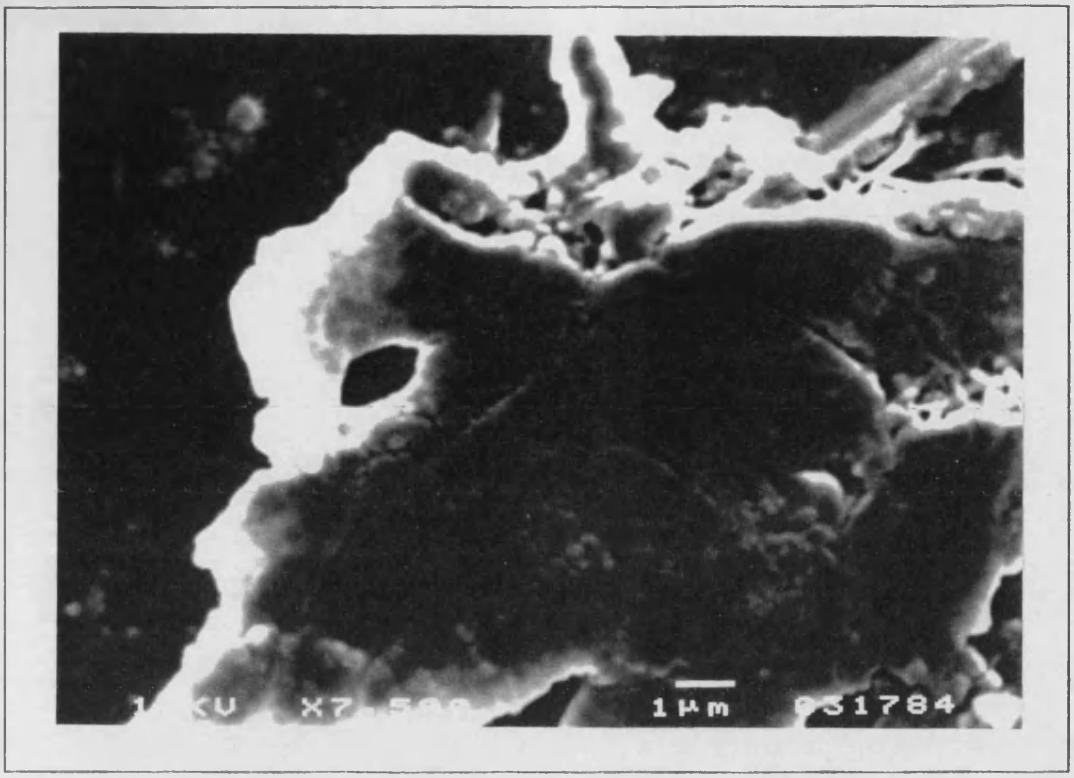

Figure 4.15 SEM photograph of POAP grown in NaCl (0.4 mol dm^{-3}) solution at pH 0.9.

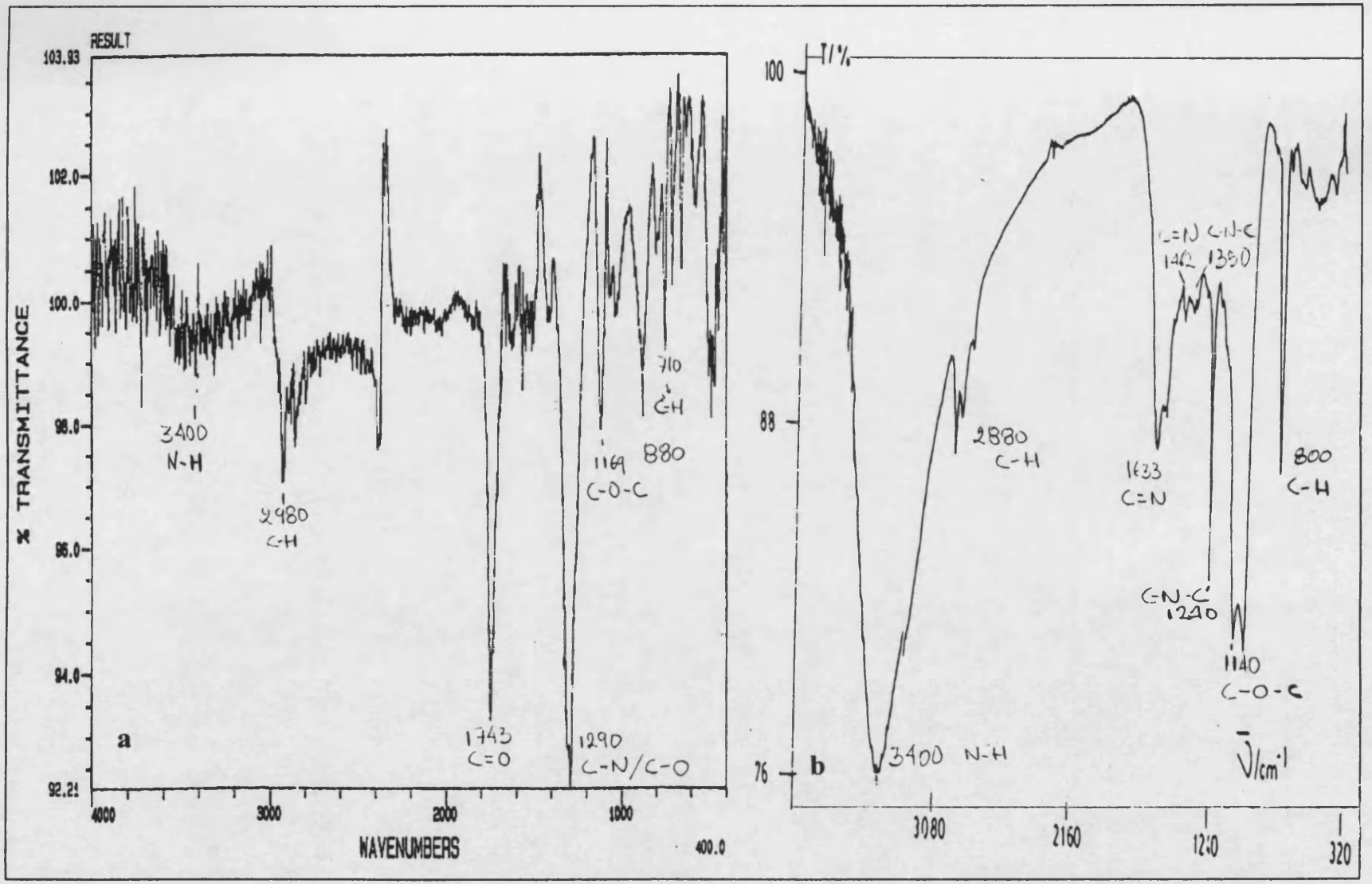

Figure 4.16 IR spectra of POAP obtained in this work (a) and the one reported by Barbero[2].

although it can also be due in part to the presence of some water. Peaks at 880 and 710 cm^{-1} may correspond to the -C-H bending vibration of aromatic rings. The absorption peak at 1290 cm^{-1} is characteristic of the C-N-C stretching vibrations of secondary amines overlapped with the C-O-H stretching vibration for aromatic rings. The peak corresponding to 1169 cm^{-1} can be assigned to C-O-C stretching mode. The peak at 1743 cm^{-1} could be ascribable to C=O stretching mode in a six membered ring[32]. The absorption peak corresponding to C=N stretching is not observable (1690 to 1640 cm^{-1}); this vibration mode is difficult to identify due to large variations in its intensity and, sometimes, to the closeness to C=C stretching region[33]. Barbero[2] and Kunimura[19] assigned this vibration mode to the peak at 1645-1633 cm^{-1}. The IR spectra of films peeled off the electrode and taken from a KBr pellet [2,19] showed also the absence of absorption of carbonyl group ($\approx$ 1700 cm^{-1}), this agrees with the closed chain structure of the polymer film (figure 4.2). By contrast, the presence of a relatively weak absorption at 3400 cm^{-1} and the strong absorption of the C=O band obtained in the present work seems to indicate that the partially opened structure shown in figure 4.2(d) is present when the polymer is extensively oxidised. Differences in the IR spectra of figure 4.16 suggest that different oxidised form of the polymer are formed : a closed structure (by Barbero[2]) and the opened ring in the present work.

The presence of quinone as a product of the atmospheric oxidation of o-AP is possible, as was proposed for anilines[34]. This would involve the existence of a carbonyl band corresponding to the contribution of quinone in the structure of the polymer.

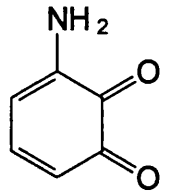

6-amino-o-quinone

In order to avoid this contamination, the monomer was recrystallised three times in ethyl acetate, dried and stored as specified in the Chapter 3, section 3.1. IR and NMR spectra were taken from the this sample. No carbonyl band was observed in the IR spectrum of the purified o-AP and all the bands fit exactly to these reported in the literature[35]. The IR spectral data for POAP and o-AP are summarised in Table 4.1 . NMR spectrum of the monomer showed the peaks corresponding to the three kind of hydrogens in the compound (-OH, $-NH_2$ and aromatics) with excellent ratio of integration, i.e. agreement in the assignment of the number of protons to each signal. The ^{13}C NMR spectrum of the purified o-AP showed the absence of signal in the range where ketones, aldehydes, carboxylic acid and quinones are active because of the carbonyl group[32] (165 - 220 ppm) so that the presence of quinone can be ruled out. On the other hand, the contribution of ClO_4^- to the spectrum is negligible[36] because of its weak band at 1092 cm^{-1}.

4.5 Cyclic voltammetry of POAP

Electrodeposited films of POAP were washed with plenty of ultrapure water and introduced into a $NaClO_4$ (0.4 mol dm^{-3}) solution, at pH 0.9, which was free of the monomer. The potential was then scanned between -0.25 and 0.7 V. A typical result is shown in figure 4.17. The polymer exhibits a broad and small oxidation peak and a sharper and higher reduction peak near, both of them, to 0.0 V. The charge consumed during the oxidation process is almost completely regained during the opposite scan,

Table 4.1
IR Absorption Spectra of PAOP film and o-AP

Vibration Mode	(C-H)[a] cm^{-1}	(C=C)[a] cm^{-1}	(C-H)[b] cm^{-1}	(N-H)[c] cm^{-1}	(C-N)[d] cm^{-1}	(C=N)[e] cm^{-1}	(C-O-C)[f] cm^{-1}	(C-O)[g] cm^{-1}	(C=O)[h] cm^{-1}
o-AP	2980	1603	846-764	3373-3302	1267	-	-	1267	absent
POAP	2980	-	880-710	3400	1290	-	1169	1290	1743

[a] Stretching vibration of the C-C and C-H bonds of benzene nuclei.[b] Out of plane bending vibration of the C-H bonds of benzene nuclei. [c] Stretching vibration of the N-H bonds. [d] Stretching of the C-N bonds for aryl NH compounds.[e] Stretching vibration for C=N bonds (about 1640cm^{-1}), undetectable in either POAP spectrum or o-AP used in this work.[f] Stretching vibration of the C-O-C bonds.[g] Stretching vibration of the C-O bonds for diaryl ethers which could be overlapped wuth *d*.[h] Stretching vibration of the C=O bonds for a six membered ring ketones.

figure 4.17(a). The differences between initial and final charge depend on the scan rates; the higher the sweep rate is, the smaller this difference becomes. It is possible that some hydrogen evolution takes place when the potential of the modified electrode reaches negative enough values. At 0.2 V s^{-1} the time scale of the experiment is short and the hydrogen evolution occurs to a lesser extent than at 0.050 V s^{-1}. Hydrogen evolution and the peeling off of the polymer were observed when the potential was scanned beyond -0.25 V, which supports this conclusion.

The charge consumed during the oxidation and reduction processes is proportional to the number of active sites or monomeric units that were involved in the reaction, so that the slopes of the q vs. E plots represent a measurement of the rate at the reaction is taking place (i.e. E changes as a function of time). It is difficult to compare rate values which have been taken at different scan rates because other factors, such as swelling or the charge transport resistance[37] of the film, could be controlling the overall process. However, comparison of the slopes corresponding to the oxidation and reduction at the same sweep rate gives an idea of the relative rates of each process. Figure 4.18(a) shows the charge change as function of time at 50 and 200 mV s^{-1} . The increasing region corresponds to the oxidation and the following decreasing one to the reduction of the film. The rate for the oxidation seems to be slower than for the reduction of the film. The set of points in figure 4.18 was taken from the interval where the anodic and cathodic voltammetric peaks appear; from the relative slopes it is possible to say that reduction occurs twice to three times faster than the oxidation.

The different shapes of the voltammetric waves have been qualitatively interpreted in terms of reduced and oxidised activity effects modulated by solvent

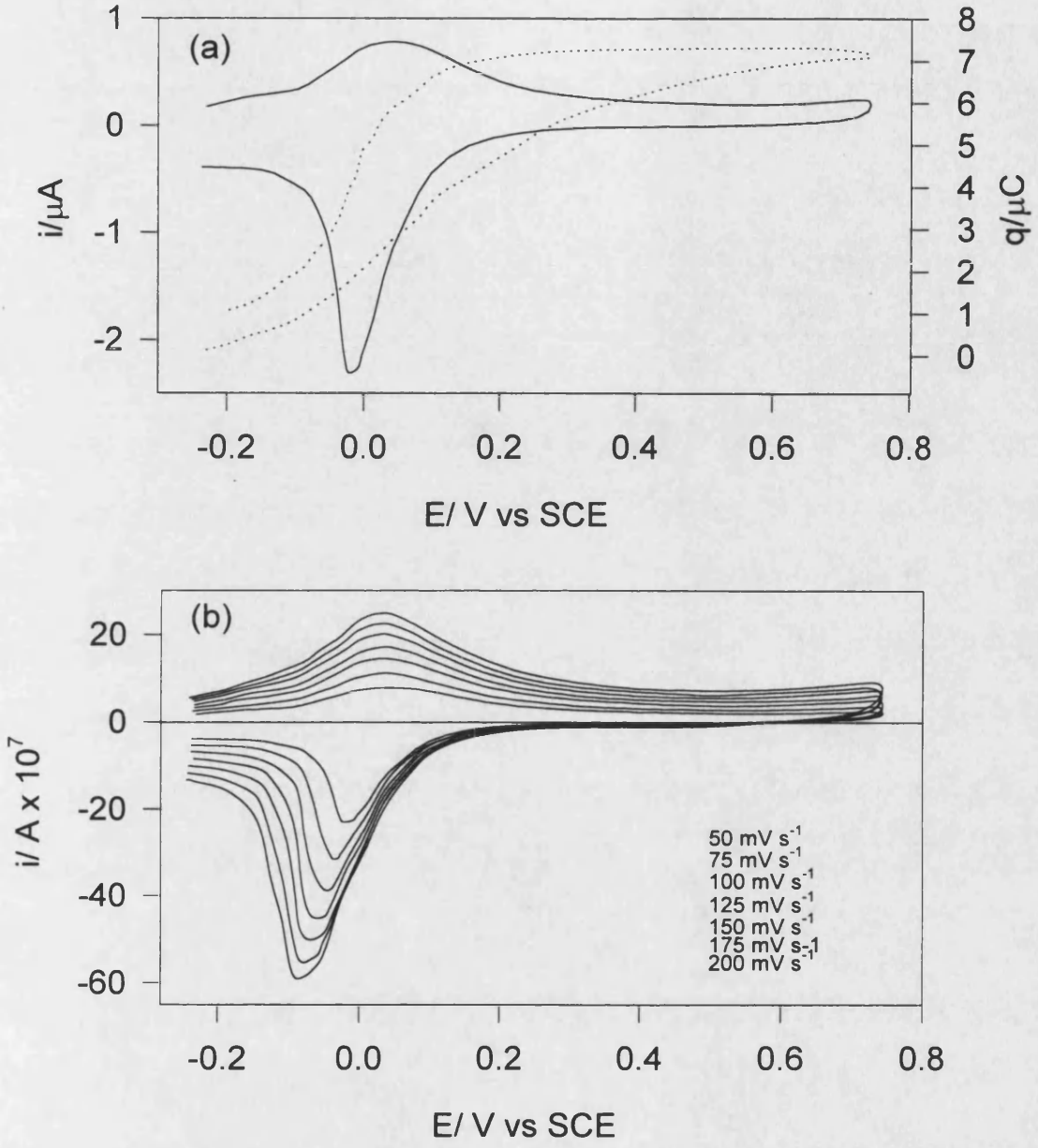

Figure 4.17 Cyclic voltammetry curves for a 32 nm thick POAP film deposited on Pt (1.9×10^{-3} cm^2). (a) Charge vs E plot and voltammogram at 50 mV s^{-1}. (b) Effect of the sweep rate on the voltammogram. Blank solution: 0.4 mol dm^{-3} $NaClO_4$ at pH 0.9 .

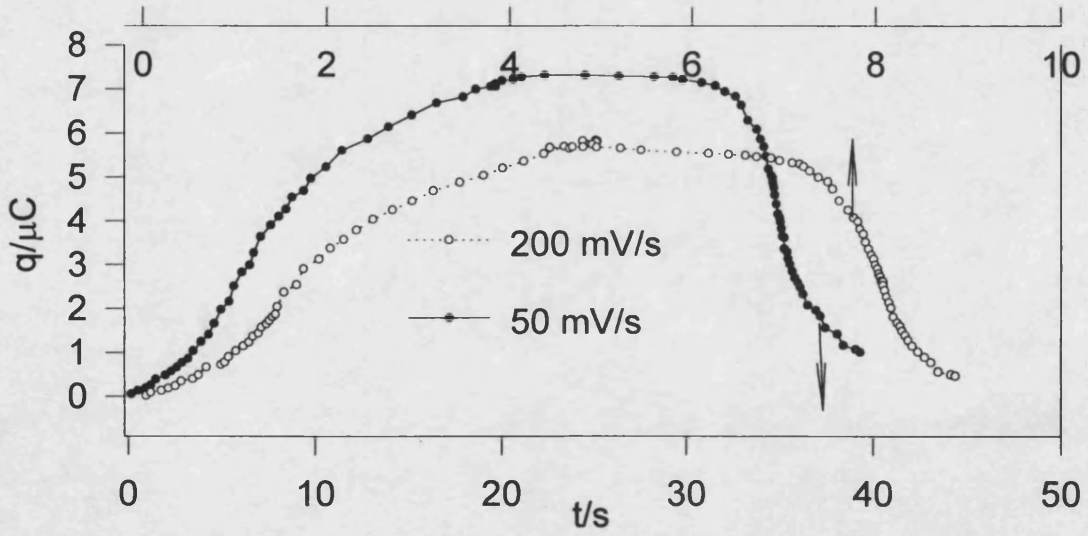

Figure 4.18 q vs t plot for reduction and oxidation of POAP at different ν, from figure 4.17.

swelling of the film[38]. The presence of a significant swelling of the polymer in one of its redox state with respect to the other will decrease the internal number of active sites per volume unit so that a small and broad peak could be expected. The affinity of the film for a particular solvent will depend on the nature of the solvent as well as the nature of the film. Polyvinylferrocene, for example, exhibits a similar and inverted set of peaks with respect to POAP, with an oxidation peak rising and falling sharply[39] when thick films are analysed in aqueous solutions. More symmetrical and broad cyclic voltammograms are obtained[40] when acetonitrile is utilised as solvent. The broadening of the waves in polyvinylferrocene has also been attributed to repulsive interactions [41] of redox centres or differences in their spatial distribution[42]. The shape of the cyclic voltammograms could also be due to the fact that the film becomes insulating when it is oxidised, so that further oxidation is limited by resistance. Reduction, on the other hand, give rises to a conducting film making further reduction easier. This is the opposite way round to polyaniline, for example, where a sharp peak is seen on oxidation[43], and a broad one on reduction.

Cyclic voltammograms of POAP at different scan rates are shown in figure 4.17(b). The anodic peak potential does not change with the sweep rate in the range studied. On the other hand, the cathodic peak potential is shifted to more negative values as the scan rate increases. The peak separation increased from 36 mV at 50 mV s^{-1} to 106 mV at 200 mVs^{-1}. This dependence of the cathodic wave on the sweep rate can probably be attributed to an uncompensated ohmic resistance of the film. If the polymer exhibits an ohmic resistance to charge flow, which cannot be compensated by the potentiostat, the actual potential at the electrode-polymer interface would be smaller than that applied potential; under this circumstance, a shift to more negative potentials

should be seen for a reduction process. The peak potential is then shifted by approximately the amount of iR drop. The fact that the cathodic wave is sensitive to the potential scan rate and the very small currents observed during the reverse reductive scan suggest that the polymer is not conducting in its oxidised form. After the reduction of the polymer, the film appears to become conductive so that the anodic peak potential is not significantly affected. This conclusion is opposite to that one given by Barbero[24] in basis to the oxidation-reduction of some redox species on POAP modified electrodes at positive potentials. Differences in the IR spectra suggest that the oxidised form of the polymer is different in both cases so that is possible to expect different electrochemical behaviour as well.

Figure 4.19 shows the change in Ep_c as a function of the cathodic peak current; data were taken from figure 4.17(b). The resistance determined from the slope of the straight line is too high to be assigned to the electrolyte resistance and the extrapolation of the plot to zero current gives the anodic peak potential in the absence of ohmic affects, which was determined to be 0.021 V. This "iR corrected" peak potential is very close to the Ep_a (0.030 V) calculated from the figure 4.17(b) so that the redox process in the polymer could be quite reversible in absence of ohmic effects. The slope of straight line in the figure 4.19 is a good approximation to the resistance of the film. Knowing the film resistance, it is possible to calculate the conductivity of the polymer layer in its oxidised form provided that the film thickness is known. The determined conductivity value found in this way is very low: 9.3×10^{-8} S cm^{-1}. This conductivity is one order of magnitude smaller than that reported by Kunimura[19] for the polymer in its dry state and four orders of magnitude smaller than that determined by Barbero[24] using redox couples. The zero current extrapolation, at different pH

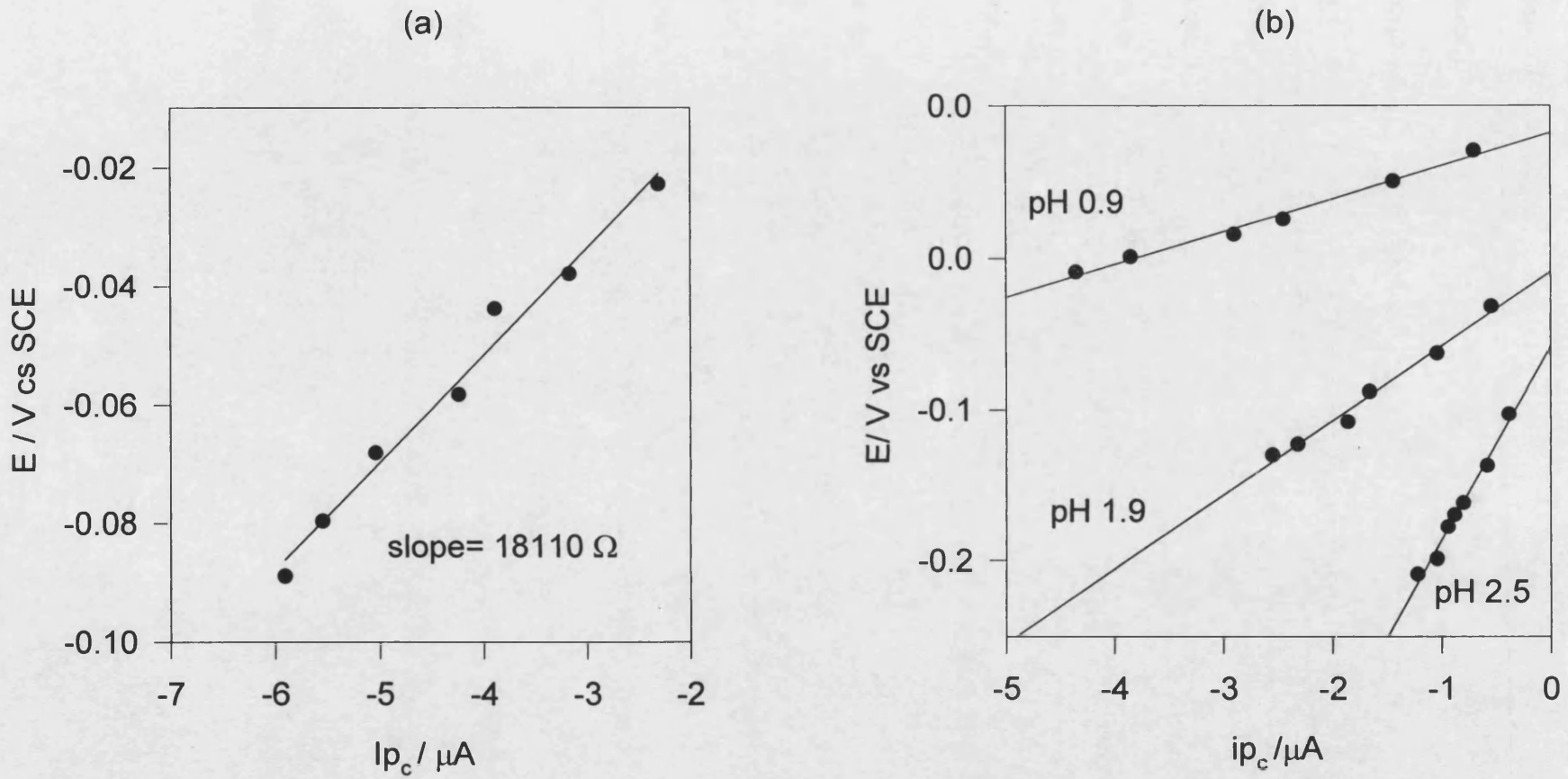

Figure 4.19 Cathodic peak potential as a function of the cathodic peak current from (a) data of figure 4.17. (b) from a 35 nm thick film at different pH values. Solutions contained $NaClO_4$ (0.4 mol dm^{-3}) and the area of the electrode was 1.9 x 10^{-3} cm^2 for all the experiments.

values, was applied in figure 4.19(b) in order to differentiate between the pH dependence of the film resistance and the effect of the film resistance on the peak potentials. Figure 4.19(b) shows an increase of the slopes, i.e. a decrease in the conductivity of the film, with the pH. Calculated conductivities were 8.7×10^{-8}, 3.7×10^{-8} and $1.4 \times 10^{-8}\ \Omega^{-1}\ cm^{-1}$ for pH 0.9, 1.9 and 2.5, respectively. Extrapolated peak potentials shift negatively as pH increases and their values are separated for less than 10 mV from the voltammetric anodic peak potentials. Thermodynamic effects are separated nicely from resistive effects by the plot. The presence of a strong band corresponding to carbonyl groups in the IR spectrum of the film indicated that the opened structure of the figure 4.2 (d) is present when the polymer is in its oxidised form; this configuration may minimise the delocalization of the charge along the polymer chains and would lower the conductivity to the value determined in this work. It has been also reported that configurations with planar arrangement, as ladder structure polymers, give rise to high conductivities in comparison with their nonladder polymeric precursors[44]. The opened ring structure breaks the ladder configuration so that a decrease in the conductivity is expected.

There are contradictory data concerning the dependence of the voltammetric behaviour of POAP on pH[19,24]. Kunimura[19] reported a linear plot of Ep vs pH in the whole pH range, but the experimental points are too widely spaced on the pH scale to characterise in detail the behaviour of the polymer. The peak currents were observed by the same author to decrease uniformly up to pH=12. On the other hand, Barbero[24] found that the anodic peak potential does not vary with the pH, while cathodic peak potential changes significantly in the range of 0.5 to 2.3 pH units, moving to more negatives values. The results in this work are different from those obtained by Barbero [24].

Figure 4.20 illustrates the changes of the peak currents and peak potentials as a function of the pH observed in the present work. There is no significant change either in the currents or in the peak potentials at pH values less than 1; a decrease of the currents can be seen at higher pH values. The cathodic current falls more steeply than the anodic current. The decrease in the current response indicates a loss in electroactivity of POAP film and an increase in the resistance of the film: ΔE_p values increase from 40 mV at pH<1 to 260 mV at pH 2.7 . The reduction peak disappears at about pH 4 but the oxidation peak is still observed, though very broad, until pH 6. The formal redox potential was estimated as the average[45,46] of the anodic and cathodic peak potentials(i.e. $(E_pa + E_pc)/2$); this value was plotted against pH giving a straight line with a slope of 97 mV/pH. This kind of plot could not be applicable because of the notable differences in behaviour between the anodic and cathodic peak potentials[24]. The slope of the anodic peak potential vs pH plot was estimated to be 55 mV/pH which corresponds to $1H^+/1$ electron ratio. The pH dependence for the reduction process is more complex: for pH values between 1 and 2 the slope of the line is 112 mV/pH and it increases to 226 mV/pH when the pH is between 2 and 3. The change in the slope occurs at approximately at pH 2. Barbero[24] reported linear plot of E_pc vs pH, with slopes of 180 mV/pH for the range of pH between 0.8 and 1.2 ; a second linear region with a slope of 90 mV/pH was observed from pH 1.2 to 2.2. This complicated behaviour cannot be explained at present, but the differences in the slopes obtained in this work and these reported by Barbero[24] are probably due to different composition of the polymer film.

The effect of the supporting electrolyte concentration on the cyclic voltammetry of POAP films was studied by introducing a modified electrode into $NaClO_4$ solutions with different concentrations at constant pH (0.9). Voltammograms

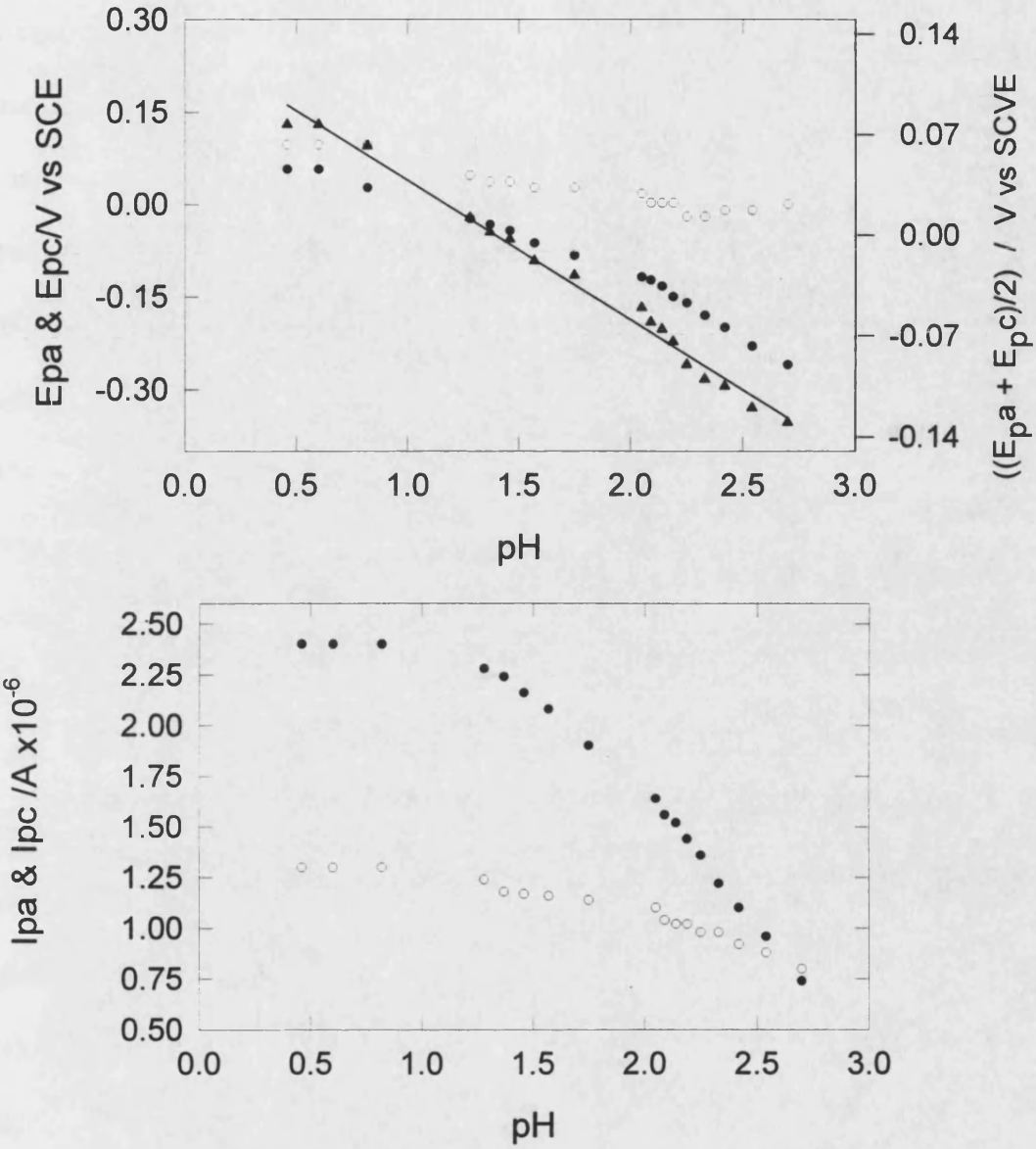

Figure 4.20 E_p vs pH (above) and I_p vs pH (below) plots for POAP modified electrode (A= 2 x10^{-3} cm^2) submerged in $NaClO_4$ (0.4 mol dm^{-3}) solution at different pH. All measurements were recorded at 100 mV s^{-1}. Thickness 0.048 μm.

○ anodic • cathodic ▲ $(E_pa + E_pc)/2$

were scanned at 100 mV s^{-1}. Figure 4.21 shows the behaviour of peak potentials and peak currents for a 60 nm thick POAP film . There is a small decrease in the peak separation from 50 mV to 36 mV when $NaClO_4$ concentration is increased from 0.1 to 0.64 mol dm^{-3}. Both peaks move to more positive potentials with the increase in the supporting electrolyte concentration. On the other hand, the cathodic current increases slightly while the anodic current remains almost unchanged. Both peaks seem to become a little sharper. This kind of variation of peak currents and peak potentials with the electrolyte has been explained by salt formation between redox sites in the film and the counterions[47,48] as well as the swelling of the polymer[46]. Interaction between water and redox centres will be extensive in the presence of counterions that lead to more soluble salts so that the degree of solvent swelling will be higher. As the electrolyte concentration is increased, films will become more compact. This effect tends to enhances the rate of electron transfer but, at higher electrolyte concentration, simultaneously restricts access of counterions into the film[46,49], minimising the rate of charge transport. The increase of peak currents and decrease of peak separation could be associated with the former effect while the decline of the currents at concentrations higher than 0.4 mol dm^{-3} could be due to a deterioration of the film permeability for counterions. The weaker influence of supporting electrolyte concentration on the anodic peak current, with respect to the cathodic peak current, may indicate that the reduced form of the polymer is comparatively swollen and the contraction of the polymer is no significant. Swelling of the film was detected by crystal impedance measurements, see section 4.10.

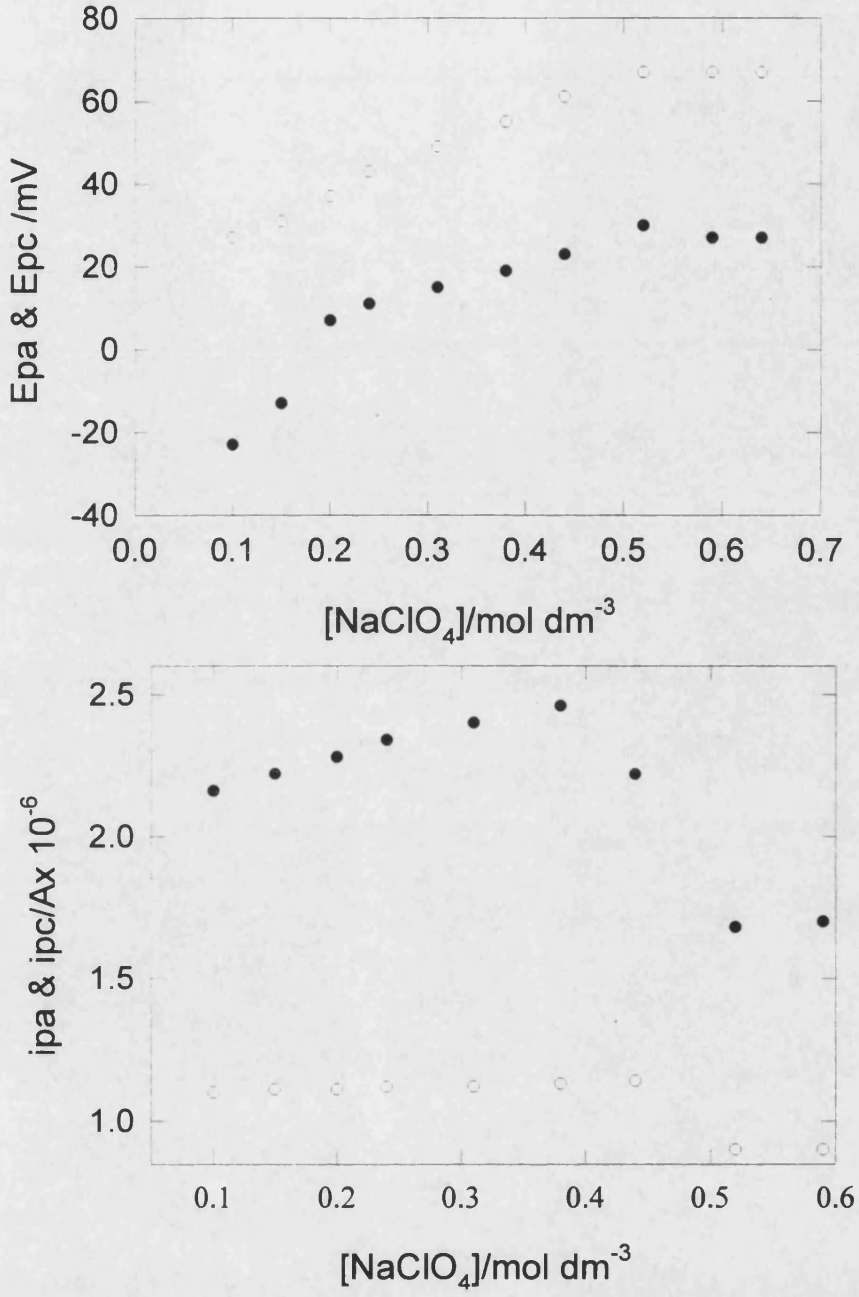

Figure 4.21 Effect of the supporting electrolyte concentration on peak potentials peak currents for POAP deposited on Pt (2 x 10^{-3} cm^2). Thickness 0.060 μm. pH 0.9. ν=100 mV s^{-1} Anodic • Cathodic

4.6 Chronoamperometry

Figure 4.22 shows potentiostatic current transients obtained by stepping the potential from -0.2 V vs SCE to a series of potentials towards the region of the oxidation of the polymer and back to initial value of potential. The duration of the pulses was 100 ms. The first peak corresponds to the oxidation of the polymer and the second to the reduction of the film. The straight line obtained by j vs $t^{-1/2}$ for the decay regions of the current transients (figure 4.23) seems to indicate that diffusion is dominant in the first stage of the redox process. In this case, incorporation of counterions into the film could be the limiting step.

The slopes of j vs $t^{-1/2}$ plots for the oxidation transients of figure 4.22 increase with increase in the potential limit following the Cottrell equation (2.23). From these slopes, the $CD^{1/2}$ values for oxidation process at 0.45V, 0.35 and 0.15 V were determined to be 1.4×10^{-7} , 1.2×10^{-7} and 0.6×10^{-7} mol cm^{-2} $s^{-1/2}$. The concentration of actives sites, C, can be calculated from the charge under the voltammogram by using the expression[51] $C = \Gamma/d$; where Γ is the number of mol of active units per area unit (mol cm^{-2}) and d is the thickness of the film. Diffusion coefficient values, calculated using $C = 3.4 \times 10^{-3}$ mol cm^{-3}, were 1.6×10^{-9} , 1.3×10^{-9} and 0.3×10^{-9} cm^2 s^{-1} , for the oxidation at 0.45, 0.35 and 0.15 V respectively. The values of diffusion coefficient reported here are in good agreement with the value reported previously[19] which is 0.36×10^{-9} cm^2 s^{-1}. It is important to note that in the calculation of C, swelling film is not considered. Dramatic changes in the concentration of actives sites could take place by the swelling of the polymer during the redox process. Because of this, calculated diffusion coefficient could be greatly affected. As will be shown in section 4.10,

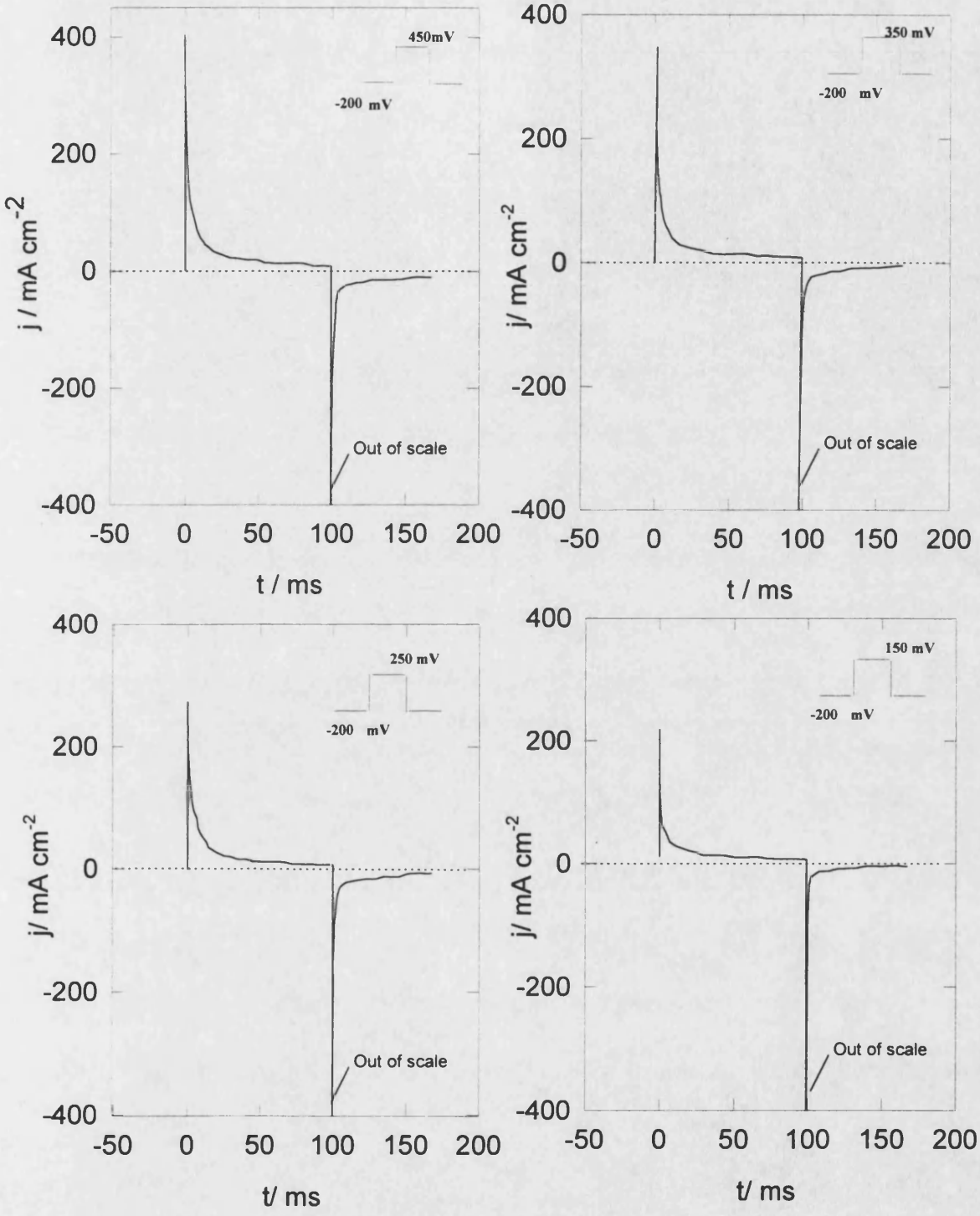

Figure 4.22 Current transients of a 37 nm POAP film on Pt electrode. Potential steps are shown in the right upper corner of each plot. Solution was $NaClO_4$ (0.4 mol dm^{-3}) at constant pH (0.9).Electrode area 0.11 cm^2.

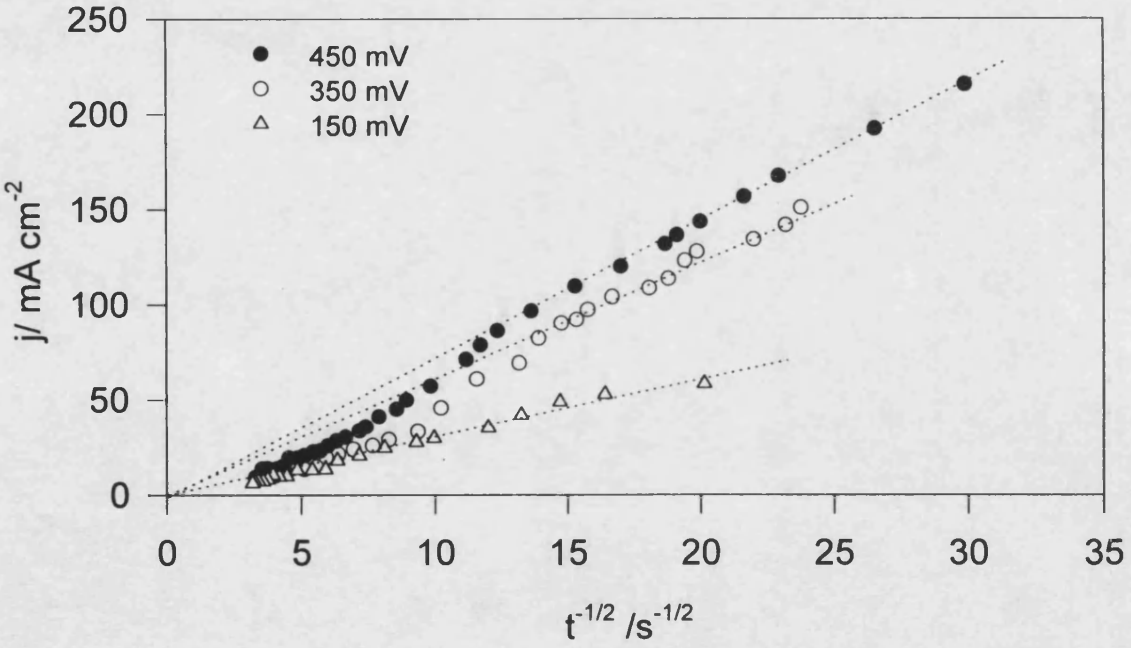

Figure 4.23 Cottrell plots of the current density (j) versus $t^{-1/2}$ obtained from the falling region of the current transients at pH 0.9.

polymer is more swollen in its reduced form so that the increase in the slopes of the figure 4.23 at higher oxidative potential steps is an artefact of the swelling of the film.

Another feature of the potentiostatic transients of the film is the short timescale in which the oxidation and reduction takes place. In 100 ms the oxidation process is almost completed, see figure 4.24(a). Although this process is quite fast it is comparably slower than the oxidation of a polyaniline[50] film of similar thickness (45 nm) which was found to be completely oxidised in less than 0.5 ms. The author reported a large diffusion coefficient of 2.0 x 10^{-4} cm^2 s^{-1} for polyaniline.

The linear regions at shorter times in Q-$t^{1/2}$ and j-$t^{-1/2}$ plots, see figure 4.24, are consistent with the Cottrell behaviour. A longer times the value of charge tends to approach a limiting value while the current density shows a negative deviation. The limiting value of charge of the figure 4.24(c) is approximately 1.2 mC cm^{-2} which is close to that charge density calculated for the oxidation of the film from the cyclic voltammogram recorded at slow scan rate (1.4 mC cm^{-2}, at 20 mV s^{-1}). The fall-off of the current density at longer times in the figure 4.24(b) indicates that the volume of polymer film cannot be taken as infinite[51,37] and a transition occurs from semiinfinite diffusion condition to a finite diffusion[52] condition. This diffusion behaviour is characteristic of thin conducting films and its theory was developed by Murray[37,23] et al. based in a thin layer approach[52]. The expression for current as a function of time is given by

$$i = \frac{nFAD^{1/2}C}{\pi^{1/2}t^{1/2}} \sum_{k=0}^{\infty} (-1)^k \left[\exp\left(-\frac{k^2 l^2}{Dt} \right) - \exp\left(-\frac{(k+1)^2 l^2}{Dt} \right) \right] \qquad (4.1)$$

Here, l is the thickness of the solution and the rest of the terms are as described in Chapter 2, section 2.2. Equation 4.1 tends to Cottrell equation when $l^2 > Dt$. At longer

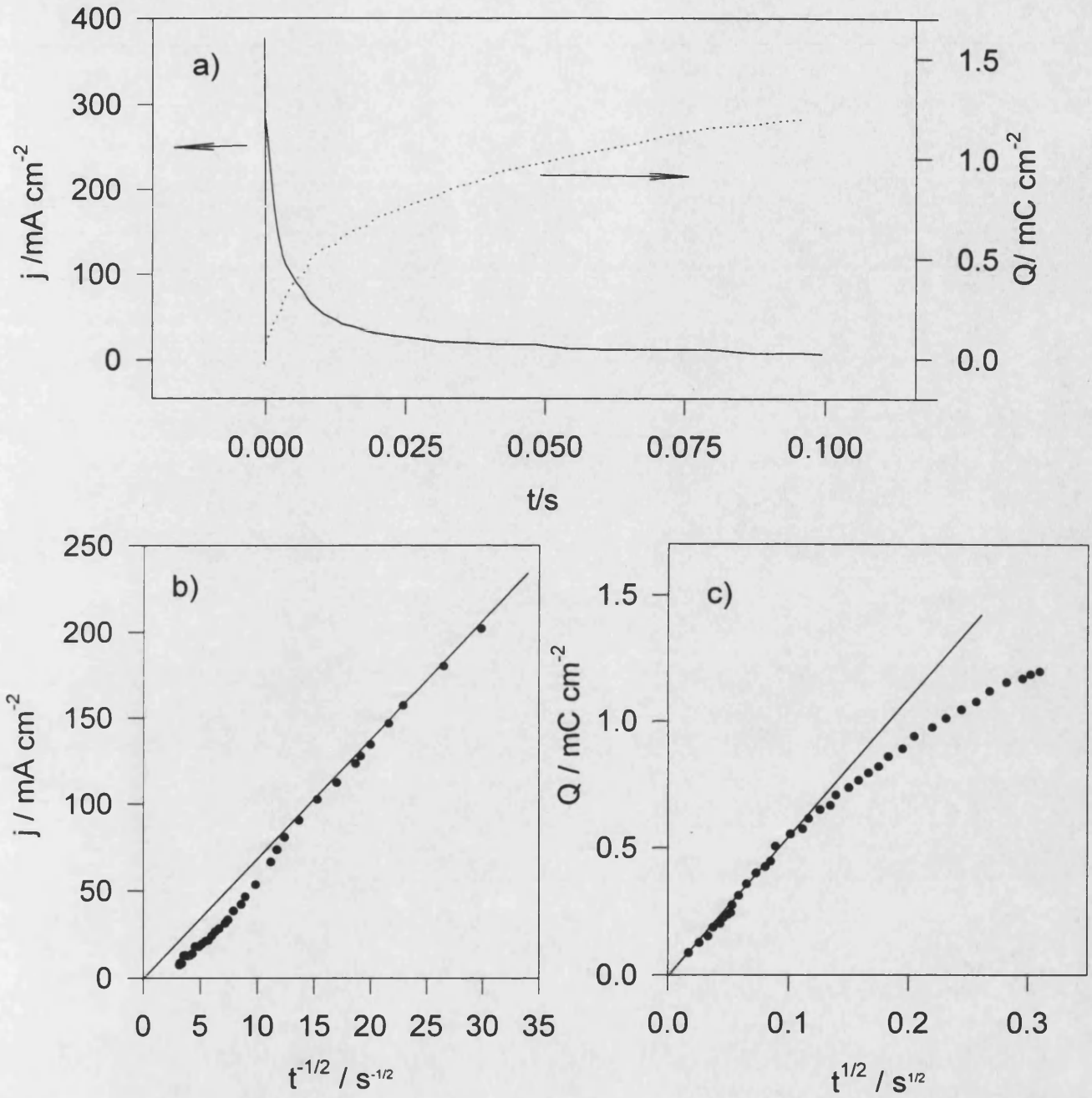

Figure 4.24 (a) I vs t and Q vs t plots for the oxidation of a 37 nm thick film. Potential step was from -0.2 to 0.45 V. (b) and (c) plots of the current density j and charge density Q obtained from the falling region of (a) as a function of $t^{-1/2}$ and $t^{1/2}$, respectively.

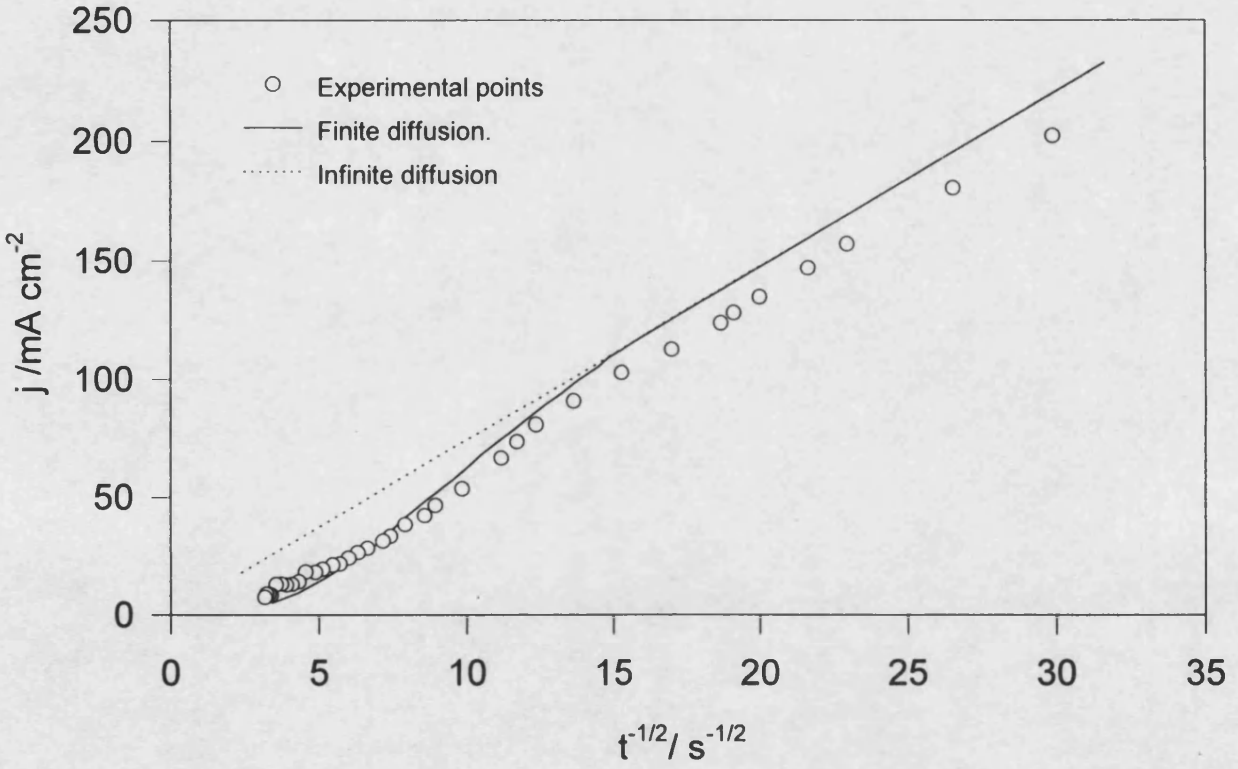

Figure 4.25 Cottrell plots for infinite (-----) and finite diffusion (——) calculated by using A=0.11 cm^2, D = 1.6 x $10^{-9}cm^2$ s^{-1} and l= 37 nm. Points represent values corresponding to the transient recorded at 450 mV.

times, the second term gives rise to a negative deviation because the diffusion profiles will impinge on the outer boundary of the polymer film. The current density-$t^{-1/2}$ data for the transient at 450 V was computed using equation 4.1 and compared with the experimental results, figure 4.25. A reasonable fitting is obtained if it is considered that the calculation of the film thickness does not take into account the possible swelling of the polymer. The better fitting of the plot at longer times, i.e. when the polymer is oxidised, may indicate that the film is less swollen that in the early stages of the application of the pulse. By ESR experiments carried out in the present work (section 4.7) it was determined that the oxidation of POAP involves formation of polarons so that this process should be accompanied by the ingress of anions for maintaining the electroneutrality; on the other hand, the proposed redox mechanism of figure 4.4 involves expulsion of protons to give the oxidised form of the film. To maintain electroneutrality the expulsion of both, protons and anions, is required. Since the mobility of protons is higher than that of anions, the slower movement of anions would be rate determining.

The cathodic currents spikes are much sharper and are always off scale at the optimum sensitivity scale for oxidation transients. In all the cases the charge density, at 50 ms, was about 40% smaller than that involves in the previous oxidation of the polymer. Current densities fell very rapidly to very small values so that the complete reduction could only be achieved if the potential is held at negative limit for longer time. Cottrell plots for this transient revealed no structure and it appears that they are controlled by the RC time constant of the cell. Consecutive trains of pulses showed random changes in the oxidation and reduction charges which agrees with the different rates of oxidation and reduction. The reduction process could proceed by a progressive

expansion of the conducting polymer strands, as will be shown in section 4.10. The 40% of the reducing charge, at early stages of the application of the pulse, could correspond to the reduction of the external layers of the film where diffusion of counterions does not play a significant role at short times and the electron transfer may be coupled to a rapid proton ingress as is indicated in figure 4.4. The remaining 60% of the charge could then be associated with the electron transfer reaction of the boundary between the conducting and no conducting regions of the film so that the slow diffusion of ions through a continuously expanding film would be rate determining.

4.8 UV-visible spectra of POAP

Figure 4.26 shows the set of spectra obtained from a 80 nm thick POAP film over the potential range from -0.30 to 0.8 V vs SCE. Each spectrum was recorded at constant potential and the wavelength was scanned from 300 to 750 nm. A waiting time of ten to twelve minutes preceded each experiment in order to allow the polymer film to equilibrate. The utilised cell is shown in figure 3.3. Solution was renewed by a fresh and oxygen free solution every thirty minutes; this procedure also helped to minimise any effect, on the spectra, due to the increase of the temperature by light absorption. The family of spectra shown in figure 4.26 illustrates the change in the oxidation state of the film. Three absorption bands are observed at 414, 492 and 690 nm. As the polymer is oxidised the absorption peaks start becoming stronger; this increase in the intensities of the bands was small in the potential ranging from -0.30 to -0.15 V vs Ag/AgCl , but large changes were observed in the spectra corresponding to -0.1 to 0.4 V. Very small modification of the peaks was noticed at potentials higher than 0.4 V.

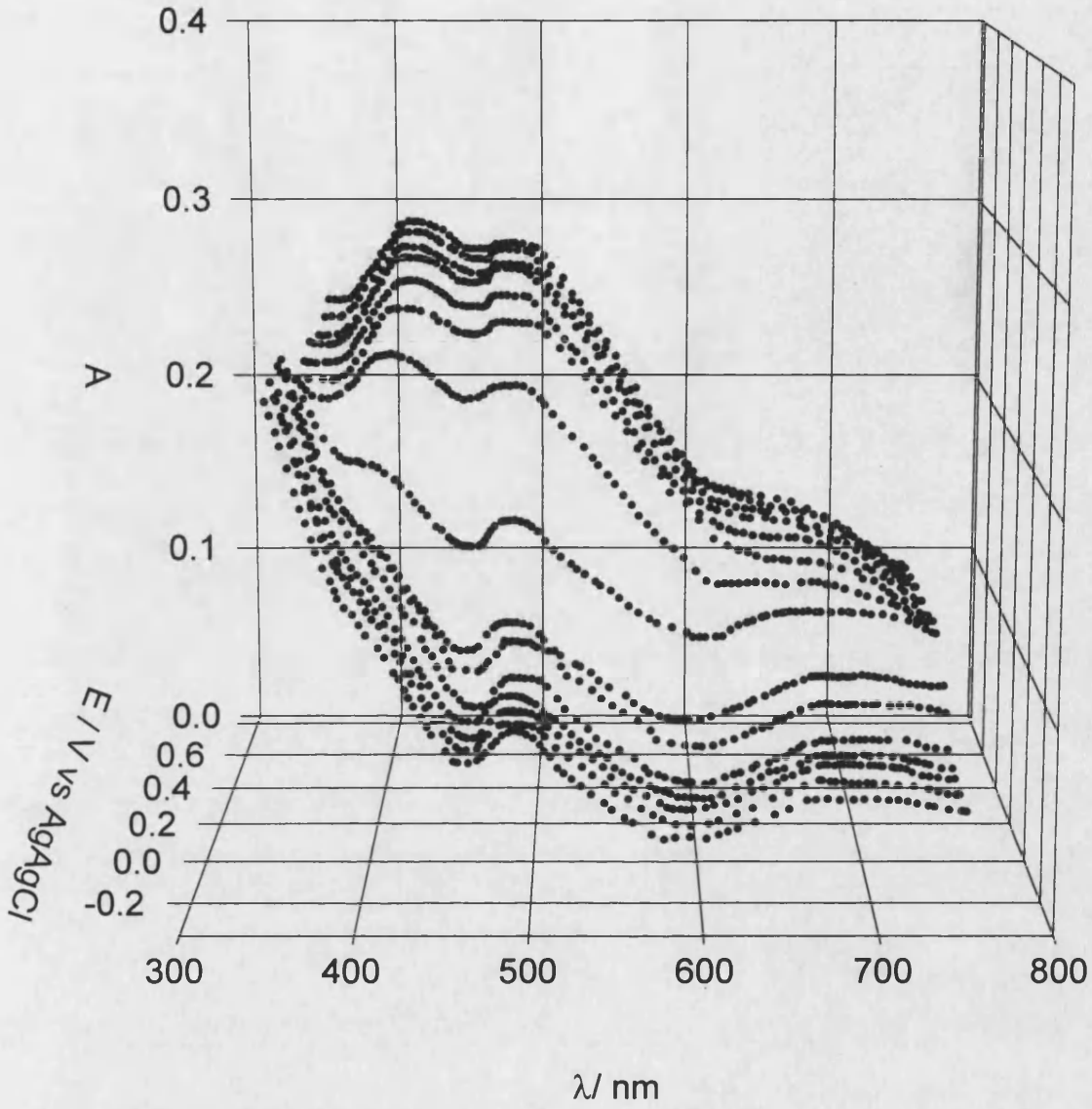

Figure 4.26 A set of absorption spectra of a 80 nm POAP film recorded at different potentials:-0.30, -0.25, -0.15, -0.1, -0.05, 0.0, 0.1, 0.2, 0.3, 0.4, 0.5, 0.6, 0.7 and 0.8 V.

The spectrum of the figure 4.26 is quite different from that reported by Barbero[22] using a thin transparent gold electrode (see figure 4.3, lower plot). In it, a broad band is observed at about 550 nm when the polymer is in its reduced form and an even broader band, very difficult to centre, is shown when the polymer is oxidised. On the other hand, the absorption spectra given by Ohsaka[20] using a ITO electrode (figure 4.3, upper plot) exhibits a peak at 600 nm while a the maximum absorption peak of the oxidised form appeared at 440 nm. In both cases the measurements were carried out using $NaClO_4$ as supporting electrolyte at pH 1. Barbero[22] polymerised oAP by cycling the potential between 0 and 1.2 V vs NHE (≈-0.25 - 1.0 V SCE) while Ohsaka[20] did it by cycling the potentials from -0.4 to 1.0 V SCE. In this work, the POAP was obtained by cycling the potential between -0.45 and 0.785 V SCE. Differences between those spectra and the one in the present work could be attributed to a dependence of the composition of the polymer with the potential range where electropolymerization is carried out.

The oxidative polymerization of oAP by $CuCl_2$ in acid medium has been followed by uv-visible spectrophotometry[21]. Two absorption peaks were observed at 410 and 460 nm which were assigned to the formation of the radical cation and an oxidised form of oAP , respectively. The shape and position of these peaks are quite similar to the ones shown in figure 4.26. On the other hand, the authors report the presence of quinoid units in the polymer by in situ Raman spectroscopy which is in agreement with the carbonyl band observed in the IR spectrum of the POAP produced in the present work.

It was no possible to observe the 330 nm peak corresponding to the π - π^* transition of the aromatic benzenic structure in figure 4.26 because glass also absorbs in the same region. Glass absorption will not be cancelled out between the sample and reference beams since the strongly absorbing glass allows so little light to pass through the cells that the detector will be effectively blind. A weak peak was observed at 424 nm in the absorption spectra of a 0.02 mol dm^{-3} *o*-aminophenol in 0.4 mol dm^{-3} $NaClO_4$ solution at pH 0.9. On the other hand, APZ spectrum has been reported[53] to show a peak at 435 nm in aqueous solution. This increase in the peak wavelength between the monomer and the precursor of POAP is associated with the increase of the conjugation of the phenyl groups[32]. For example, the spectra of aniline and aniline dimer have been reported to show absorption peaks at 250 and 280 nm, respectively[54]. The 492 nm peak, in the figure 4.26, can be attributed to the reduced form of the conjugated polymer; the nonbonding electrons on oxygen and nitrogen may also be involved in extending that conjugation[32]. The weak absorption of the reduced state of the POAP film is expected because this form exhibits a very pale yellow color and is highly transparent in contrast with the oxidised form of polymer which is reddish-brown color. Spectra for polyaniline films has been reported by Vuki[50]; the oxidation of those films produced an increase of the 420 nm and 820 nm peaks ascribable[55] to the formation of polarons (radical cations) and bipolarons (dications).

A schematic band structure for polyaniline is shown in the figure 4.27 . The leucoemeraldine state (fully reduced) has a π - π^* transition between the highest occupied band (valence band) and the lowest unoccupied band (conduction band) at 318 nm (3.9 eV). When a half of the electrons in the valence band is removed the polaron defect is formed; the valence band moves up slightly due to the destabilization

Figure 4. 27 Schematic energy band diagram for polyaniline, *Huang*[55].

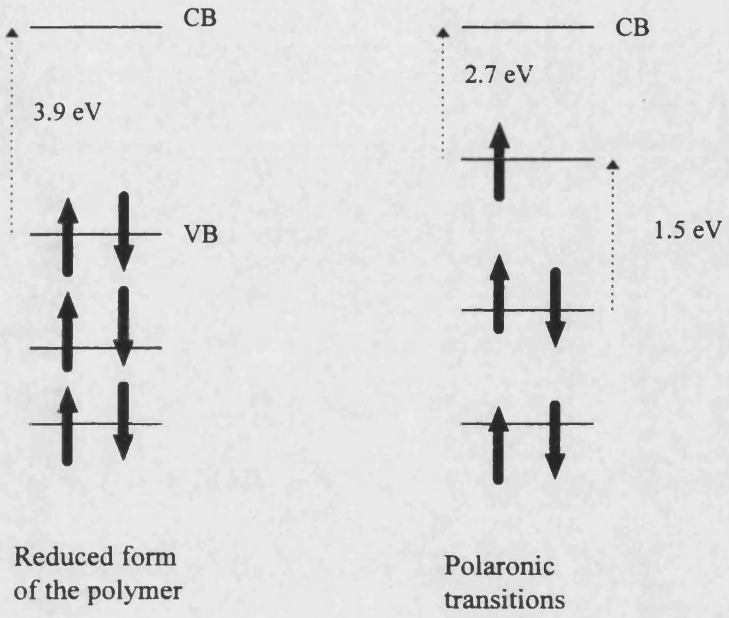

of the band. The conduction band almost remains unchanged exhibiting approximately the same energy. In this case, transitions from semifilled valence band to conduction band are detected at longer wavelength (500 nm, 2.7 eV)) and other transitions from lower electronic levels to the valence band were also observed at 826 nm (1.5 eV). As in polyaniline[55], two gap defect bands could be formed in the oxidation of POAP . The 414 and 690 nm peaks can be attributed to the formation of the radical cation and dication form of POAP which is common among polyaniline-like structures[54] and polypyrrole derivatives[56] . However, the peak at 492 nm is no common to polyaniline or polypyrroles polymers and it must correspond to the formation of other oxidised form of the polymer. All these transitions are responsible for the changes to the color of the film when it is oxidised. Absorption of blue from white light leaves the complementary colors, which appear yellow/orange to the human eye. Progressive absorption from 400 nm upward leads to progressive darkening through yellow, orange, red, green, blue, violet and black so that the complementary color at 690 nm darkens the orange/yellow appearance of the film to brown color.

Deconvolution of the spectra was carried out in order to determine their development as the potential increases. Figure 4.28 illustrates the results of this procedure. Experimental results fitted quite well to the deconvoluted peaks . The large peak at wavelength under 350 nm was assigned to the absorption of the glass which is not completely compensated by the double beam system of the spectrophotometer. Peaks located at higher wavelength, except for the 690 nm, increase their absorption as the potential goes to more positive values without no significant change on the λ_{max}. The 690 nm peak move to smaller wavelengths as the oxidation takes place and a small decrease is observed at potentials higher than 0.3 V. The free carrier electron band for

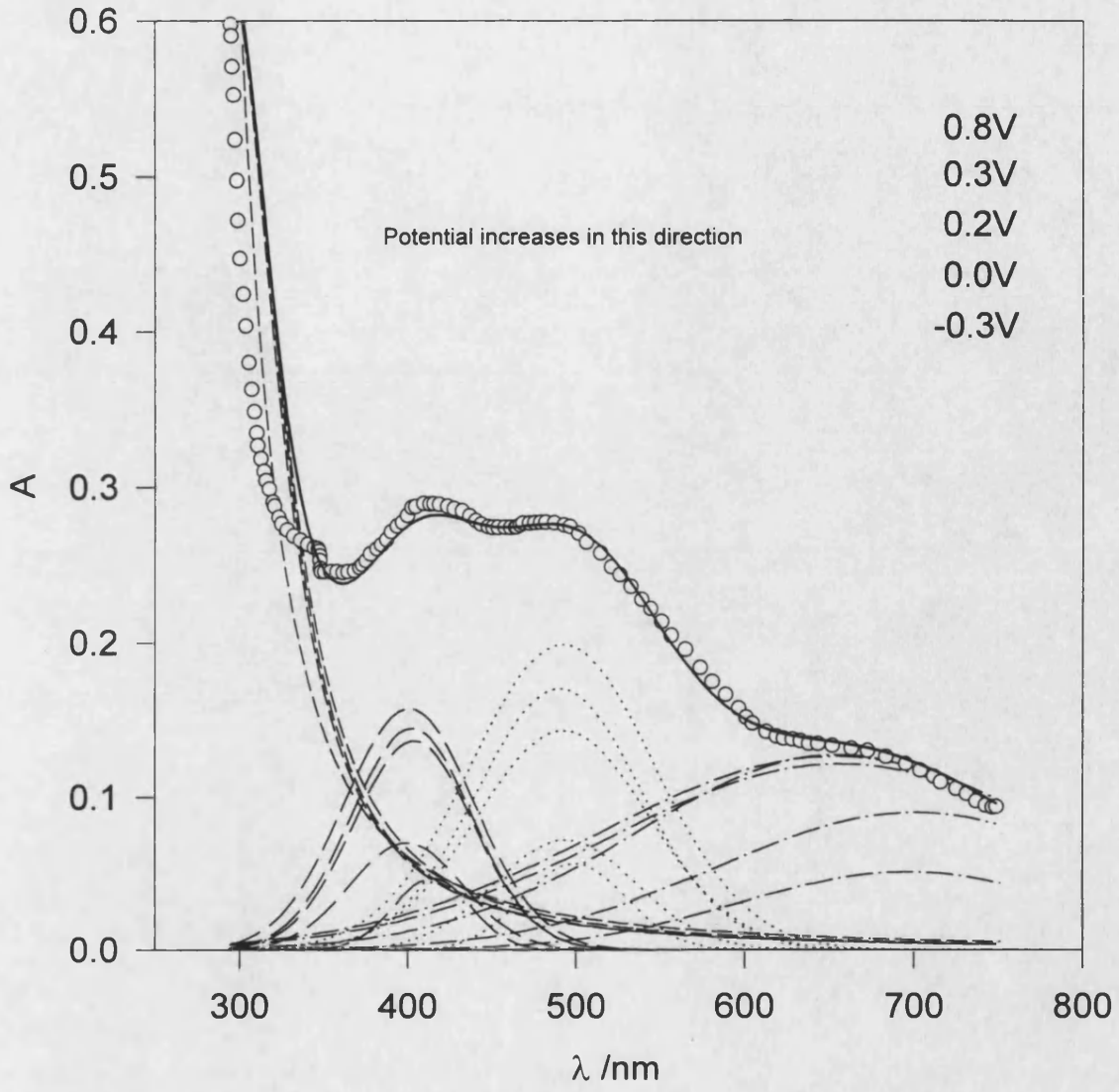

Figure 4.28 Deconvoluted spectra for POAP as a function of the potential. Upper curve corresponds to the fitting of the spectrum recorded at 0.8 V.

○ Experimental points (——) Fitted curve

conducting polyaniline has been represented[54] by an absorption at about 820 nm. Unfortunately, it was no possible to scan further than 750 nm with our spectrophotometer; however, the blue shift of the 690 nm band with increasing potential suggest that the combination of radicals can give rise to dications in a structure quinoid like in polyaniline[57] . Stilwel[54] *et al* ascribed the observed broad band of polyaniline at 610 nm to the fully oxidised film with repeating aromatic-quinoid structures . Ohsaka[25] *et al* stated that the polaronic form of POAP is possible; this observation is based in the electrocatalytic activity of this film in the reduction of oxygen which could be mediated by the POAP radical cation.

Electropolymerization of oAP (section 4.2) seems to agree with the presence of a slow cyclization reaction that gives rise to the cyclic precursor 3APZ and its polymer (POAP). On the other hand, IR spectrum of the film obtained at the present work shows that the polymer has carbonyl groups when it is oxidised. It is possible that a composite polymer of opened and closed structure is formed. Both kinds of structures could be involves in the redox process. Figure 4.29 proposes a structural representation of those systems for POAP. The reduced species could undergo oxidation to the polaronic form of the polymer. At higher positive potentials, the population of polarons increases giving rise to combination of radicals to produce the bipolaronic form of the polymer which, by proton elimination, can produce the oxidised form. Bipolaronic and oxidised forms exhibit quinoide structures which have also been reported as possible for POAP [25,87].

It has been reported[9] that APZ is produced by the chemical reaction between *o*-benzoquinone monoimine (*o*-BQMI) and orthoaminophenol (*o*-AP). The reaction was followed by uv-visible spectroscopy and it was observed that in addition to APZ peak a

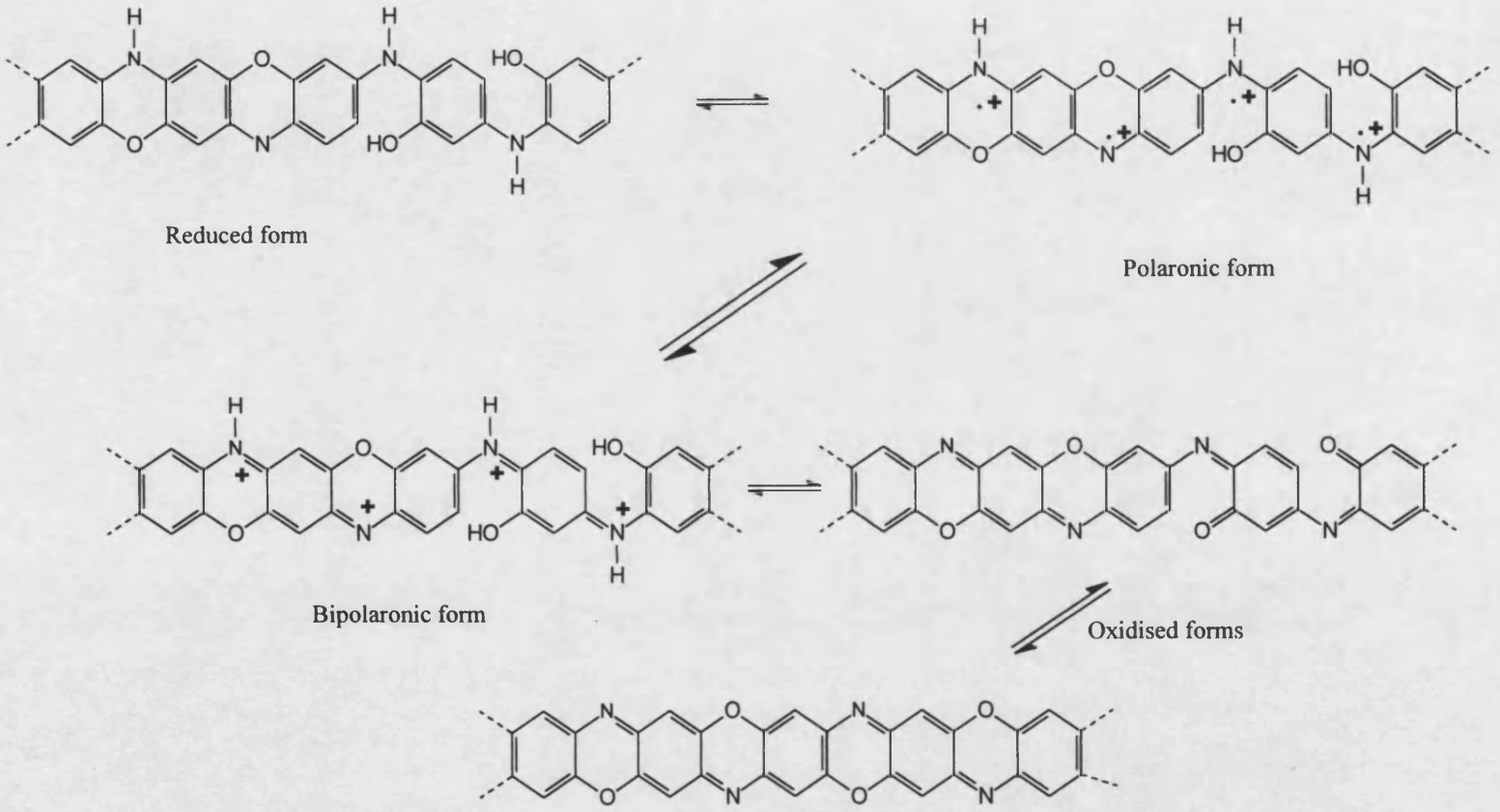

Figure 4.29 Possible structural representation of POAP forms as the oxidation process is taking place. Oxidised structures are tautomers, i.e they can interconvert by a cyclization reaction.

second peak appeared at 492 nm. This band was assigned to 2-amino-*o*-indophenol (AIP) but it could not be isolated because of its easy conversion to APZ by a cyclization reaction. Many indophenol derivatives are reported[58,59] to have their absorption peaks between 470 and 510 nm.

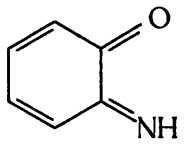

o-BQMI

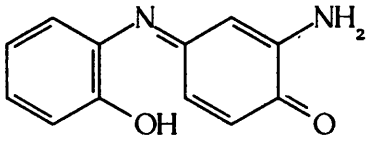

API

The experimental peak observed at 492 nm, in the figures 4.26 and 4.27, seems to correspond to the formation of the opened structure similar to API. Initially, this opened structure with carbonyl group seems to be present in a no large proportion in the reduced state of the polymer due to the protonation of the oxygen atom, but as the potential becomes more positive the proton elimination give rise to the oxidised forms. The IR spectrum of the fully oxidised form of the polymer revealed the presence of C=O groups which support this assumption. The presence of a weak 492 nm band in the spectrum of the reduced form of polymer seems to support the idea of formation of isolated "islands" of the oxidised form which are not reduced at the same timescale[60], even when the polymer was reduced for thirty minutes at -0.3 V vs Ag/AgCl before scanning the spectrum. This oxidised structure may also be related to the low conductivity of the film when it is fully oxidised.

The spectroelectrochemical transient of the figure 4.30 was recorded after thirty minutes of application of 0.8 V to the POAP film; it is reasonable to assume that the polymer was completely oxidised after that period. A potential step from 0.8 to -0.3 V vs Ag/AgCl was applied for forty three seconds before the potential went back to the

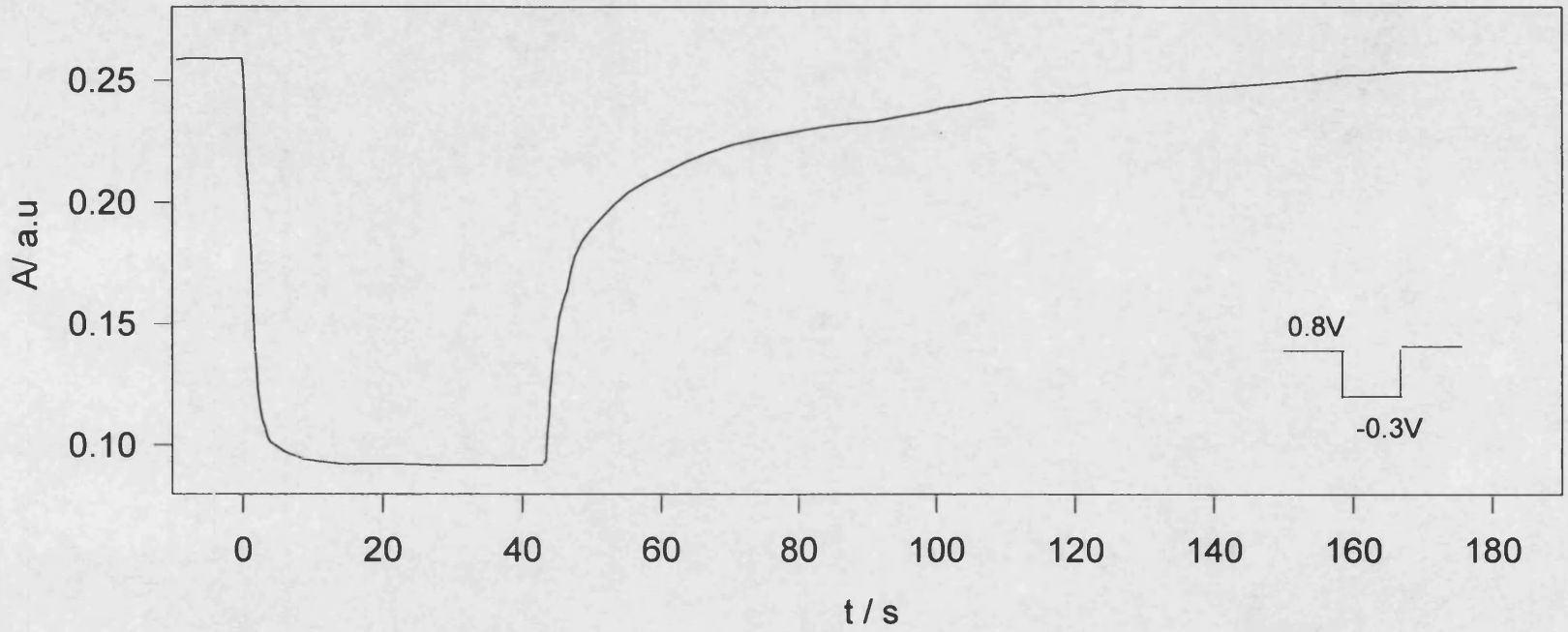

Figure 4. 30 Spectroelectrochemical transient of a 80 nm thick POAP film on electrical conducting glass electrode (A= 3 cm^2). Submerged in 0.4 mol dm^{-3} $NaClO_4$ solution at pH 0.9. Potential step is shown in the right lower corner of the plot.

initial value. Wavelength was fixed at 492 nm because this peak represents the change between the reduced and the fully oxidised forms of the polymer. The difference in the rates of reduction and oxidation process is clearly shown in the figure 4.30. The initial decreasing region corresponds to the reduction of the film; 75% of the total change of the color is achieved in three seconds and the 100% at about 12 seconds. In contrast, the oxidation process is very slow, 99% of the change in the color was reached at 189 seconds after the application of the pulse. No change in the transmittance response was observed after applying consecutive potential stepping for two hours.

4.8 Electron Spin Resonance Measurements

Electron Spin Resonance (ESR) is a spectroscopic method that is sensitive to materials with unpaired electrons, such as organic and inorganic free radicals, radical anions and cations. The electrochemical reduction or oxidation of neutral organic molecules[61] typically involves formation of these radicals. In recent years studies on the electroconducting organic polymers by ESR have been developed increasingly[62,63,64] . Based on the radical nature of the transition of POAP at 410 nm, it could be expected that polarons exhibit activity in ESR spectroscopy. Films deposited on Pt electrode were introduced into a $HClO_4$ solution (pH 0.9) which was free of monomer. Next, the solution and the cell was completely deaerated by passing argon gas through the system. Finally, the cell was sealed using parafilm paper to avoid the entrance of oxygen and the destruction of the radicals. SCE was used as reference electrode in all ESR spectra but the values of potential are given in Ag/AgCl scale in order to facilitate their comparison with these shown in figure 4.28. ESR spectra of POAP film were recorded a different potentials, scanning forward and back from -0.3 to 0.55 V vs Ag/AgCl. Figure 4.31 shows the appearance of a weak signal at negative potentials which

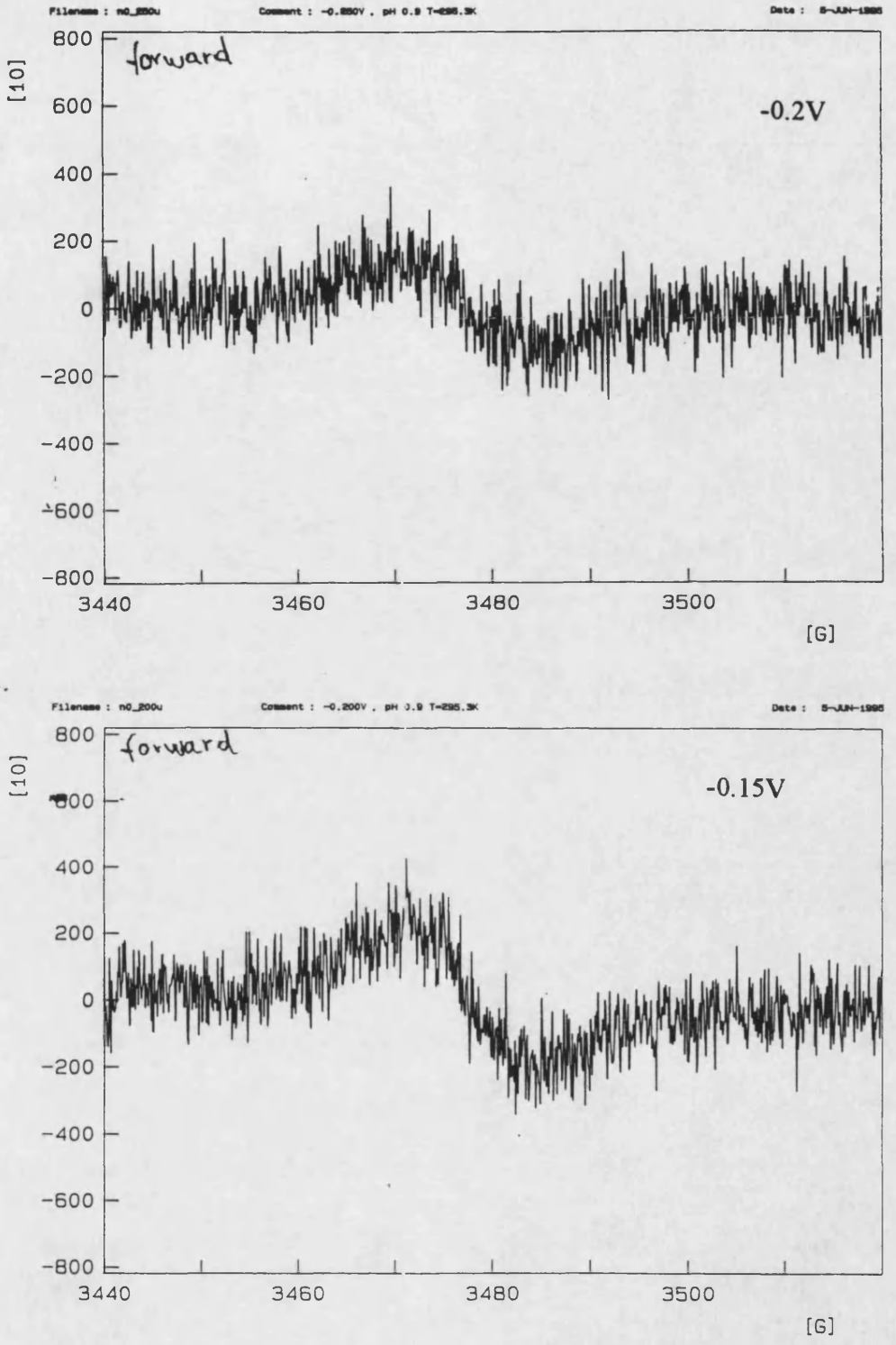

Figure 4.31 ESR spectra of a 80 nm thick POAP film on Pt electrode at different potentials. Solution was o.1 mol dm^{-3} $HCLO_4$. ν= 9.770416 Ghz. Last plot illustrates the changes in the ESR intensities as a function of the potential.

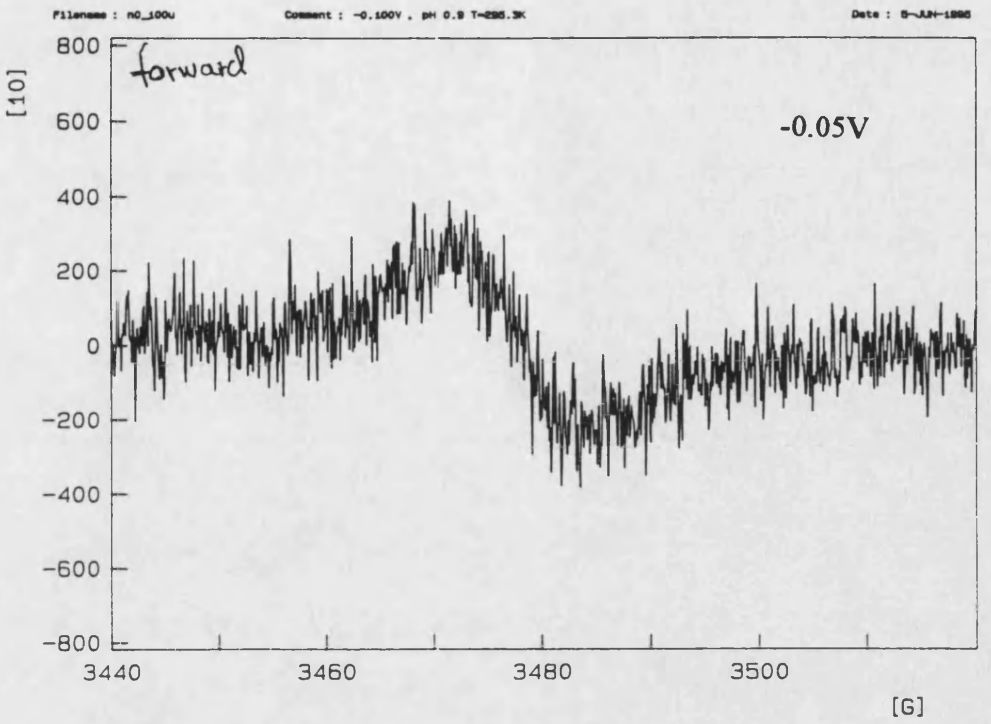
forward
-0.05V
[10]
800
600
400
200
0
-200
-400
-600
-800
3440
3460
3480
3500
[G]

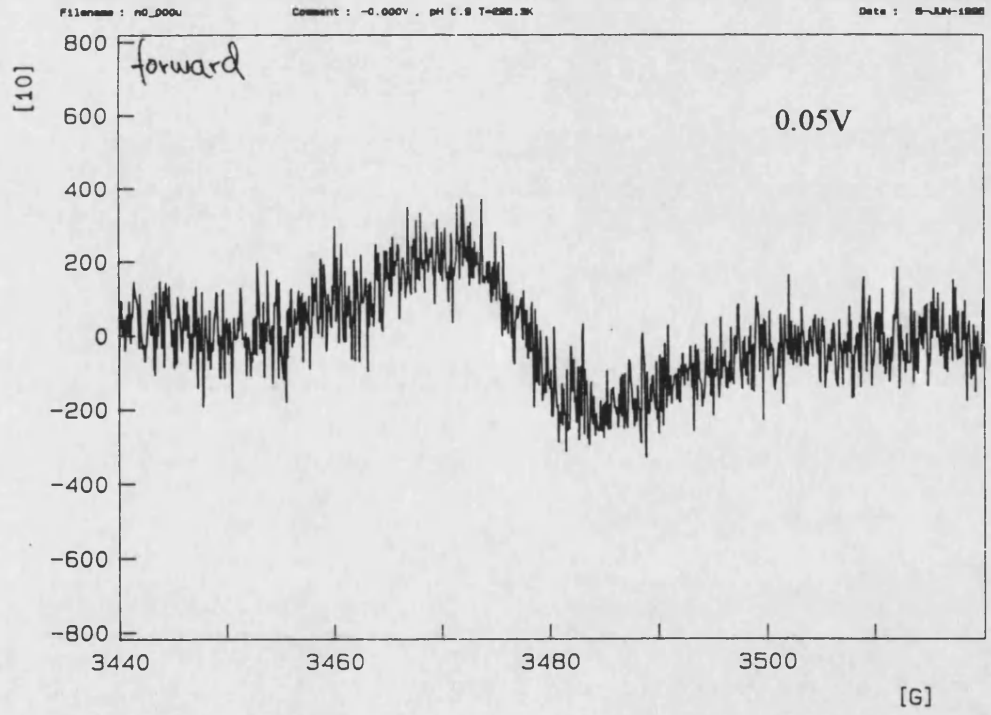
forward
0.05V
[10]
800
600
400
200
0
-200
-400
-600
-800
3440
3460
3480
3500
[G]

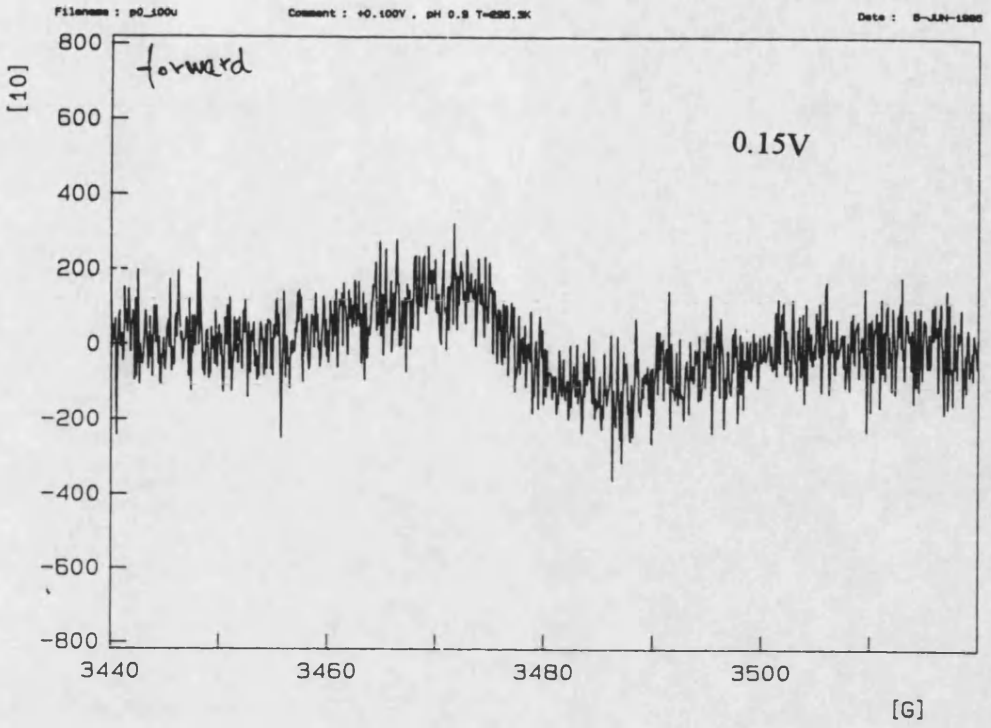
Filename : p0_100u
Comment : +0.100V , pH 0.9 T=295.3K
Date : 8-JUN-1988
forward
0.15V
[10]
800
600
400
200
0
-200
-400
-600
-800
3440
3460
3480
3500
[G]

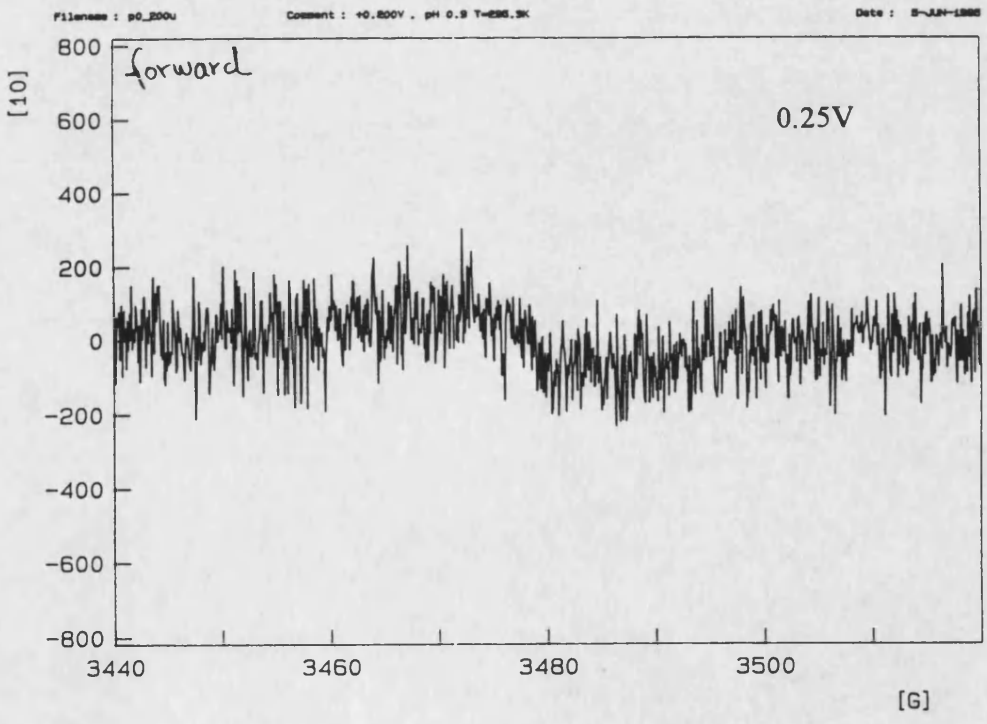
Filename : p0_200u
Comment : +0.200V , pH 0.9 T=295.3K
Date : 8-JUN-1988
forward
0.25V
[10]
800
600
400
200
0
-200
-400
-600
-800
3440
3460
3480
3500
[G]

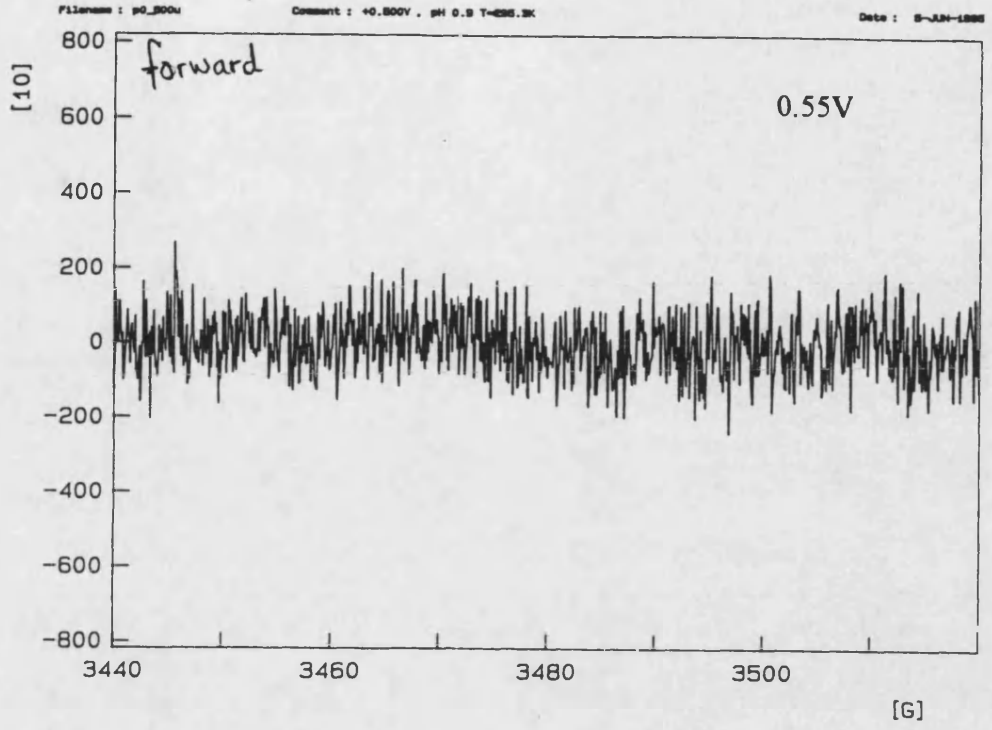
forward
0.55V
[10]
800
600
400
200
0
-200
-400
-600
-800
3440
3460
3480
3500
[G]

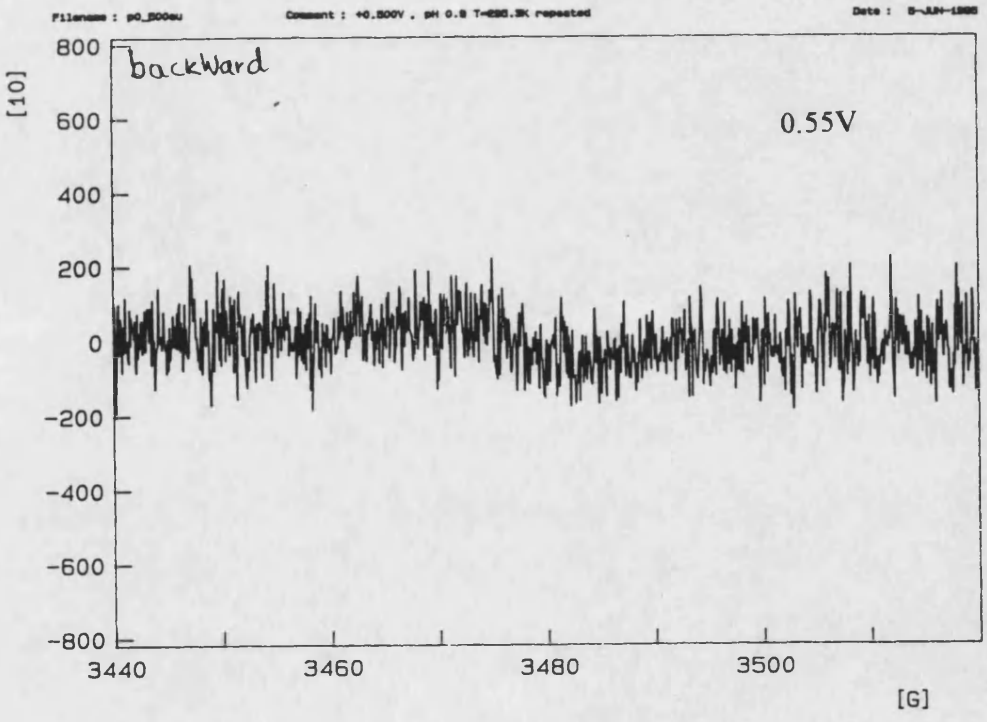
backward
0.55V
[10]
800
600
400
200
0
-200
-400
-600
-800
3440
3460
3480
3500
[G]

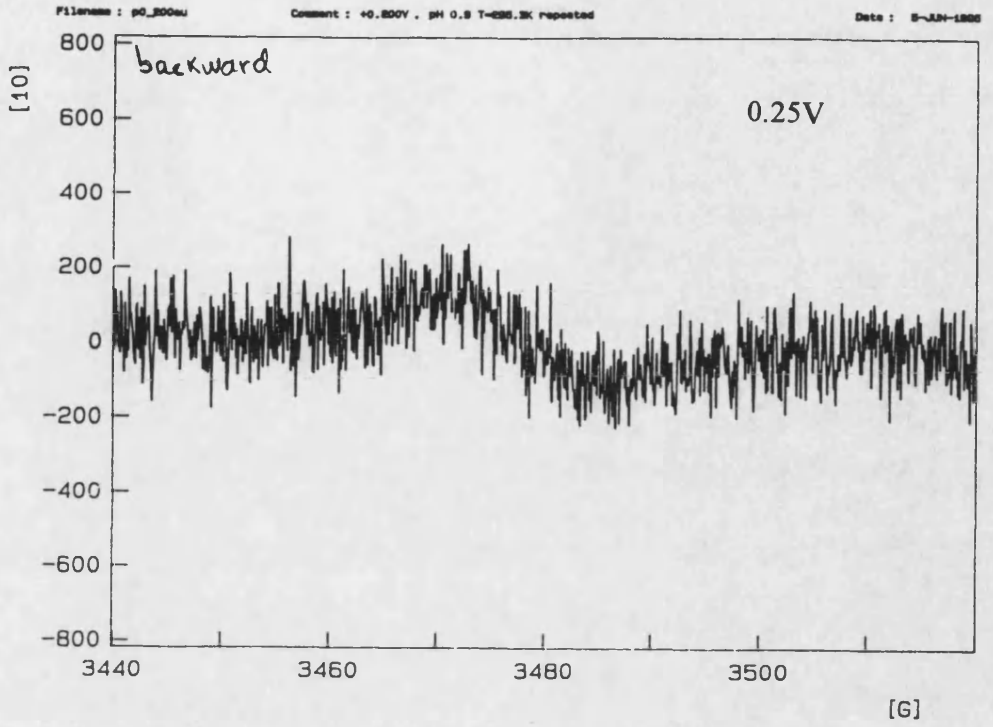
backward
0.25V
[10]
800
600
400
200
0
-200
-400
-600
-800
3440
3460
3480
3500
[G]

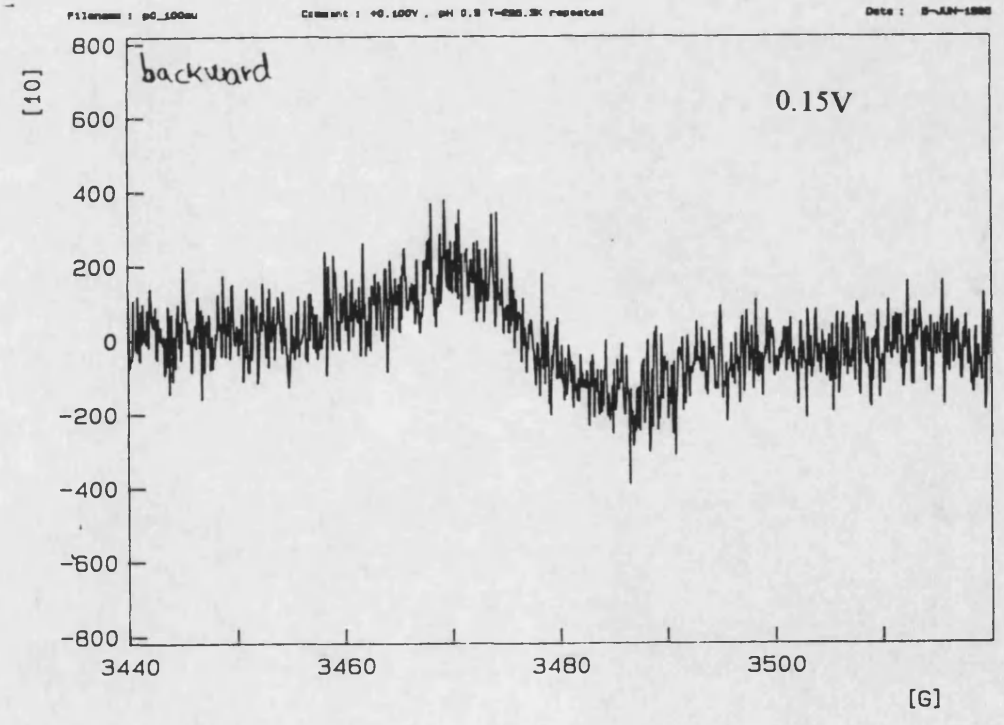
backward
0.15V
[10]
800
600
400
200
0
-200
-400
-600
-800
3440
3460
3480
3500
[G]

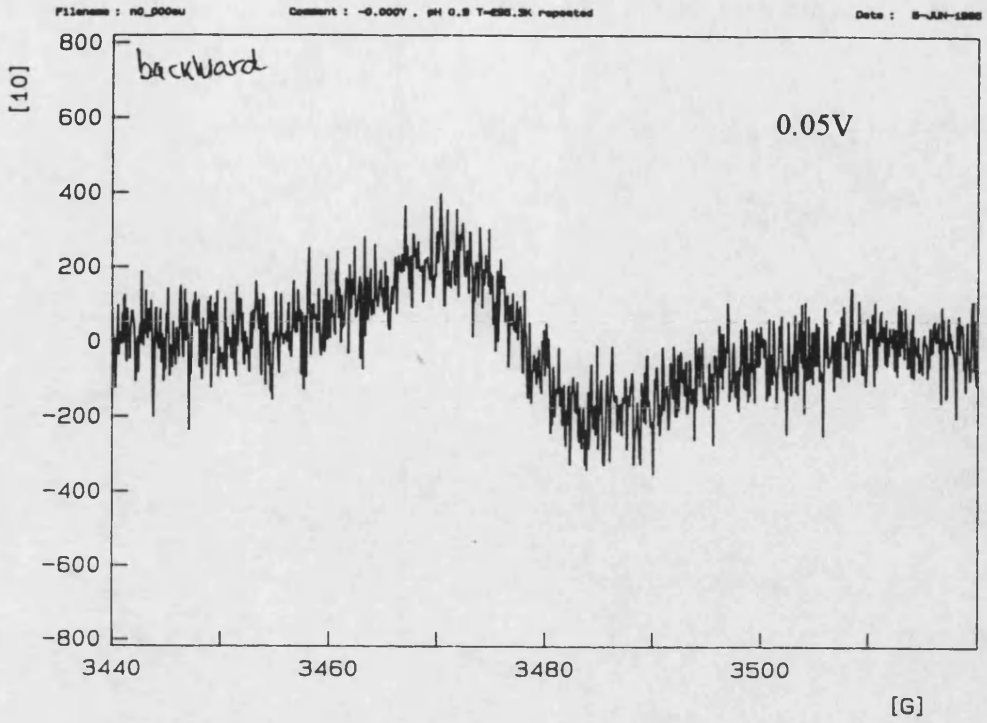
backward
0.05V
[10]
800
600
400
200
0
-200
-400
-600
-800
3440
3460
3480
3500
[G]

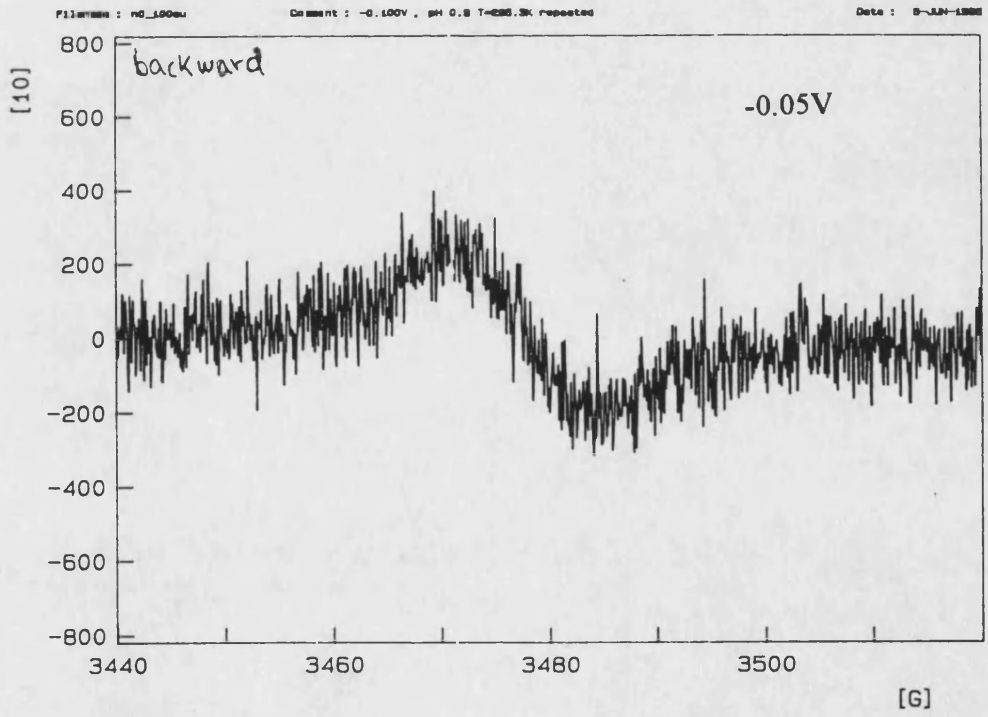
backward
-0.05V
[10]
800
600
400
200
0
-200
-400
-600
-800
3440
3460
3480
3500
[G]

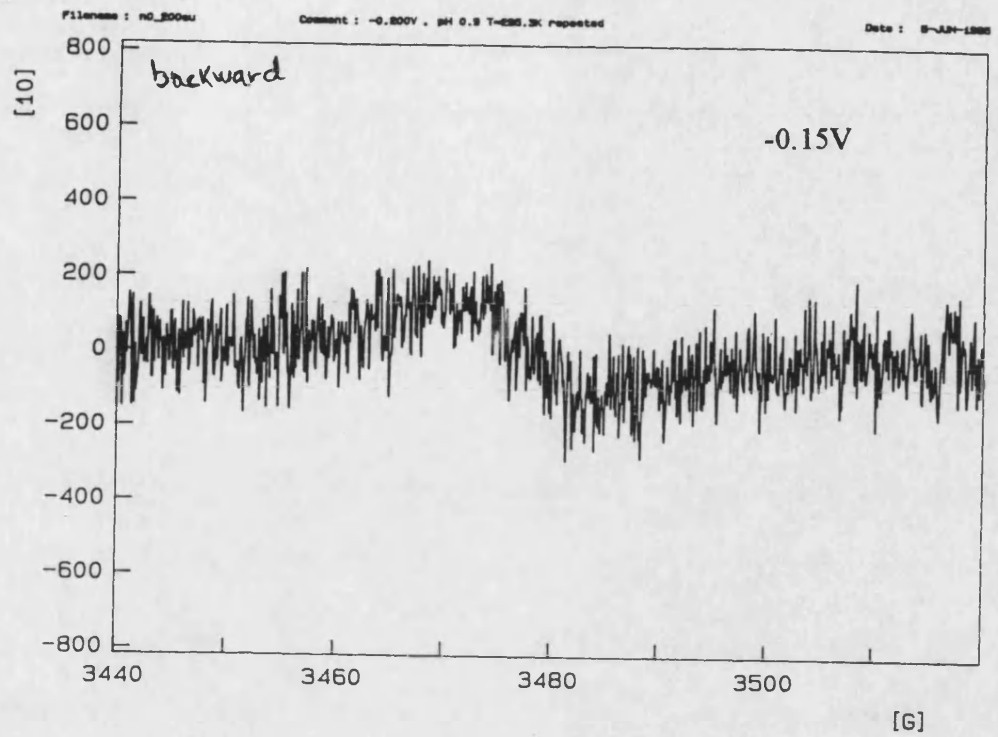
backward
-0.15V
[10]
800
600
400
200
0
-200
-400
-600
-800
3440
3460
3480
3500
[G]

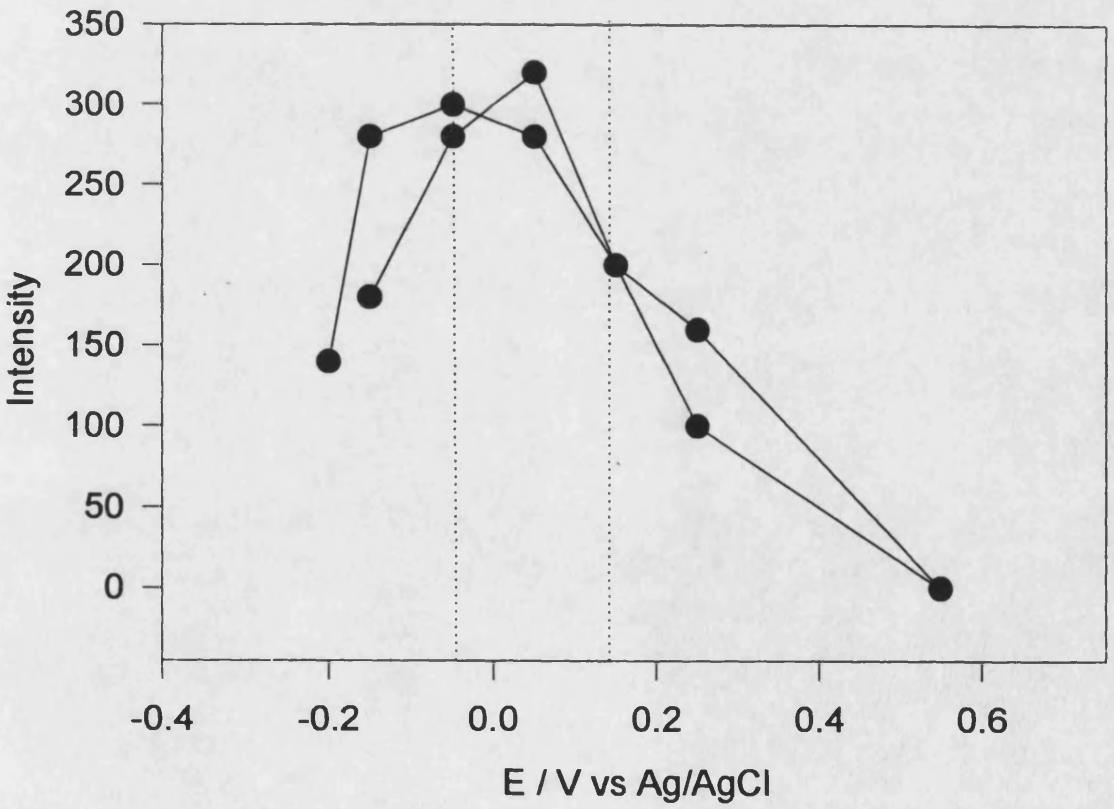
Intensity
350
300
250
200
150
100
50
0
-0.4
-0.2
0.0
0.2
0.4
0.6
E / V vs Ag/AgCl

becomes gradually stronger as the potential increases in the positive region; the ESR signal reaches a maximum at about -0.05 and 0.150 V and starts decreasing to very small values at 0.55 V. The determined *g* values were 2. 0071± 0.00002 for the spectra recorded from -0.2 to 0.05V and 2.0076 for the one at 0.15 V. This small change in *g* may indicate the presence of two different structures in the polymer[65]. The maximum in the ESR spectra occurs in the range where the 414 nm absorption peak shows large increase with the potential. The assignment of this peak to radical species is consistent with the in situ ESR behaviour.

The decrease and further absence of a detectable ESR signal at higher potentials than 0.55 V suggests combination of radical to give rise the dication species which is not active in ESR because of its paired spin. The absorption band ascribed to dication species reaches a maximum at 0.2 V, see figure 4.28, and it does not change significantly a more positive potentials. It is possible that only a fraction of it is transformed into the oxidised POAP as potential increases. The presence of the dication species could also produce the small change in g factor due to the change in the nature of the electrostatic interactions between the charges in the polymer[66].

The 414 nm peak, corresponding to the radical species in the polymer, should decrease as the combination of electrons gives rise to the dications[50,54]. No decrease was observed in the figure 4.26; however, figure 4.28 shows that the contribution of all the other bands to the absorption at 414 nm is very significant so that any change in this absorption peak could be obscured by the other peaks in the spectrum.

Assuming that the absorbance changes shown in figure 4.26 follow the Beer's law it is possible to treat experimental data according to the Nernst equation[54,67,68,69]:

$$E = E_o + \frac{0.059}{n}\log\frac{A - A_{\min}}{A_{\max} - A} \qquad (4.2)$$

where E_o is the formal potential for the redox process, n is the number of electrons transferred and A_{max} and A_{min} denote absorbances of fully oxidised and reduced forms of the polymer, respectively. A_{min} is that measured at negative potentials while A_{max} is the absorbance value at highly positive potentials. The increase in the absorption peak at 492 nm is related to the formation of the fully oxidised form of the polymer. Changes associated with this band were plotted against E by using the equation 4.1. Figure 4.32 shows the variation of the absorbance as a function of the potential. At negative values of potential the absorbance is low but it increases up to steady state value as potential becomes more and more positive. The plot of E vs log (A - A_{min} / A_{max} - A) is linear, see figure 4.32(b) . The value of E_o , determined from the intercept, was 95 mV vs Ag/AgCl (46 mV vs SCE) which agrees with that determined from cyclic voltammetry curve of figure 4.17 at 50 mV s^{-1}. The n value obtained from the slope of the figure 4.32(b) was 0.34 which means that the transformation of POAP from a conducting form to a insulating one requires about 0.34 electrons per monomeric unit. This approach has been reported to give excellent agreement between the n values calculated from chronocoulometric data for polyaniline[54] and from ESR measurements for polyindole films[67]. However, this spectroelectrochemical method may introduce some errors because the redox reactions in POAP film cannot be represented by reactions involving two species but by a mixture of different structures. This is supported by the absence of isobestic points in the absorption spectra; moreover, overlapping of the absorption bands in uv-visible spectra can leads to misinterpretation the calculated values[70].

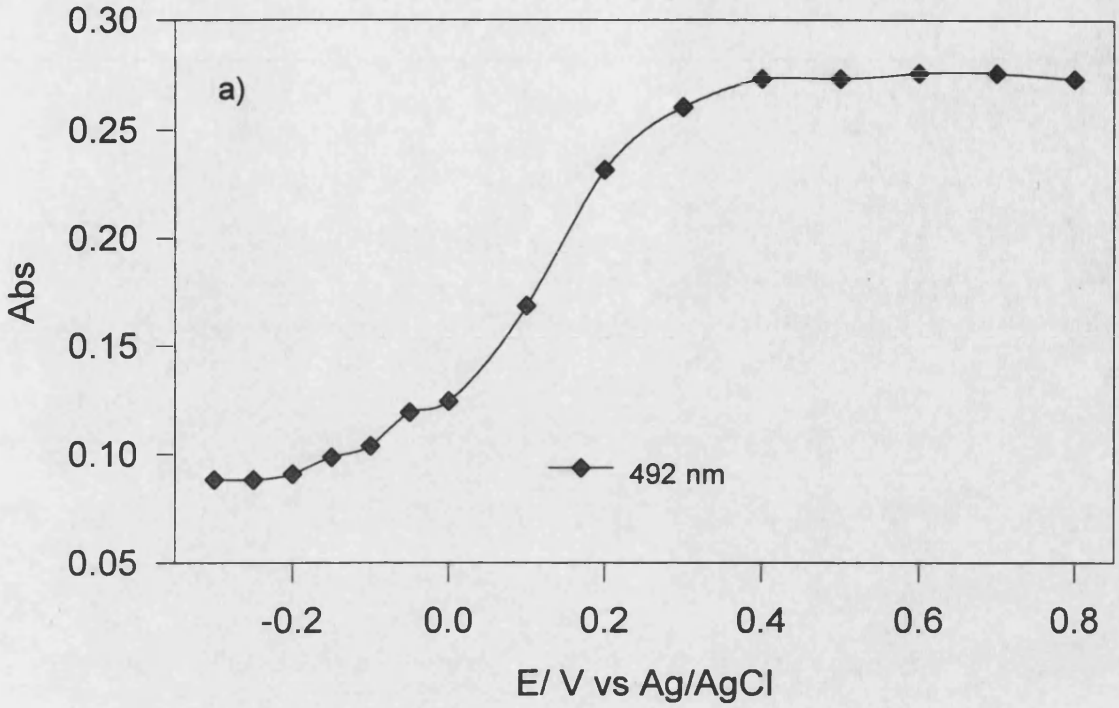

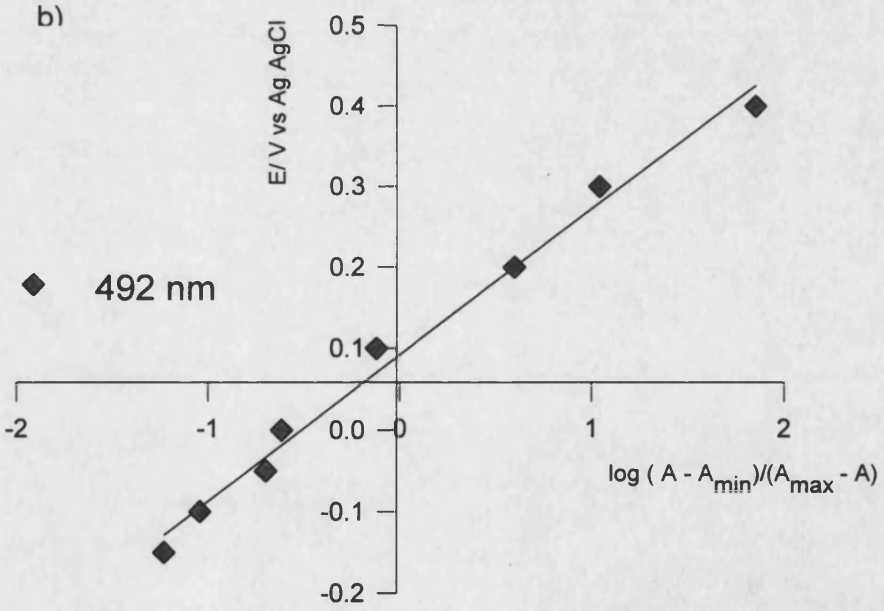

Figure 4.32 A vs E plots (a) and Nernst plot (b) obtained from absorbance data in figure 4.25.

4.9 Test of conductivity of POAP using redox couples

One method of testing the conductivity in electrochemical systems consist in using the modified electrode as a working electrode against solutions of redox couples of known behaviour[71,72] . These substances with lower redox potentials than the formal potential of the film will be reduced at the modified electrode so that a set of peaks corresponding to the conducting polymer and the redox couple is expected. A similar explanation is applicable to these species with redox potentials more positive than the formal potential of the polymer.

POAP modified electrodes were introduced into $NaClO_4$ (0.4 mol dm^{-3}) solutions at pH 0.9, containing 10^{-3} mol dm^{-3} of $Fe(CN)_6^{4-}$. The electrochemical reaction of this species is as follows[73] :

$$Fe(CN)_6^{3-} + e^- \rightleftharpoons Fe(CN)_6^{4-}$$

with a redox potential strongly dependent in acid solutions due to formation of $HFe(CN)_6^{3-}$. The E_o for $Fe(CN)_6^{3-}$ at pH 0.9 is located in the region where POAP is in its oxidised form (0.36 V SCE).

Figure 4.33(a) shows the voltammograms corresponding to redox process of the $Fe(CN)_6^{-4}$ at a Pt electrode and of the conducting film in presence and absence of the hexacyanoferrate. There is no peak ascribable to the $Fe(CN)_6^{-4}$ redox process in the region ranging from 0 to 0.75 V SCE when a polymer modified electrode is used. Increasing concentrations of hexacyanoferrate (up to 5 x 10^{-2} mol dm^{-3}) were used but no peak was observed. A change in the color of the solution, from yellow to green and further to dark blue, took place when high concentrations of $Fe(CN)_6^{4+}$ and protons were present. This color can be attributed to formation of a mixed-valence compound

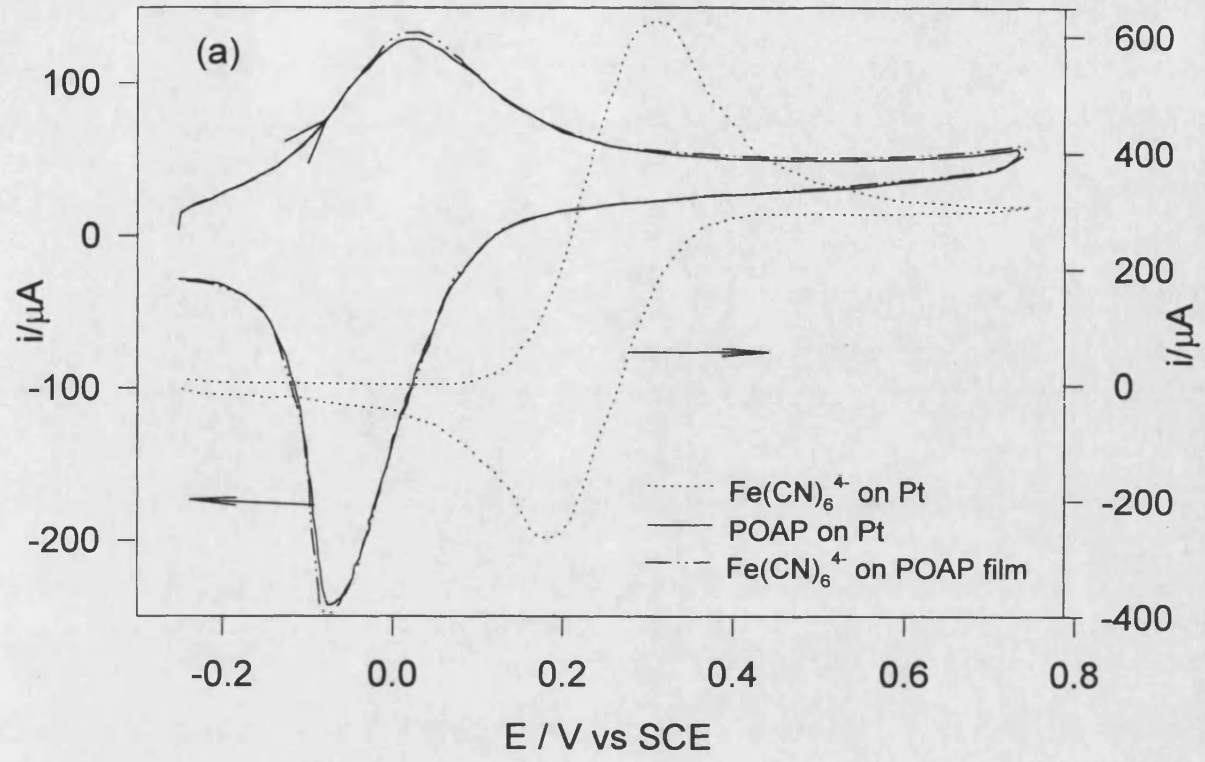

Figure 4.33 Voltammograms corresponding to (a) 80 nm thick POAP in presence and in absence of $Fe(CN)_6^{4-}$ (10^{-2} mol dm^{-3}). Solution was $NaClO_4$ (0.4 mol dm^{-3}) at pH 0.9. A= 0.33 cm^2. ν= 20 mV s^{-1}. (b) 0.06 μm thick POAP film in KCL (0.4 mol dm^{-3}) at pH 0.9; in presence and absence of $Fe(CN)_6^{4-}$.

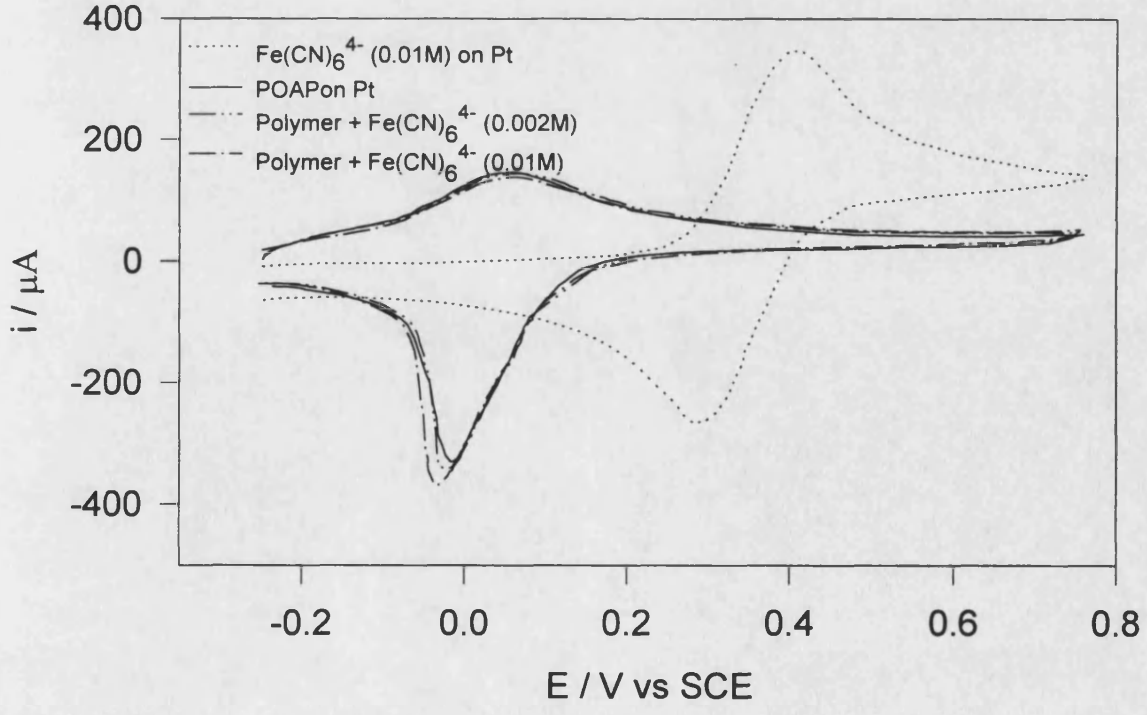

known as prussian blue[74,75] ($Fe_4^{3+}[Fe^{2+}(CN)_6]_3$) which was deposited all over the cell, blocking the frit at the reference electrode. KCl (0.4 mol dm^{-3}) solution, at the same pH, was also utilised but the formation of prussian blue was still quite fast. Figure 4.33(b) shows the voltammograms of POAP in this medium. No peak, attributable to the $Fe(CN)_6^{4-}$ redox reaction, was detected in the potential range from 0.2 to 0.75 V. However, an increase of the cathodic peak current was observed as the concentration of the $Fe(CN)_6^{4-}$ increases. It is probable that very small amount the $Fe(CN)_6^{3-}$, is oxidised during the forward scan through pores formed from the swollen reduced form of the polymer; during the reverse scan, the polymer becomes more compact and the $Fe(CN)_6^{3-}$ is reduced when the polymer becomes conducting. This agree with the assumption of a higher conductivity of POAP in the potential range from -0.25 to 0 V.

In order to avoid the formation of prussian blue, $FeCl_2$ solutions were utilised. Oxidation of Fe^{2+} to Fe^{3+} is reported[73] to take place at a formal potential of 0.8 V NHE in acid medium, in the region where POAP is in its oxidised form. Figure 4.34 illustrates the behaviour of POAP in that system. No peak ascribable to the oxidation of Fe^{2+} was observed.

Copper has been deposited at about -280 mV vs SCE on glassy carbon electrode and H_2SO_4 medium[76], which is in the potential range where the POAP is reduced. The conductivity of POAP in its reduced state was tested by the use of Cu^{2+} species. Figure 4.35 compares the voltammograms corresponding to copper deposition from an acid solution containing 3.5 x 10^{-3} mol dm^{-3} $Cu(ClO_4)_2$ onto bare platinum and a POAP modified electrode. Deposition of Cu^{2+} onto platinum, figure 4.34(b), exhibits a diffusion shaped peak at -0.025 V SCE in the anodic scan while in the cathodic sweep a sharp peak, corresponding to the stripping of Cu deposited on the

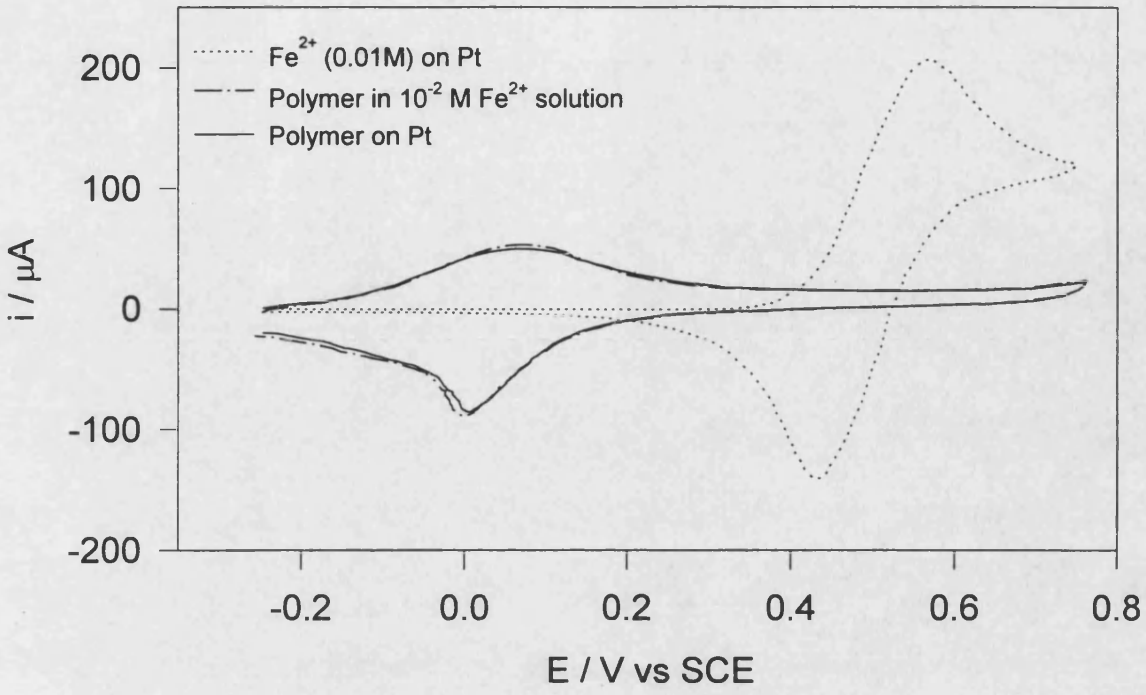

Figure 4.34 Voltammograms corresponding to a 30 nm thick POAP film in presence and absence of Fe^{2+} in acid $NaClO_4$ (0.4 mol dm^{-3}) solution at pH 0.9. Scan rate 20 mV s^{-1}.

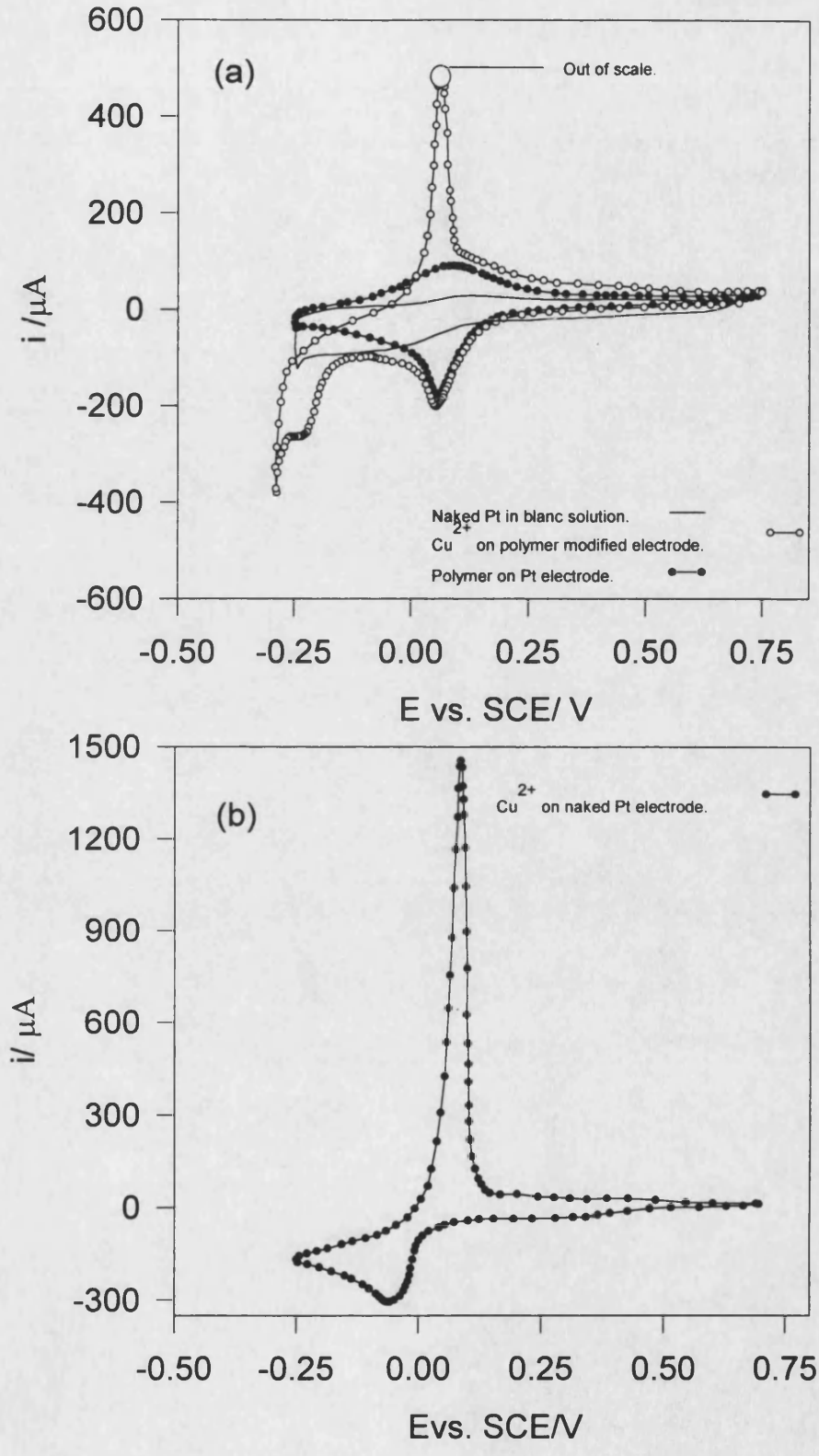

Figure 4.35 Voltammograms of (a) 70 nm thick POAP film immersed in a 3.5×10^{-3} mol dm^{-3} in Cu^{2+} and $NaClO_4$ (0.4 mol dm^{-3})solution at pH 0.9. ν= 20 mV s^{-1}. (b) Cu^{2+}/Cu on bare platinum in the same medium that (a).

previous step, is observed. The sharpness of the cathodic peak is explained since the Cu is deposited on the electrode and it does not need to diffuse there in order to react.

A current loop between the forward and the reverse direction was detected for scan rates smaller than 15 mV s^{-1}. This is because the potential has to be more negative to deposit Cu on Pt that on Cu itself[77]. Thus, on the cathodic sweep, a potential significantly more negative than the equilibrium potential is required before the deposition takes place and, on the reverse step, the deposition is occurring on a Cu surface and thus continues until the equilibrium potential is reached. The low is the scan rate, the longer is the time the working electrode is held at negative potentials so that a larger coverture of Cu is expected and the cross-over of the voltammogram takes place.

A voltammogram of POAP modified electrode submerged in Cu^{2+} solution, figure 4.35(a), clearly shows the oxidation and reduction peaks corresponding to the polymer and Cu^{2+}/Cu couple. Copper reduction peak appears shifted to more negative potentials, probably due to the resistivity of the film while the cathodic current does not change significantly. However, the oxidation peak is not shifted in the modified electrode. Voltammograms recorded at different scan rates showed that the reduction peak of Cu^{2+} depends on this parameter in the same way as the reduction peak of POAP, i.e. it moves to more negative potential as the sweep rate increases. Changes in the scan rates do not affect either the oxidation peak of the Cu or the oxidation peak of the polymer. De most reasonable for this behaviour is that the film is conductive in its reduced form.

Those results disagrees with these reported by Babero[24] in which $Fe(CN)_6^{4+}$ oxidation showed reversible behaviour in a 200 nm POAP film and no peak was

observed in the range where the polymer is reduced when other redox couples were used. Similar voltammograms for the oxidation-reduction of $Fe(CN)_6^{4+}$ were obtained in this work when very thin films (20 nm) were utilised but under such conditions complete coverage of the electrode surface is not ensured and the $Fe(CN)_6^{4+}$ redox reaction could be taking place at the Pt solution interface.

Other redox substances were also used. Europium (III) can be reduced to Eu(II) in aqueous solution by electrochemical methods[78]. However, europium(II) is gradually oxidised to europium (III) by atmospheric air so that precautions must be taken. The Eu^{3+}/Eu^{2+} redox couple has been reported[79] to have formal potential of -622 mV SCE. Eu^{2+} and Eu^{3+} forms complexes with many ions[80]; the curves are reported to be shifted for different anions and the relative shifts depend on the strength of these complexes[81,82]. A stock solution of Eu(III) was prepared by dissolution of the Eu(III) carbonate in an excess of $HClO_4$ and dilution with water to a known volume; the obtained solutions were usually 4 to 5 milimolar. A mercury pool working electrode, see figure 3.2, was utilised to reduce Eu(III) at a potential step of -1.050 V SCE for 20 hours. A constant stream of nitrogen gas was passed into the system in order to avoid the reoxidation of Eu(II) by air. A platinum electrode modified with a 50 nm thick POAP film was then used as working electrode. The potential was cycled from -0.25 to 0.75 V SCE. The scan rate was 100 mV s^{-1} for all the voltammograms of figure 4.36 . It was expected that the electrochemical reoxidation of Eu(II) to Eu(III) on the film would occur in the range where the polymer is conducting so that some additional current should be seem at one side of the POAP formal potential ($\cong$ + 60 mV). Figure 4.36 shows the voltammograms of the Eu(III)/Eu(II) redox process on mercury electrode and these corresponding to the polymer in the presence and absence of Eu^{+2} species. No

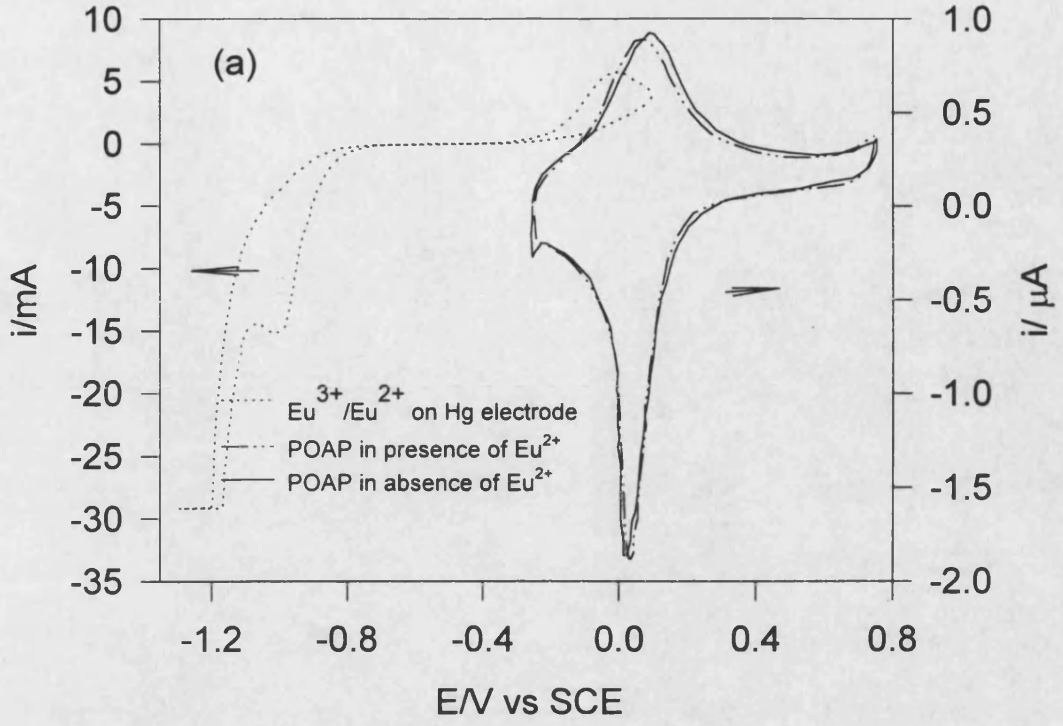

Figure 4.36 Voltammograms of POAP in (a) Eu^{2+} (about 3×10^{-3} mol dm^{-3}) solution, pH 0.9, and in (b) paraquat (about 3×10^{-3} mol dm^{-3}) solution, pH 3. Area of mercury electrode was 12 cm^2 area and of Pt electrode 1.9×10^{-3} cm^2 for both systems.Supporting electrolyte was $NaClO_4$ (0.4 mol dm^{-3}) for (a) and KCl (0.1 mol dm^{-3}) for (b).

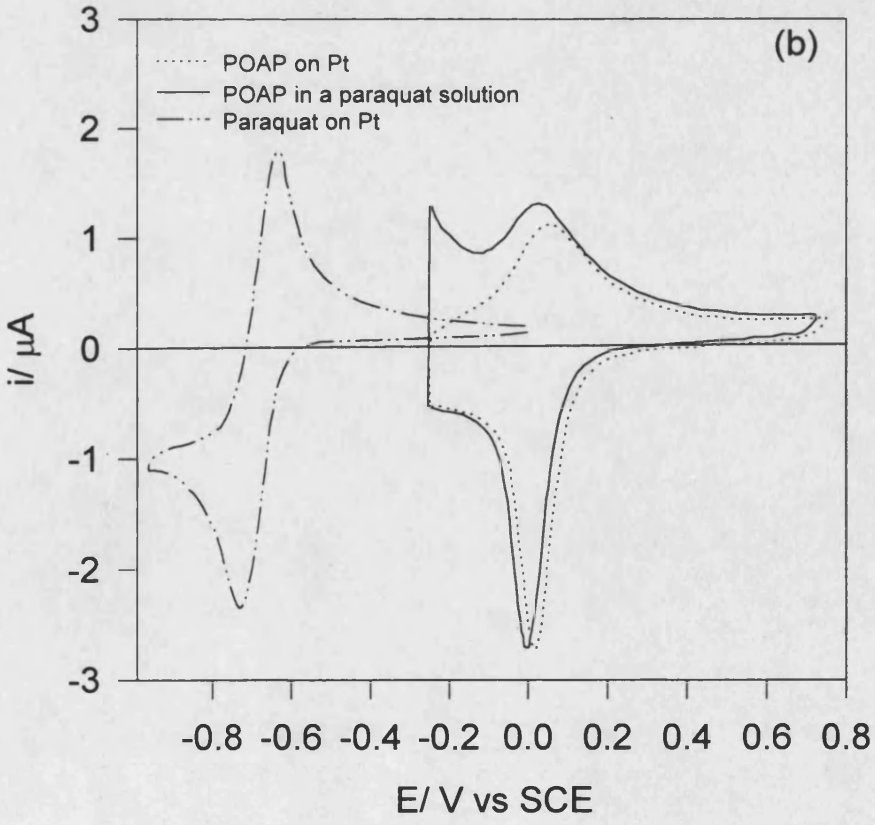

peak or additional current was observed at both sides of the POAP voltammogram. None peak corresponding to Eu(II) was observed when bare Pt electrode was used in the range -0.25 to 0.75 V SCE; it is possible that the Eu(II) oxidation peak on Pt is located at more negative potentials than that for the hydrogen evolution. Voltammogram of Eu(III)/Eu(II) on mercury exhibits very slow kinetic (ΔEp= 1 V); it has been reported[83] values of kinetic heterogeneous rates in the order of 10^{-4} cm s^{-1} for this system in $NaClO_4$ solutions so that the redox reaction is possibly even slower on POAP than on mercury. Eu(III)/Eu(II) is not a suitable system for determining the conductivity of the POAP film. In addition, some traces of no removed oxygen could oxidise the Eu(II) produced on the potential step. Attempts were made to increase the current corresponding to Eu(II) oxidation by using higher concentration of Eu(III) and longer reduction times but no change occurred on the cyclic voltammetry curves.

Paraquat (1,1'-dimethyl-4,4'-bipyridylium or methyl viologen) is a foliage contact herbicide used in the control of a variety of plants[84]. The reversible reduction of this species leads to a violet radical which is stable for a short period of time[85] (5-10 minutes). Paraquat has been reported[86] to exhibits two reversible peaks at -0.7 V vs Ag/AgCl, in aqueous solution at pH=4. A stock solution of 1 x 10^{-3} mol dm^{-3} paraquat was prepared by dissolving the compound in a KCl (0.1 mol dm^{-3}) at pH 2. The utilised cell is that of the figure 3.2. Reduced paraquat was produced on Hg electrode by applying a potential step from 0 to -0.85V SCE for four minutes; after that time, the concentration of reduced paraquat was estimated to be about 0.5 x 10^{-3} mol dm^{-3} from the charge consumed during the potential step. The appearance of a dark blue color indicated the formation of the methylviologen radical. A voltammogram of paraquat redox reaction on bare platinum was recorded in a neutral solution to avoid the

hydrogen evolution. A 40 nm thick POAP film on a Pt electrode was used as working electrode. The results are shown in figure 4.36(b). In this case, an additional current is observed in the potential ranging from -0.25 to 0.060 V, exactly in the region where the polymer is in its reduced form; moreover, current decreases to values close to those of POAP film in a solution free of paraquat after the potential where the ESR signal is maximum (about 0.0 V SCE). This agrees with a conducting form of the POAP in the potential range from -0.25 to 0.0 V SCE where polarons seem to be the most important phenomenon of charge transfer.

Returning to the results presented in figure 4.35, it can assumed that the shift of the reduction peak of copper on POAP modified electrode, with respect to that for naked Pt electrode, originates from the different nature of the substrate, i.e. from the potential-dependent resistance of the film. Reduction currents at the modified electrode are also very similar to these recorded when a bare Pt electrode was used. These features suggest that the deposition of copper takes place on the polymer-solution interface, otherwise, an appreciable decrease in the current because of the diffusion of copper through the film would be observed. In the case of POAP films, no pinholes were visible in the scanning electron micrographs, which supports this assumption. The difference between the current-potential profiles for the reduction of copper on the POAP modified electrode and naked Pt can be related to the resistance of the polymer film by

$$R = \rho \, L/A \tag{4.3}$$

where R and L are the resistance and thickness of the film, respectively; A is the area of the electrode and ρ is the resistivity of the film (Ω cm). Knowing that conductivity (σ) is $1/\rho$ and $R = i/\Delta E$, the equation 4.3 becomes

$$\sigma = \frac{i}{\Delta E}\frac{L}{A} \tag{4.4}$$

where i is the current and ΔE is the difference of potential between points with the same magnitude of current for the reduction of copper curves on POAP modified and naked Pt electrodes.

Voltammograms of POAP modified Pt rotating disc electrode were recorded at different rotation rates. No change was observed in the POAP voltammogram when the rotation rate were under 50 rad s^{-1} because the process is controlled by charge transfer in the polymer matrix. At rotation rates higher than 50 rad s^{-1}, some portions of the polymer are removed by the whirlpool created by gyration of the electrode. Since the concentration of Cu^{2+} on the electrode surface is determined by the potential, while its rate of diffusion depends on the thickness of the diffusion layer, i.e. on the rotation rate of the disc, the voltammograms were recorded at sufficiently slow scan rates (3 mV s^{-1}) that steady state conditions applied. Under such conditions, the polymer should also have time to reach its equilibrium conductivity at each potential. In order to avoid any loss of polymer by turbulence, the rotation rate was 13 rad s^{-1} .

Figure 4.37(a) shows the voltammograms corresponding to the reduction of copper on naked Pt and on a POAP modified Pt electrode. The smaller hump observed in the i-E curve of reduction of copper on the modified electrode represents the reduction of the polymer while the larger one involves the reduction of the metal ion on the polymeric material. Small changes in the potential produce large changes in the current for the reduction of copper on naked platinum at about 0.0 V. However, the curve corresponding to the POAP modified electrode is less steep; this is due to the potential-dependent resistance of the film which controls the copper deposition. Then,

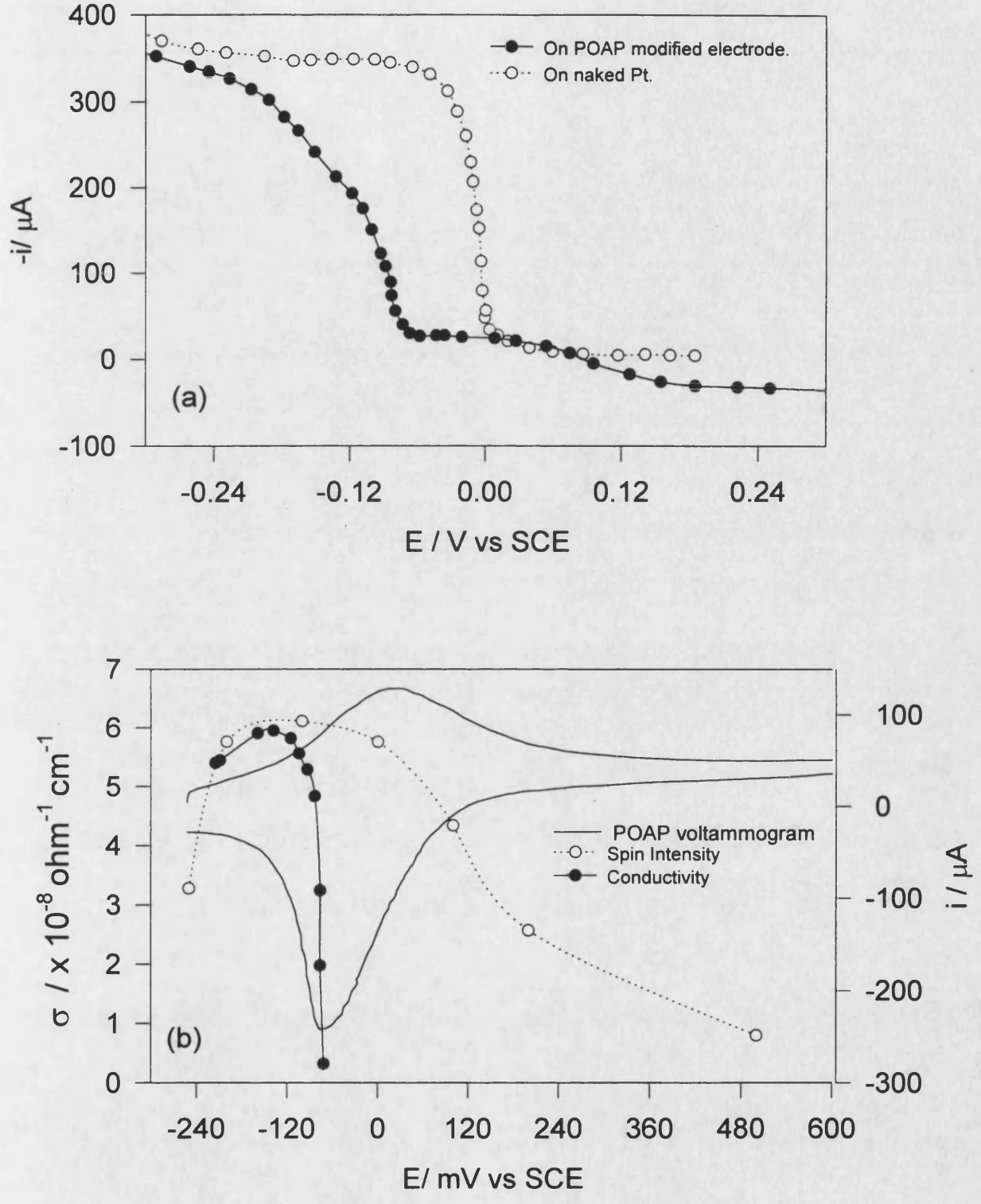

Figure 4.37 (a) Voltammograms on the rotating Pt/POAP and naked disc electrode in aqueous solution containing 3.5 mol dm^{-3} Cu^{2+} at pH 0.9 . Scan rate was 3 mV s^{-1} rotation rate 13 rad s^{-1}. (b) Changes in the conductivity of the film as a function of the potential and its correlation with the spin intensity showed in figure 4.29.

for a surface area of the electrode of 0.33 cm^2 and a thickness of the film of 80 nm, the conductivity of the film was determined as a function of polarisation potential by using equation 4.3. The resulting σ-E plot (figure 4.37(b)) is compared with the spin intensity-E (figure 4.31) characteristic. The conductivity increases very sharply at about -67 mV, peaks at about -120 mV and starts decreasing at more negative potentials. The conductivity and the spin intensity both exhibit maxima at -0.120V which clearly shows the polaronic nature of the conductivity of the film at that potential range. At more positive potentials the number of polarons decreases but not so steeply as the conductivity. It is possible that when the concentration of polarons is high they start to combine to give rise to bipolarons; some of these bipolarons are converted to the fully oxidised form of the polymer (figure 4.29) minimising the conductivity in the polymer. Some polaron islands surrounded by fully oxidised units, can still be present in segments of the chains so that the conductivity of the film is strongly minimised while ESR spectra still show the presence of radicals. Calculated conductivity values are in the same order of magnitude as the value reported by Oh-Kil[87] (1×10^{-8} ohm^{-1} cm^{-1}) from four-point probe measurements and from that calculated in section 4.5 of this chapter (9.3×10^{-8} ohm^{-1} cm^{-1}); however, these values are four orders of magnitude smaller that that measured by Barbero[24] at more positive potentials using hexacyanoferrate couple. In the present work no evidence of redox activity was observed in this region so that the films studied by Barbero evidently have quite different properties.

4.10 Crystal Impedance Measurement†

Caution must be exercised when interpreting frequency changes in the quartz crystal microbalance simply on the basis of the Sauerbrey equation (equations 2.36 and 2.37). Measurements of Δf are not sufficient to distinguish actual mass changes from contributions from viscosity (η_f) and density (ρ_f) changes of the polymer films investigated; for example, it has been found that polyacrylamide films impregnated with hexokinase gave much larger Δf values than expected when glucose binds to the enzyme in the film[88].

In order to distinguish more clearly between mass changes occurring at the electrode surface and changes in the resonant frequency due to the contacting liquid, equivalent circuits for QCM have been considered[89,90]. The actual electrical representation of a quartz resonator (figure 4.38a) with a rigid polymer deposited on it includes components such as an inertial parameter related to the displaced mass during oscillation (L_1), a capacitor representing the energy stored during oscillation (C_1) and the energy dissipation during oscillation due to internal friction and mechanical losses (R_1). This circuit also includes a capacitance (C_o) in parallel which represents the static capacitance of the quartz resonator with the electrodes. When a quartz crystal electrode is in contact with a viscous liquid or/and polymer film, a mechanical restriction to the oscillation is introduced[91]. The equivalent circuit of the figure 4.38(a) is then modified to include the mass loading density component (L_l) and a resistive viscosity component (R_l) of the liquid as well as the mass loading due to the film (L_f). Energy dissipation of the film (R_d) as well as the elasticity of the film (μ_f) are also represented in figure 4.38.

† The author gratefully acknowledges Professor R. Hillman's assistance in perfoming these measurements at the University of Leicester.

a)

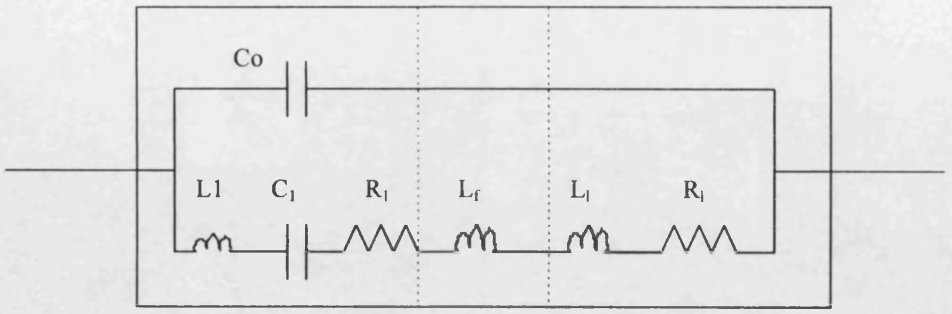

b)

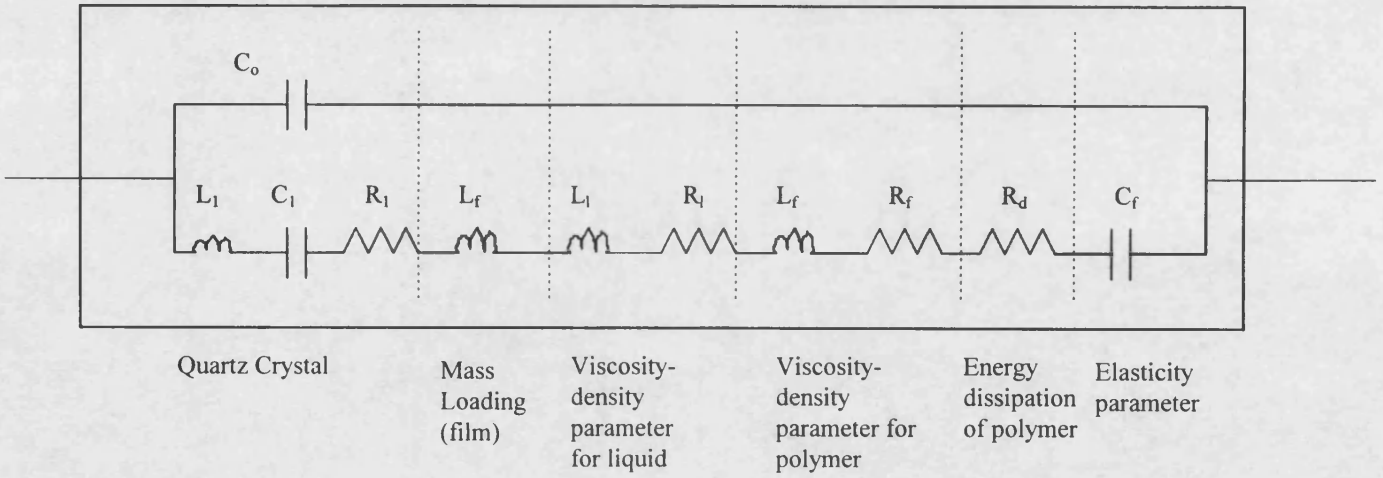

Figure 4.38 a) The general equivalent circuit representation for a quartz crystal electrode with contributions from the mass of a rigid film and the viscosity and density of a liquid in contact with one face of the crystal. b) Equivalent circuit representation for a quartz crystal with a viscoelastic polymer film in a liquid. *Buttry et al* [94].

All these circuits are based on the coupling of the mechanical displacement electric potential within the piezoelectric quartz. The impedance and admittance equations for the circuit 4.37(a) have been reported[92,93]; film and liquid contributions have been included by extension[94].

Admittance versus frequency plots (crystal impedance measurements) have been utilised to determine non-rigidity and viscosity effects on the frequency of resonance of quartz crystals[95]. This kind of plot exhibits a maximum at the frequency of resonance of the crystal, see figure 4.39. The shape of the curve and the position of the maximum will depend on the interaction of the crystal with its surrounding environment. Curve (a), figure 4.39, shows a very sharp peak centred at 9.9983 MHz corresponding to the naked quartz crystal exposed to air. This system is represented by figure 4.38 (a) where there is no mass loading and the viscosity-density effect are negligible. Curve (b) represents the admittance spectrum for a 27 nm thick POAP film deposited on the crystal electrode and dried under vacuum overnight. The crystal was exposed to air so that under such conditions the shift in the frequency of resonance, with respect to the naked electrode, is due to the mass loading of the polymer. The increase in the bandwidth is associated with a small contribution from density, viscosity and elasticity of the polymer to the impedance of the crystal. The mass of the deposited polymer was calculated from the difference between the peaks frequencies of **a** and **b** in the figure 4.39, with a calibrated mass sensitivity of 1.1 Hz/ ng. A value of 12.5 $\mu g\ cm^{-2}$ was determined. This value is approximately twice that that calculated from the anodic charge (see, section 3.7) of the voltammogram of the same film at 5 $mV\ s^{-1}$ which was 5.0 $\mu g\ cm^{-2}$. The difference between the frequencies of resonance is associated with the total mass the polymer, while the charge is related to the mass of the

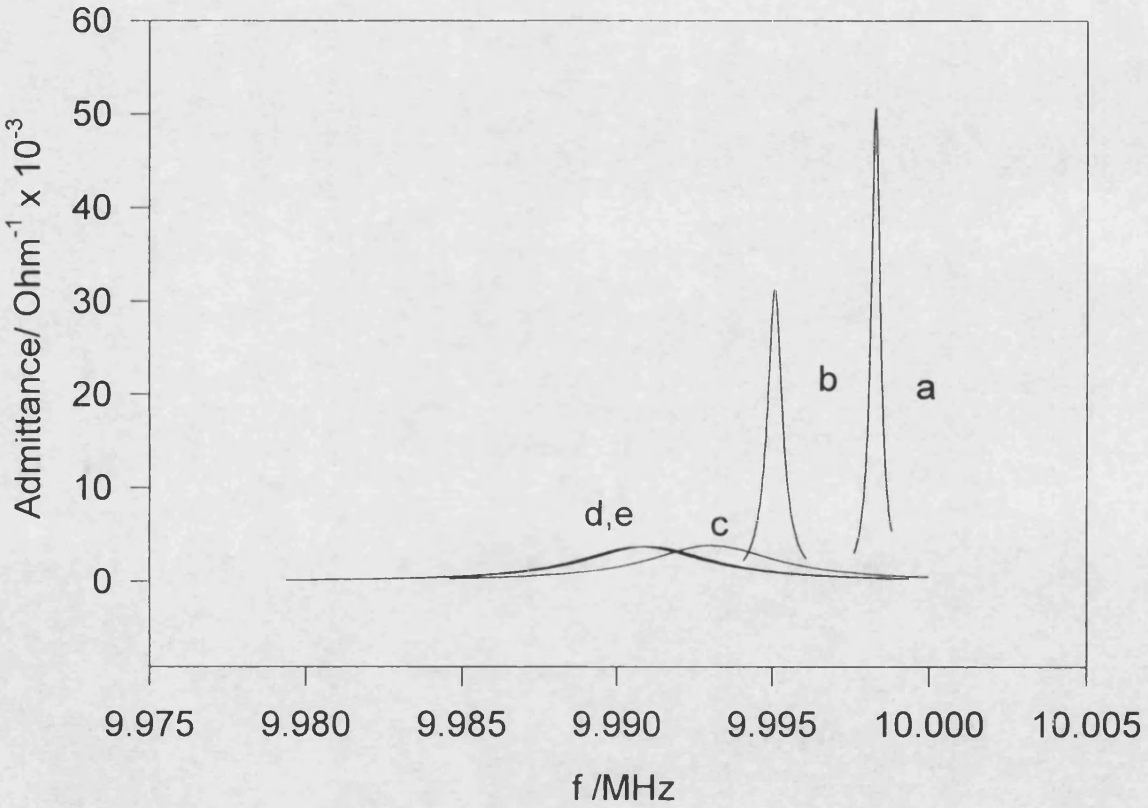

Figure 4.39 Effect of the presence of the film and solution on the admittance spectrum of the crystal. Admittance spectra for (a) naked and dried crystal, b)polymer coated and dried crystal, (c) naked crystal immersed in water, (d) polymer coated crystal in water and (e) polymer coated crystal in a $HClO_4$ solution (pH 0.9).

polymer that was electrochemically oxidised; it is possible to conclude that about 60% of the POAP film is electrochemically oxidised. Formation of the oxidised structures proposed in figure 4.29 as the electrochemical oxidation takes place can prevent the complete oxidation of the polymer chains as well as produce the decay of the conductivity of the film.

Curve (c) in figure 4.39 shows the admittance spectrum for the naked crystal immersed in water. In this case the viscosity-density (R_l and L_l) components of the figure 4.38(b) are not negligible; a decrease in the frequency of resonance and a significant increase in the bandwidth are observed. There is no polymer film on the electrode so that the presence of the liquid decreases the frequency of resonance in 5200 Hz. Typical frequency changes in aqueous media[96] are 6-7 kHz, although additional contributions due the surface roughness of the crystal may increase this value by some kilohertz[97]. The polymer coated quartz crystal immersed in water and in a $HClO_4$ solution (pH 0.9) is illustrated by curves **d** and **e**. In this case, all the components of the electric circuit from figure 4.38(b) are present. However, the fact that no appreciable change in the bandwidth with respect to the curve **c** may indicate that the polymer is rigid[98] and that viscoelastic effects are not important.

In order to determine any change in the rigidity condition with the thickness of the film, admittance spectra of the crystal were recorded during the deposition of POAP in $HClO_4$ (pH 0.9) by cycling the potential between -0.25 and 0.75 V SCE at 100 mV s^{-1}. Measurements were made at 103 points centred about the fundamental resonant frequency. Spectra were recorded every minute for the first ten minutes; afterwards, each spectra was taken in periods of ten minutes. Figure 4.40 shows the set of spectra for the deposition of POAP from 0 to 130 minutes. There is no change either in the frequency of resonance or in the bandwidth during the first ten minutes of the

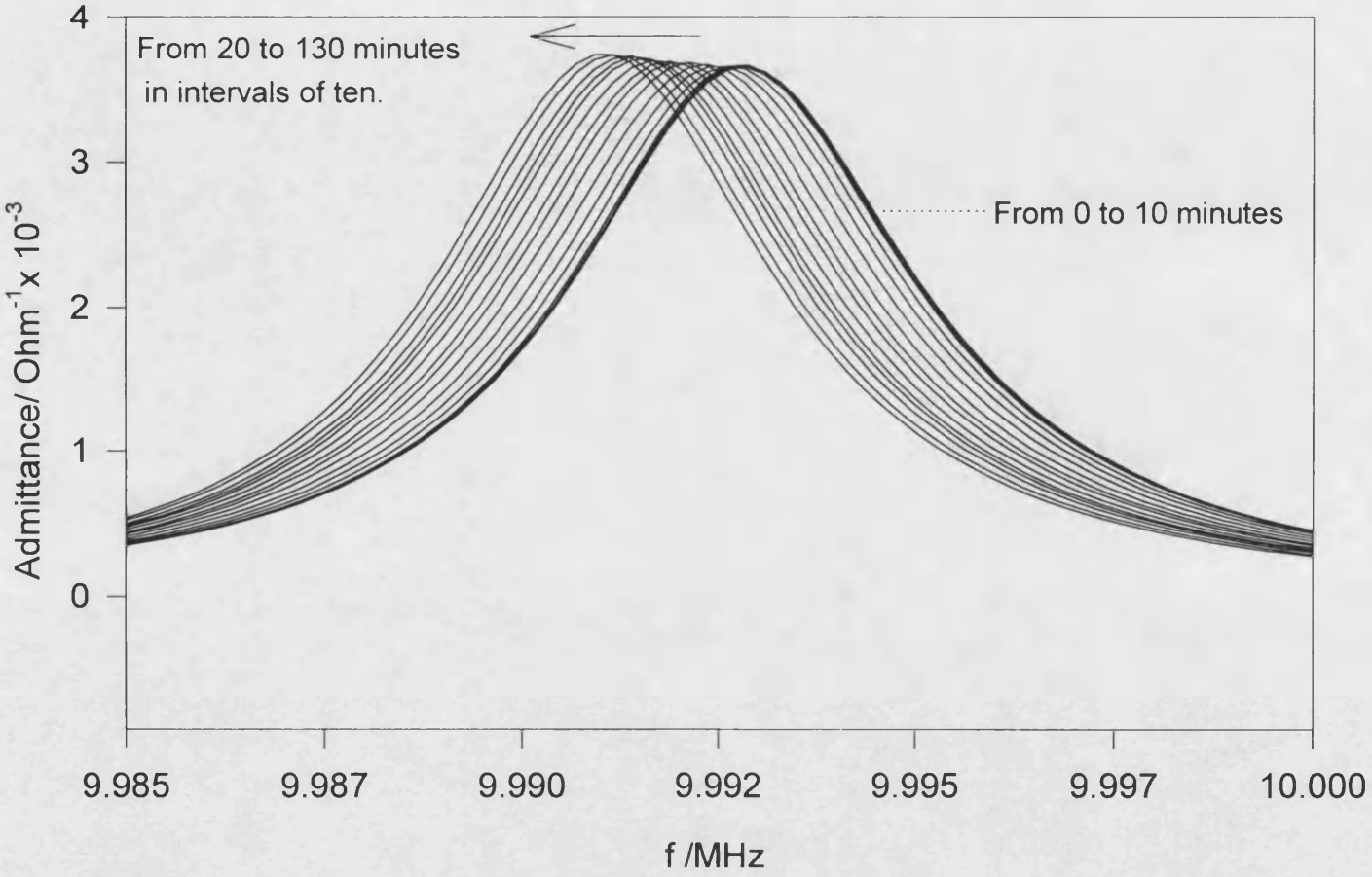

Figure 4.40 Admittance spectra for the electrodeposition of POAP in a $HClO_4$ solution (pH 0.9) at different times.

Monomer concentration 5 x 10^{-3} mol dm^{-3}. Area of electrode was 0.23 cm^{-2}.

deposition process which agrees with the induction time observed by cyclic voltammetry (section 4.2); the appearance of the voltammetric peaks corresponding to POAP coincided with the beginning of the displacement of the admittance spectra. As the deposition takes place, the spectra move toward smaller frequencies due to the mass loading; however, the bandwidth does not change. Since broadening of the spectrum is a clear signal of non-rigidity[98], so that it is possible to conclude that POAP is rigid under the experimental conditions used in this work.

The coated electrode of figure 4.40 was dried at room temperature and stored in a dessicator overnight. The mass of deposited polymer was calculated from the different frequecies between the admittance spectrum at the naked and coated crystal electrode. The mass of the polymer was calculated to be 2.9×10^{-6} g (6.1×10^{-8} mol of repeating units of the polymer cm^{-2}) The crystal was then immersed in deoxygenated water and the admittance spectrum was recorded. The decrease in the frequency represents the mass of water that went into the polymer. A value of 1.8×10^{-6} g of water was determined (4.4×10^{-7} mol of H_2O cm^{-2}, electrode area 0.23 cm^2). The liquid modulation was corrected by taking the difference in frequencies between the coated crystal and the naked crystal in water. The ratio between surface coverages gives 7.2 mol of water per POAP unit which is about 62% (w/w) of the polymer. Due to the increase in the surface roughness brought about by the presence of the polymer, the entrainment of water within the polymer boundary layer is expected to be greater than at a naked crystal electrode[99]. This effect cannot be corrected for so that the amount of water actually resident within the polymer may be less than that calculated . It is important to note that all measurement were carried out at open circuit and that the film is fully oxidised.

The admittance versus frequency plots of the oxidised form of the polymer at open circuit becomes slightly sharper as the supporting electrolyte is increased from 0.0 to 0.7 mol dm^{-3} at pH 0.9, see figure 4.41. The sharpening of the curves suggests that the polymer becomes more rigid at higher concentration of the electrolyte. This conclusion agrees with the behaviour of the Ip vs [$NaClO_4$] plots in figure 4.21, where the decrease in the peak currents of the polymer was attributed to the restriction of the access of the counterions into the film. Admittance spectra of the naked crystal electrode in the range of supporting electrolyte concentrations used in figure 4.41 showed non appreciable viscoelastic effect; the narrowing of the curves of figure 4.41 is then related mostly to changes in the rigidity of the polymer.

Figure 4.42 compares admittance spectra for the oxidised and reduced POAP film on the quartz crystal electrode. The concentration of supporting electrolyte was changed by the addition of small volumes of a more concentrated $NaClO_4$ solution (0.7 mol dm^{-3}, pH 0.9). The set of spectra of the oxidised form were recorded at open circuit. Next, for each concentration, the film was cycled between 0.7 to -0.2 V during five minutes; afterwards, the potential was held at -0.2 V for thirty minutes. All the curves of the figure 4.42(a) exhibited sharpe bands centred at 9.9911 MHz. On the other hand, the reduced form of the polymer shows broader and less intense bands at 9.9989 MHz. The shift of the resonant frequency of the reduced form of POAP with respect to the spectra for the oxidised species indicates that some mass of the polymer film increased during the reduction. This agrees with the presence of polarons in the potential range -0.25 to 0.0 V because, in order to maintain the electroneutrality of the film, the ingress of anions is required. Protonation of nitrogen atoms and the ingress of water or even of salt is possible. The broadening of the curves clearly indicates that the

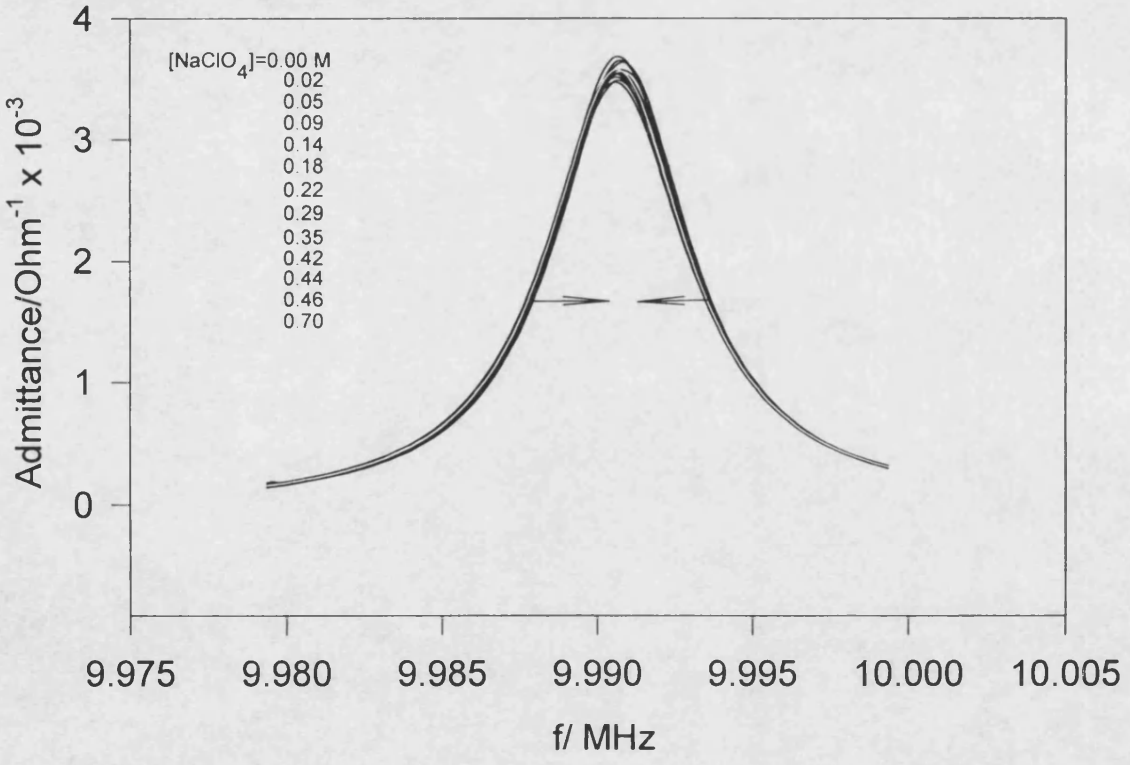

Figure 4.41 Admittance spectra for a POAP film (40 nm thick) on exposure to increasing $NaClO_4$ concentration at pH 0.9.

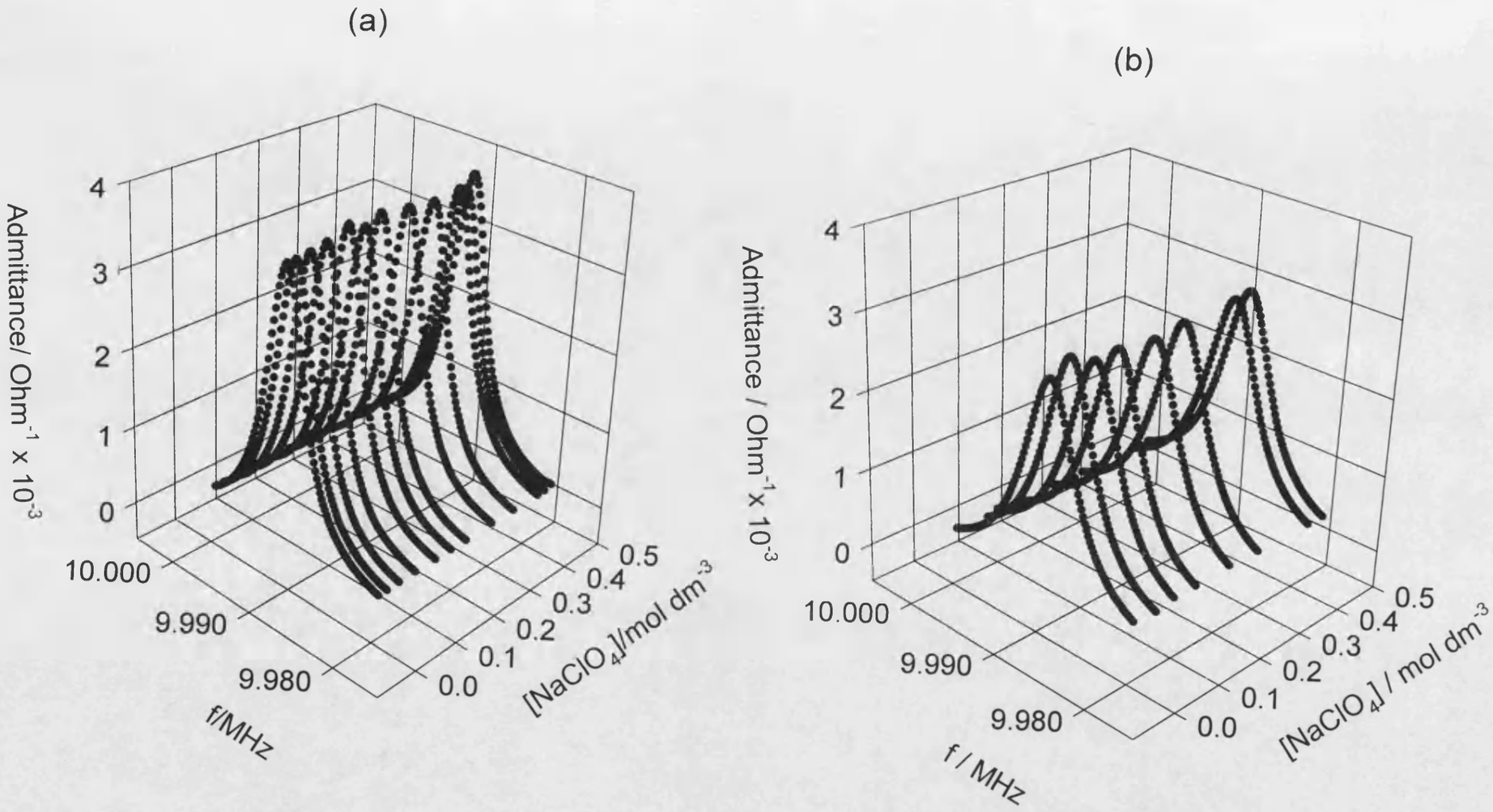

Figure 4.42 Admittance spectra for polymer coated crystal at different [$NaClO_4$] at pH 0.9 (a) oxidised film at opened circuit and (b) reduced film at -0.2 V SCE. Thickness of film: 40 nm.

polymer is less rigid. Swelling of the film is favoured by the electrostatic repulsion of the polaronic and bipolaronic states[100]. Some viscoelastic contribution to the shift in the frequency due to the change in the rigidity of the film should also be considered.

Summing up, despite the ingress of about seven molecules of water per equivalent unit of polymer in its oxidised form and the increase of mass when the polymer is reduced, POAP films showed characteristic rigidity under the experimental conditions used in this work. On the other hand, the polymer is approximately 60% oxidised by electrochemical via. The presence of an induction time, before deposition of the polymer takes place, was also observed by this method.

Mass changes during the redox process of the polymer in $HClO_4$ solution at pH 0.9 were recorded using a quartz crystal microbalance. The circuit used to make the crystal oscillate was described by Bruckenstein[91]. A 40 nm thick film was deposited on the crystal electrode by cycling the potential as has been explained in other sections of this chapter. After two hours of deposition, the solution containing the monomer was taken out and the cell was rinsed several times with ultrapure water and monomer free $HClO_4$ solution at pH 0.9. Finally, the cell was filled with the former solution and introduced into a Faraday cage. Figure 4.43 shows the mass and charge changes of the polymer under potentiodynamic conditions at three scan rates. Negative values in the mass coordinate mean loss of material while tendency toward positive values represents an increase in the mass of the polymer. The mass changes in the polymer revealed a complex behaviour; large changes were observed where the anodic and cathodic voltammetric peaks appear. In each case, some loss of mass takes place during the first half of the voltammetric peaks; after a maximum, the mass increases. There is no significant change between the mass at the initial and the end of the cycle, which means

Figure 4.43 Cyclic voltammogram and the corresponding change of mass for a 40 nm thick POAP film. Scan rate is indicated in each plot. All the scans were carried out in a $HClO_4$ solution at pH 0.9 . Dotted lines represent the mass change.

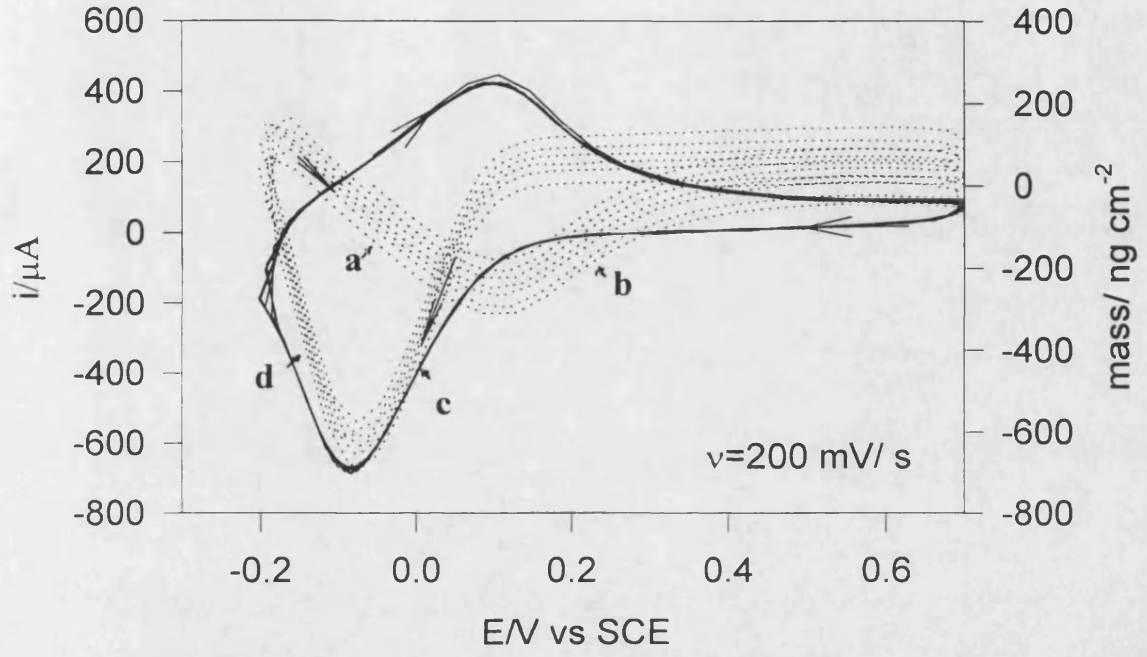

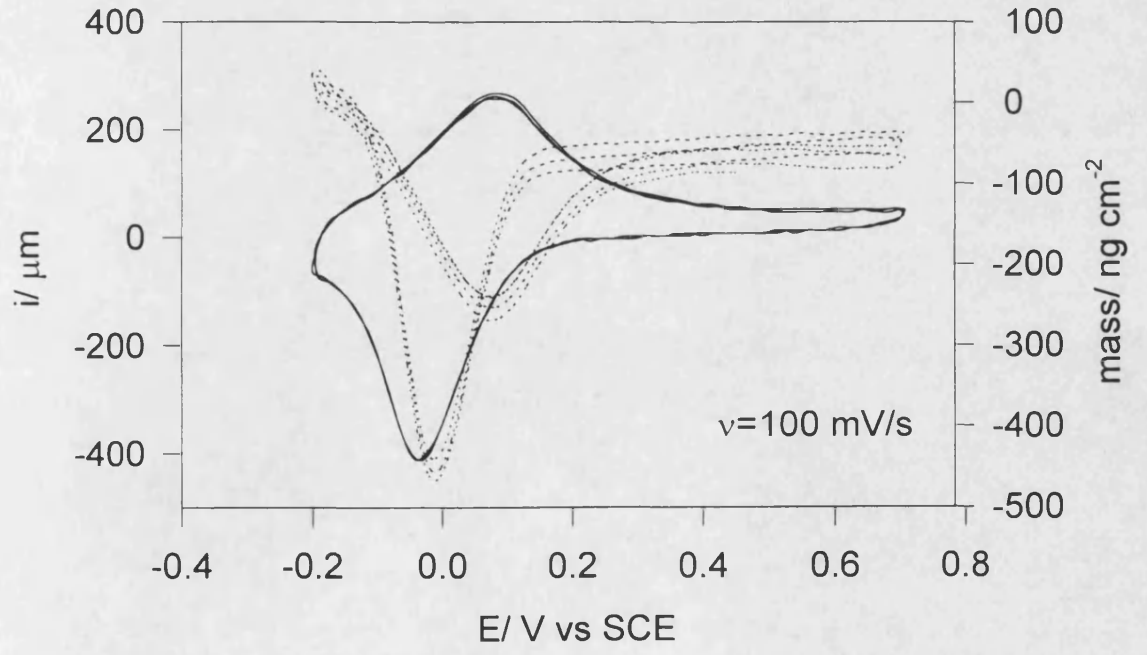

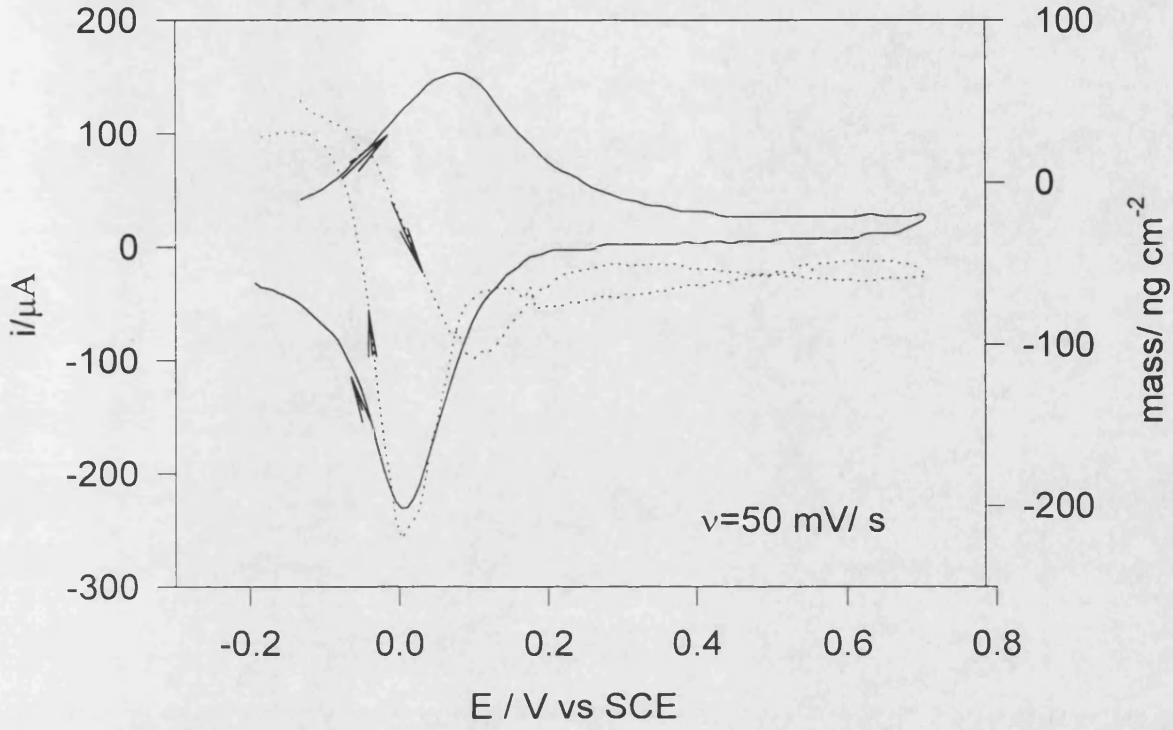
200
100
0
-100
-200
-300
i/μA
100
0
-100
-200
mass/ ng cm-2
ν=50 mV/ s
-0.2
0.0
0.2
0.4
0.6
0.8
E / V vs SCE

that the overall process is reversible. Differences in consecutive curves could be due to a slow polymer relaxation i.e. failure of the polymer to achieve its equilibrium configuration on the time scale of the experiment[98]. It is important to note that the potential range where the mass changes are maximum corresponds to the potential range where the spin density was also observed to exhibit a maximum (figure 4.37a), suggesting that the formation of polarons is involved in the mass transfer.

The net mass change per unit of area of electrode, occurring at the polymer-electrolyte interface is given by[101,102]

$$\Delta M = \sum m_i \Delta\Gamma_i + \sum m_n \Delta\Gamma_n \qquad (4.5)$$

where $\Delta\Gamma$ is the change in the molar population of species within the polymer and m is the molar mass; subscripts **i** and **n** denote ionic and neutral species, respectively. On the other hand, the net charge passed at the polymer is

$$Q = \int i dt = -\sum z_i F \Delta\Gamma_i \qquad (4.6)$$

where z_iF is the charge carried per mol of ionic species **i**. Combination of (4.5) and (4.6) yield the total mass change per mol of redox sites converted (g mol^{-1})

$$\Delta MF/Q = [\sum m_n \Delta\Gamma_n + \sum m_i \Delta\Gamma_i]/[\sum z_i \Delta\Gamma_i] \qquad (4.7)$$

ΔMF vs Q plot (normalised plot) will have a slope proportional to the average of molar mass of the species involved in the redox process.

Normalised plots for the figure 4.43 were drawn and the determined molar mass were calculated from their slopes. Averaged values are reported in the table 4.2.

Table 4.2

Apparent Molar mass from the normalised plots for figure 4.43 data.

Scan Rate mV s^{-1}	Apparent molar mass, region "a" g mol^{-1} *	Apparent molar mass, region "b" g mol^{-1}	Apparent molar mass, region "c" g mol^{-1} *	Apparent molar mass, region "d" g mol^{-1}
200	-22.9 ± 3.2	25.1 ± 2.8	-85.4 ± 5.9	93.1 ± 3.9
100	-30.4 ± 4.1	14.9 ± 2.5	-45.5 ± 6.0	31.7 ± 3.9
50	-12.5 ± 2.2	6.6 ± 0.9	-17.5 ± 1.2	20.4 ± 1.9

* Negative values indicate that the apparent molar mass is lost by the polymer film.

The previous table indicates a dependence of the mass transfer on the scale of time of the experiment. At high scan rate, the oxidation seems to involve the loss and gain of protons (H_3O^+) whereas the reduction seems to be more related to the movement of CLO_4^- ions (99.5 g mol^{-1}). As the scan rate decreases other low molecular weight species get involved (possibly salt, water) and the apparent molar mass decreases. Although this kind of plot has successively been utilised to determine the identity of the transferred species in systems as polyvinylferrocene, where little or no change in solvent content of the film was observed[103], the interpretation of much more complex behaviour like those observed for POAP films requires further experiments. In the POAP film case, mass transport is a summation of the various process occurring at any given time, so that the slopes of the normalised plots are weighted averages of the various transport processes.

4.10 Conclusions

The polymer films produced in this work exhibited different characteristics from these reported in the literature. First of all, their compact morphology contrasts with the granular appearance reported by Kunimura[19] and the bundles structures observed by Cornelison[30]. Secondly, the measured conductivity values are of the order of $10^{-8}\ \Omega^{-1}\ cm^{-1}$, four orders of magnitude smaller than that determined by Barbero[24], and are inversely dependent on the pH. Observed changes of the peak potentials as a function of the pH revealed different behaviour from Barbero's[24]. The asymmetric chronoamperometric curves for the oxidation and reduction of POAP films disagree with these reported by Kunimura[20]. Finally, uv-visible spectra of the films produced in this work differ from those reported in the literature[20,22]. All those discrepancies can be attributed to formation of films with different structural composition. Poly-orthoaminophenol films produced in the present work appear to be a composite of two repeating units: a closed ring structure originated by coupling of 3APZ precursor, and an opened structure originated by coupling, during the path "c" shown in figure 4.1, of a species similar to API. This species and 3APZ could be formed simultaneously.

The presence of a mixture of structures in the polymer chain significantly affects the conductivity of the film by a decrease of the planarity of its structure. The IR spectrum reported by Barbero[2] does not show any band corresponding to carbonyl groups while an intense band at 1743 cm^{-1} was observed for films obtained in this work which supports the presence of an opened structure.

Characterisation of the changes in the oxidation state of the polymer by uv-visible spectroscopy revealed three peaks at 414, 690 and 492 nm which were assigned

to formation of polarons, bipolarons and an oxidised form of the polymer similar to 2-amino-o-indophenol (AIP), respectively. The band at 492 nm agrees with the presence of carbonyl groups when the polymer is oxidised. The absence of isobestic points indicates the presence of a mixture of structures as the oxidation occurs.

Morphology of the films is quite compact and smooth, and independent of the supporting electrolyte used ($NaClO_4$, Na_2SO_4 , $NaNO_3$ and NaCl).

From the limiting voltammetric behaviour observed during growth of the polymer and from the experiments with redox couples, it was demonstrated that this polymer exhibits conducting properties at potentials more negative than the formal potential of the film which is opposite to the conclusion reached by Barbero[24] by using species with redox potentials more positive or negative that the anodic peak potential of the film. The presence of an opened structure affects the range of potential where the polymer is conducting. Formation of non conducting oxidised forms of POAP in different sections of the polymer chains significantly decreases the conductivity of the film since polarons and bipolarons become insulated defects along the chains. This conclusion is also supported by the ESR experiments which indicated formation of polarons in that potential region. Creation of bipolarons by combination of polarons is also possible, but it seems that dications are not an important factor in the charge transfer.

About 60% of the polymer was determined to be electrochemically oxidised; formation of oxidised non conducting forms along the chains prevents further oxidation of the polymer. The number of molecules of water per POAP equivalent in its oxidised form was determined to be approximately 7. As the reduction proceeds, swelling of the film takes place but it still exhibits rigidity features.

The change in the polymer mass during the oxidation-reduction of the film under potentiodynamic conditions reflects the electroneutrality requirement for counterion insertion. However , the overall process is complex and needs to be analysed with more detail in the future.

References

1 . D. Goncalves, B. Matvienko, L.O.S Bulhoes, *J. Electroanal. Chem.*, 371 (1994) 267.

2 . C. Barbero, J. J. Silber, L. Sereno, *J. Electroanal. Chem.*, 263(1989) 333.

3 . A.F. Díaz, J. I. Castillo, J.A. Logan, W. Y Lee, *J. Electroanal.Chem.*, 129 (1981) 115.

4 . T. Kobayashi, H. Yoneyama, H.Tamura, *J. Electroanal. Chem.*, 177 (1984) 281.

5 . J.C. Lacroix, P. García. J. P. Audiere, R. Clement, O. Kahn, *New J. Chem.*, 14(1990)87.

6 . K. Jackowska, J. Bukowska, A. Kudelski, *J. Electroanal.Chem.*, 350 (1993) 177.

7 . K. Jackowska, J. Bukowska, A. Kudelski, *Polish J. Chem.*, 68 (1994) 141.

8 . E.M. Genies, M. Lapkowski, C. Tsintavis, *New J. Chem.*, 12 (1988) 181.

9 . T. Nogami, T. Hishida, M. Yamada, H. Mikawa, Y. Shirota, *Bull. Chem. Soc. Jpn.*, 48 (1975) 3709.

10 . O.K Kim, *J. Polym. Sci., Polym. Lett. Ed.*, 23 (1985) 137.

11 . J.F. Stille, M. E. Freeburger, *J. Polym. Sci., Polym. Chem. Ed.*, 6 (1968) 161.

12 . A.M. Heras, J. L. Avila, J.J. Ruiz, F. García-Blanco, *Electrochim. Acta.*, 29 (1984) 541.

13 . S. Taj, M. F. Ahmed, S. Sankarapapavinasam, *J. Electroanal. Chem.*, 338 (1992) 347.

14 . T.L. Porter, P. I. Oden, *Synth. Met.*, 53 (1993) 309.

15 . K. B. Prater, *J. Electrochem. Soc.*, 120 (1973) 365.

16 . S. Sankarapapavinasam, *J. Polymer Science. Poly Chem.*, 31 (1993) 1105.

17 . S. Sankarapapavinasam, *Synth. Met.*, 58 (1993) 173.

18 . K. Chiba, T. Ohsaka, N. Oyama, *J. Electroanal.Chem.*, 219 (1987) 117.

19 . S. Kunimura, T. Ohsaka, N. Oyama, *Macromolecules*, 21 (1988) 894.

20 . T. Ohsaka, S. Kunimura, N. Oyama, *Electrochim. Acta.*, 33 (1988) 639.

21. A.Q. Zhang, C.Q. Cui, Y.Z. Chen, J.Y. Lee, *J. Electroanal. Chem.*, 373 (1994) 115.

22. C. Barbero, J. Zerbino, L. Sereno, D. Posadas, *Electrochim. Acta.*, 32 (1987) 693.

23. P. Daum, R. W. Murray, *J. Phys. Chem.*, 85 (1981) 389.

24. C. Barbero, J. J. Silber, L. Sereno, *J. Electroanal. Chem.*, 291 (1990) 81.

25. T. Ohsaka, T. Watanabe, F. Kitamura, N. Oyama, K. Tokuda, *J. Chem. Soc. Chem. Commun.*, (1991) 1072.

26. J. R. Reynolds, *Journal of Molecular Electronics.*, 2 (1986) 1.

27. V. M. Schmidt, J. Heitbaum, *Electrochimica Acta.*, 38 (1993) 349.

28. A.F. Díaz, B. Hall, *IBM J. Res. Dev.*, 27 (1983) 342.

29. M. Irene Montenegro, M. Arlete Queirós, John L. Daschbach(Eds),*Microelectrodes: Theory and Applications.*, NATO ASI Series, Vol. 197, Kluwer Academic Publisher, Netherlands (1990).

30. D.M. Cornelison, G.E. Bowman, T.L. Porter, *Synth. Met.*, 58 (1993) 383.

31. G.E. Bowman, D.M. Cornelison, G. Caple, T.L. Porter, *J. Vac. Sci. Technol.*, A, 11 (1993) 2266.

32. William Kemp, *Organic Spectroscopy*, third edition, MacMillan Press, Hong Kong, (1991).

33. H. Dudley, Fleming Ian, *Spectroscopy Methods in Organic Chemistry*, fifth edition, McGraw-Hill Book Company, London, (1995).

34. R. L. Hand, R. F. Nelson, *J. Electrochem. Soc.*, 125 (1978) 1053.

35. *The Aldhich Library of Infrared Spectra*, Charles J. Pouchert (Ed), Aldrich Chemical Company Inc.

36. F. A. Miller, C. H. Wilkins, *Anal. Chem.*, 24 (1952) 1253.

37. P. Daum, J.R. Lenhard, D. Rolison, R. W. Murray, *J. Am. Chem. Soc.*, 102 (1980) 4649.

38. P. Daum, R.W. Murray, *J. Electroanal. Chem.*, 103 (1979) 289.

39. M.D. Ward, *J. Phys. Chem.*, 92 (1988) 2049.

40. C. Iwakura, T. Kawai, M. Nojima, H. Yoneyama, *J. Electrochem. Soc.:Electrochem Sci and Technology.*, 134 (1987) 791.

41. J. R. Lenhard, R.W. Murray, *J. Am. Chem. Soc.*, 100 (1978) 7870.

42. F. B. Kaufman, E.M. Engler, *J. Am. Chem. Soc.*, 101 (1979) 547.

43. M.C. Miras, C. Barbero, R. Kötz, O. Haas, *J. Electroanal. Chem.*, 369 (1994) 193.

44. J. L. Gillson, W. R. Hertler, *J. Polym. Sci. Polym. Lett. Ed.*, 14 (1976) 151.

45. R.J. Nowak, F.A. Schultz, M. Umaña, R. Lam, R.W. Murray, *Anal. Chem.*, 52 (1980) 315.

46. G. Inzelt, J. Bácskai, *Electrochimica. Acta.*, 37 (1992) 647.

47. G. Inzelt, *Electrochim. Acta.*, 34 (1989) 83.

48. G. Inzelt, J. Bácskai, J. Q. Chambers, R.W. Day, *J. Electroanal. Chem.*, 201 (1986) 301.

49 G. Inzelt, L. Szabo, *Electrochimica. Acta.*, 31 (1986) 1381.

50. M. Vuki, Ph.D Thesis, Southampton University, 1993.

51. P. Daum, R.W. Murray, *J. Phys. Chem.*, 85 (1981) 389.

52. D.M. Oglesby, S.H. Omang, C.N. Reilley, *Anal. Chem.*, 37 (1965) 1312.

53. T. Nogami, T. Hishida, M. Yamada, H. Mikawa, Y. Shirota, *Bull. Chem. Soc. Jpn.*, 48 (1975) 3709.

54. D. E. Stilwell, S. Park, *J. Electrochem. Soc.*, 136 (1989) 427.

55. W. S. Huang, A. G. MacDiarmid, *Polymer.*, 34 (1993) 1833.

56. M. Lapkowski, G. Bidan, *J. Electroanal. Chem.*, 362 (1993) 249.

57. S.H. Glarum, J.H. Marshall, *J. Electrochem. Soc.*, 134 (1987) 142.

58. J. F. Corbett, *J. Chem. Soc.*, B (1970) 1502.

59. S. P. Harmalker, D. T. Sawyer, *J. Org. Chem.*, 49 (1984) 3579.

60. M. Kalaji, L. Nyholm, L.M. Peter, *J. Electroanal. Chem.*, 313 (1991) 217.

61. T. M. McKinney, *Electroanal. Chem.*, 10 (1977) 97.

62. E. M. Genies, J. M Pernaut, *Synth. Met.*, 10 (1984/1985) 117.

63. P. Marque, J. Roncali, *J. Phys. Chem.*, 94 (1990) 8614.

64. J. Tang, R. D. Allendoerfer, R. A. Osteryoung, *J. Phys. Chem.*, 96 (1992) 3531.

65. E. M. Genies, M. Lapkowski, *J. Electroanal. Chem.*, 236 (1987) 199.

66. M. Nechtschein, F. Devreux, F. Genoud, E. Vieil, J. M. Pernaut, E. M. Genies, *Synth. Met.*, 15 (1986) 59.

67. K. Jackowska, A. Kudelski, J. Bukowska, *Electrochim. Acta.*, 39 (1994) 1365.

68. S. N. Hoier, D.S. Ginley, S. Park, *J. Electrochem. Soc.*, 135 (1988) 91.

69. D. D. Cunningham, A. Galal, C. V. Pham, E. T. Lewis et al, *J. Electrochem. Soc.*, 135 (1988) 2750.

70. T. Amemiya, K. Hashimoto, A. Fujishima, K. Itoh, *J. Electrochem. Soc.*, 138 (1991) 2845.

71. A. F. Díaz, J. M. Vasquez Vallejo, A. Martínez Durán , *IBM J. Res. Dev.*, 25 (1981) 42.

72. M. Skompska, L. M. Peter, *J. Electroanal. Chem.*, 383 (1995) 43.

73. Standard Potentials in Aqueous Solution, A.J. Bard, R. Parsons and J. Jordan (Eds.), Marcel Dekker Inc, New York (1985).

74. A. Roig, J. Navarro, J. J. García, F. Vicente, *Electrochim. Acta.*, 39 (1994) 437.

75. P. J. Kulesza, S. Zamponi, M. Berrettoni, R. Marassi, M. A. Malik, *Electrochim. Acta.*, 40 (1995) 681.

76. J. Crousier, I. Bimaghra, *J. Applied. Electrochem.*, 23 (1993) 775.

77. Southampton Electrochemistry Group, *Instrumental Methods in Electrochemistry*., Ellis Horwood Series in Physical Chemistry, New York (1990).

78. Z. Borkowska, H. Elzanowska, *J. Electroanal. Chem.*, 76 (1977) 287.

79. M. J. Weaver, F. C. Anson, *J. Electroanal. Chem.*, 65 (1975) 711.

80. J. A. Rard, *Chemical Reviews.*, 85 (1985) 555.

81. I. Kisova, M. Sluyters-Rehbach, J.H. Sluyters, *J. Electroanal. Chem.*, 40 (1972) 29.

82. J. Tabib, J. T. Hupp, M. J. Weaver, *Inorg. Chem.*, 25 (1986) 1916.
J. Chlistunoff, H. Elzanowska, Z. Galus, *Polish Journal of Chemistry.*,57 (1983) 301.

84. K. A. Hassall, *The Chemistry of Pesticides: Their Metabolism, Mode of Action and Uses in Crop Protection*, Verlag Chemie, Weinheim (1982).

85 P. Shivhare, V.K. Gupta, *Analyst.*, 116 (1991) 391.

86 J. M. Pinilla Macías, L. Hernández Hernández, J. M. Moreno Sobrino, M. T. Sevilla Escribano, *Electroanalysis.*, 5 (1993) 79.

87. K. Oh-Kil, *J. Poly. Sci: Polymer Letter.*, 23 (1985) 137.

88. S. J. Lasky, D.A. Buttry, *ACS Symp. Ser.*,403 (1989) 237.

89. H. Muramatsu, E. Tamiya, I. Karube, *Anal. Chem.*, 60 (1988) 2142.

90. S. J. Martin, V. E. Granstaff, G. C. Frye, *Anal. Chem.*, 63 (1991) 2272.

91. S. Bruckenstein, M. Shay, *Electrochim. Acta.*, 30 (1985) 1295.

92. C. -S. Lu, *J. Vac. Sci. Technol.*, 12 (1975) 578.

93. C. -S. Lu, O. Lewis, *J. Appl. Phys.*, 43 (1972) 4385.

94. D.A. Buttry, M. D. Ward, *Chem. Rev.*, 92 (1992) 1355.

95. A. Glidle, A. R. Hillman, S. Bruckenstein, *J. Electroanal. Chem.*, 318 (1991) 411.

96. A. R. Hillman, D. C. Loveday, M. J. Swann, S. Bruckenstein, C. P. Wilde, *ACS Symposium Series.*, chapter 12, vol. 487 (1992) 150.

97. R. Schumacher, J. G. Gordon, O. Melroy, *J. Electroanal. Chem.*, 216 (1987) 127.

98. A. R. Hillman, D. C. Loveday, A. Glidle, J. G. Vos, A. P. Clarke, D. Kelly, S. Bruckenstein, *Macromol. Symp.*, 80 (1994) 323.

99. R. Beck, U. Pittermann, K. G. Weil, *J. Electrochem. Soc.*, 139 (1992) 453.

100. S. B. Tuwiner, *Diffusion and Membrane Technology.*, Chapman and Hall, New York (1992).

101. A. R. Hillman, D. C. Loveday, M.J. Swann, S. Bruckenstein, C. P. Wilde, *J. Chem. Soc. Faraday Trans.*, 87 (1991) 2047.

102. A.R. Hillman, M. J. Swann, S. Bruckenstein, *J. Phys. Chem.*, 95 (1991) 3271.

103. P. T. Varineau, D. A. Buttry, *J. Phys. Chem.*, 91 (!987) 1292.

Chapter 5

Electrodeposition of Copper on Poly-o-Aminophenol

CHAPTER 5

ELECTRODEPOSITION OF COPPER ON POLY-o-AMINOPHENOL

5.1 Introduction

The reduction of copper on POAP modified Pt electrodes is possible by application of negative enough potential, as it was shown in the previous chapter, section 4.9. This redox process involves a phase transformation on the electrode surface and the term *electrocrystallisation* is used to describe it. Metallic deposits find extensive application in plating processes[1], plating of printed circuit boards[2] and production of conductive copper tracks on polymer base materials[3]. Adding organics is widely used to control the plating process and the quality of the deposits; these organics do not take part in the electrode reaction, but influence the electrocrystallisation process[4]. The most of investigations deal with metal deposition onto metal electrodes. Electrodeposition of metals on conducting polymers is less explored. This change in the nature of the substrate can modify the characteristics of the electrodeposition process and so the features of the electrodeposit itself. Adhesion between the polymer and metal layers, for example, can be enhanced by chemical functionalisation of the surface polymer chains[5]. In this chapter, the transients corresponding to the reduction of copper on POAP films at different overpotentials are discussed. A comparison between the behaviour predicted by electrocrystallisation theory and that observed by scanning electron microscopy photographs is reported.

5.2 Electrocrystallisation Theory

Electrocrystallisation is defined as the process of electrochemically induced phase transformation on a electrode surface. This solid new phase can occur by a reduction process as in metal deposition or the oxidation of the electrode surface followed by reaction with anion to form an anodic film[6]. The process is not a simple step phenomenon. It involves a number of distinct steps[7] as follows

a.- Diffusion of ions to the electrode.
b.- Electron transfer.
c.- Partial or complete loss of the solvation sheath.
d.- Surface diffusion of ad-atoms.
e.- Clustering of ad-atoms to form critical nuclei.
f.- Incorporation of clusters at lattice sites.
g.- Development of crystallographic and morphological characteristic of the deposit.

The growth of a solid phase from its supersaturated vapour is necessarily generated from metastable systems by nuclei formation. The Gibbs free energy change associated with growth of the solid phase is given by

$$\Delta G = -RT \ln\left(\frac{p}{p^*}\right) \qquad (5.1)$$

where R and T have their usual meaning; p and p^* are the vapour pressure of the system and the equilibrium vapour pressure at a particular temperature, respectively. Equation 5.1 is valid for macroscopic bodies where ratio of their surface area to their volume is effectively zero. For small particles the contribution of the surface free energy is important. At the equilibrium, the vapour pressure p is given by Kelvin equation[7]

$$\ln\left(p/p_{\infty}\right)=\left(\frac{2\gamma V}{RT}\right)\frac{1}{r} \qquad (5.2)$$

where γ is the molar surface free energy (surface tension), V is the molar volume of the condensed phase and p_{∞} is the equilibrium vapour pressure in the limit that the radius of the curvature, r, tends to infinity ($1/r \rightarrow 0$). The smaller the radius of the droplet, the larger should be the pressure of vapour in equilibrium with the droplet of liquid if stable small centres are formed. The overall free energy of change is the sum of surface and bulk components for a spherical centre

$$\Delta G_s = 4\pi r^2 \gamma \qquad (5.3)$$

$$\Delta G_b = \frac{4}{3}\pi r^3 \Delta G_v \qquad (5.4)$$

where ΔG_v is the free energy change per unit volume associated with the formation of the bulk phase.

$$\Delta G_v = -\frac{RT}{V}\ln\left(p/p^*\right) \qquad (5.5)$$

Figure 5.1 illustrates the behaviour of the equations (5.3) and (5.4) and the overall change of ΔG as a function of the radius of the particle. The bulk component of the free energy ΔG_b is always negative because of (5.5). On the other hand, ΔG_s is always positive. For small values of r, ΔG_s is large and predominant in the overall free energy, defined as $\Delta G_{net} = \Delta G_b + \Delta G_s$; for large values of r, ΔG_b dominates. This change in the sign of the overall energy indicates the formation of a maximum characterised by

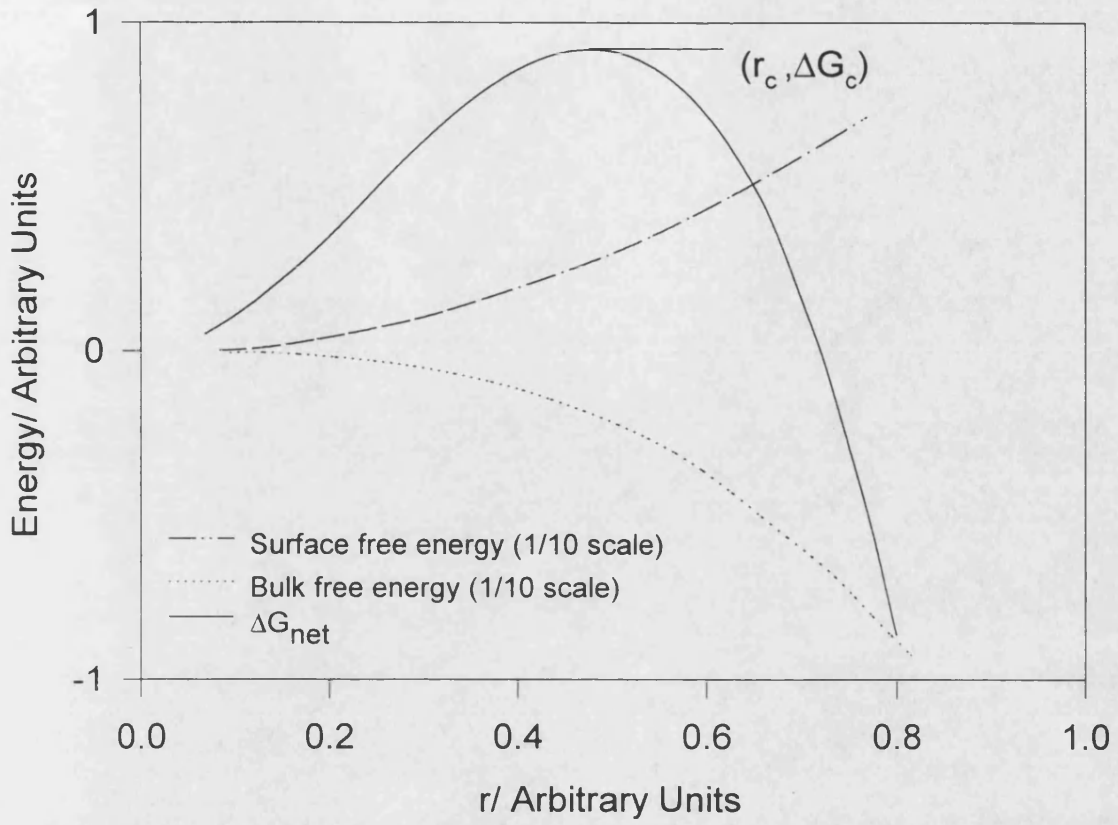

Figure 5.1 Gibbs free energy curves for the homogeneous nucleation of a spherical mercury drop from the vapour phase. Contributions from surface and bulk energy are also shown.

a critical free energy and radius. A stable nucleus is formed only if its radius exceed the critical radius by overcoming of the energy barrier ΔG_c.

In the case of electrochemical phase formation, equilibrium is established by electron transfer

$$M^{n+} + ne^- \rightleftharpoons M$$

and the surface activity of ad-atoms (a_{Mads}) at a given potential will differ from its equilibrium value (a^*_{Mads}) following the Nernst equation

$$\frac{a_{Mads}}{a^*_{Mads}} = \exp(-nF\eta/RT) \qquad (5.6)$$

where η (overpotential) is the shift of the potential with respect to the equilibrium potential. The free energy of formation of the condensed phase is

$$\Delta G_v = {}^{nF\rho\eta}/_{M} \qquad (5.7)$$

where M is the molecular weight and ρ is the density of the deposit. ΔG_{net} for spherical centre formed on the electrode surface is given in this case by

$$\Delta G_{net} = \frac{4\pi r^3 \rho nF\eta}{3M} + 4\pi r^2\gamma \qquad (5.8)$$

Expressions for ΔG_c and r_c are determined by taking the derivative of (5.8) with respect to r.

$$\Delta G_c = \frac{16\pi M^2\gamma^3}{3\rho^2 n^2 F^2 \eta^2} \qquad (5.9)$$

$$r_c = -\frac{2M\gamma}{nF\eta\rho}$$

A ΔG_{net} versus r plot will exhibit the same shape that figure 5.1 but in this case the maximum of the curve will depend on the overpotential , i.e. critical radius and ΔG_c decrease with the overpotential.

The classical approach to nucleation considers the clusters as one unique species; their surface tension and composition are assumed to be identical to those of the bulk phase at equilibrium which is not true for clusters of only a few angstroms in diameter[8] . At the same time, the subdivision of free energy terms into bulk and surface contributions implies an abrupt discontinuity in the molecular environment at the interface; the surface thickness of the liquid - vapour transition for argon was calculated to be only seven or eight molecular diameters[9] .

Walton[10] considered the concentration of clusters using statistical mechanics, avoiding the use of surface energy concepts. In this case, the small clusters are defined not in terms of macroscopic physical quantities but instead, on the frequency of attachment and detachment of individuals atoms or ions of the form

$$n-1 \rightleftharpoons n \rightleftharpoons n+1$$

In the steady state, the rates of addition or loss of particles must be equal but, as the cluster size increases up to a critical value, further addition of particles results in the formation of stable growth centres. In other to fit the non steady-steady state distribution of particles, the stable clusters are viewed in terms of removal and re-introduction of particles with a steady state rate (j_{st}) given by

$$J_{st} = Z\alpha^* c^* \qquad (5.10)$$

where α^* is the rate at which particles are added to the critical cluster and c^* is the equilibrium concentration of critical clusters. The Zeldovich factor (Z) is a

dimensionless parameter which accounts for the fact that clusters are removed from the steady distribution as they approach to the critical size. The concentration of critical clusters ,c^*, is related to the concentration of particles by the Boltzmann expression

$$c^* = c_1 \exp\left(\frac{-\Delta G_n}{\kappa_B T}\right) \qquad (5.11)$$

where c_1 is the number of single adsorbed atoms and ΔG_n is the energy of formation of the cluster which is identical to ΔG_c in (5.9).

In practice, a real surface exhibits a differentiated array of sites at which an atom can be incorporated so that nuclei may be formed at preferred active sites on the surface. The rate of appearance of stable nuclei follows first order kinetics with the number density of centres given by

$$N_{(t)} = N_o\left(1 - \exp^{(-At)}\right) \qquad (5.12)$$

where N_o is the number of actives sites under particular experimental conditions and A is the first order nucleation rate constant. Two limiting cases can be distinguished[11] . If A is large, all the sites are converted to nuclei virtually instantaneously and (5.12) becomes

$$N \cong N_o \qquad (5.13)$$

where the number of active sites is independent of time. This limiting is referred to as *instantaneous* nucleation.

On the other hand, if A is smaller (5.12) is given by

$$N \cong AN_0 t \qquad (5.14)$$

In this case, new nuclei are formed at a constant rate, and the process is referred as to *progressive* nucleation.

The new phase starts with the formation of new centres followed by their growth. The growth of metals on electrodes and anodic films has been analysed by considerations of the geometry of their growing centres[11,12]. In the case of formation of a monolayer, the growth centres can be thought of as disc shapes one atom or molecule thick which grow by the incorporation of atoms or molecules to the edges of the discs (determining step). The current density associated with the growth for instantaneous and progressive nucleation is given by

$$\begin{aligned} j_{inst} &= \frac{2N_0 \pi n F k^2 h M}{\rho} t \\ j_{prog} &= \frac{2AN_0 \pi n F k^2 h M}{\rho} t^2 \end{aligned} \qquad (5.15)$$

where k is the rate of incorporation (mol cm^{-2} s^{-1}) and h is the height of the cylinder. If the process of nucleation and growth extends over a considerable period of time, the predicted current from the set of equations (5.15) does not apply because of the overlapping of growing centres. The theorem developed by Avrami[13] relates the normalised area covered by growing centres (S) to the normalised extended area (S_{ex}) by the expression

$$S = 1 - \exp(-S_{ex}) \qquad (5.16)$$

a b c

Figure 5.2 Representation of Avrami theorem. (a) Overlapping of growth centres, (b) real area corresponding to (a) and the extended area (c).

The consideration of the extended area into (5.15) leads to the following expressions

$$j_{inst} = \frac{2\pi nFMhN_o k^2 t}{\rho} \exp\left(\frac{-\pi N_o M^2 k^2 t^2}{\rho^2}\right)$$
$$j_{prog} = \frac{\pi nFMhAN_o k^2 t^2}{\rho} \exp\left(\frac{-\pi M^2 AN_o k^2 t^3}{3\rho^2}\right) \qquad (5.17)$$

These equations can be simplified to the normalised forms

$$\frac{j_{ins}}{j_m} = \frac{t}{t_m} \exp\left(\frac{-\left(t^2 - t_m^2\right)}{2t_m^2}\right)$$
$$\frac{j_{prog}}{j_m} = \frac{t^2}{t_m^2} \exp\left(\frac{-2\left(t^3 - t_m^3\right)}{3t_m^3}\right) \qquad (5.18)$$

The shapes of the curves originated from (5.18) are shown in figure 5.3(a) and are useful diagnostic criteria for the kind of nucleation involved[14].

The shape of three dimensional growth centres has been represented by considering simple geometries[15,16] which lead to analytical expressions for the current transient under potentiostatic conditions. A simple approach to the three dimensional growth model is obtained by considering the centre to be a circular cone[16]. The growth

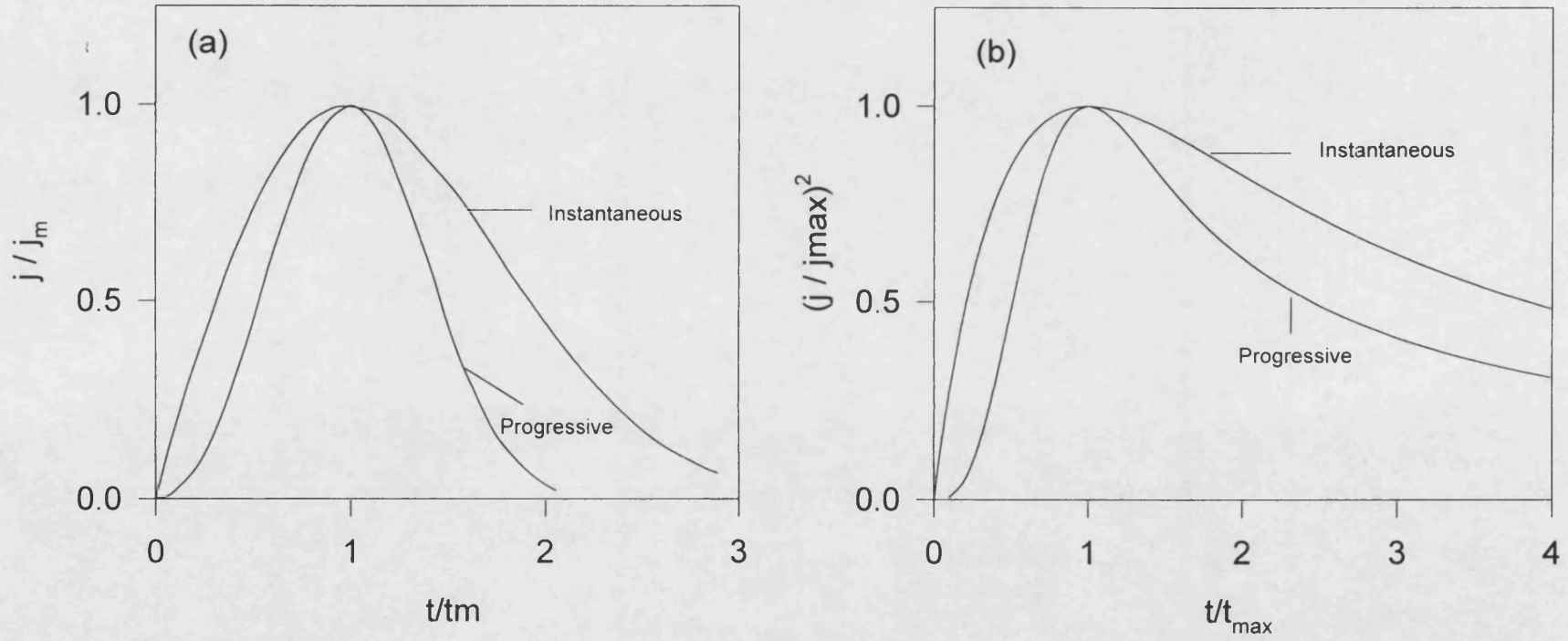

Figure 5.3 (a)Dimensionless plots for the growth of monolayer deposits by instantaneous and progressive nucleation cases. (b) Dimensionless plots for three dimensional nucleation under diffusion controll.

in the direction parallel to the substrate surface takes place with the rate constant k_3 and that which is normal to the surface, (k'_3). The solutions, for the instantaneous and progressive nucleation, have the forms

$$j_{inst} = nFk'_3\left(1-\exp\left(\frac{-\pi M^2 k_3^2 N_o t^2}{\rho^2}\right)\right)$$

$$j_{prog} = nFk'_3\left(1-\exp\left(\frac{-\pi M^2 k_3^2 A_3 t^3}{3\rho^2}\right)\right) \qquad (5.19)$$

In the case of hemispherical growth centres, the current transient for instantaneous and progressive nucleation in their reduced forms is given by[17]

$$\frac{j_{inst}}{j_m} = (t/t_m)^2 \exp\left(-2/3\left\{[t/t_m]^3 - 1\right\}\right)$$

$$\frac{j_{prog}}{j_m} = (t/t_m)^3 \exp\left(-3/4\left\{[t/t_m]^4 - 1\right\}\right) \qquad (5.20)$$

In all the preceding cases, the incorporation of material into the lattice is the slowest step in the three dimensional growth. Diffusion controlled growth of hemispheric centres was considered by Hills[18] et al who derived the next expression for the nucleation of a single centre

$$i_{(t)} = \frac{nf\pi(2DC)^{3/2}M^{1/2}}{\rho^{1/2}}\left[1-\exp\left(\frac{-nF\eta}{RT}\right)\right]^{3/2} t^{1/2} \qquad (5.21)$$

where the instantaneous or progressive limiting cases of nucleation can be obtained by multiplying (5.21) by N_o or $A't$, respectively.

In a multiple nucleation under diffusion control, the nuclei grow independently of each other only at the early stages of the transients; at longer times the overlap between the diffusion fields of the growing nuclei takes place. In this case, the application of the Avrami theorem is no possible because of the three dimensional nature of the growth. To overcome this, Scharifker[15,19] et al considered the equivalent area of plane surface towards which diffuses, by linear diffusion, the same amount of material that would be transferred, through spherical diffusion, to a hemispherical growing centre. The overlap problem is thus reduced to a two dimensions frame. The current transient expressions were obtained by considering the linear diffusion of the active species to the area of the projected diffusion fields and are given by[15]

$$j_{inst} = \frac{zFD^{1/2}C}{\pi^{1/2}t^{1/2}}\left[1-\exp(-N\pi kDt)\right]$$

$$j_{prog} = \frac{zFD^{1/2}C}{\pi^{1/2}t^{1/2}}\left[1-\exp\left(-AN_o\pi k'Dt^2/2\right)\right] \qquad (5.22)$$

where $k= (8\pi CM/\rho)^{1/2}$ and $k'= 4/3\ (8\pi CM/\rho)^{1/2}$. At short times, the transients from (5.22) approach those predicted for the non-interacting centres (equation 5.21), whereas a long times they tend to the Cottrell equation. The dimensionless expressions from the analysis of the current maxima for instantaneous and progressive nucleation are[15] given below and their shapes are illustrated in figure 5.3(b).

$$\left(\frac{j_{inst}}{j_m}\right)^2 = \frac{1.9542}{t/t_m}\left\{1-\exp\left[-1.2564(t/t_m)\right]\right\}^2$$

$$\left(\frac{j_{prog}}{j_{m\sim}}\right)^2 = \frac{1.2254}{t/t_m}\left\{1-\exp\left[-2.3367(t/t_m)^2\right]\right\}^2 \qquad (5.23)$$

The projection of the planar diffusion on the nucleation plane gives rise to cylindrical diffusion zones which were considered[20] to have different height for nuclei created at t≠0. Sluyters[21] et al proposed that those diffusion zones have the same height and expressed them as a function independent of the time at which the new nuclei are formed (u).

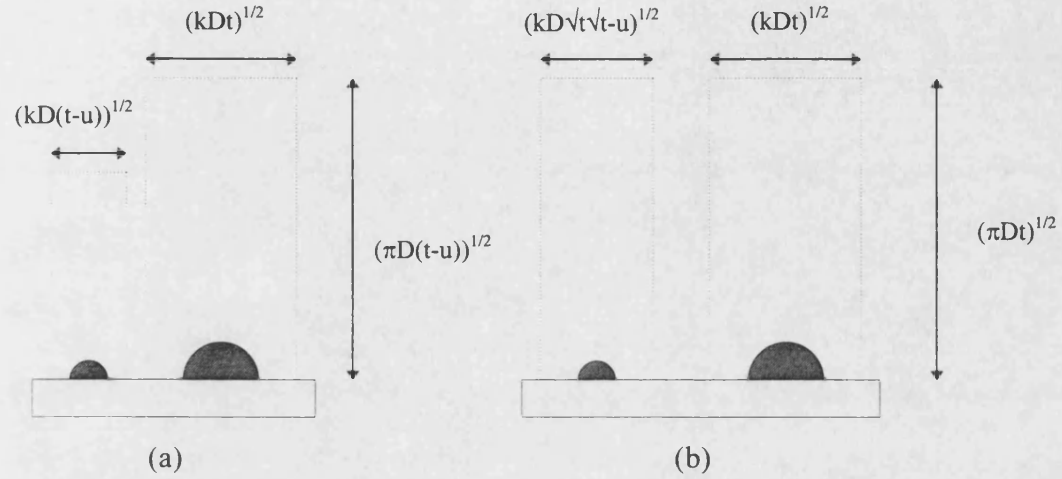

Figure 5.4 Schematic representation of the cylindrical diffusion zones by (a) Gunawardena[20] and (b) Sluyters[21].

Sluyters et al tried to derive an equation applicable to any nucleation system, at shorter times, where the two limiting cases were integrated. The equation for the current transient is given by

$$j_{(t)} = \frac{nFCD^{1/2}}{(\pi t)^{1/2}}\left[1 - \exp\left(-ANk\pi Dt^{1/2}\int_0^t (t-u)^{1/2}\exp(-At)du\right)\right] \quad (5.24)$$

with $k = (8\pi C\, M/\rho)^{1/2}$. When u=0, i.e. instantaneous nucleation, the radii and heights of the diffusion zones in figure 5.4 (b) becomes (a) and the equation (5.24) can be rewritten as

$$j_{inst} = \frac{nFCD^{1/2}}{(\pi t)^{1/2}}\left[1 - \exp(-N\pi kDt)\right] \quad (5.25)$$

The current for progressive nucleation is given by

$$j_{prog} = \frac{nFCD^{1/2}}{(\pi t)^{1/2}}\left[1 - \exp\left(-\frac{1}{2}AN\pi kDt^2\right)\right] \qquad (5.26)$$

Equations (5.25) and (5.26) are the same that these proposed by Gunawardena[20].

5.3 **Electrodeposition of Copper on POAP Modified Electrode**

POAP films were grown on a previously polished Pt electrode by cycling the potential between -0.25 and 0.7 V SCE in a 10^{-2} mol dm^{-3} oAP solution, at pH 0.9. Dismantleable and reusable platinum electrodes (see figure 3.4, area 1.9 x 10^{-3} cm^2) were utilised in the experiments where SEM photographs were required. After formation of the polymer, electrodes were rinsed with plenty of ultrapure water and monomer free solution at the same pH. Next, the modified electrodes were introduced in the latter solution and the potential was cycled between -0.25 and 0.7 V for several minutes. POAP voltammograms recorded after this procedure were used to check the integrity of the film at the end of each set of nucleation experiments. Finally, electrodes were introduced into the cell containing a 3.5 x 10^{-2} mol dm^{-3} $Cu(ClO_4)_2$ solution, at pH 0.9; the potential was kept at 0.279 V for six or eight minutes before each cathodic pulse to ensure a total redissolution of metallic copper deposited in previous steps.

Figures 5.5 and 5.6 show the potentiostatic transients for the copper deposition on POAP modified electrodes at two different polymer thicknesses. The initial potential in all the transients shown in the figures was 0.279 mV SCE, the final potentials are specified in the upper right corner of the plots and correspond to values more negative that the potential of reduction of the polymer. At the beginning of each transient there is a charging current that decays during the process of nucleation; this charging current is

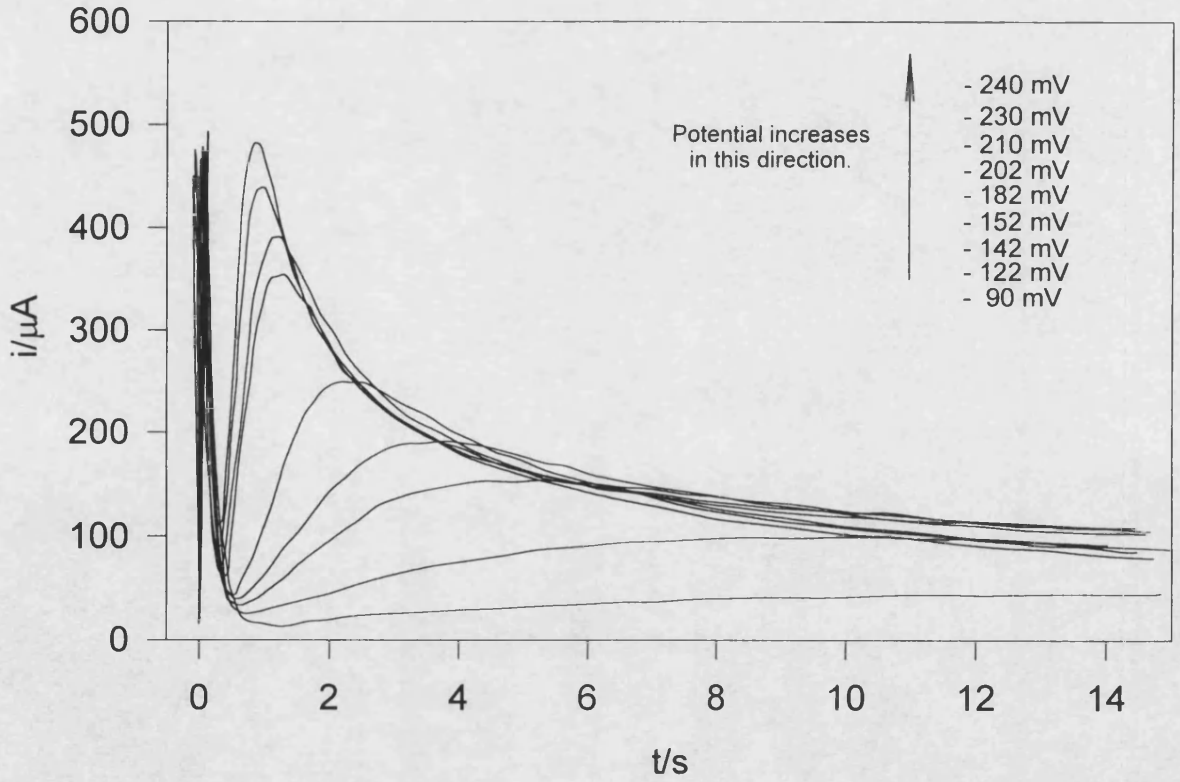

Figure 5.5 Set of potentiostatic transients for the deposition of copper on POAP modified Pt electrode (0.031 cm^2) in aqueous 3.5 x 10^{-2} mol dm^{-3} Cu^{2+} solution at pH 0.9. Thickness of the film 90 nm. All the potentials steps started at 0.279 V SCE.

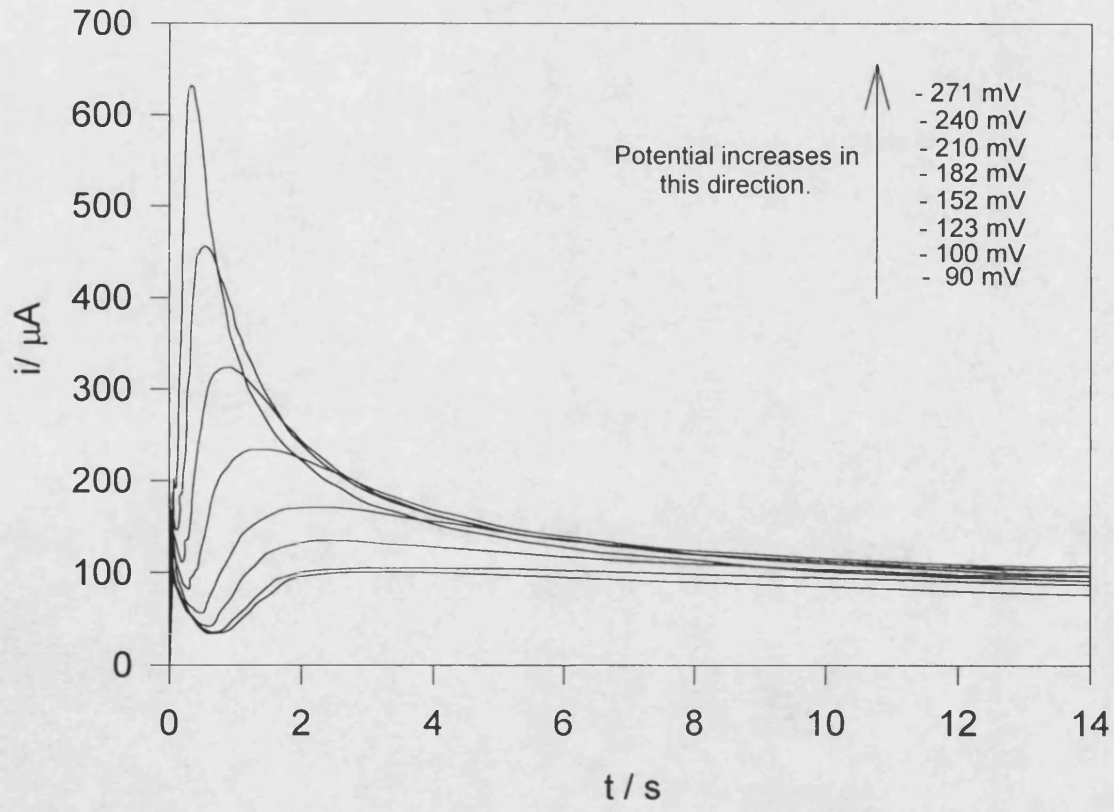

Figure 5.6 Set of potentiostatic transients for the deposition of copper under the experimental conditions shown in figure 5.5. Thickness of polymer film 32 nm.

related to the reduction of the polymer before the electrocrystallisation of copper occurs. The charge under the anodic curve of the voltammogram corresponding to the 90 nm thick film was 5.1mC cm^{-2} which is close to that calculated from the transients for the same film (2.3 mC cm^{-2}). The charging current is smaller when the polymer thickness decreases, as can be seen in figure 5.6, which supports this conclusion.

The succeeding part of the transients reflects the rise in current as the electroactive area increases because of the growth of independent nuclei and/or the number of them. The current reaches a maximum and then starts decreasing as the diffusion fields of the nuclei overlap. The maxima are higher and occur at shorter times as the potential step increases suggesting that the number of active sites and nuclei increases with the potential[22].

The transients were contrasted with these corresponding to the limiting cases for nucleation and two dimensional growth predicted by the set of equations (5.18). No fit was observed for any of the two film thicknesses. At longer times, the current decays more slowly that that predicted by the theory[7]. This characteristic seems to indicate that the process is mass transport controlled. Figure 5.7 compares the 32 nm film transient with the theoretical 2D instantaneous and progressive nucleation curves. It is clear that the growth of the copper centres does not follow the 2D characteristics.

At longer times, the transients of figure 5.5 and 5.6 converge on a falling line similar to that corresponding to linear diffusion to the electrode surface. This behaviour agrees with the set of equations (5.22) for a three dimensional nucleation and growth under diffusion control. A set current versus $t^{-1/2}$ plots of the transients is shown in figure 5.8; from their slope it is possible to determine the diffusion coefficient of the

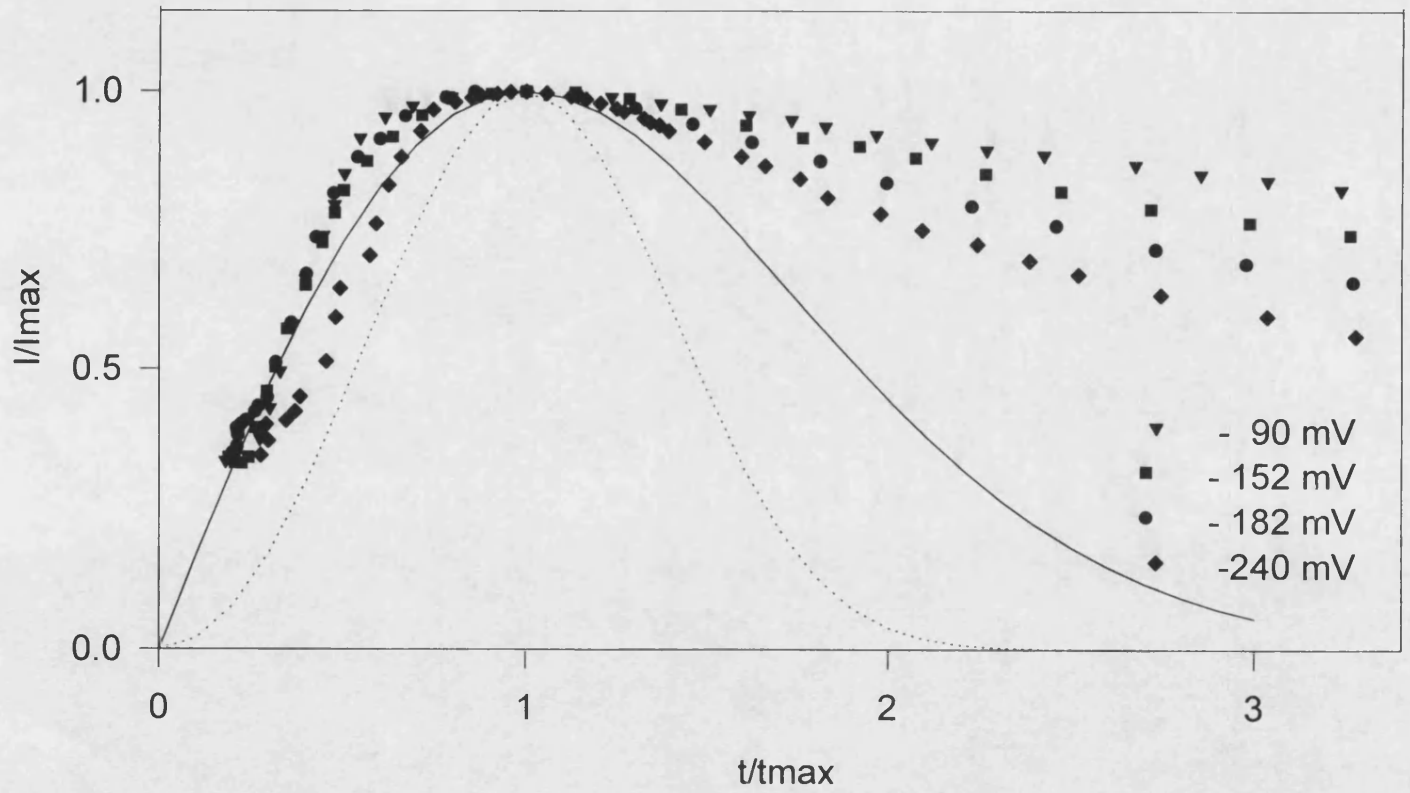

Figure 5.7 Diomensionless plots according to the set of equations (5.18) for two dimensional growth of deposits. ····· Progressive —— Instantaneous limiting cases. Points represent experimental curves at different potential steps. Thickness of the film 32 nm.

electroactive species. The average calculated value of this parameter is (6.4 ± 0.3) x 10^{-6} cm^2 s^{-1} which is very close to that reported in the literature[23,24] (5.9 x 10^{-6} cm^2 s^{-1}).

The current and time data of the reduction of copper were normalised according to the set of equations (5.23) and the values $(j/j_m)^2$ were plotted against t/t_m .

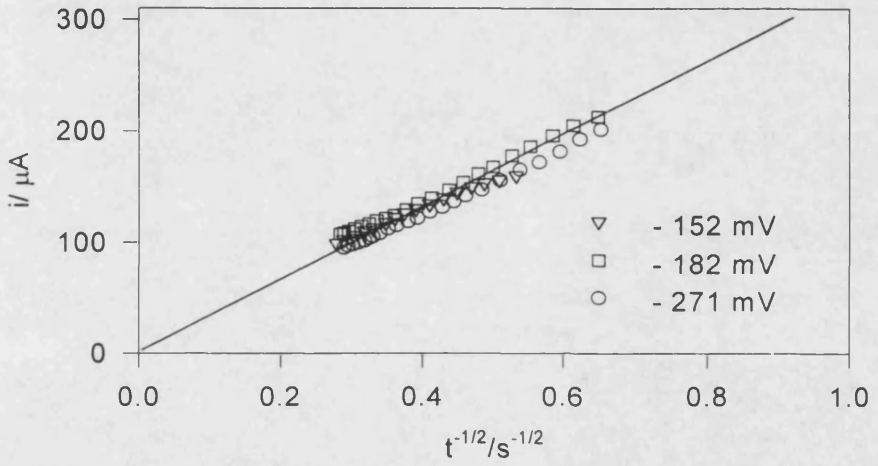

Figure 5.8 Current vs $t^{-1/2}$ plot for potentiostatic transients of figure 5.5 at longer times. Potential steps are specified in the plot.

Figure 5.9 compares the experimental results with the two limiting cases (i.e. instantaneous and progressive) of the theoretical three dimensional nucleation growth model proposed by Scharifker[15] et al. Those authors considered a set of hemispherical nuclei randomly distributed on the electrode surface and growing under diffusion control. Experimental data for the 32 nm film fit reasonably between the two limiting cases of nucleation. The results suggest that nucleation is instantaneous at low overpotentials, whereas it becomes progressive as the potential increases. This behaviour could be explained if electrodeposition takes place onto a conducting

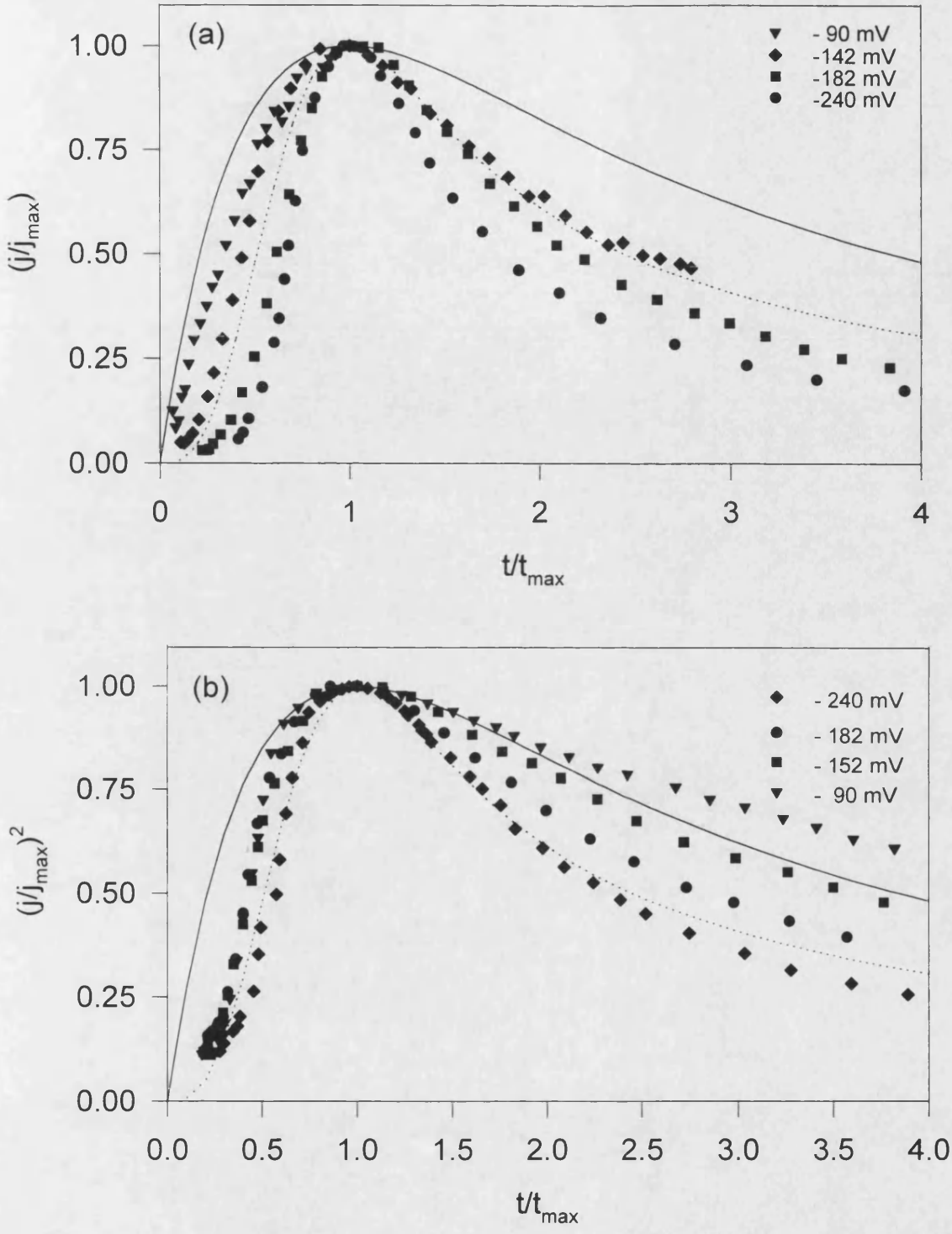

Figure 5.9 Nondimensional plots, $(j/j_{max})^2$, as a function of t/t_{max} for the transients of figures 5.5 and 5.6. ····· progressive —— Instantaneous nucleation. Points represent experimental data at different potential steps. (a) 90 nm and (b) 32 nm thick POAP films.

polymer because a larger number of active sites will be formed at the surface of the polymer by to reduction of the polymer at higher overpotentials.

The nondimensional plots for 90 nm thick POAP film in figure 5.9 do not fit the theoretical lines for progressive and instantaneous nucleation. However, the experimental curves followed the same tendency that observed for the thinner film in the falling region of the transients, i.e. a steeper decay of the normalised current as the potential increases.

Plots of i vs $t^{1/2}$ and vs $t^{3/2}$ were made using the early rising parts of the transients[7,15] to test for instantaneous and progressive nucleation with diffusion controlled growth respectively. However, linear plots were not obtained, probably due to the distortion at short times by the charging current of the polymer and at longer times by the overlapping of diffusion fields of the growing centres.

If a narrow distribution of the size of the particles is assumed at higher overpotentials, the number density of copper particles can be calculated from the following equation[22,15] for an instantaneous nucleation

$$N = j_m^2 \Big/ \left[(0.6382nFDC)^2 (8V_mC/\pi)^{1/2} \right] \qquad (5.27)$$

where j_m is the current density at the maximum, D is the diffusion coefficient of Cu^{2+} species (6.4×10^{-6} cm^2 s^{-1}) and V_m is the molar volume of the deposit ($V_m = M/\rho$, M is the molar mass and ρ is the density of copper, 8.9 g cm^{-3}). Figure 5.10 shows the calculated dependence of the number density of nuclei as a function of potential. N rises sharply at potentials more negative -140 mV and seems to be independent of the film thickness.

Figure 5.11 shows a set of SEM photographs corresponding to the electrodeposition of copper on a 40 nm thick POAP film. The potential was held at -90

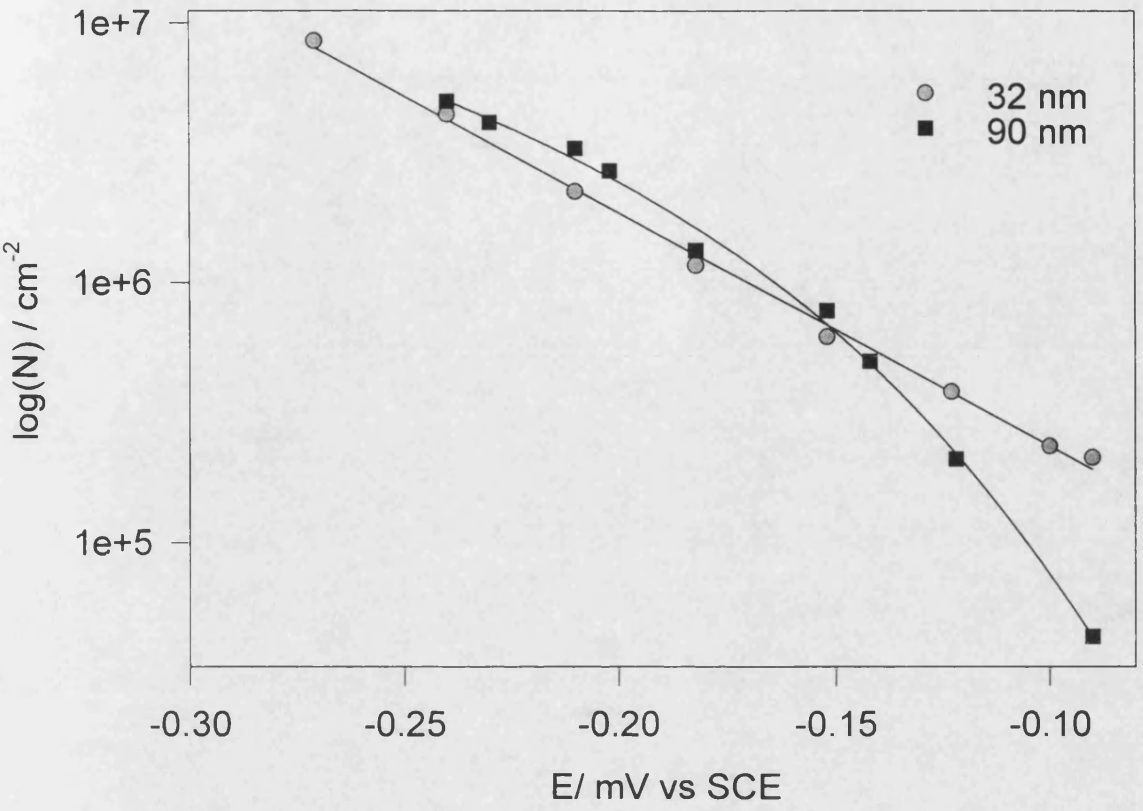

Figure 5.10 Number density of copper particles on 32 and 90 nm thick POAP films as a function of the potential.

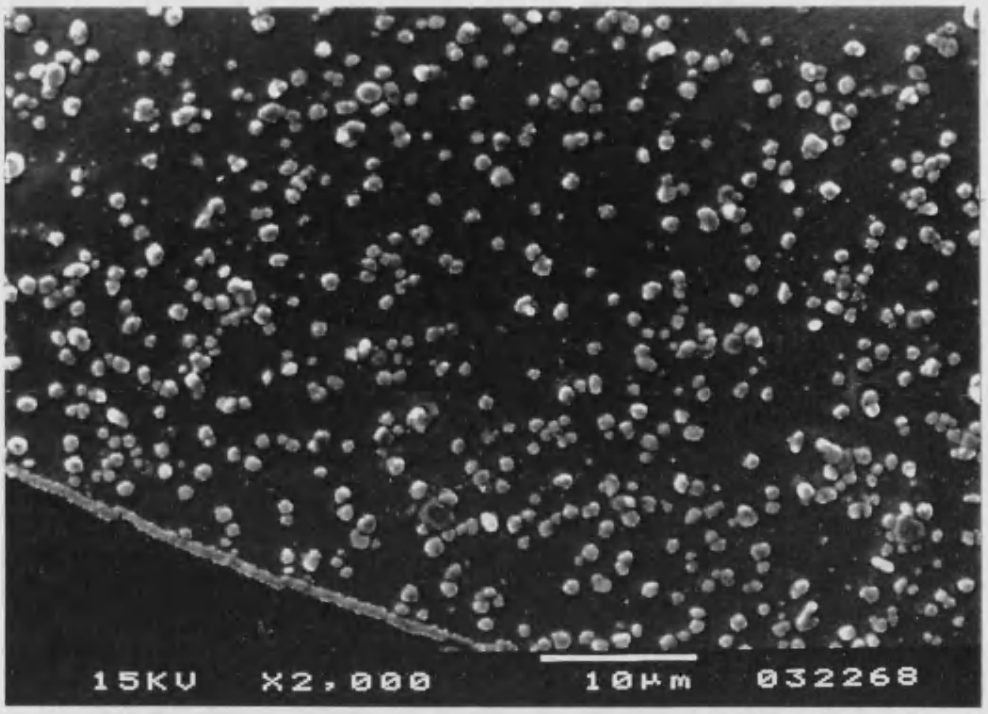

a

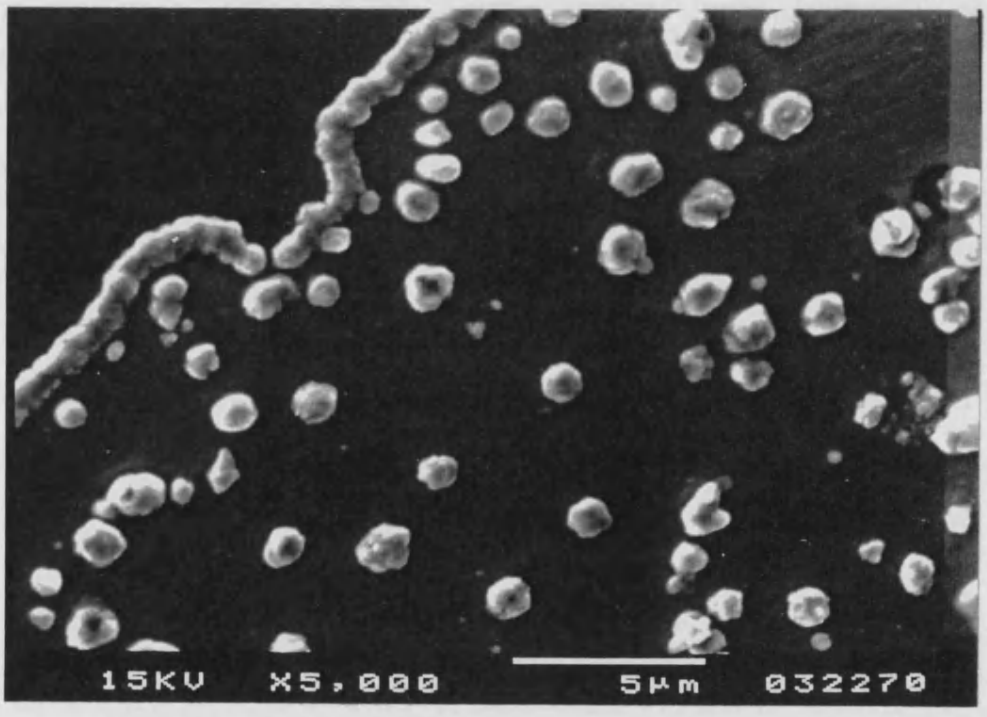

b

Figure 5.11 Set of SEM photographs corresponding to the electrodeposition of copper on a 40 nm thick POAP modified electrode. Potential was stepped from 279 to -90 mV SCE and held at the latter value for 18.5 seconds. Electrode area 1.9 x 10^{-3} cm^2. Density number 2.0 x 10^7 particles cm^{-2}.

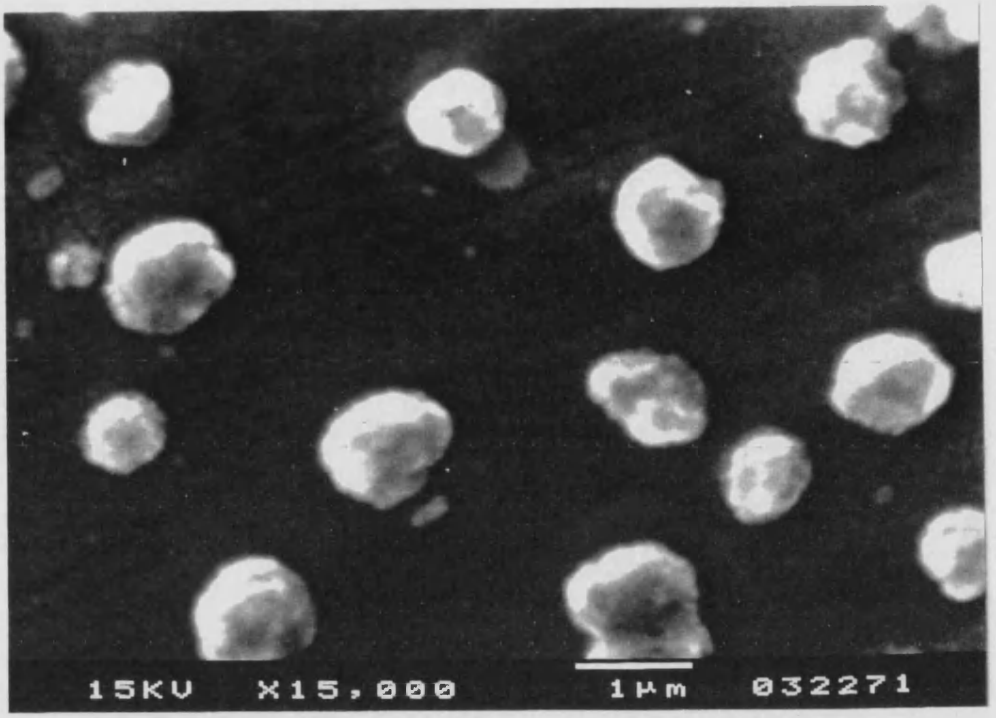

c

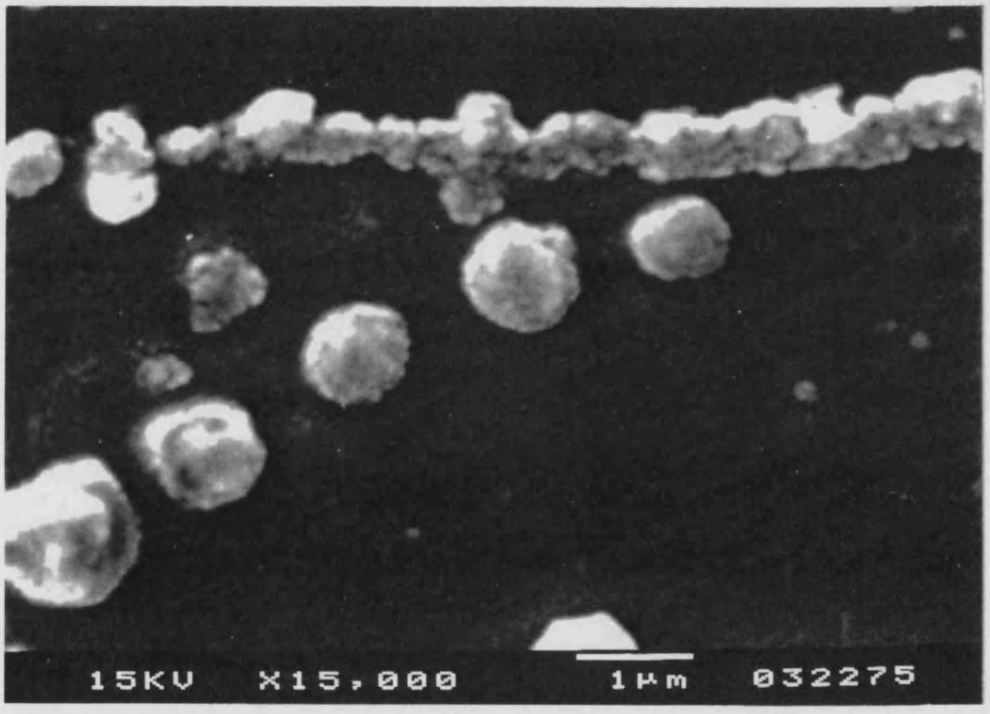

d

mV SCE for 18.5 seconds. The images reveal the formation of hemispherical centres randomly distributed on the electrode surface. The nuclei number density calculated from photographs was 2.0 x 10^7 particles cm^{-2} which is higher than that calculated from equation (5.24) at the same potential (2.1 x 10^5 particles cm^{-2}). Photographs (a), (b) and (d) show the formation of very close centres on the border between the platinum modified electrode and the glass. This edge effect could be associated to a poor coverage of the polymer in that area and/or the distortion of the diffusion fields in that region. The results indicate a instantaneous nucleation because growing centres exhibit similar sizes; this agrees with the figure 5.9.

Electrodeposition of copper at higher overpotentials on a POAP film of similar thickness was also studied by SEM, figure 5.12. In this case the potential was held at -240 mV SCE for the approximately 18 seconds. The centres looks like cauliflowers. If each cauliflowered unit is considered a growing centre, the number density calculated from photographs is approximately 3.1x 10^7 particles cm^{-2} . Although some distribution of sizes can be observed in the photographs, the number of active sites clearly does not depend on the potential as can be seen by comparing figures 5.11 and 5.12. The apparent progressive nucleation deduced from figure 5.9 at higher potentials is clearly an artefact due to progressive transformation of multiple centres in clusters located at the original nucleation sites. In consequence, the distribution of nuclei is not random.

The fact that the number density does not depend on the potential suggests that electrodeposition takes place through pores, in the electrode solution interface. For a thin porous film at low potentials, the electron transfer rate to the copper cation in the pore could be very small so that no depletion of Cu^{2+} would occur. If the polymer

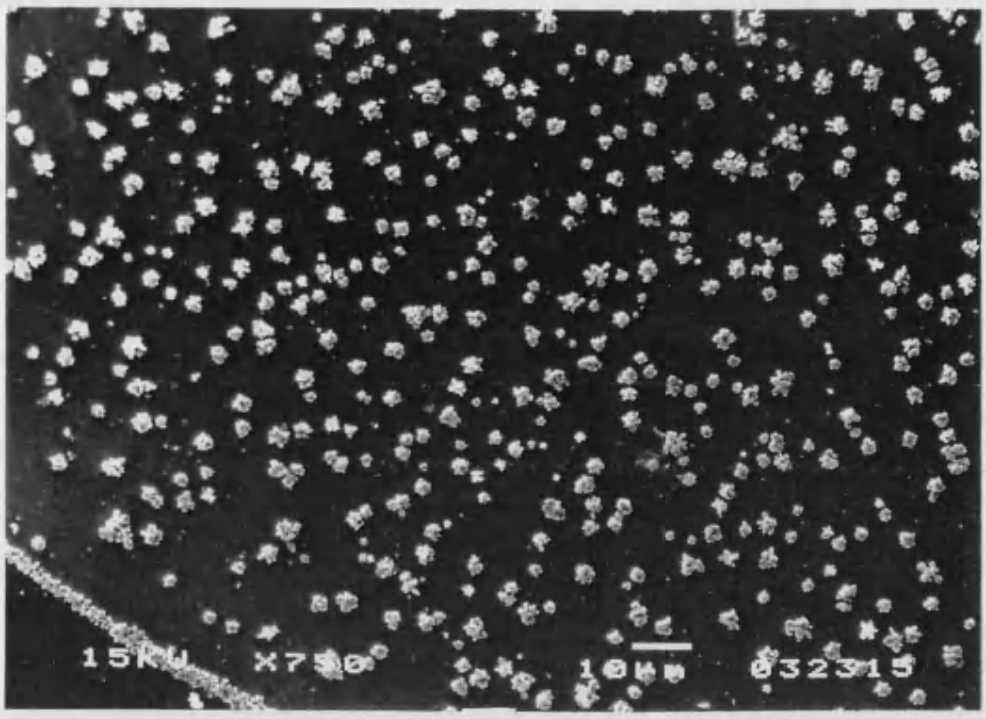

a

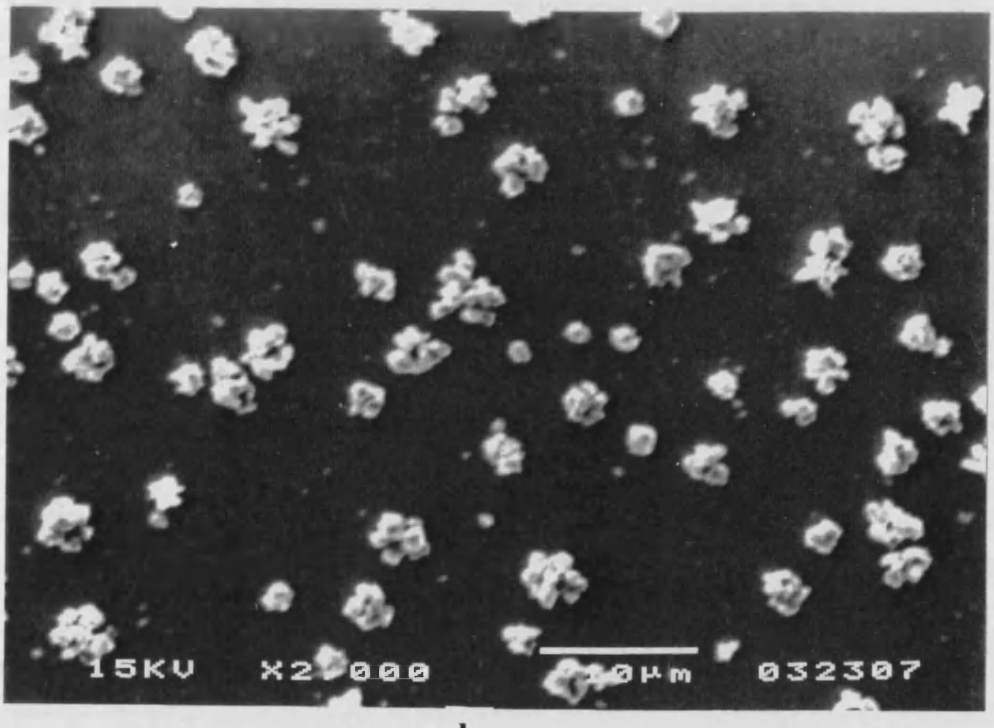

b

Figure 5.12 Set of SEM photographs corresponding to the electrodeposition of copper on a 42 nm thick POAP modified electrode. Potential was stepped from 279 to -240 mV SCE and held at the latter value for 18 seconds. Electrode area 1.9 x 10^{-3} cm^2. Density number 2.0 x 10^7 particles cm^{-2}.

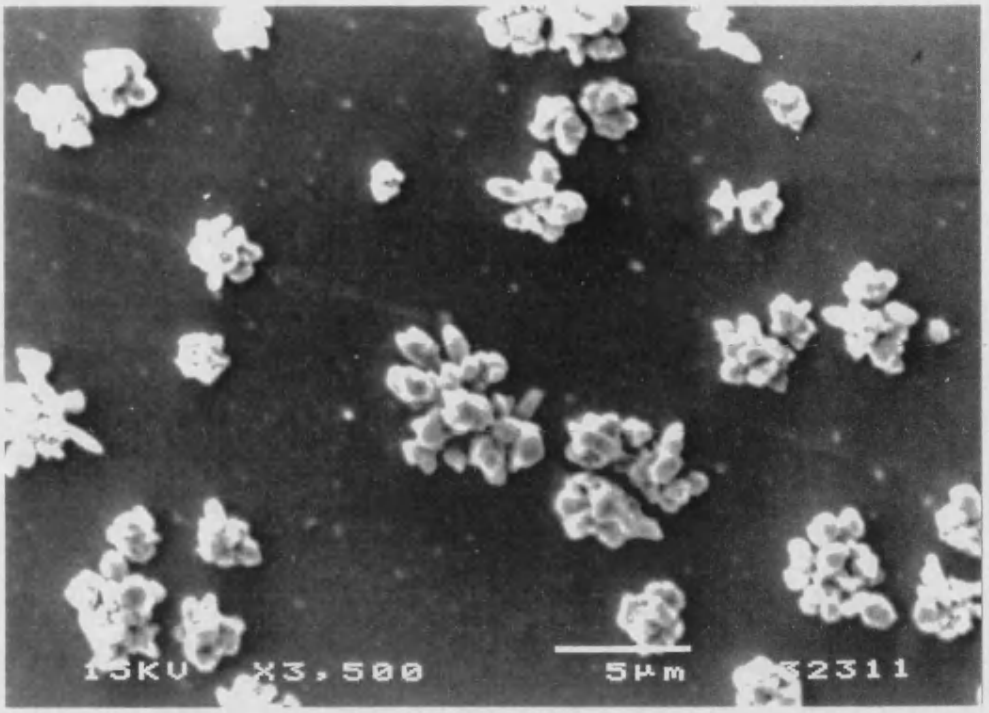

c

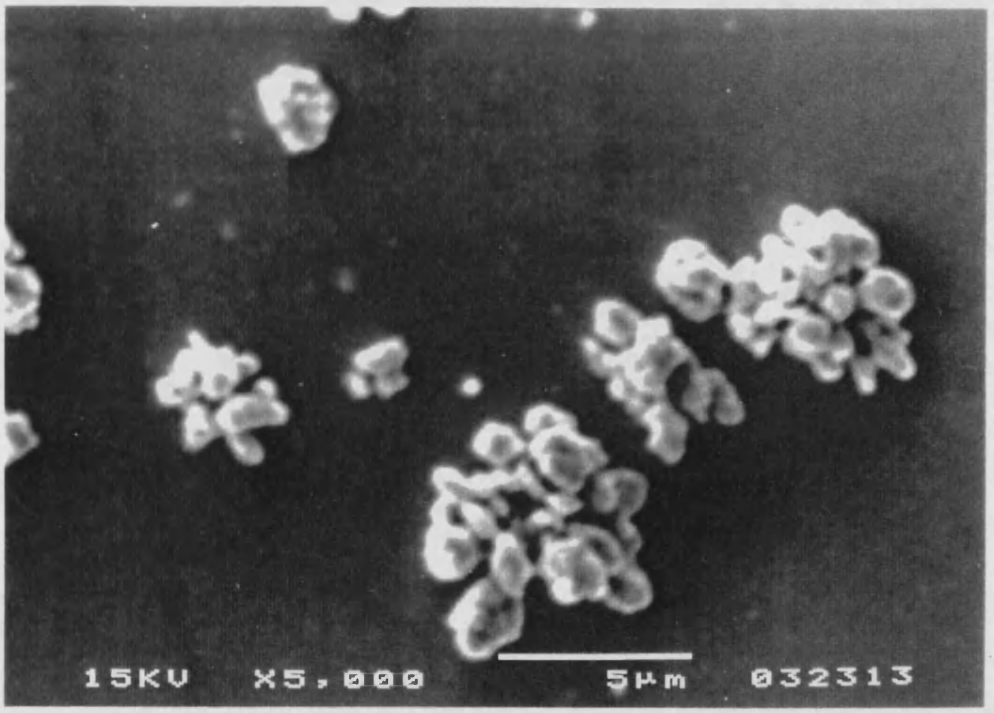

d

If the polymer contains initially copper ions in its pores, these would be reduced at the same rate and the metallic copper formed would reaches the surface at approximately the same time. Under such conditions instantaneous-like nucleation would be observed. At higher potentials electron transfer is no longer a limiting factor and the morphology of the pores would limit the diffusion of Cu^{2+} to the electrode surface; in this case, the moment at which the copper reaches the polymer solution interphase would depend on the tortuousity of the pores and progressive-like nucleation would result.

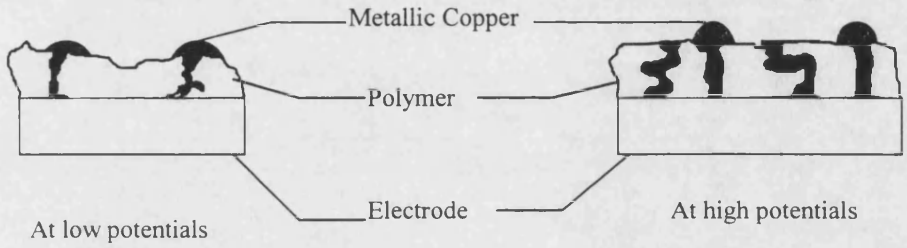

Figure 5.13 Representation of copper deposition on the POAP modified electrode at low and high potentials. Porous model.

Attempts were made to observe the 'mushroom' corresponding to growing centre by SEM, but no evidence of pores was found. On the other hand, the results shown in section 4.9 indicate that the polymer is a conductor in the region where copper is reduced. Since that the polymer is conducting in that region, the potential drop occurs at the polymer-solution interphase so that it is probable that the electrodeposition of the metal takes also place in that region. Moreover, the fact that the cathodic current for reduction of copper ion on the POAP modified electrode did not show a significant decrease with respect to the reduction of the ion on naked platinum (see section 4.9) means that the metallic ions do not to diffuse through pores. Finally, this model does not explain the assemblies of clusters at higher overpotentials.

A closer examination of the SEM photographs from figure 5.12 shows multiple growing centres clustered around a nucleation site. Such a consideration will increase the density of number so that the number of actives sites depends on the potential. It is probable that nucleation occurs on conducting strands of the polymer which reach the surface. At low potentials, these reduced conducting strands are less extended so that the growth of particles occurs on a few number of nuclei and the nucleation is effectively instantaneous. At higher overpotentials where the chains are extensively reduced, the number of actives sites increases but only in the area where the conducting strands are present. The conducting chains may be represented by those with a lower proportion of open units. The existence of large areas without nuclei agrees with the conclusion of that only about one half of the total mass of the polymer participates in the redox reaction (section 4.1).

Figure 5.14 Representation of the deposition of copper on POAP modified electrode. Points represents the extension of the reduction of the conducting strands. Model of conducting strands.

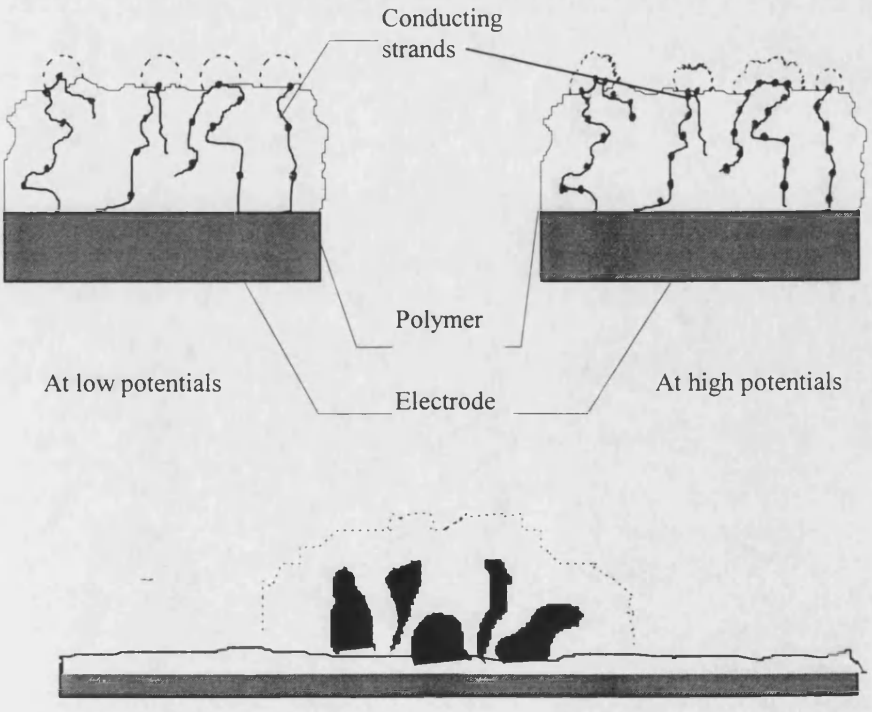

The set of equations (5.23) assumes single hemispherical centres growing independently and randomly at the early stages of nucleation. SEM photographs at low overpotentials seem to agree with that assumption. However, the calculated nuclear number density at -90 mV by using (5.24) is two orders of magnitude smaller than that calculated from SEM. The actual charge density involved in the deposition of copper of figure 5.11 was calculated by integration of the area in the transient; this value was 0.041 C cm^{-2} which is markedly smaller than that expected if the nuclei in figure 5.11 were hemispherically shaped (0.150 C cm^{-2}). This discrepancy between charges may indicate that the growing centres are not hemispherical but possibly have a truncated spherical shape.

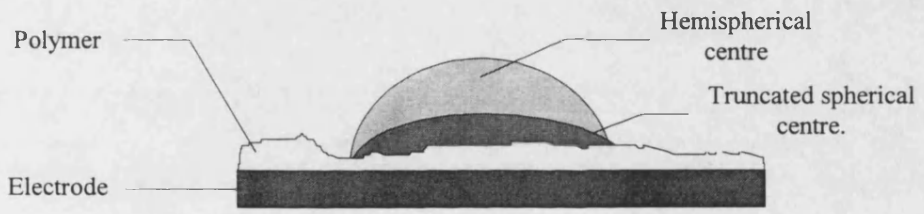

Figure 5.15 Comparison between hemispherical and truncated spherical growing centres for the deposition of copper on POAP modified electrode.

On the other hand, at high overpotentials, the assemblies of clusters shown in figure 5.12 indicate early overlapping of the diffusion fields which explains the non linear relation of the current with t^2 and $t^{3/2}$ for the increasing region of the transients.

Copper electrocrystallization is closely related to the substrate used. On glassy carbon[25,26] and steel[26], for example, it follows the response predicted for 3D instantaneous nucleation with diffusion control[15]. Progressive nucleation and growth has been reported[27] when Au(111) is used as electrode. Others authors have reported

island growth mode on amorphous carbon[28,29], polycrystalline silver[28,29] and tungsten[30]. The electrodeposition of copper on conducting polypyrrole benzenesulfonate[31] has been characterised by an instantaneous nucleation and 3D growth; AFM images showed that the number of growth centres is greater at more negative overpotentials and that they were randomly distributed on the polymer surface. The random distribution of nuclei illustrates the formation of new active sites in regions where, at low overpotentials, no nuclei was present. This behaviour was not observed at the present work where new nuclei surrounding the original sites are formed at higher overpotentials, supporting the idea of large regions of poor conducting polymer chains and the presence of conducting polymer strands where the nucleation takes place. Instantaneous 3D nucleation with diffusion control seems to be also the mechanism for other metal deposition processes on conducting polymer, for example palladium on polyaniline and polypyrrole films[22].

5.4 Conclusions

The conductivity of POAP at potentials more negative than the reduction potential of the polymer has been demonstrated by the electrodeposition of copper.

Potentiostatic transients were fitted to the three dimensional nucleation and growth with diffusion control proposed by Scharifker[15] et al. Nondimensional plots showed a transition from instantaneous nucleation, at low overpotentials, to progressive nucleation at higher potentials. The formation of nuclei with approximately the same diameter at low overpotentials and the presence of a major dispersion in the size of the clusters at higher overpotential agrees with the fitting. However, discrepancies between the charge consumed during the formation of the copper deposit, at low potential, and that calculated by assuming hemispherical centres suggests that the nuclei are not hemispherically shaped but probably truncated spheres. Nuclei formed at large potential steps are not single centres but clusters of copper around a central site which produces a early overlapping of diffusion fields.

The shape of the nucleation centres is explained in terms of electrochemical reduction forming conducting strands in a poorly conducting matrix. The overpotential controls the number of active sites in the strands so that at low potentials a small number of centres is created in the conducting chains giving rise to instantaneous nucleation. An increase of the overpotential creates new centres in the neighbourhood where the surface conducting strands are located. The distribution of clusters is fixed by the presence of these conducting strands.

The potentiostatic transients showed that charging currents are related to the thickness of the polymer film. A larger charging current is required as the polymer thickens because of the mass of the film to be reduced is also larger.

General conclusions and further work

The experimental differences between the polymer films obtained in this work and these reported in the literature clearly indicate that the former has a different structural composition to that found in previous literature. An opened ring structure is possibly formed during the electrochemical oxidation of monomer. This species is attached to the growing chains during the building up of the polymer. A composite of both units, i.e. opened and closed ring structures, is eventually produced. Formation of the opened ring species, possibly API, could be detected in situ during oxidation of monomer by FTIR (Fourier Transform Infrared Spectroscopy) because of the strong absorption of carbonyl group at 1700 cm^{-1}. On the other hand, changes in the structure of the polymer as a function of the applied potential could be also followed by this technique which will help to determine the overall redox mechanism of the POAP films.

The origin of the differences in the structural composition between POAP films reported in the literature and these reported in this work is not clear. Some authors[32,33,34] used oAP without further purification reporting formation of coloured solutions which were not observed in this work. Barbero[35] purified the monomer before using it and the obtained polymer exhibited conducting properties at positive potentials which disagrees with the results in this thesis. Effect of the temperature at which the electropolymerisation is carried out as well as the pH of the solution and the nature of the solvent on the polymer composition will be studied in the future in order to ascertain the origin of these differences.

Determination of the thickness of polymer films by using equation (3.3) assumes that the total charge is completely associated with the redox reaction in the polymer and that the film is completely oxidised and reduced in each cycle. This

assumption is not valid because it was demonstrated in this thesis that only a 60% w/w of the polymer participates on the redox reaction. On the other hand, this thickness determination does not take into account the swelling of the solvent. Thickness determined in this work are an approaching to the real values and the use of in situ techniques, such as ellipsometry, are highly recommended.

Conducting properties of POAP films at negative potentials was demonstrated by oxidation of paraquat and reduction of Cu^{2+} on polymer modified electrodes. Films become non conducting as the oxidation of the film takes place.

The number of molecules of water per POAP equivalent in its oxidised form was determined to be approximately seven. Reduction of the polymer gives rise to a more swollen film but it still exhibits rigidity features. Mass changes during oxidation and reduction of the film under potentiodynamic conditions revealed a complex process. A study of the effect of the pH and nature of anions and cations on the mass changes by QCMB will be carried out to make clear the role of each species in the redox process of the polymer; non aqueous system will be also tried.

Nucleation and growth of copper on polymer modified electrodes is explained in terms of formation of conducting strands in a poorly conducting matrix. The overpotential controls the number of active sites in the strands so that at high overpotentials new centres are created in the neighbourhood where the conducting strands are located. Scharifker[15] equations are not suitable to explain this behaviour and a new model should be considered. This model must assume the formation of truncated spherical nuclei instead of spherical ones with a located distribution of growing centres. Electrodeposition of other metals (Cd, Cr) on POAP modified electrode will be studied in the future.

Finally, copolymerisation of oAP with other monomers, for instance aniline, could give rise to new composite polymers with interesting characteristics. The use of POAP modified electrodes as a sensor to some particular species represents an interesting possible field to study in the future.

References

1. H. Fischer, *Elektrolytische Abscheidung und Elektrokristallisation von Metallen.*, Springer, Berlin (1954).
2. H. Meyer, R. J. Nichols, D. Schröer, L Stamp, *Electrochimica Acta.*, 39 (1994) 1325.
3. D. Schröer, R. J. Nichols, H. Meyer, *Electrochimica Acta.*,40 (1995) 1487.
4. W. Plieth, *Electrochimica Acta.*, 37 (1992) 2115.
5. K. L. Mittal, *J. Vac. Sci. Technol.*, 13 (1976)19.
6. B. Scharifker, Ph.D Thesis, University of Southampton (1979).
7. Southampton Electrochemistry Group, *Instrumetal Methods in Electrochemistry.*, Ellis Horwood Series in Physical Chemistry, New York (1990).
8. E. A. Guggenheim, *Trans. Faraday Soc.*,36 (1940) 408.
9. K. S. C. Freeman, I.R. McDonald, *Molec. Phys.*, 26 (1973) 529.
10. D. Walton, *J. Chem. Phys.*, 37 (1962) 2182.
11. M. Fleischmann, H.R. Thirsk, *Advances in Electrochemistry and Electrochemical Engineering*, Delahay (Ed.), Interscience, New York (1963).
12. A. Bewick, M. Fleischmann, H. R. Thirsk, *Trans. Faraday Soc.*, 58 (1962) 2200.
13. M. Avrami, *J. Chem. Phys.*, 7 (1939)1130.
14. *Annual Report on the Progress of Chemistry.*, Section C: Physical Chemistry, Vol. 87, The Royal Society of Chemistry, Cambridge (1990) 127.
15. B. Scharifker, G. Hills, *Electrochimica Acta.*, 28 (1983) 879.
16. R. D. Armstrong, M. Fleischmann, H. R. Thirsk, *J. Electroanal. Chem.*, 11 (1966) 205.
17. M. Y. Abyaneh, M. Fleischmann, *J. Electroanal. Chem.*, 119 (1981) 187.
18. G. J. Hills, D. J. Schiffrin, J. Thompson, *Electrochim. Acta.*, 19 (1974) 657.
19. G. A. Gunawardena, G. J. Hills, I. Montenegro, B. R. Scharifker, *J. Electroanal.Chem.*, 138 (1982) 225.

20. G. Gunawardena, G. Hills, I. Montenegro, B. Scharifker, *J. Electroanal. Chem.*, 138 (1982) 225.

21. M. Sluyters-Rehbach, J. H. O. J. Wijenberg, E. Bosco, J. H. Sluyters, *J. Electroanal. Chem.*, 236 (1987) 1.

22. A. Leone, W. Marino, B. R. Scharifker, *J. Electrochem. Soc.*, 139 (1992) 438.

23. G. Fabricius, K. Kontturi, G. Sundholm, *Electrochimica Acta.*, 39 (1994) 2353.

24. J. T. Hinatsu, F. R. Foulkes, *J. Electrochem. Soc.*, 136 (1989) 125.

25. G. Fabricius, K. Kontturi, G. Sundholm, *Electrochimica Acta.*, 39 (1994) 2353.

26. L. Bonou, M. Eyraud, J. Crousier, *J. App. Electrochem.*, 24 (1994) 906.

27. M. H. Hölzle, V. Zwing, D. M. Kolb, *Electrochimica Acta.*, 40 (1995) 1237.

28. P. V. Brande, R. Winand, *Surface and Coatings Technology.*, 52 (1992) 1.

29. P. V. Brande, R. Winand, *J. App. Electrochem.*, 23 (1993) 1089.

30. M. Peykova, E. Michailova, D. Stoychev, A. Milchev, *Electrochimica Acta.*, 40 (1995) 2595.

31. R. J. Nichols, D. Schröer, H. Meyer, *Electrochimica Acta.*, 40 (1995) 1479.

APPENDIX I

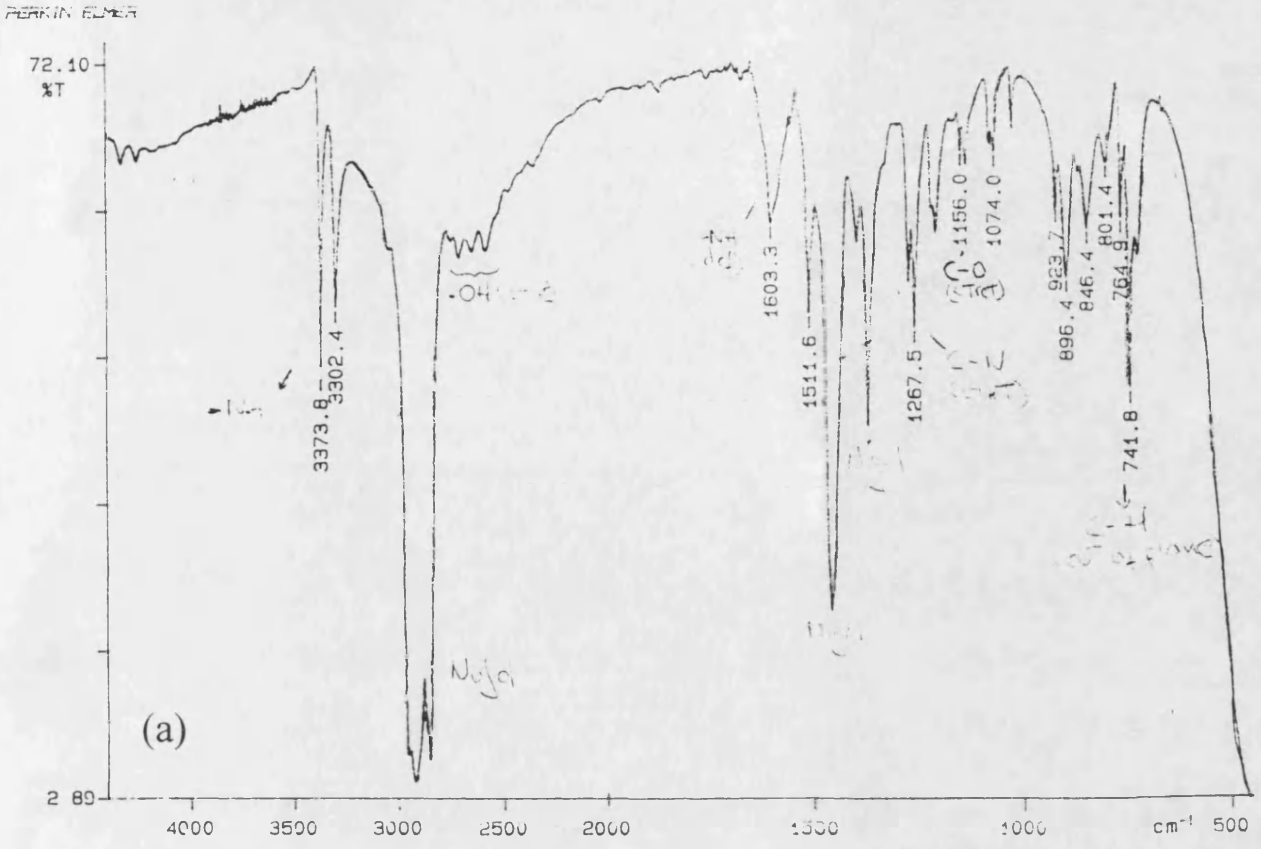

(b)

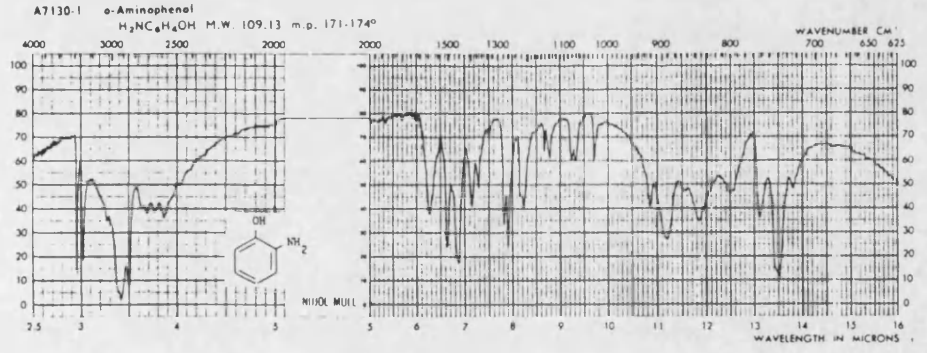

(a) IR spectrum of purified orthoaminophenol in nujol. (b) Reported spectrum in nujol from *The Aldrich Library of Infrared Spectra*, by Charles J. Pouchert, Aldrich Chemical CO. Inc.

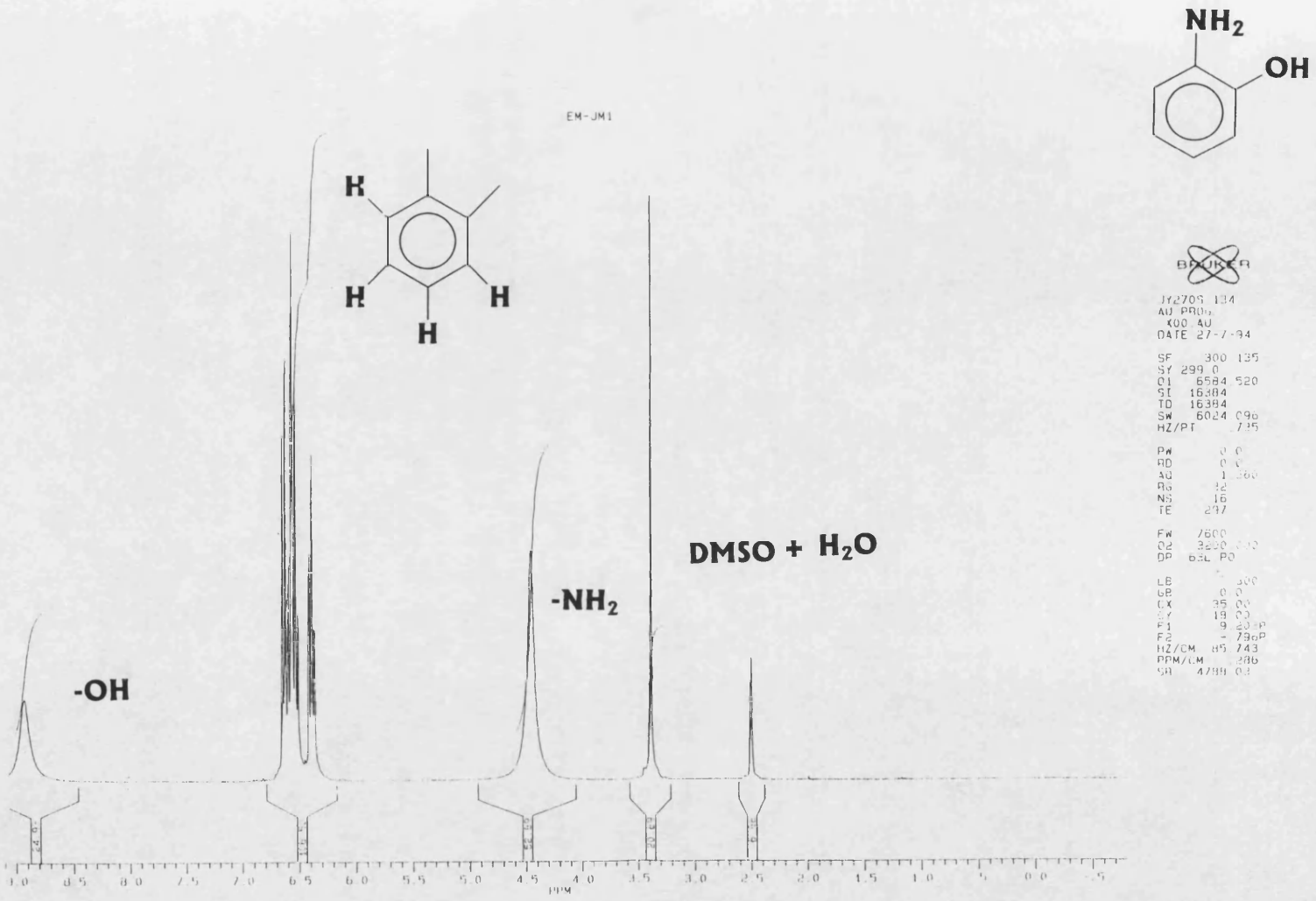

NMR spectrum of purified orthoaminophenol in DMSO.

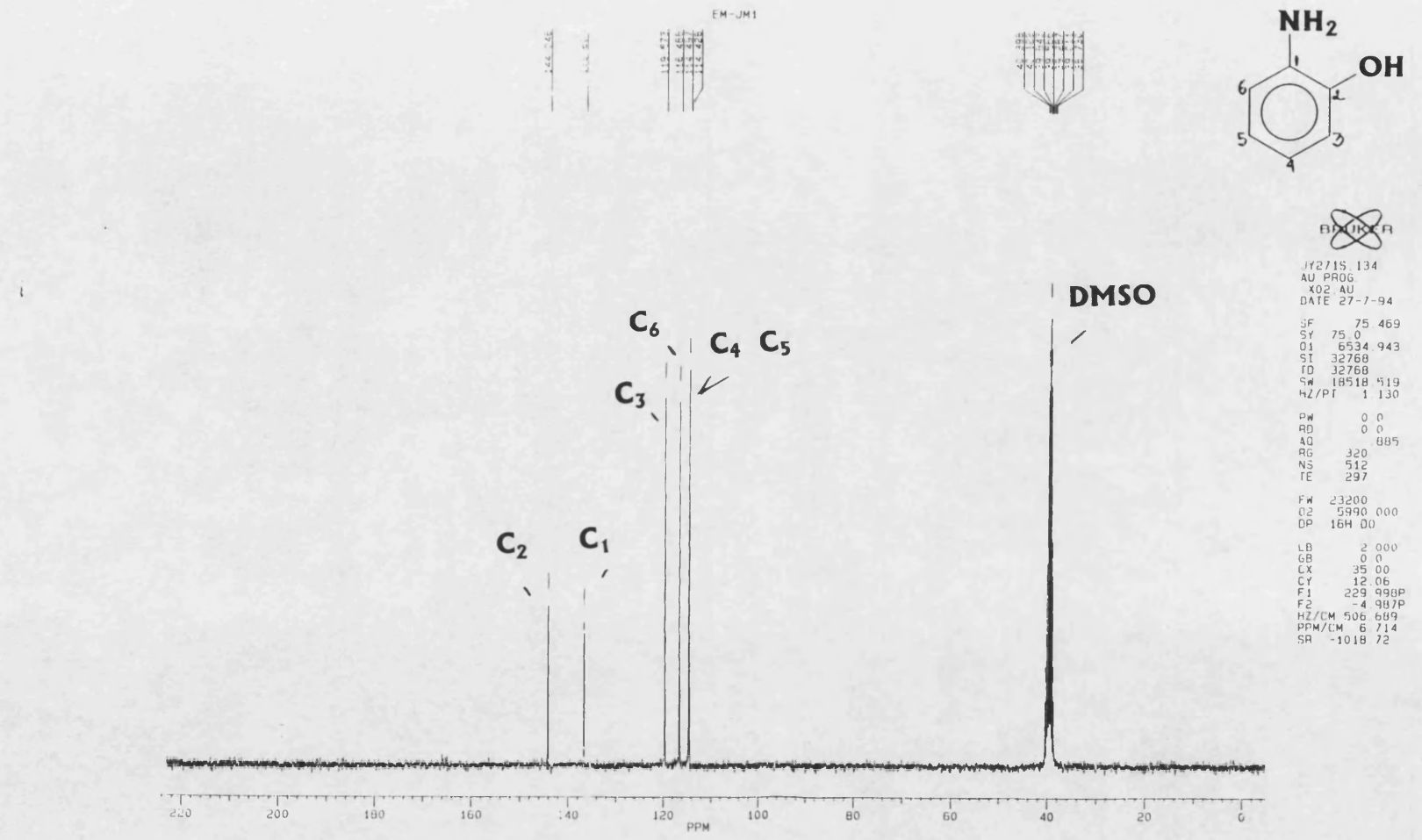

^{13}C spectrum of purified orthoaminophenol in DMSO.